

Binary Neutron Star Mergers: Equation of State and the Hadron-Quark Phase Transition

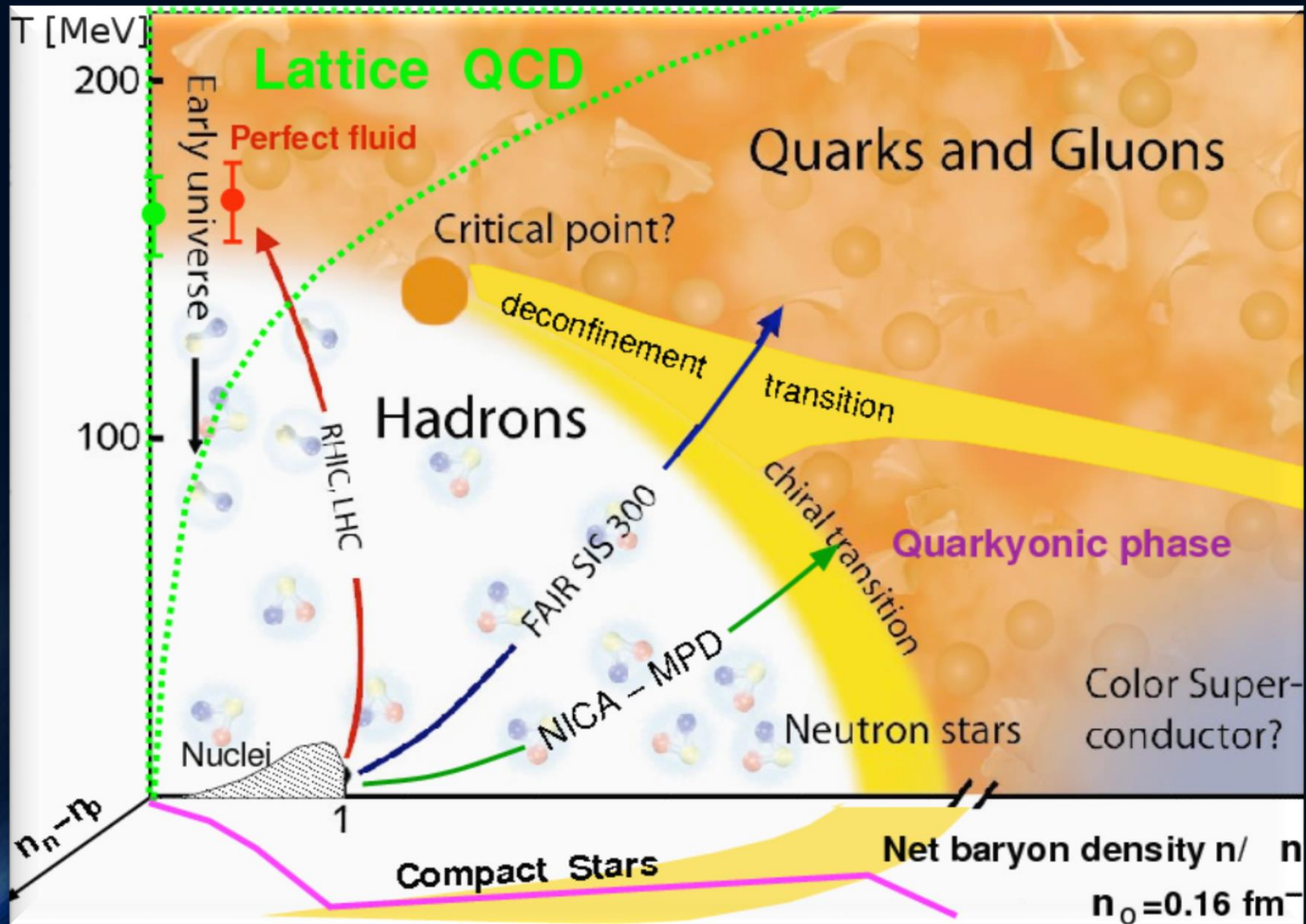
PHYSICS AND ASTROPHYSICS AT THE EXTREME (PAX) III WORKSHOP

PENN STATE, USA, 05. FEBRUARY 2018

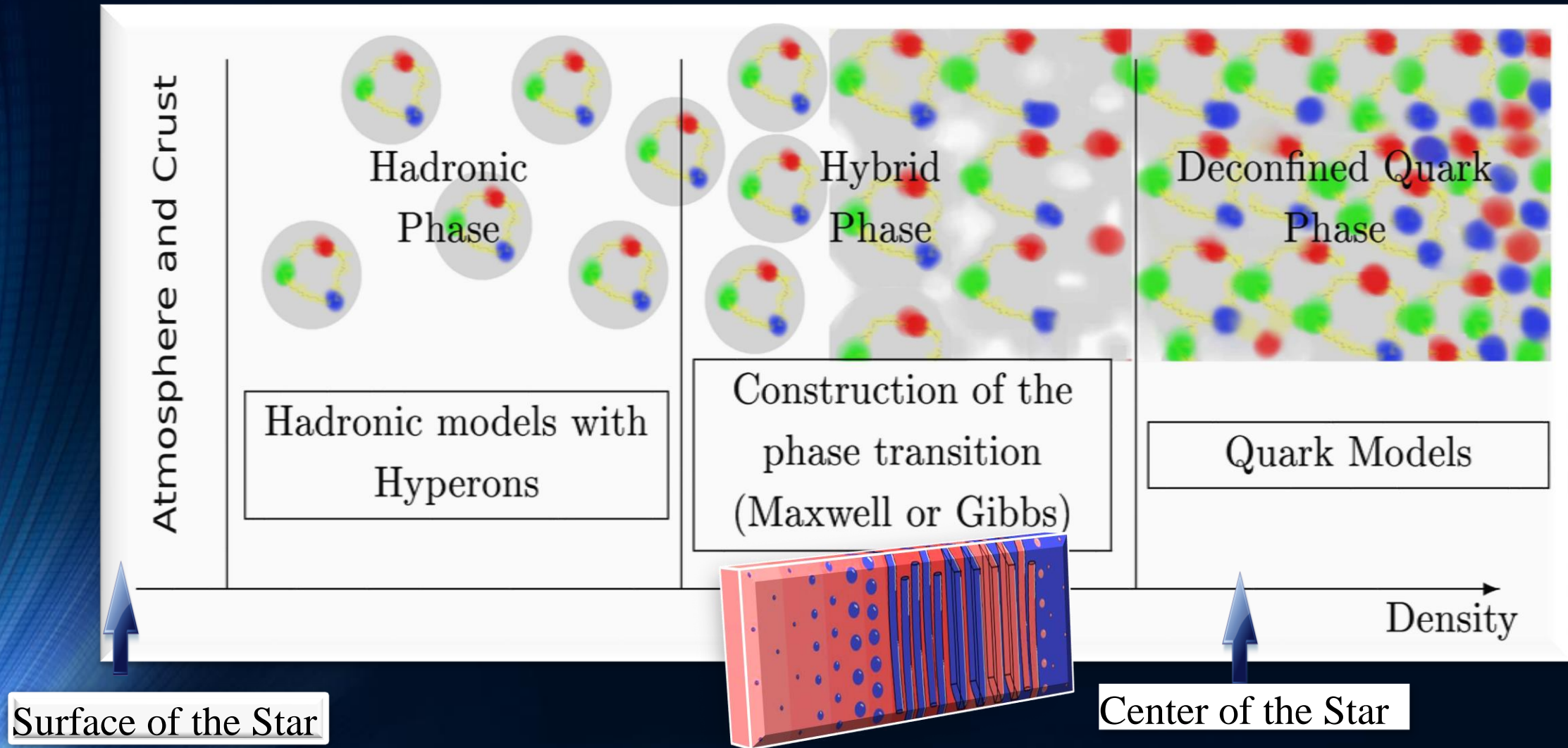
MATTHIAS HANAUSKE, KENTARO TAKAMI, LUKE BOVARD, JOSE FONT,
FILIPPO GALEAZZI, JENS PAPPENFORTH, LUKAS WEIH, ELIAS MOST,
FEDERICO GUERCILENA, NATASCHA WECHSELBERGER, ZEKIYE SIMAY
YILMAZ, CHRISTINA MITROPOULOS, JAN STEINHEIMER, STEFAN
SCHRAMM, DAVID BLÄSCHKE, MARK ALFORD, KAI SCHWENZER,
ANDREAS ZACCHI, JÜRGEN SCHAFFNER-BIELICH, LAURA TOLOS,
GLORIA MONTAÑA, MICHAEL RATTAY, HORST STÖCKER AND LUCIANO
REZZOLLA

FRANKFURT INSTITUTE FOR ADVANCED STUDIES
JOHANN WOLFGANG GOETHE UNIVERSITÄT
INSTITUT FÜR THEORETISCHE PHYSIK
ARBEITSGRUPPE RELATIVISTISCHE ASTROPHYSIK
D-60438 FRANKFURT AM MAIN

The Hadron-Quark Phase Transition



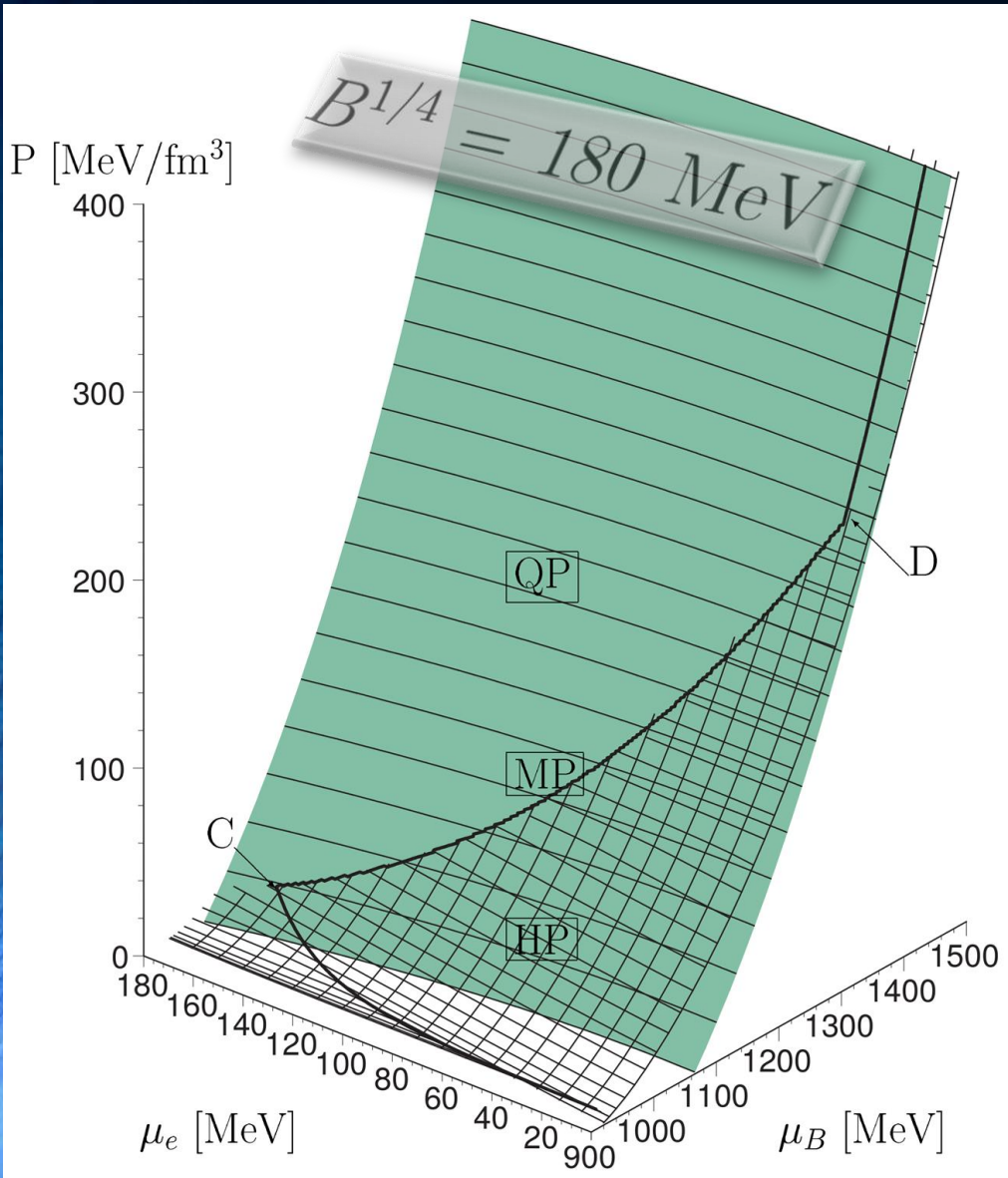
The QCD – Phase Transition and the Interior of a Hybrid Star



See: *Stable hybrid stars within a SU(3) Quark-Meson-Model*,
A.Zacchi, M.Hanuske, J.Schaffner-Bielich, PRD 93, 065011 (2016)

The Gibbs Construction

Hadronic and quark surface:

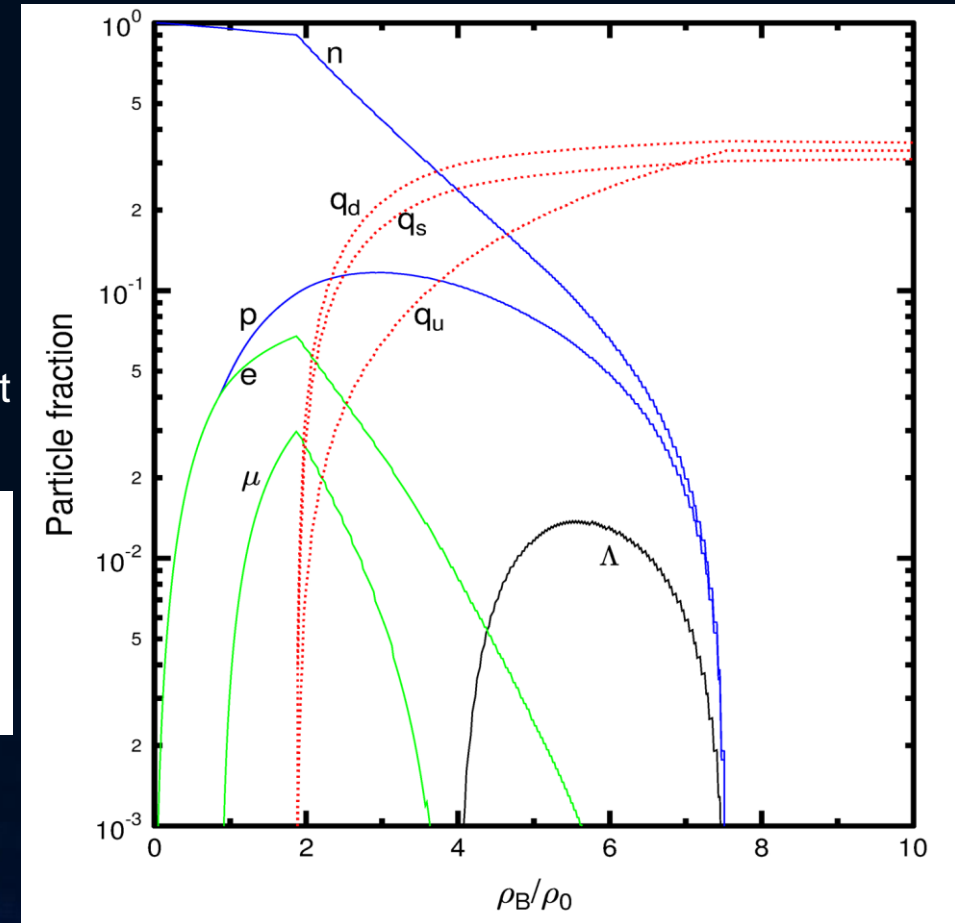


Charge neutrality condition is only globally realized

$$\rho_e := (1 - \chi)\rho_e^H(\mu_B, \mu_e) + \chi\rho_e^Q(\mu_B, \mu_e) = 0.$$

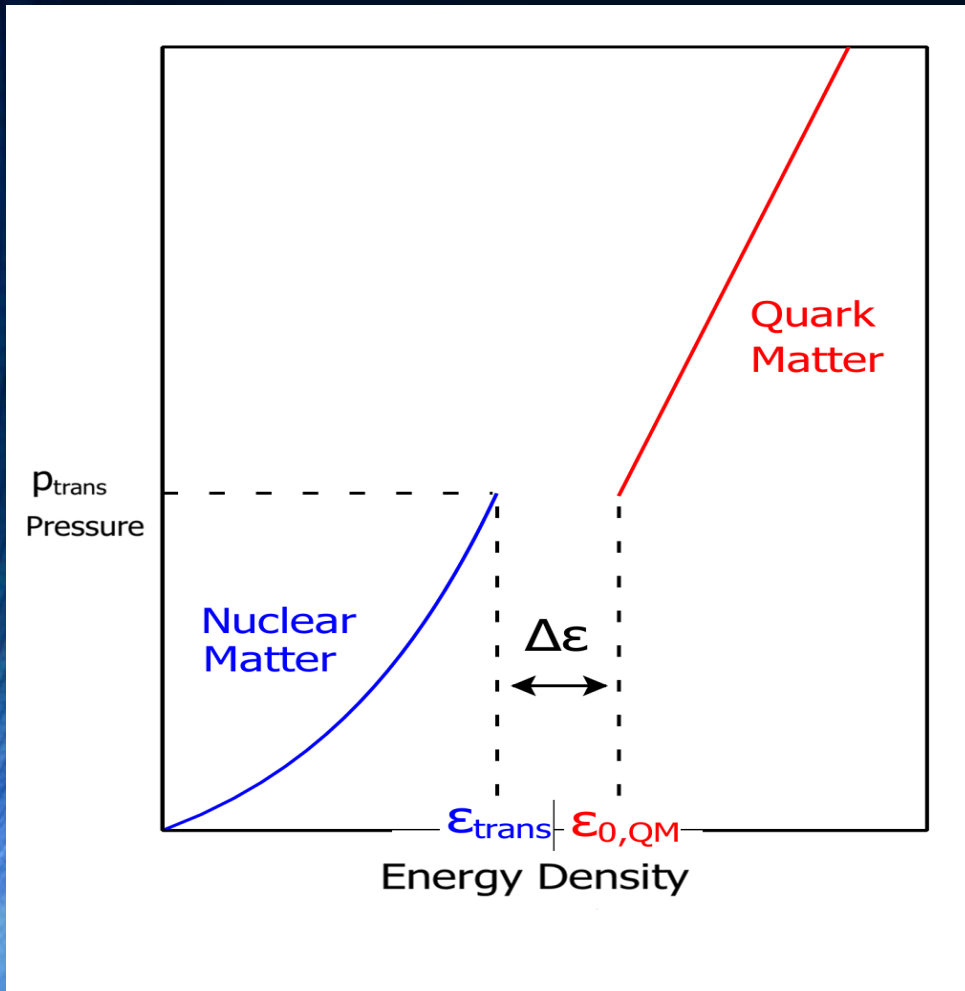
The pressure in the mixed phase depends on two independent chemical potentials

$$\begin{aligned} P^H(\mu_B, \mu_e) &= P^Q(\mu_B, \mu_e), \\ \mu_B &= \mu_B^H = \mu_B^Q, \\ \mu_e &= \mu_e^H = \mu_e^Q \end{aligned}$$

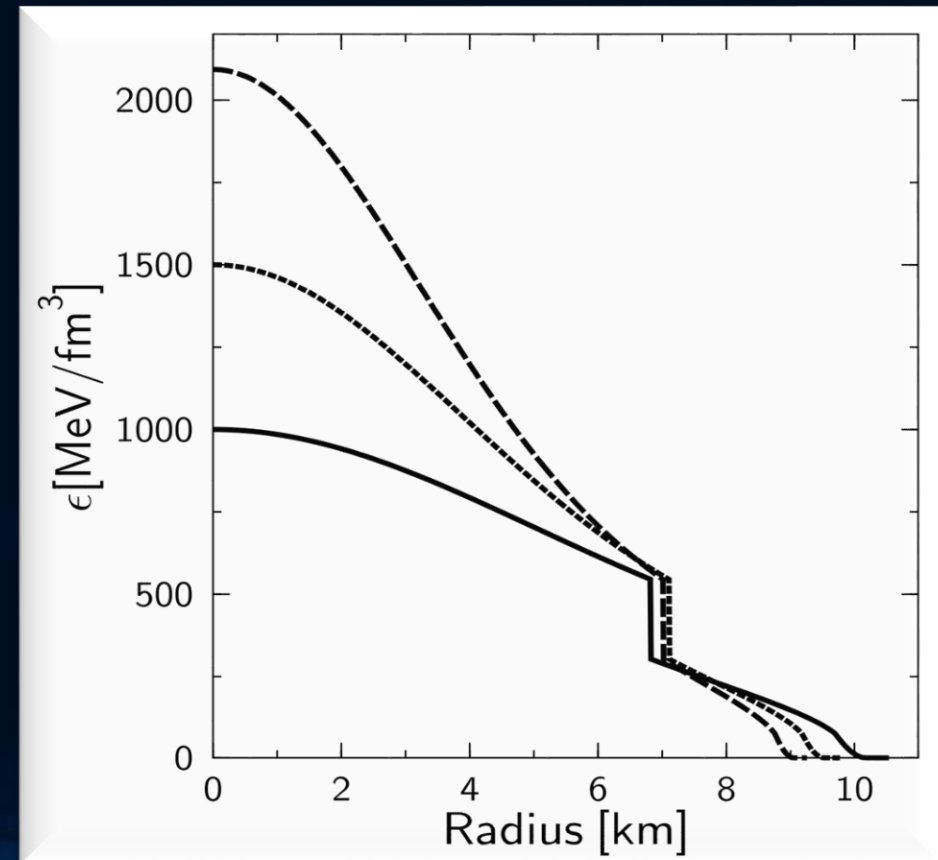


The Maxwell Construction

If the surface tension between the hadron and quark phase is relatively large, the mixed phase could completely disappear, so that a sharp boundary between the two phase exists. The Hadron-quark phase transition is then described using a Maxwell construction.



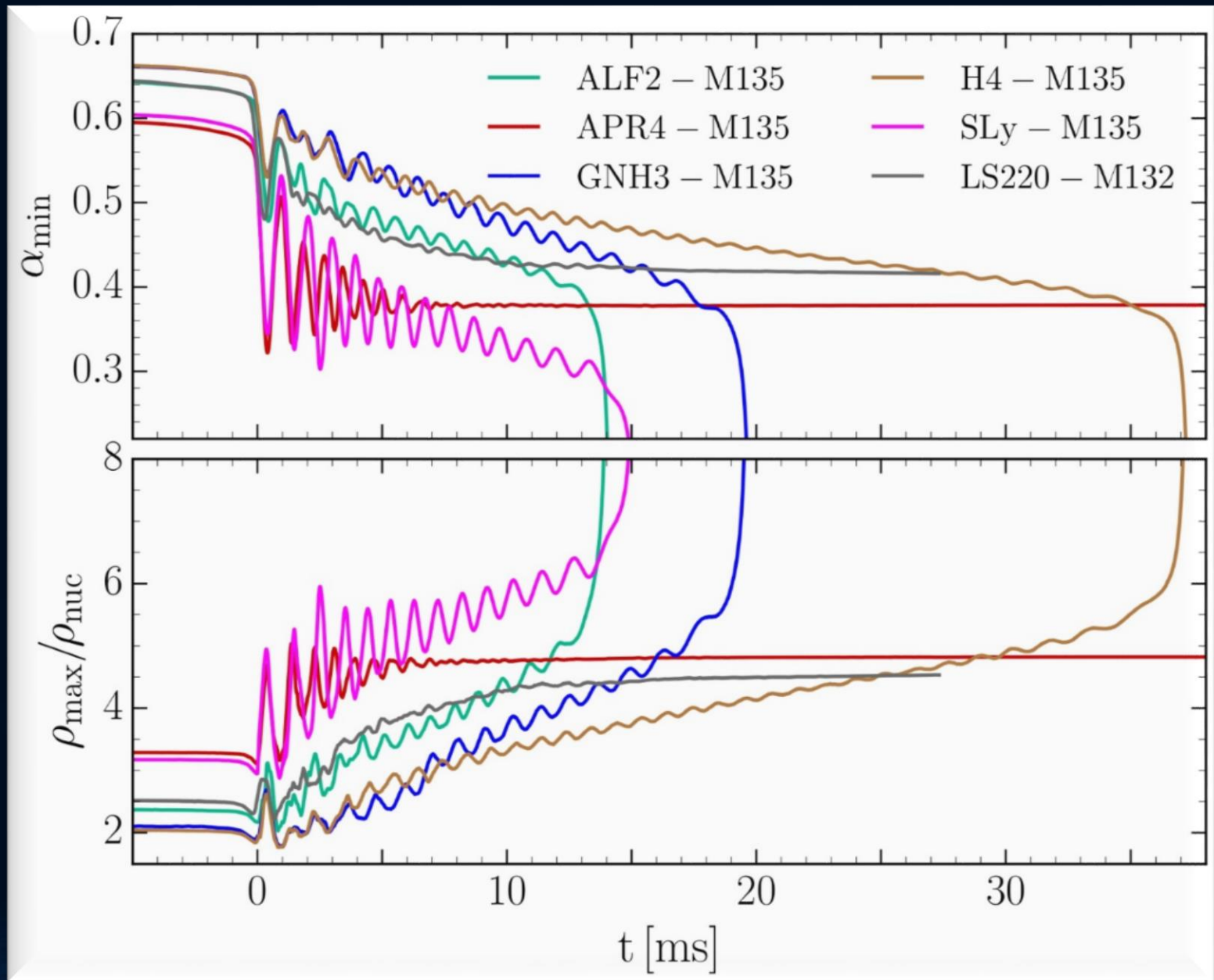
Pressure and baryon chemical potential stays constant, while the density and the charge chemical potential jump discontinuously during the phase transition.



HMNS Evolution for different EoSs

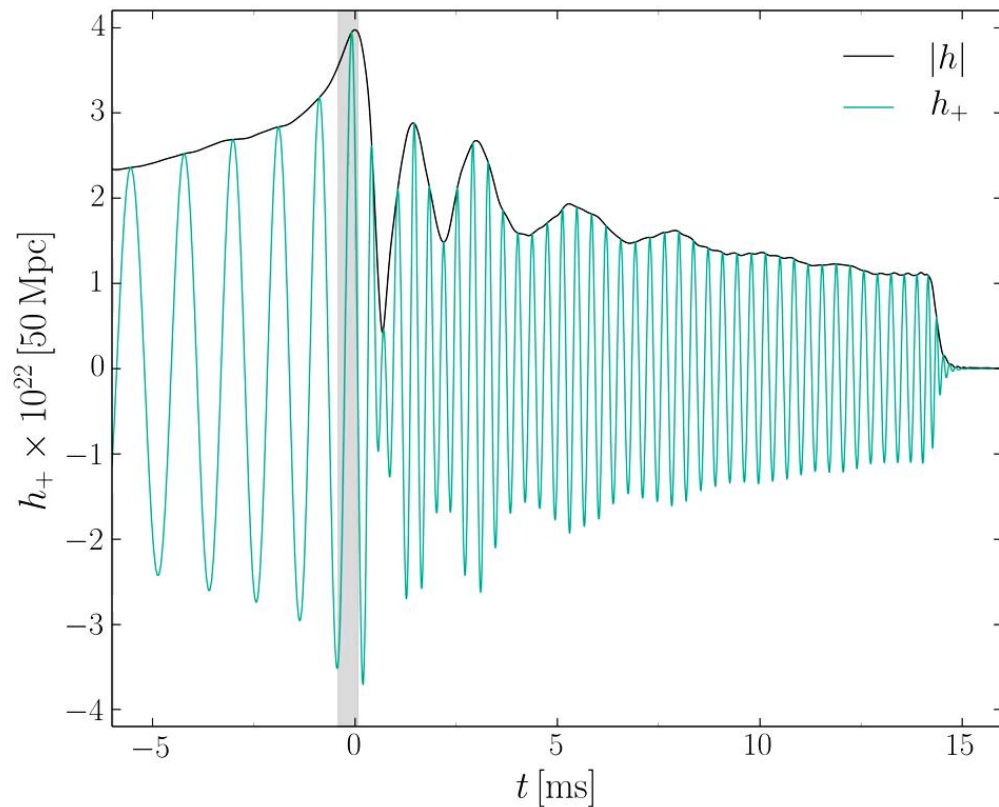
High mass simulations
($M=1.35 M_{\text{solar}}$)

Central value of the lapse function α_c (upper panel) and maximum of the rest mass density ρ_{max} in units of ρ_0 (lower panel) versus time for the high mass simulations.

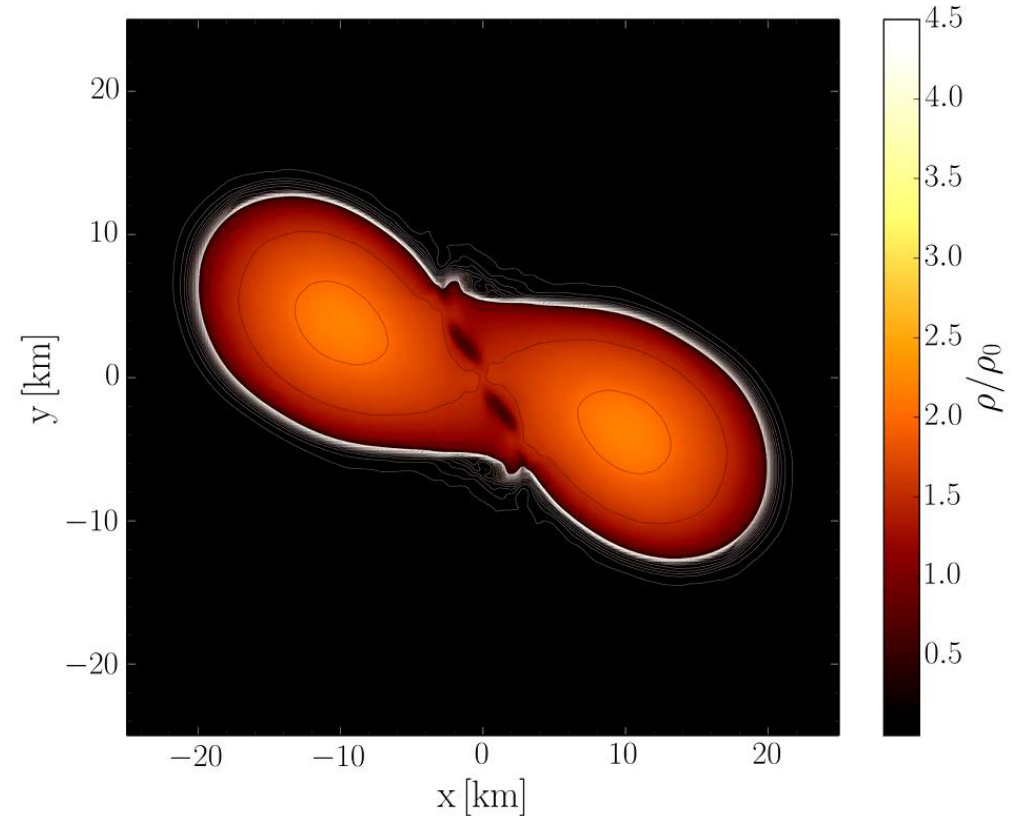


Evolution of the rest-mass density distribution

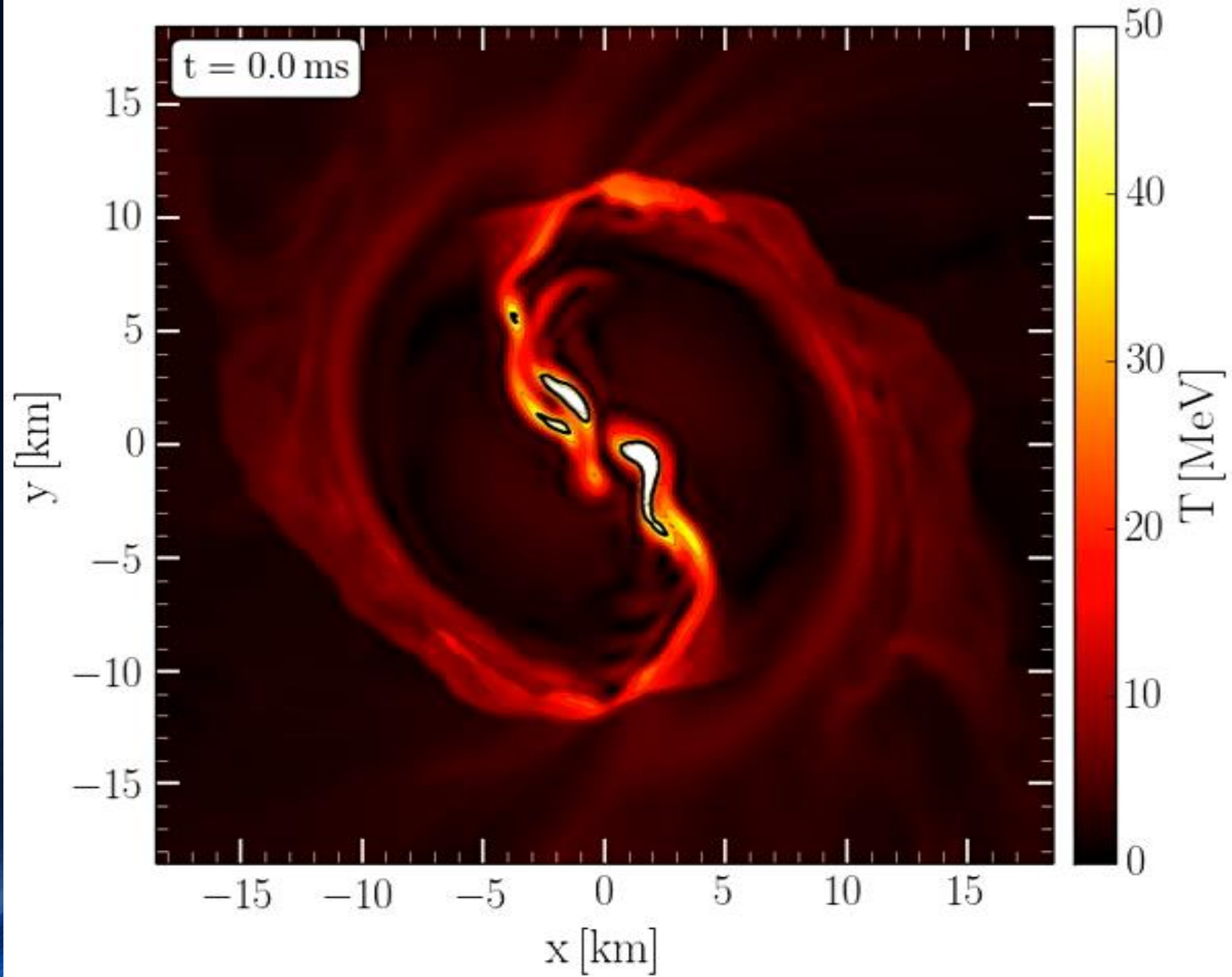
ALF2, High mass model: Mixed phase region starts at $3\rho_0$, initial NS mass: $1.35 M_{\text{solar}}$



Gravitational wave amplitude
at a distance of 50 Mpc

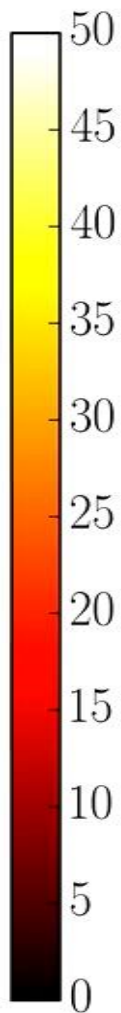
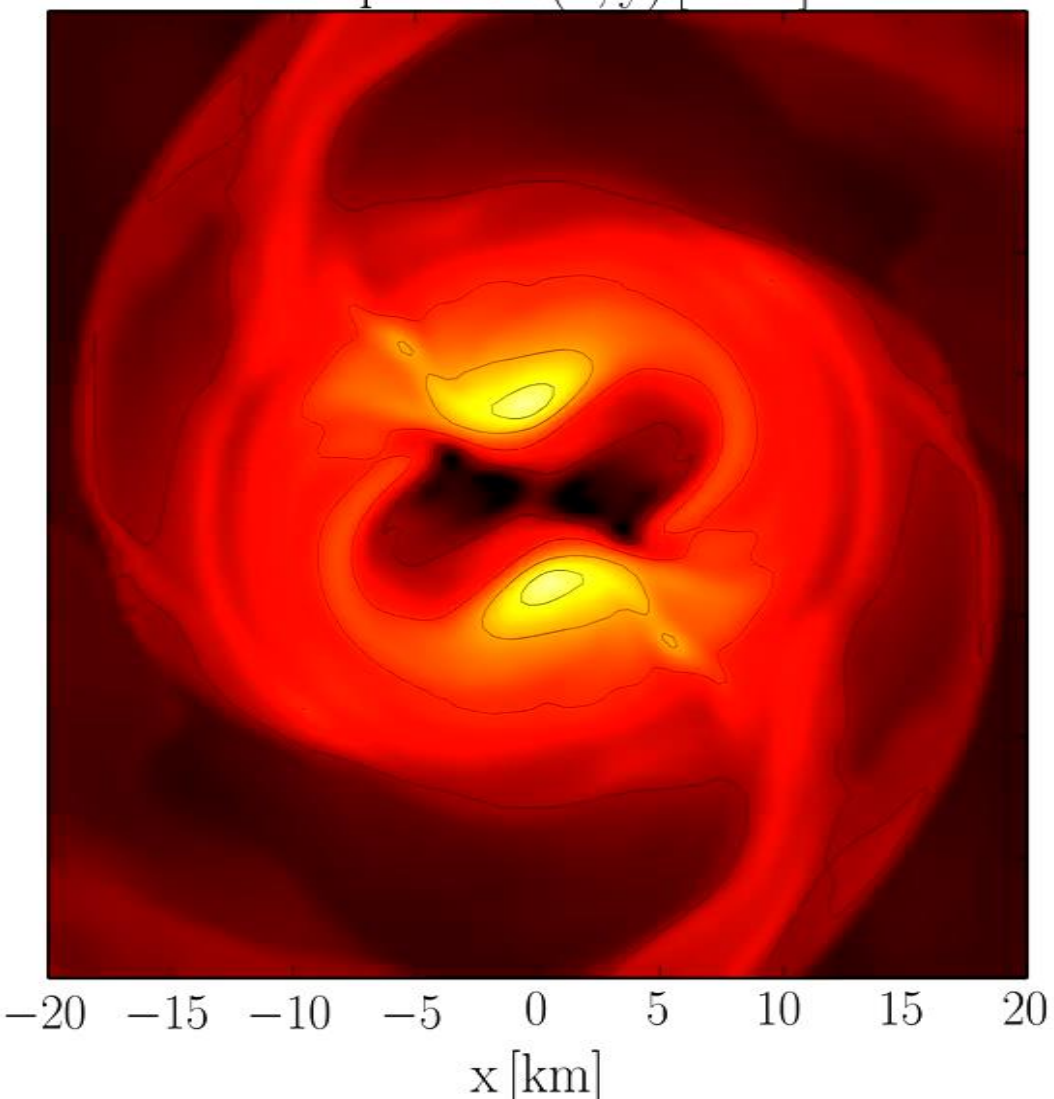


Rest mass density distribution $\rho(x,y)$
in the equatorial plane
in units of the nuclear matter density ρ_0



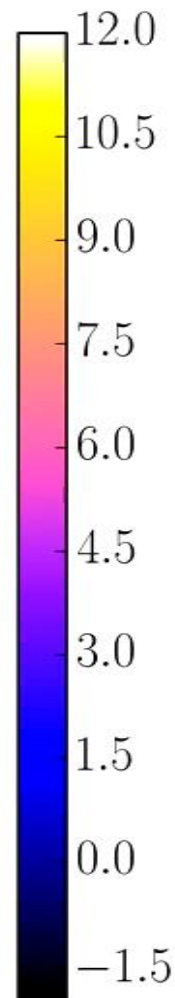
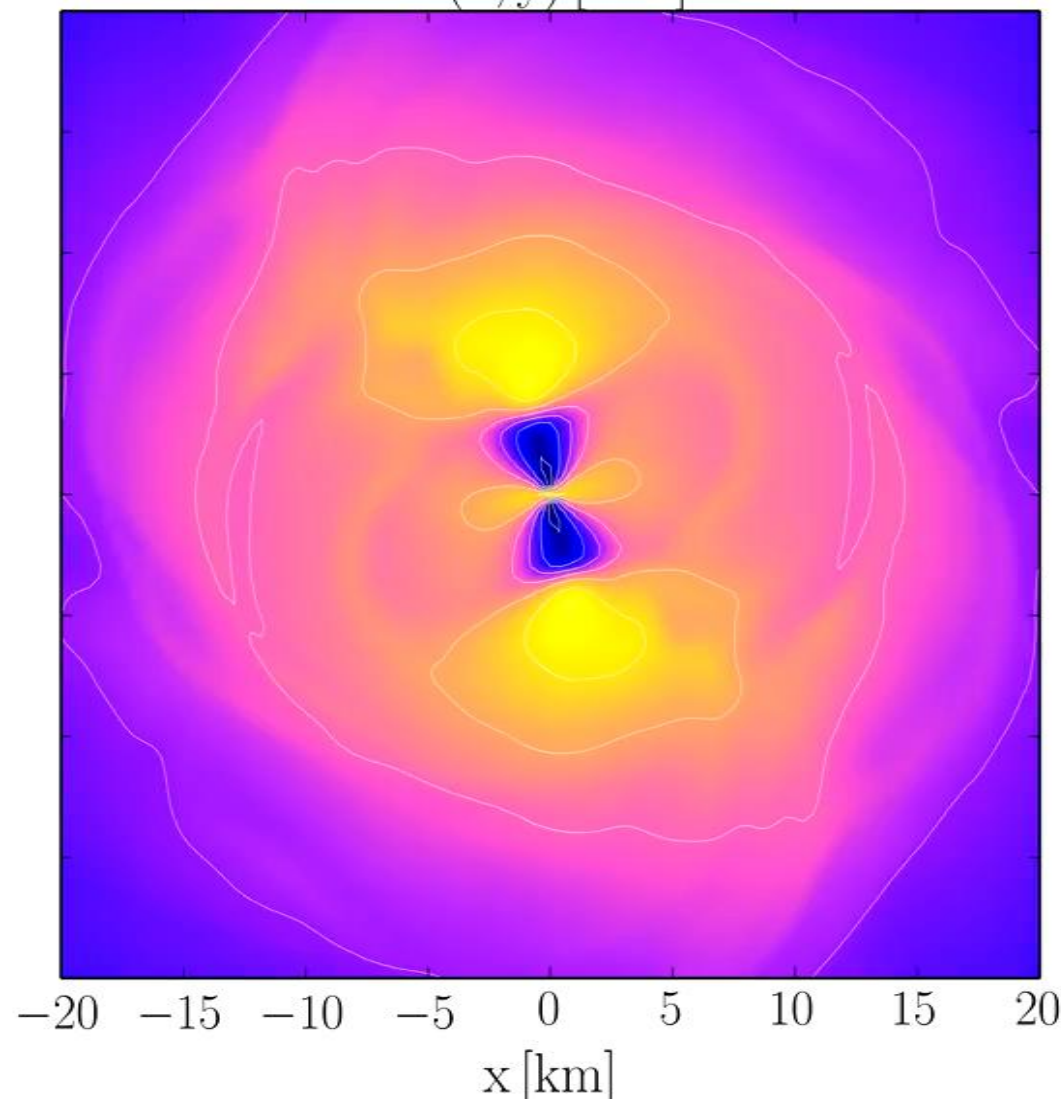
Temperature

Temperature(x, y) [MeV]



Angular Velocity

$\Omega(x, y)$ [kHz]

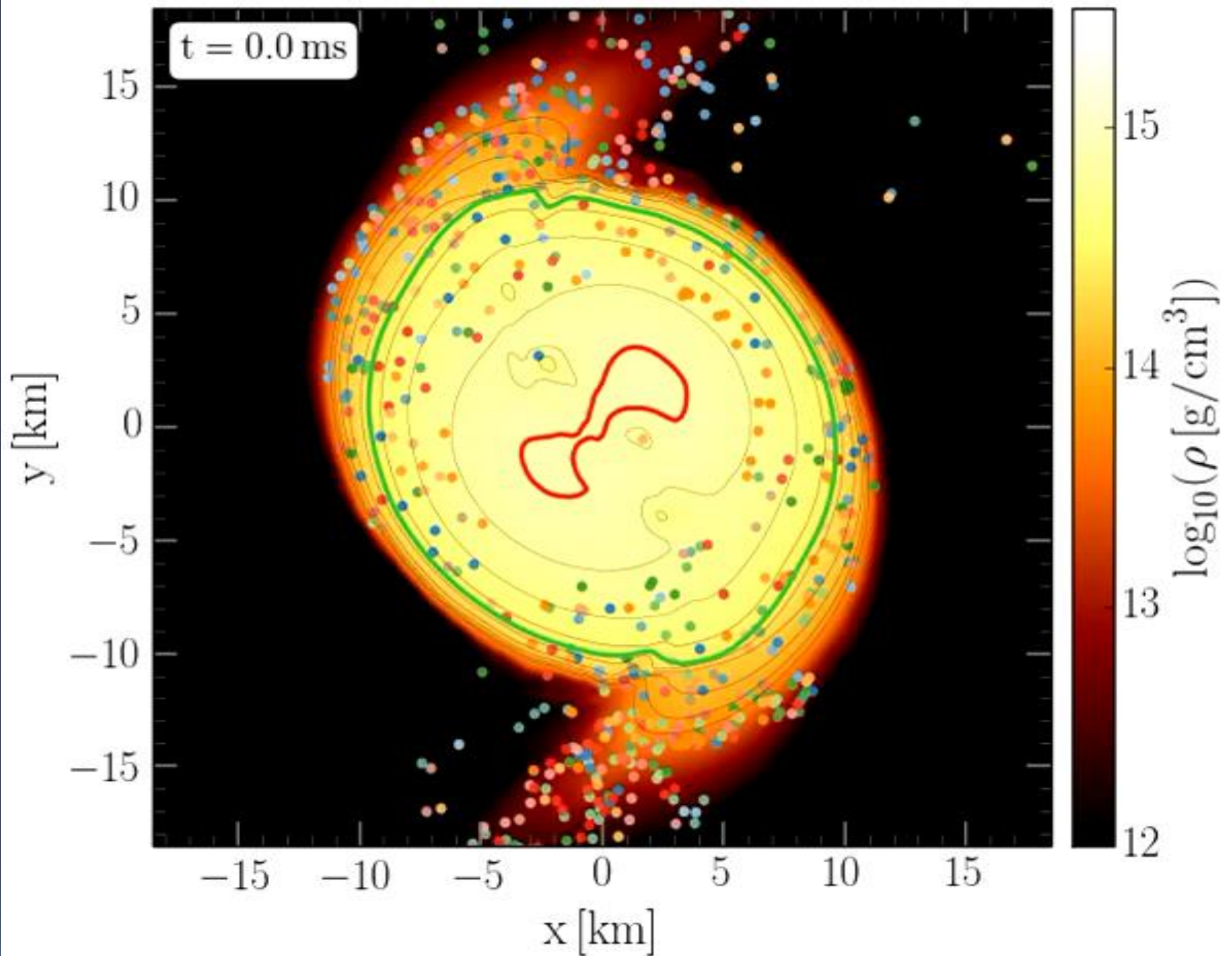


Evolution of Tracer-particles tracking individual fluid elements in the equatorial plane of the HMNS at post-merger times

M.G. Alford, L. Bovard, M. Hanauske, L. Rezzolla and K. Schwenzer

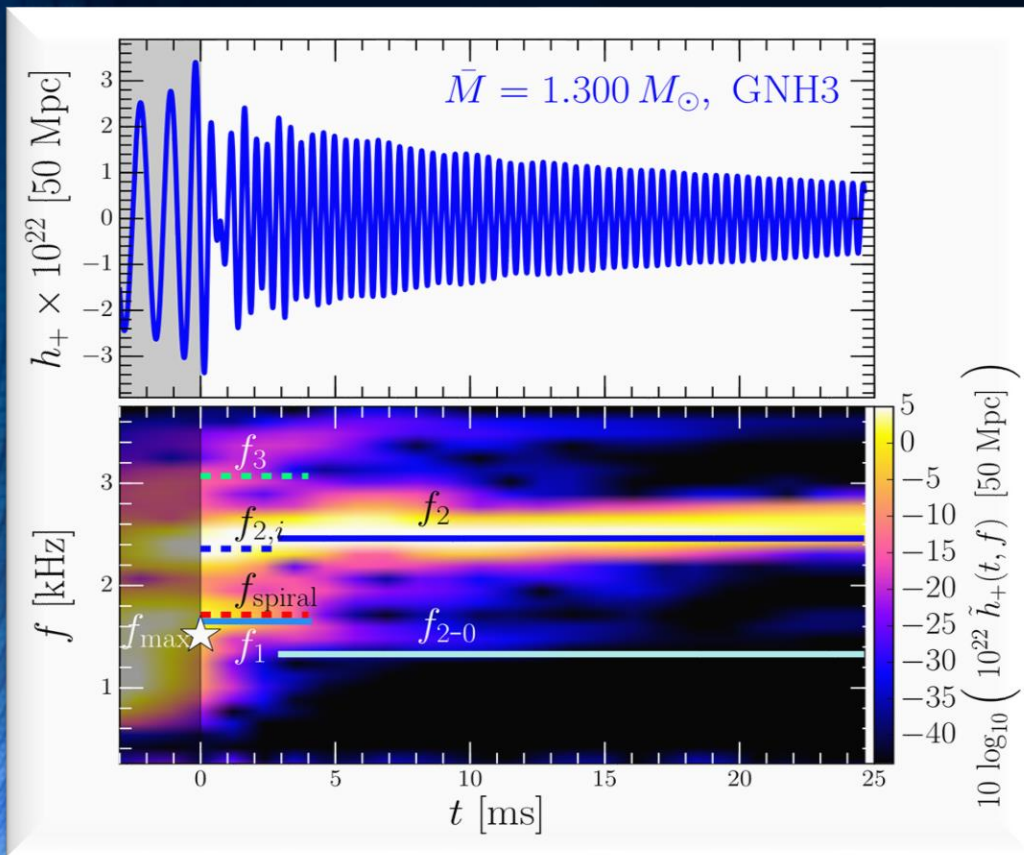
“On the importance of viscous dissipation and heat conduction in binary neutron-star mergers” (submitted to PRL, see arxiv)

Different rotational behaviour of the quark-gluon-plasma produced in non-central ultra-relativistic heavy ion collisions
L. Adamczyk et.al., “Global Lambda-hyperon polarization in nuclear collisions: evidence for the most vortical fluid”, Nature 548, 2017

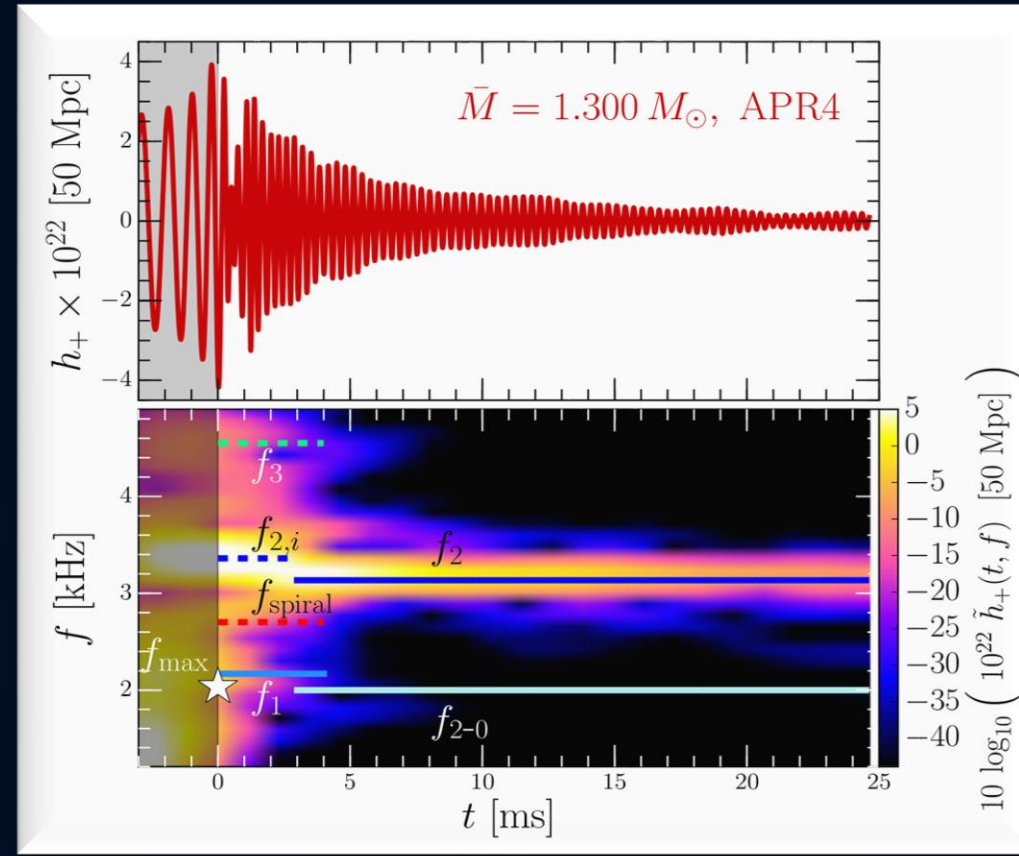


Time Evolution of the GW-Spectrum

The power spectral density profile of the post-merger emission is characterized by several distinct frequencies f_{\max} , f_1 , f_2 , f_3 and f_{2-0} . After approximately 5 ms after merger, the only remaining dominant frequency is the f_2 -frequency (See L.Rezzolla and K.Takami, arXiv:1604.00246)



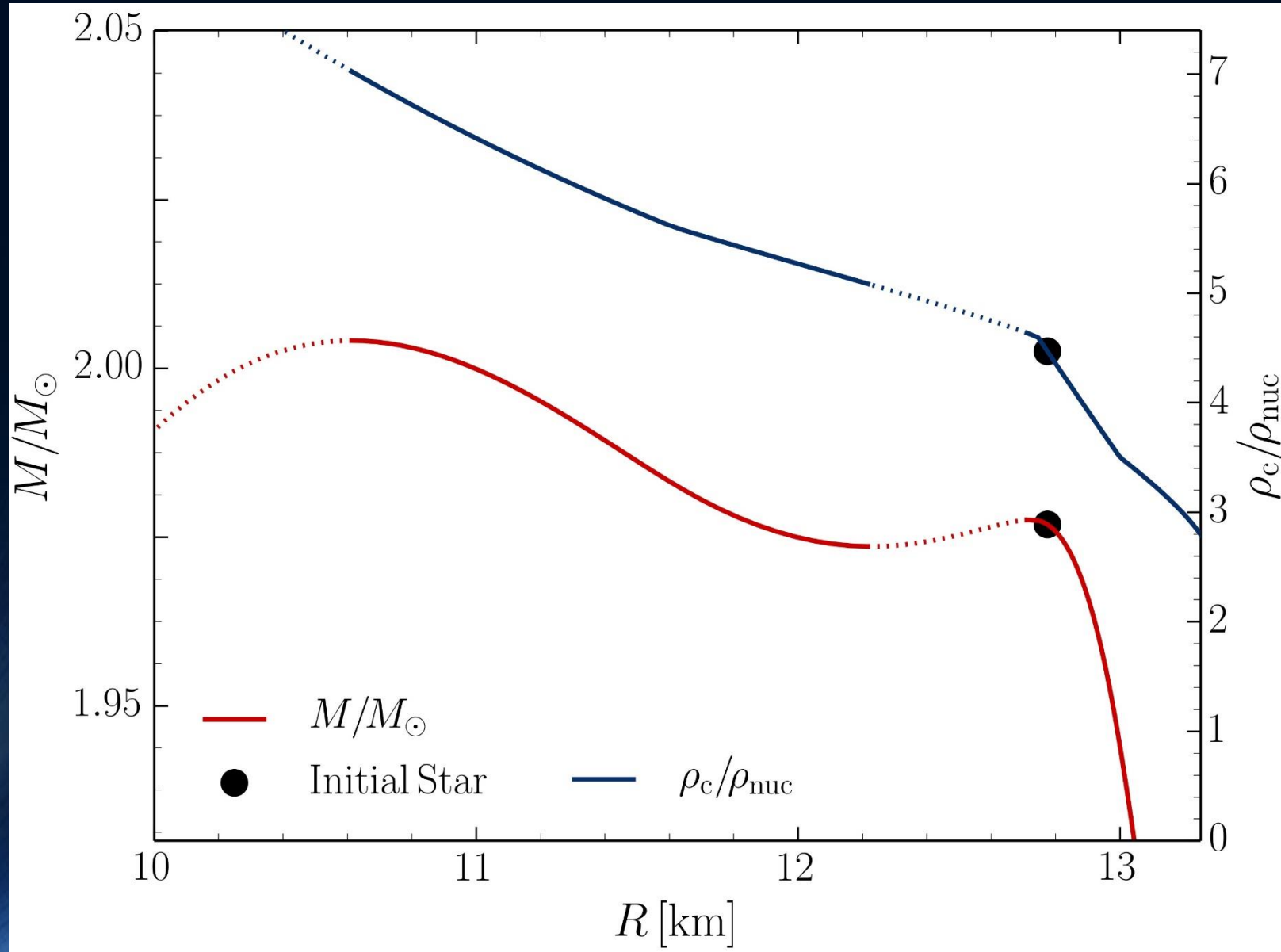
Stiff EOS



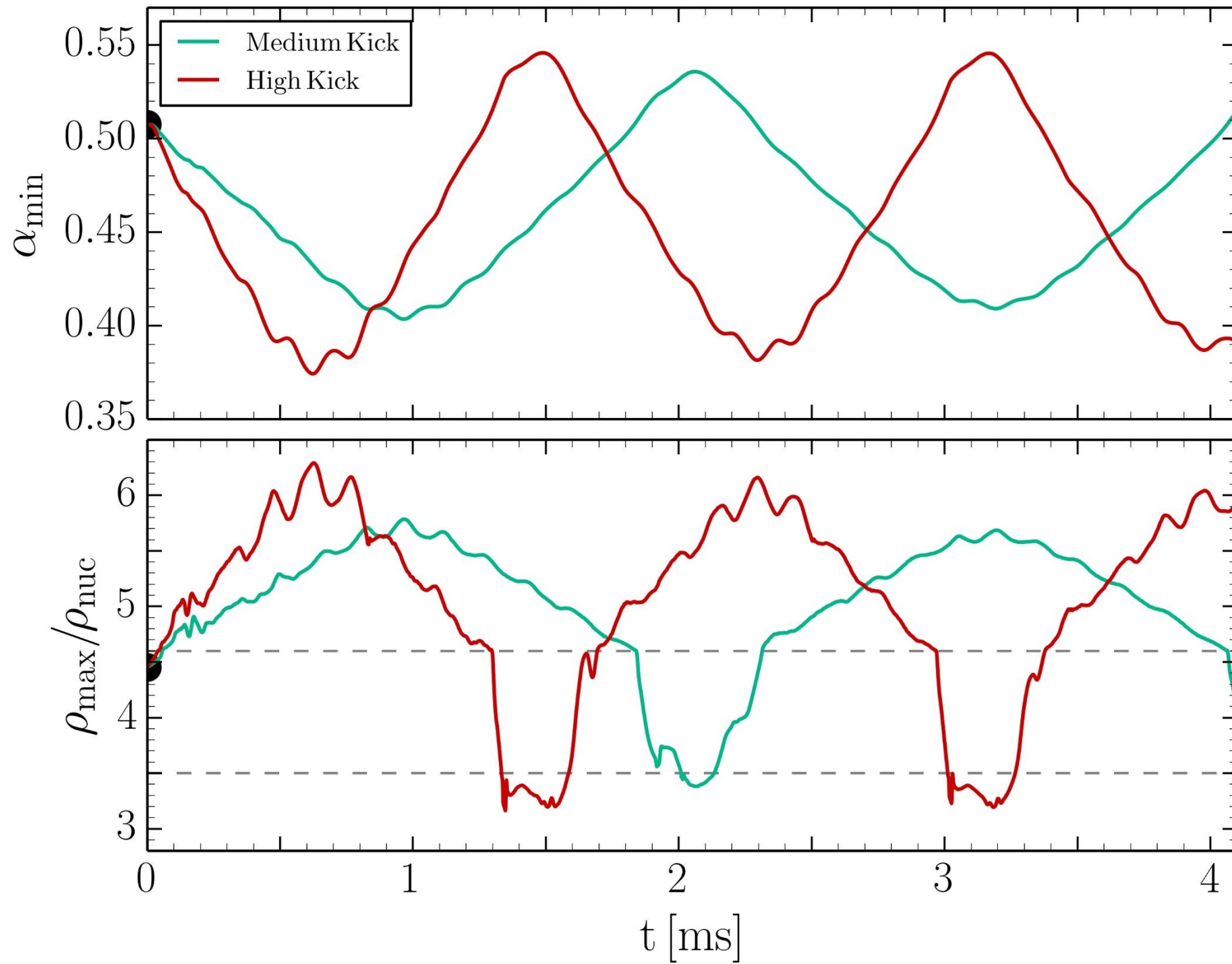
Soft EOS

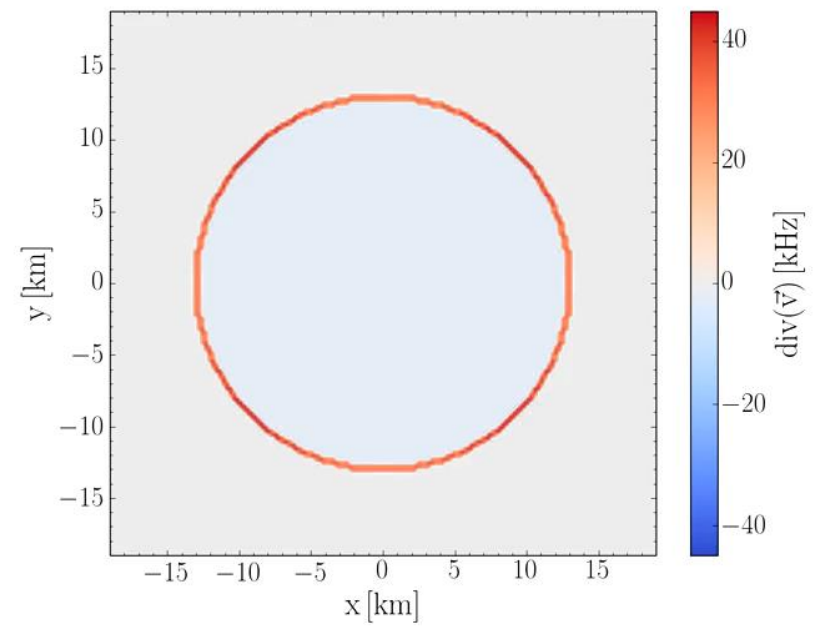
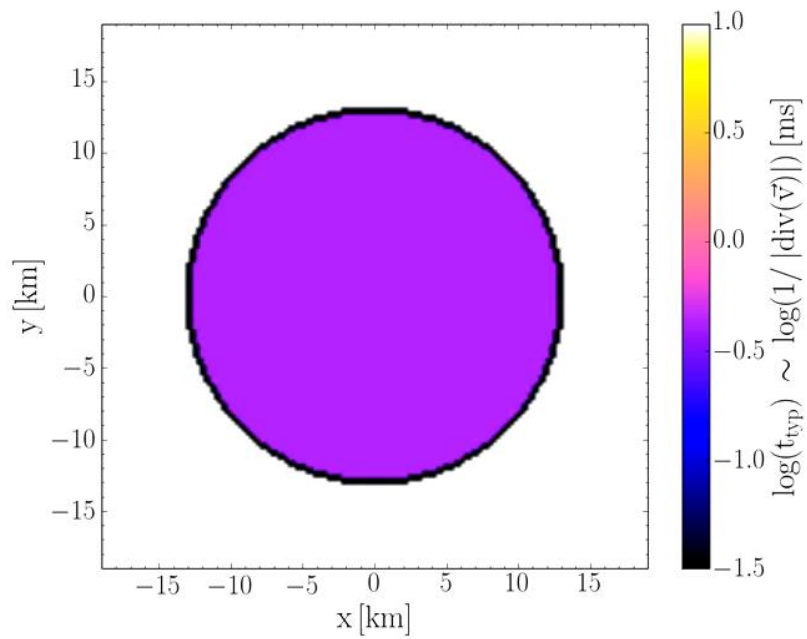
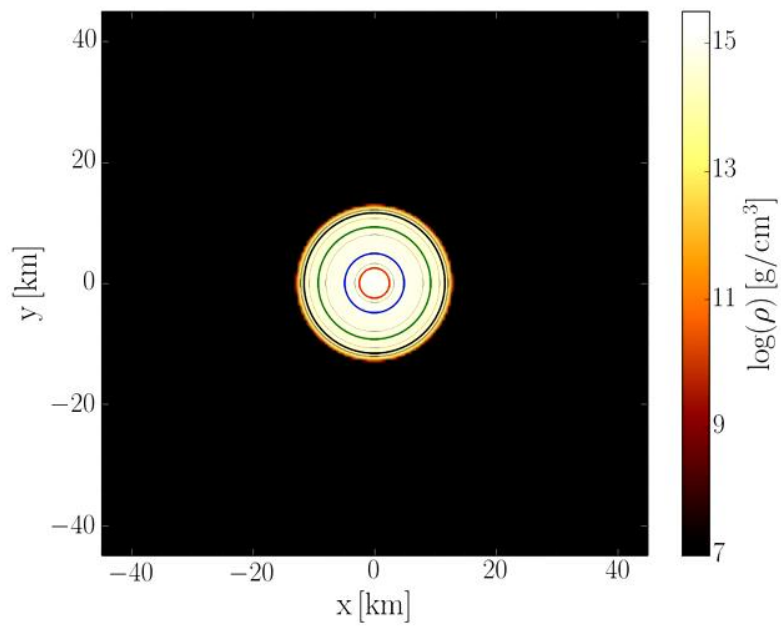
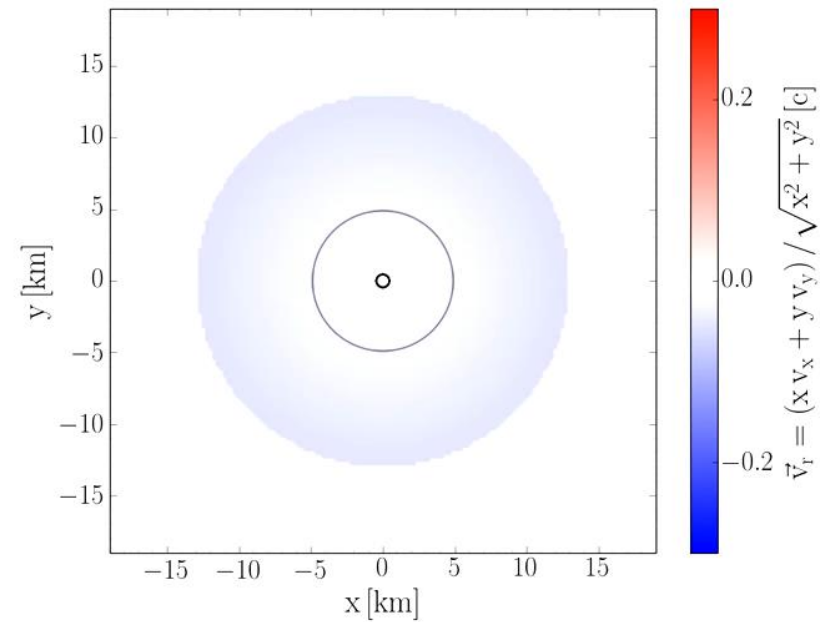
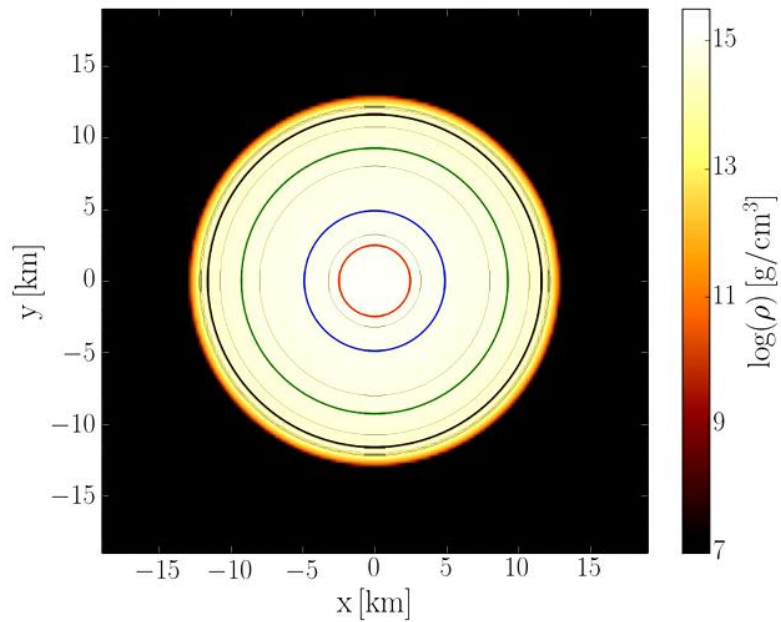
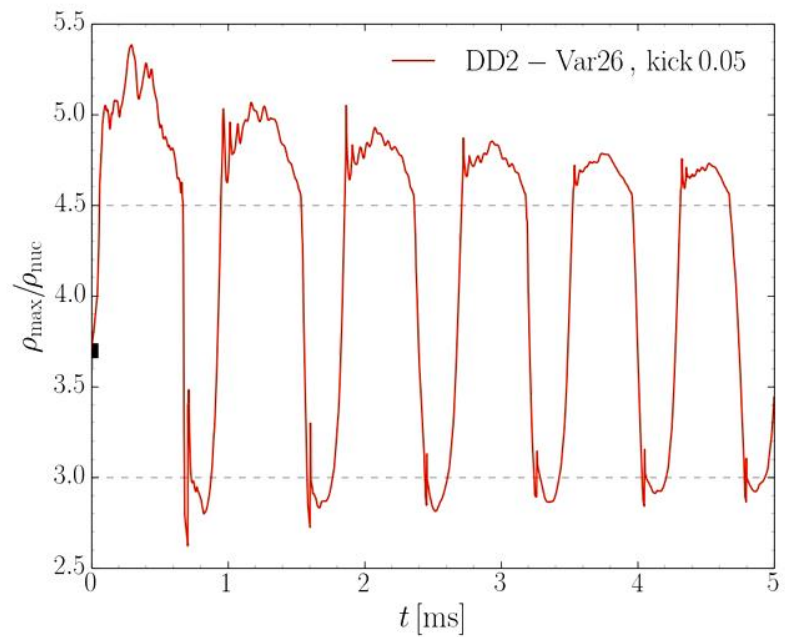
Unfortunately, due to the low sensitivity at high gravitational wave frequencies, no post-merger signal has been found in GW170817.

But advanced detectors / next-generation detectors will be able to detect!



I.N. Mishustin, M. Hanauske, A. Bhattacharyya, L.M. Satarov, H. Stöcker, and W. Greiner, "Catastrophic rearrangement of a compact star due to quark core formation", Physics Letters B 552 (2003) p.1-8





Additional Slides

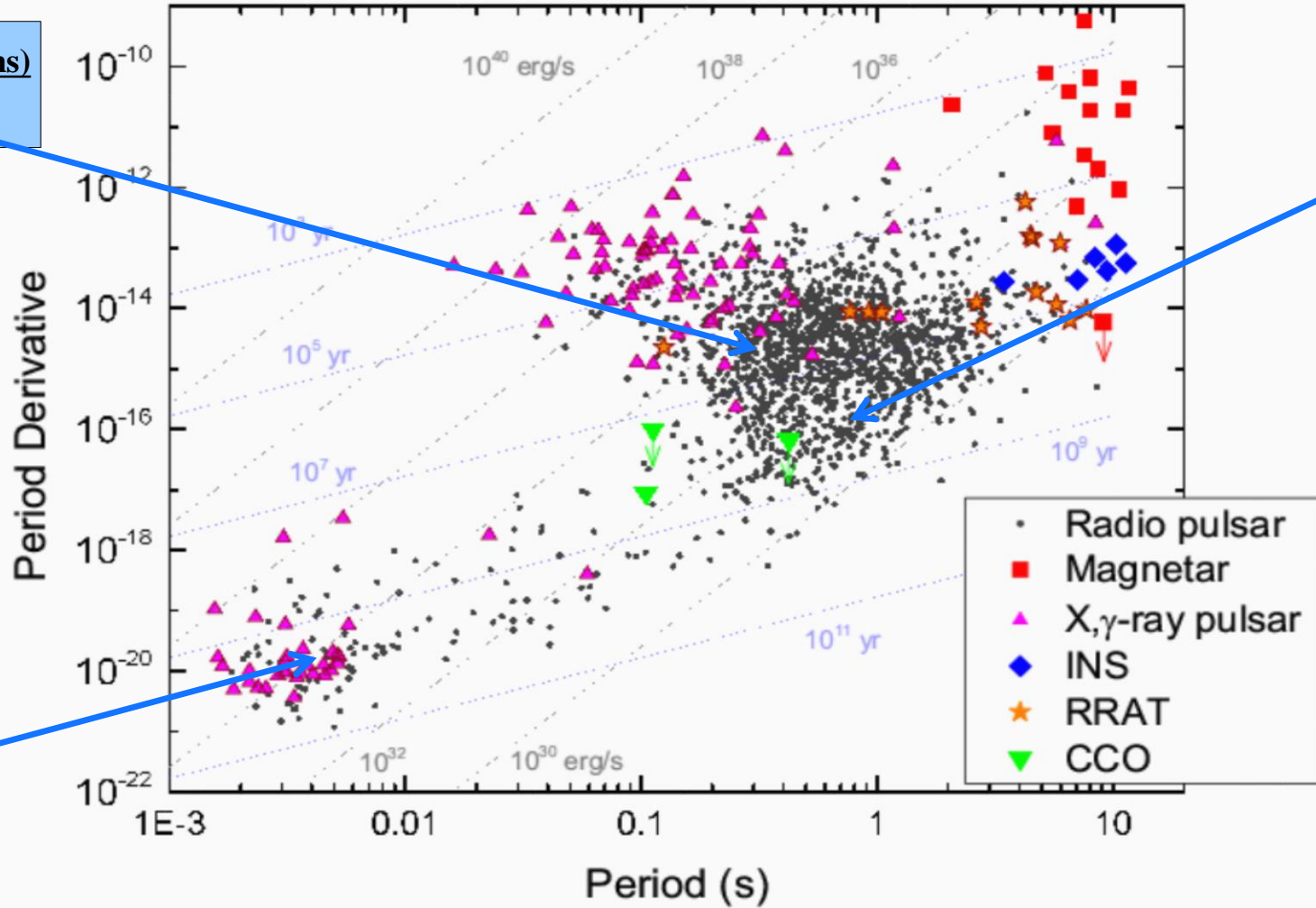
Millisecond and Second Pulsars



PSR B0531+21 (33.5 ms)
Crab Pulsar



PSR B0329+54 (0.715 s)



PSR B1937+21 (1.56 ms)

Observed Masses in Binary Neutron Star Systems

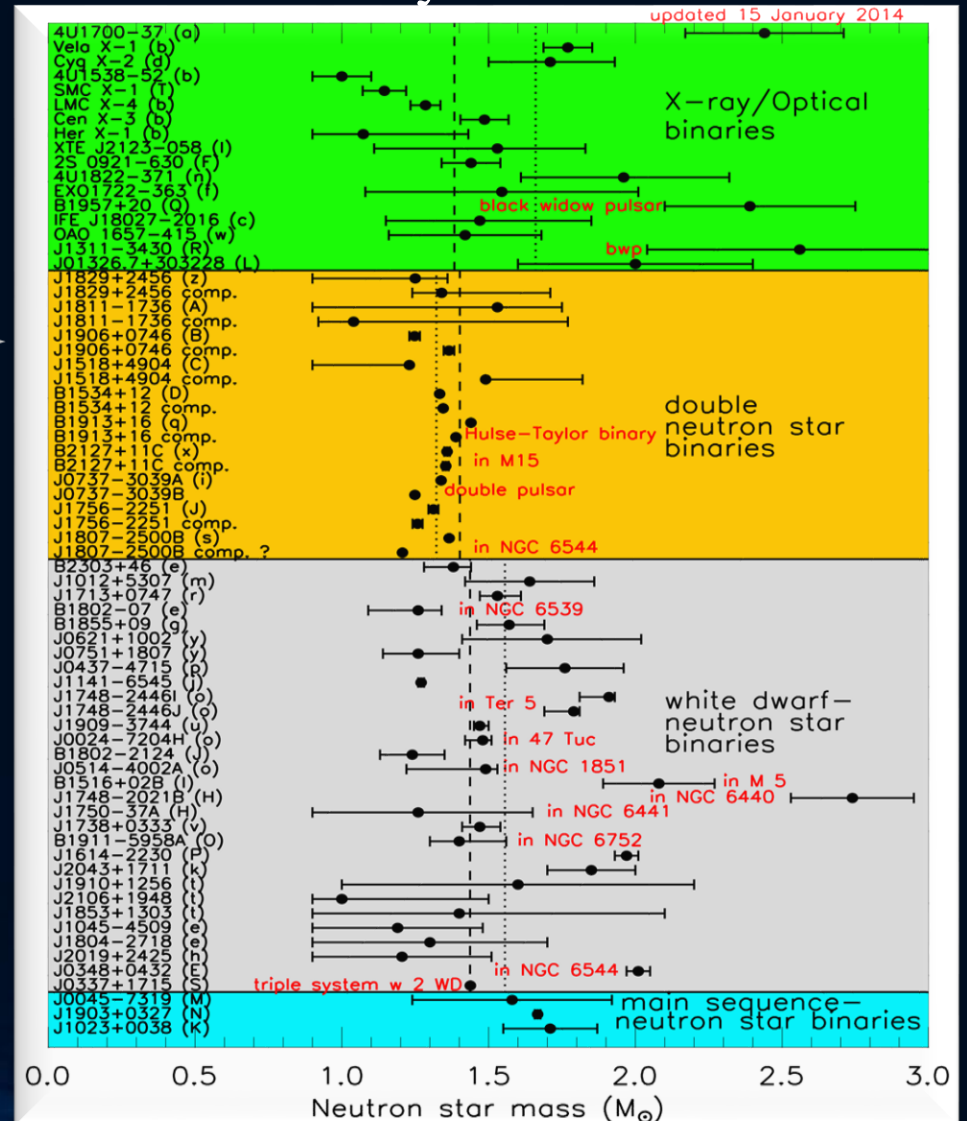
Some of the known Neutron Stars (NS) are in binary systems:

NS-Planet, NS-(white dwarf) or NS-NS binary

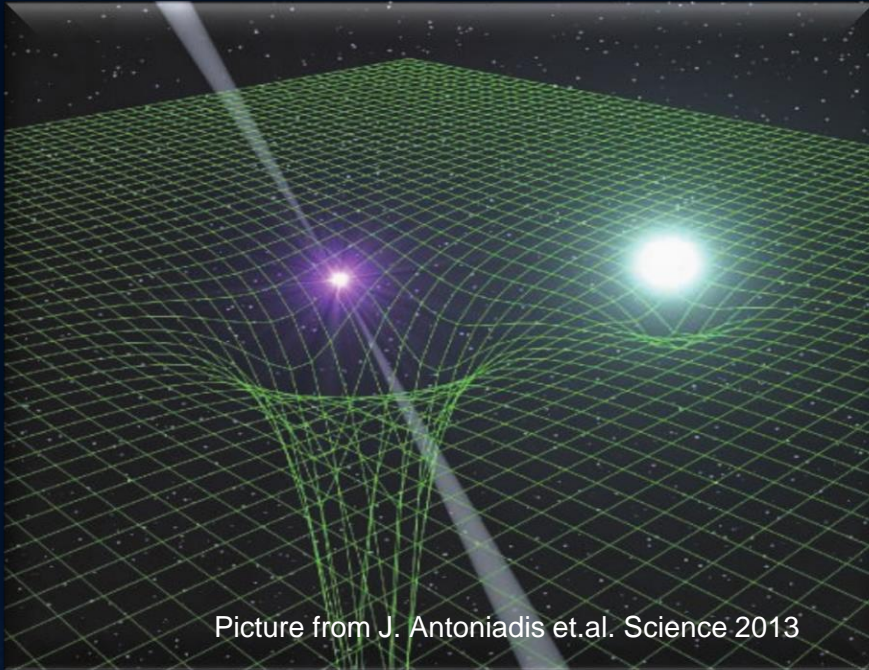
PSR J1906+0746

144-ms Pulsar, observed in 2004
 Orbital Period: 3.98 hours,
 Eccentricity: 0.085
 Pulsar Mass: 1.291(11)
 Mass Companion: 1.322(1)
 Observed between 1998-2009,
 after 2009, the pulsar disappeared
 because of spin precession

Van Leeuwen et al, arXiv:1411.1518



A Two Solarmass Neutron Star



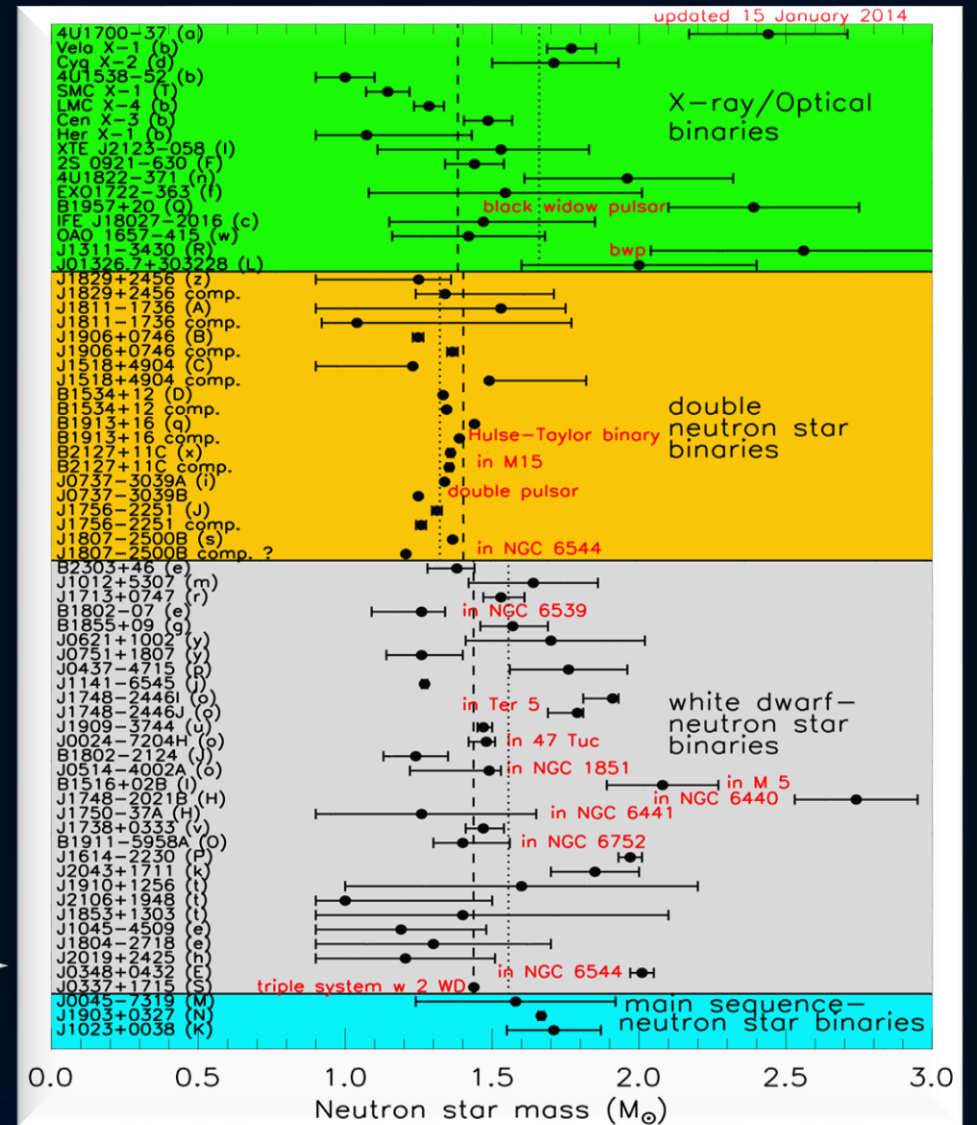
PSR J0348+0432

Orbital Period: 2.46 hours

Pulsar mass: 2.01 ± 0.04

Mass of the white dwarf:

$M = 0.172 \pm 0.003$

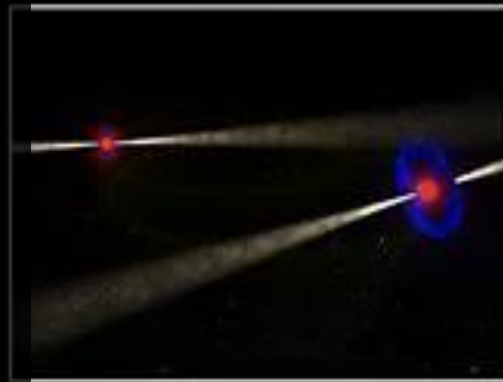


Binary Neutron Star Systems

Kramer, Wex, Class. Quantum Grav. 2009

The Double Pulsar (PSR J0737-3039A/B):
Observed in 2003
Eccentricity: 0.088
Pulsar A: $P=23$ ms, $M=1.3381(7)$
Pulsar B: $P=2.7$ s, $M=1.2489(7)$
Only separated 800,000 km from each other
Orbital period: 147 Minuten
Pulsar A is eclipsed by Pulsar B
(30 s for each orbit)

Distance shrinks
due to Gravitational Wave emission
→ They will collide in 85 Million Years!



Binary Neutron Star Systems

Recently some new interesting Neutron Star Binary Systems has been found:

J0453+1559

$P = 17 \text{ ms}$

(similar to the Doublepulsar)

J1913+1102

$P = 27 \text{ ms}$

$P_b = 4.95 \text{ h}$

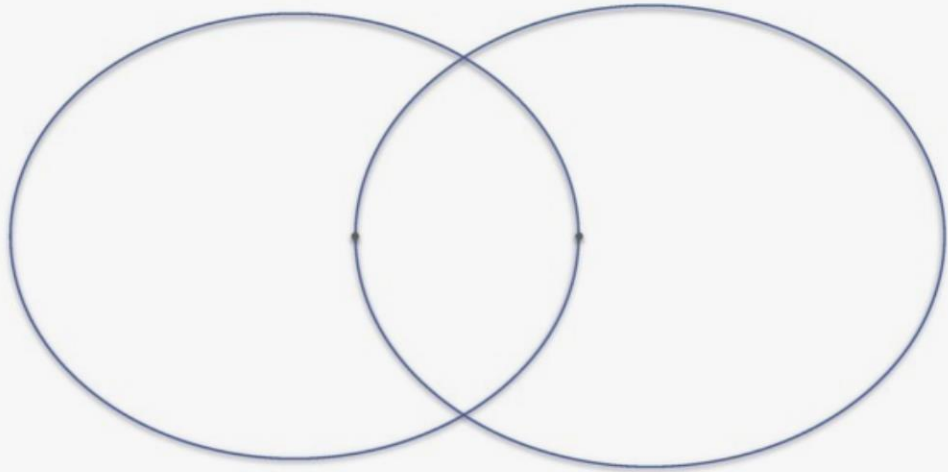
J1757-1854

$P = 215 \text{ ms}$

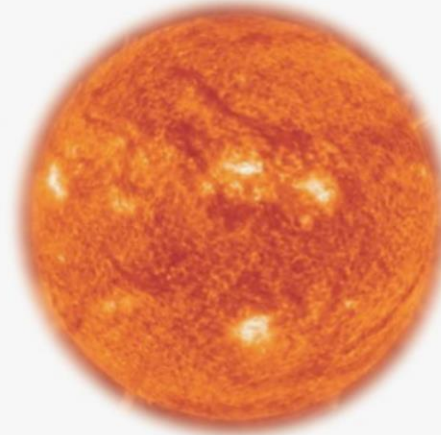
$P_b = 4.4 \text{ h}$

$E = 0.606$

Hulse-Taylor-Pulsar



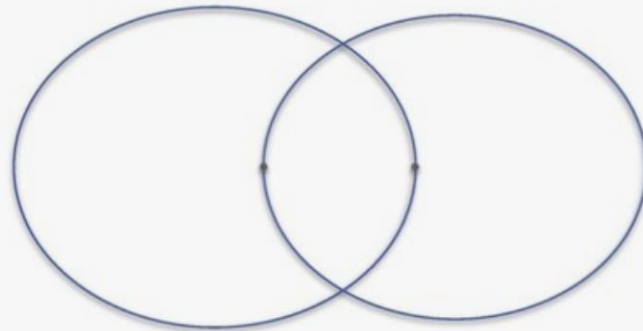
Sonne



Doppelpulsar

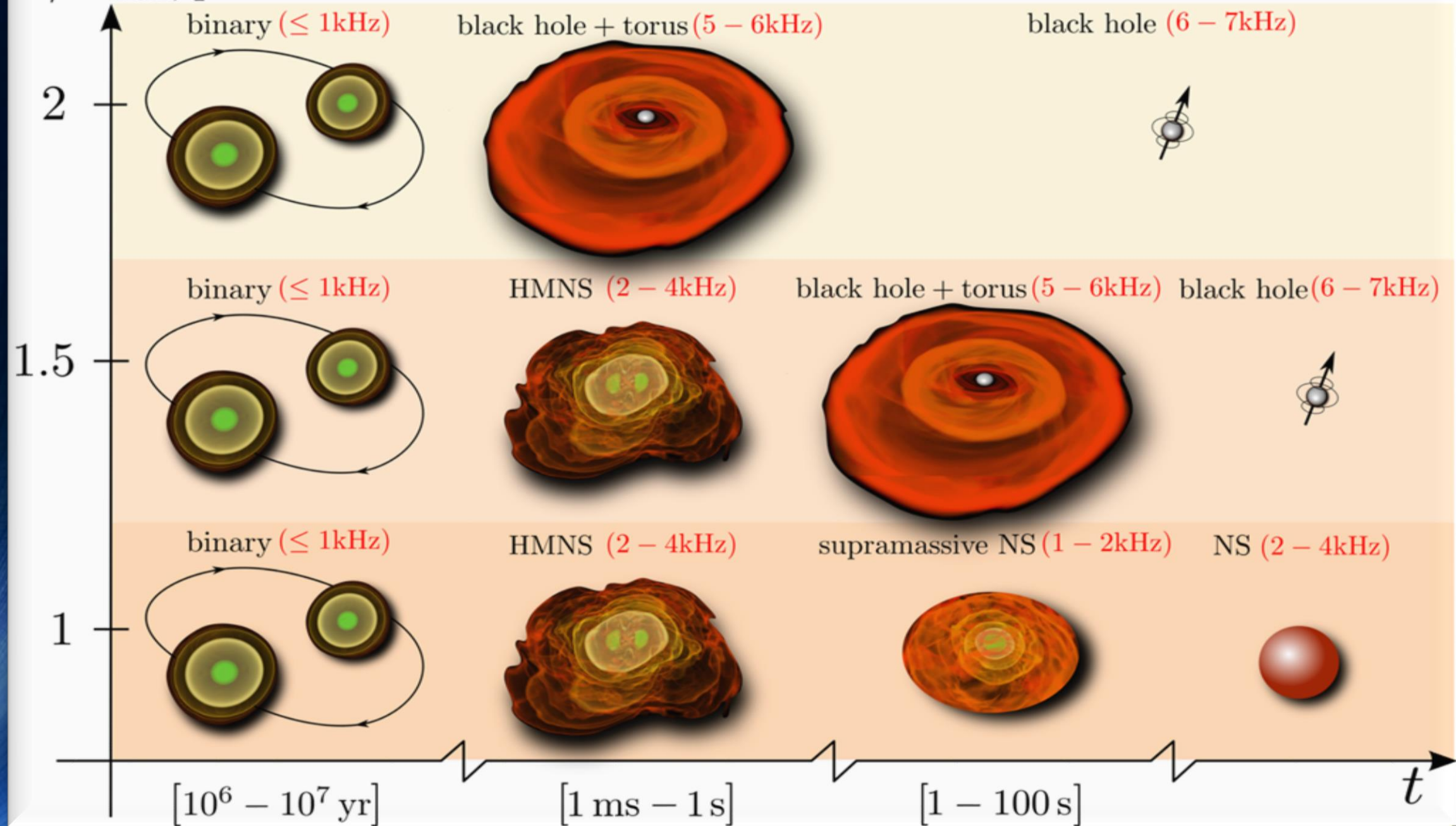


J1757-1854



Currently we know ~25 Double-NS Systems and one triple System

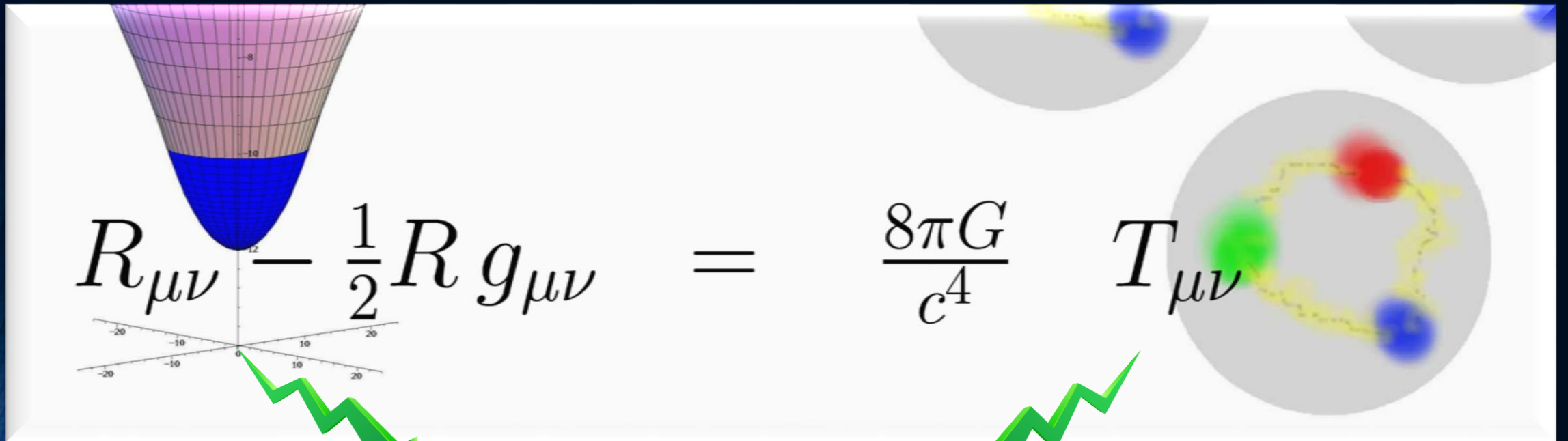
$M/M_{\max}, q \simeq 1$



General Relativity

The Einstein Equation

100 years ago, Albert Einstein presented the main equation of general relativity: **The Einstein-Equation**


$$R_{\mu\nu} - \frac{1}{2}R g_{\mu\nu} = \frac{8\pi G}{c^4} T_{\mu\nu}$$

Spacetime curvature

Properties of the
spacetime metric

Mass, Energy and Momentum of the System

Equation of state of elementary matter
(density, temperature)

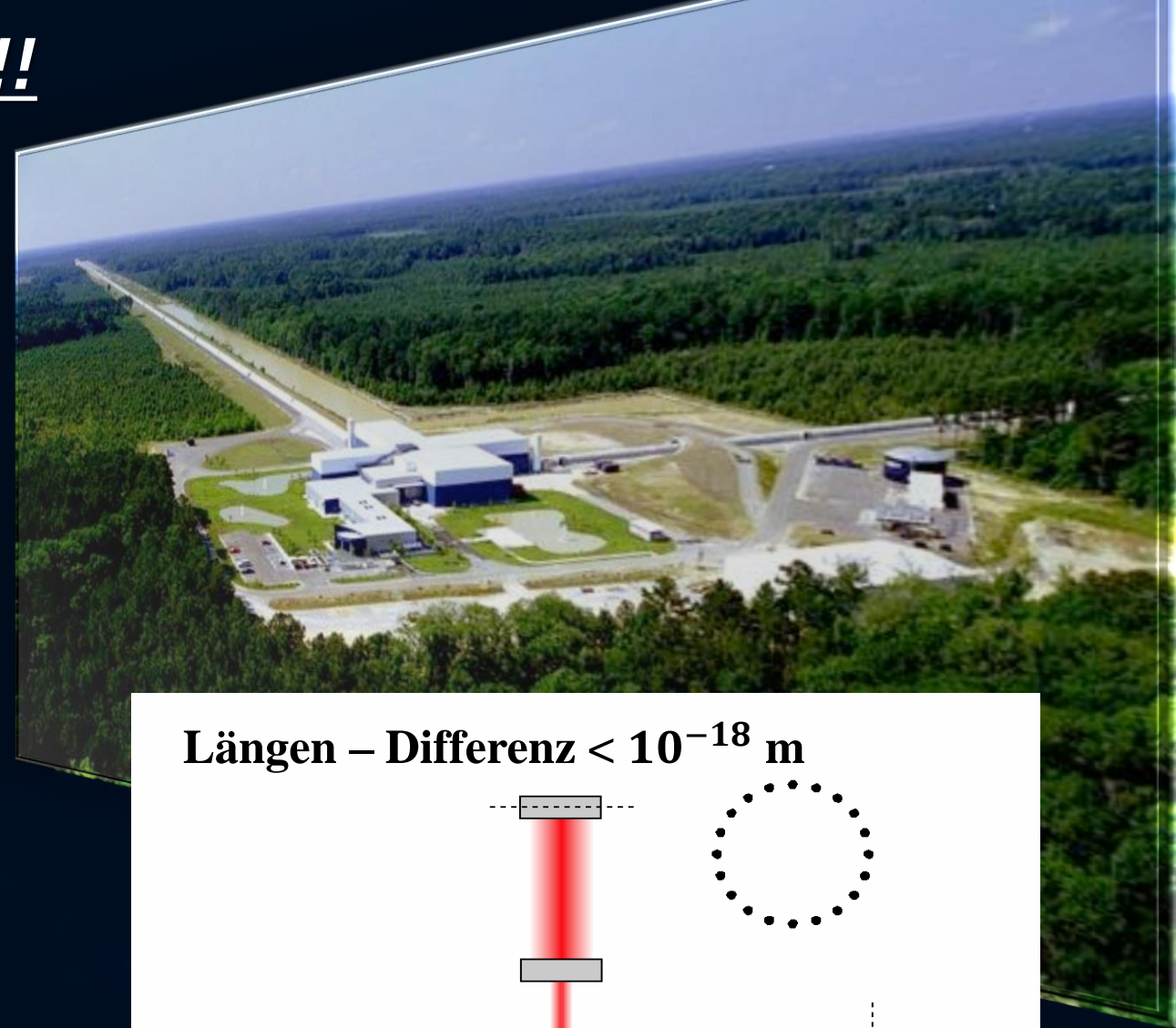
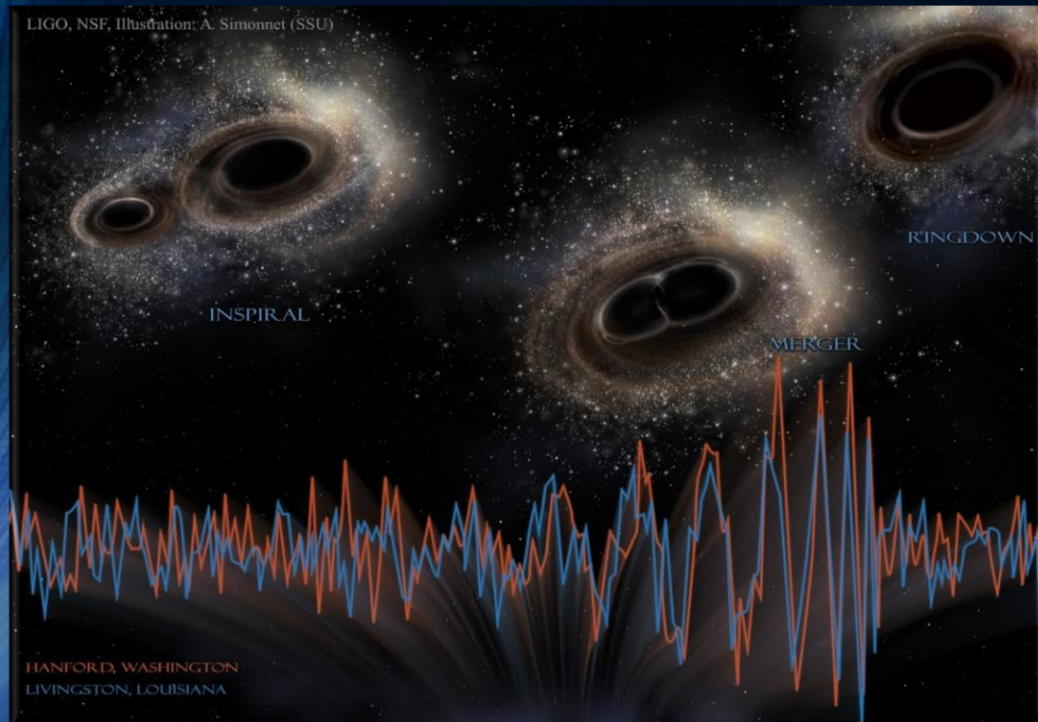
Gravitational Waves (A.Einstein, 1916)

Gravitational Waves detected!!!

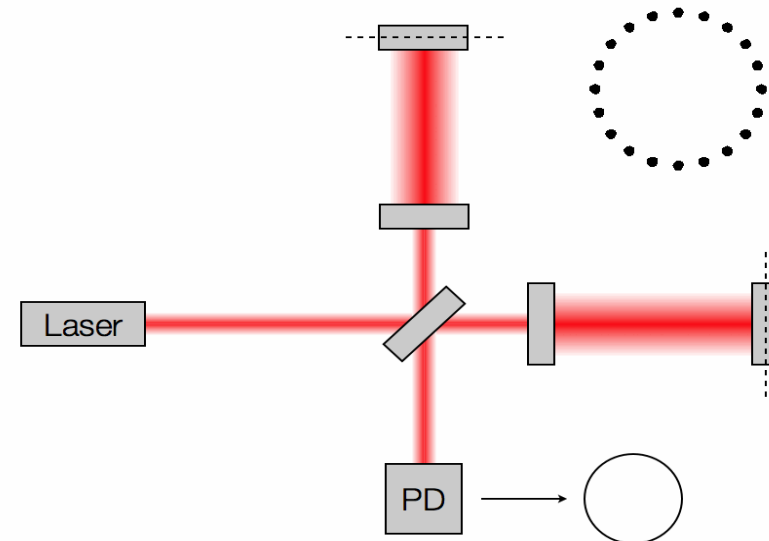
Collision of two Black Holes GW150914

Masses: 36 & 29 Sun masses

Distance to the earth 410 Mpc
(1.34 Billion Light Years)

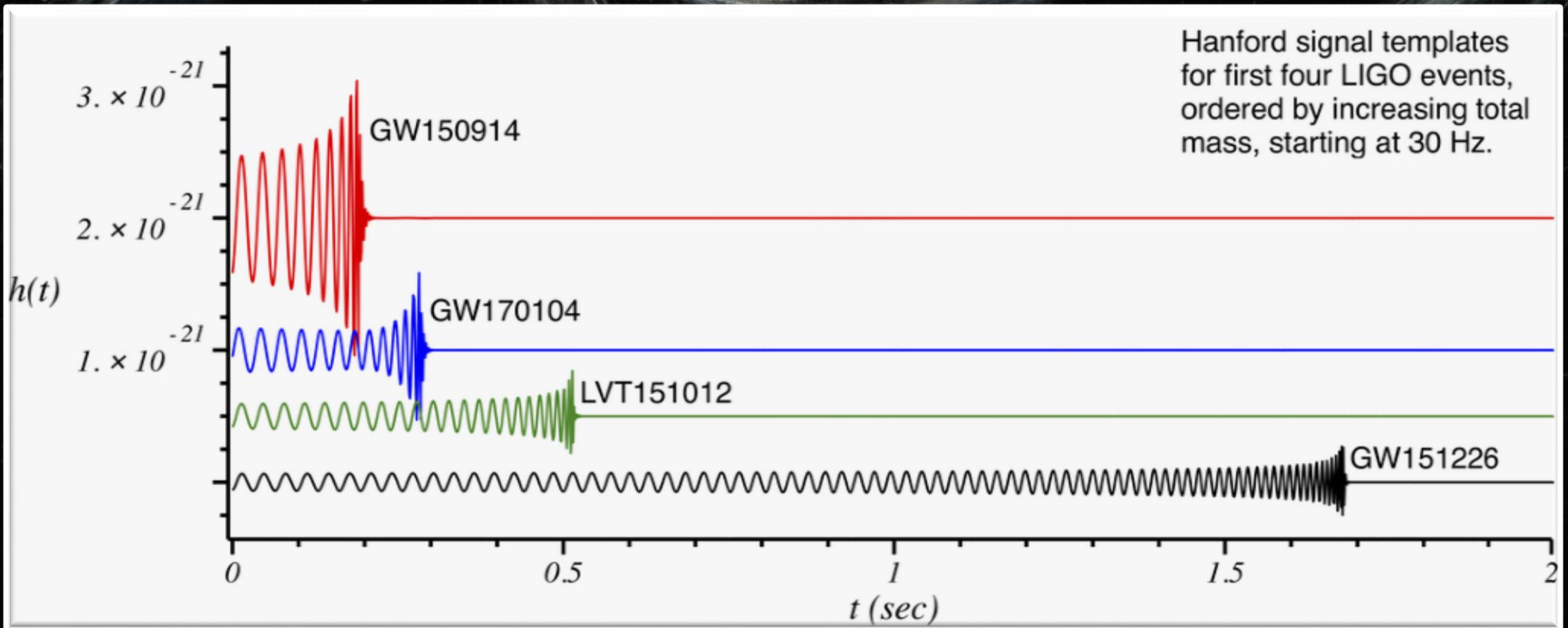


Längen – Differenz $< 10^{-18}$ m



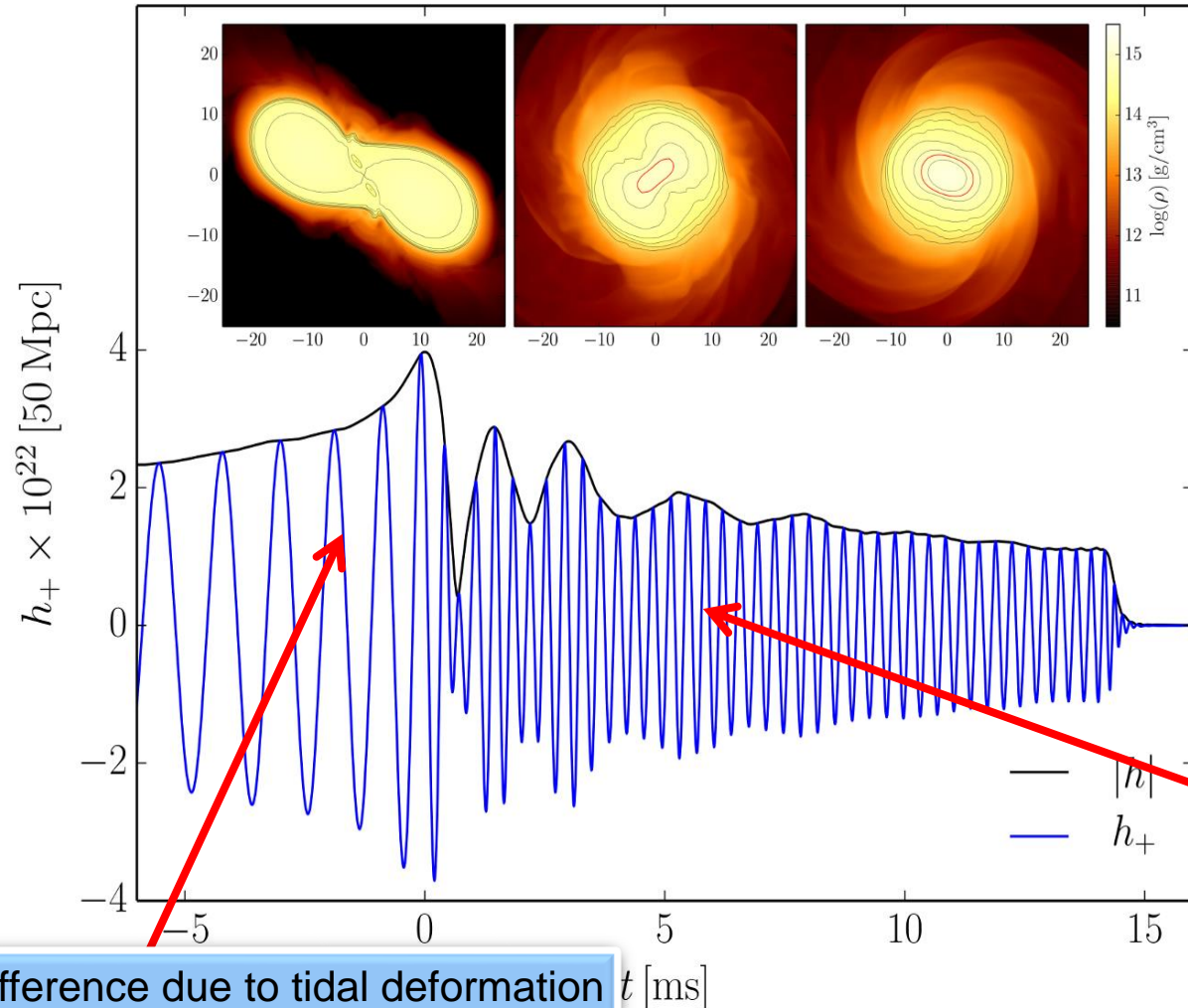
Credit: Les Wade from Kenyon College

Three (maybe four) GWs from BH-Mergers detected

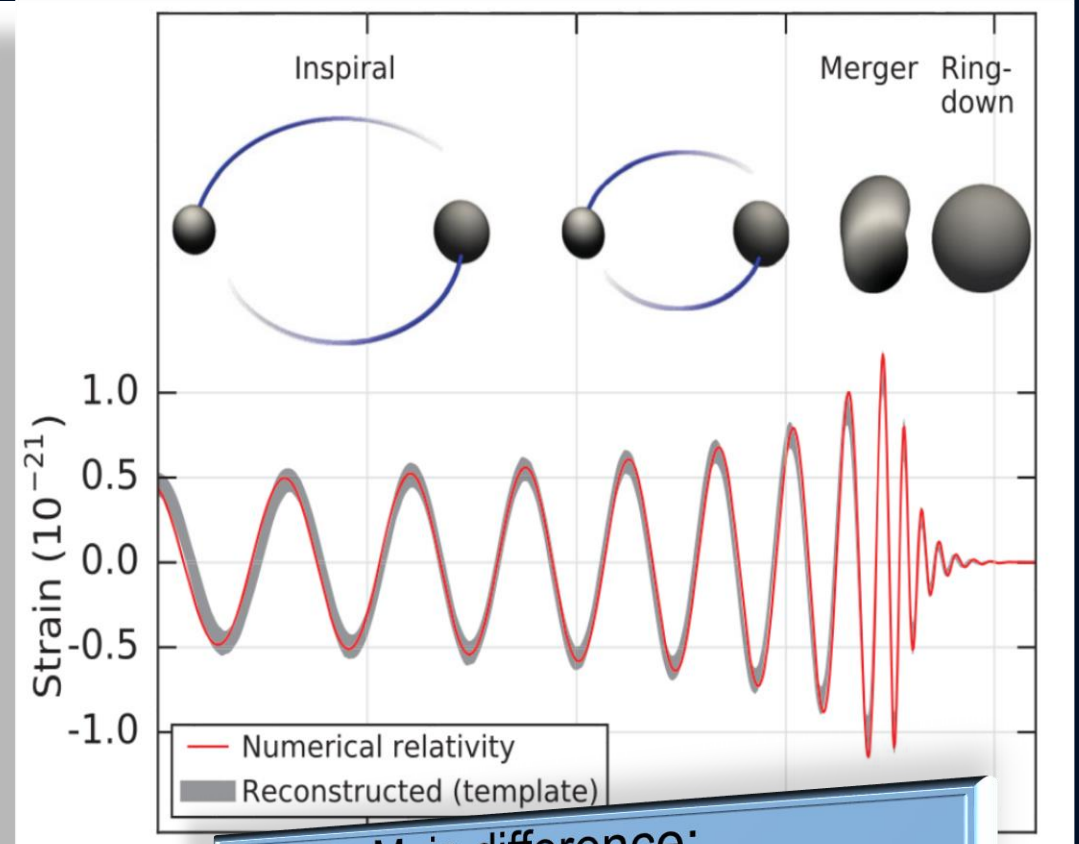


Gravitational Waves from Neutron Star Mergers

Neutron Star Collision (Simulation)



Collision of two Black Holes

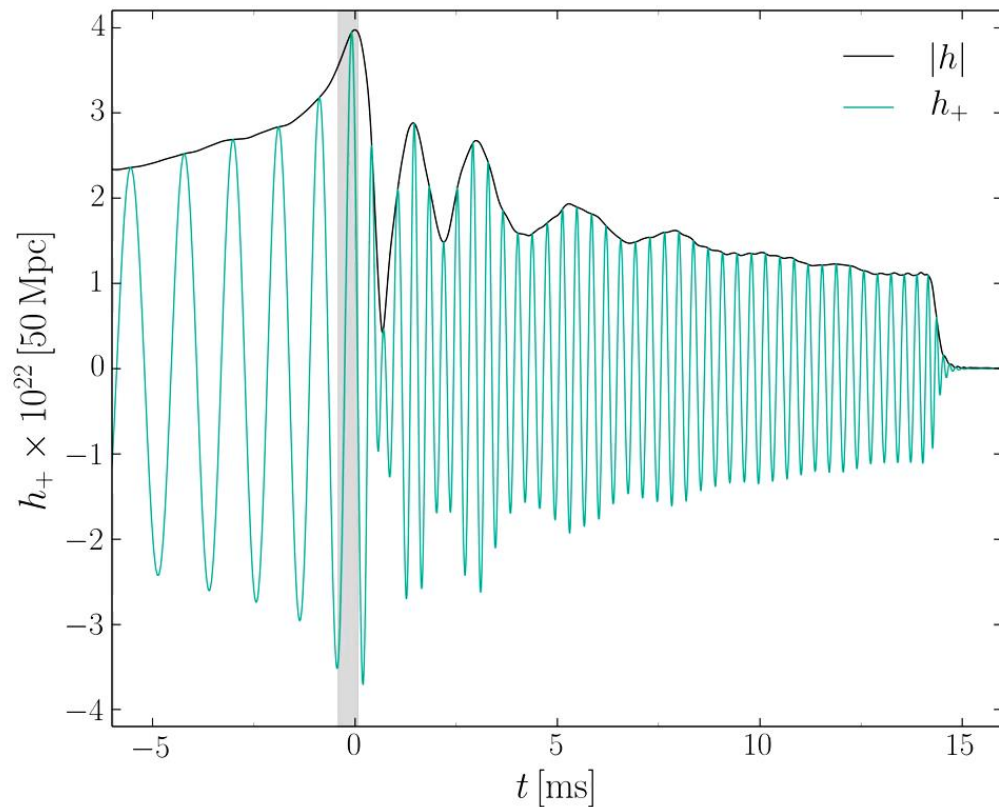


Main difference:
In binary neutron star mergers a **Post-Merger Phase** often exists

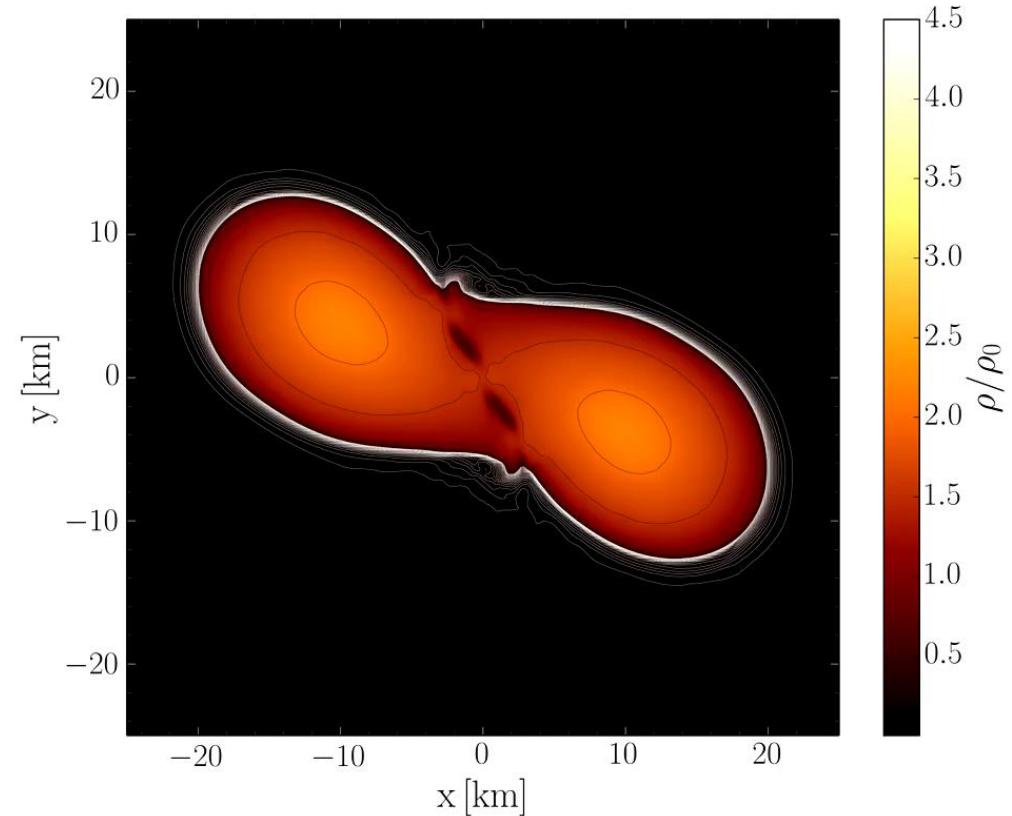
Difference due to tidal deformation in the late Inspiral phase

Evolution of the rest-mass density distribution

ALF2, High mass model: Mixed phase region starts at $3\rho_0$, initial NS mass: $1.35 M_{\text{solar}}$



Gravitational wave amplitude
at a distance of 50 Mpc



Rest mass density distribution $\rho(x,y)$
in the equatorial plane
in units of the nuclear matter density ρ_0

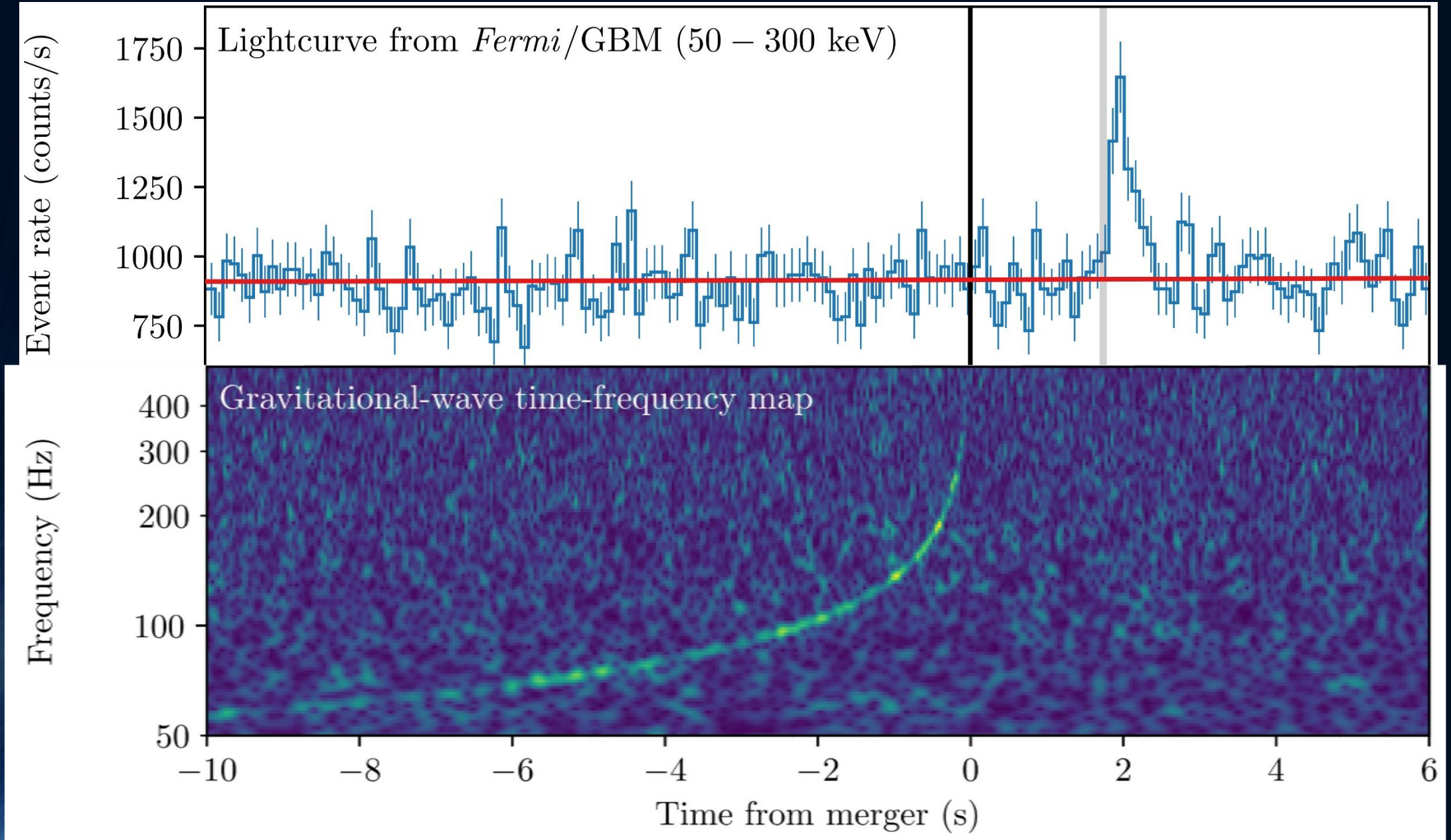


The Neutron Star Merger Dance
Credits to Riedberg TV

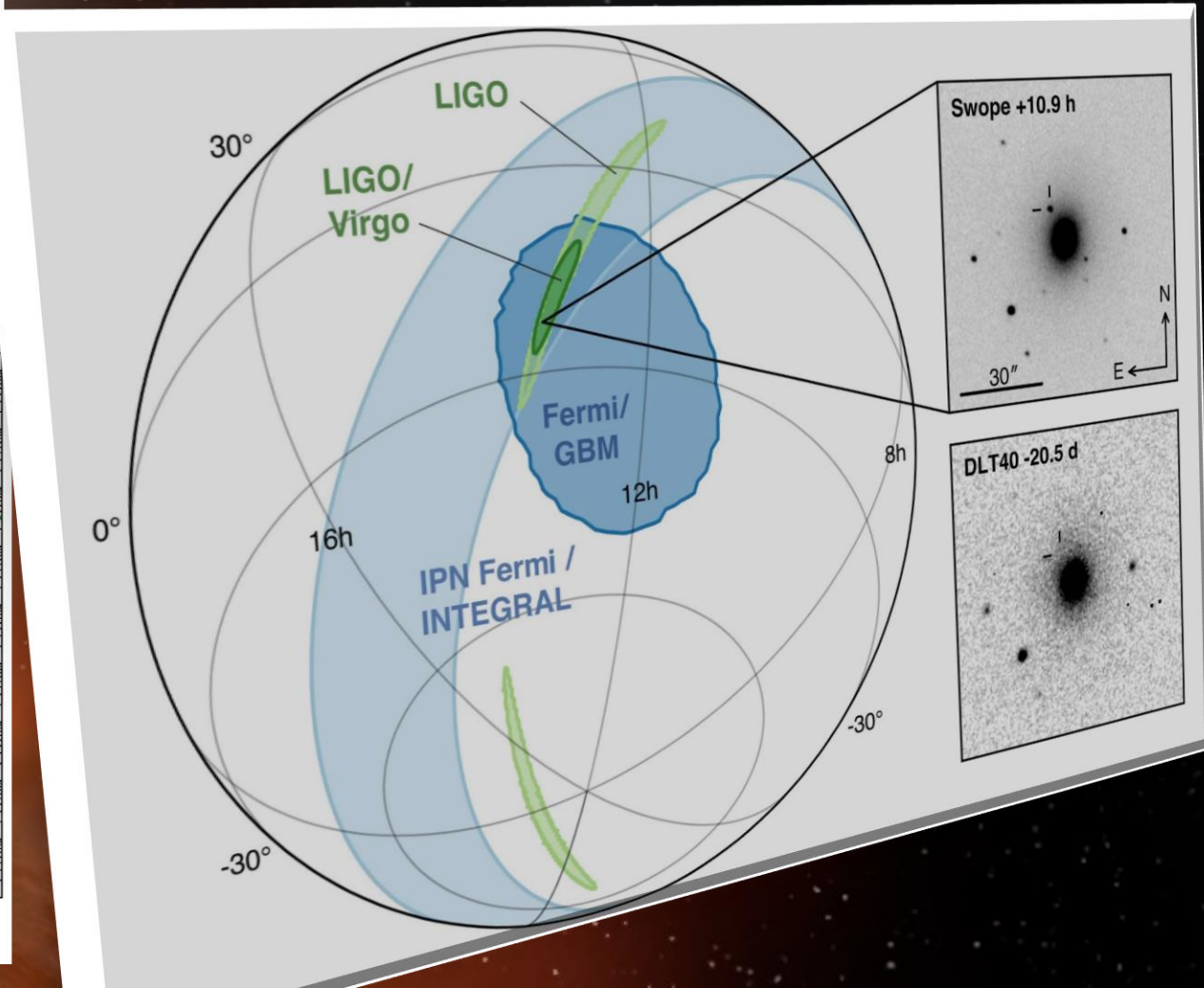
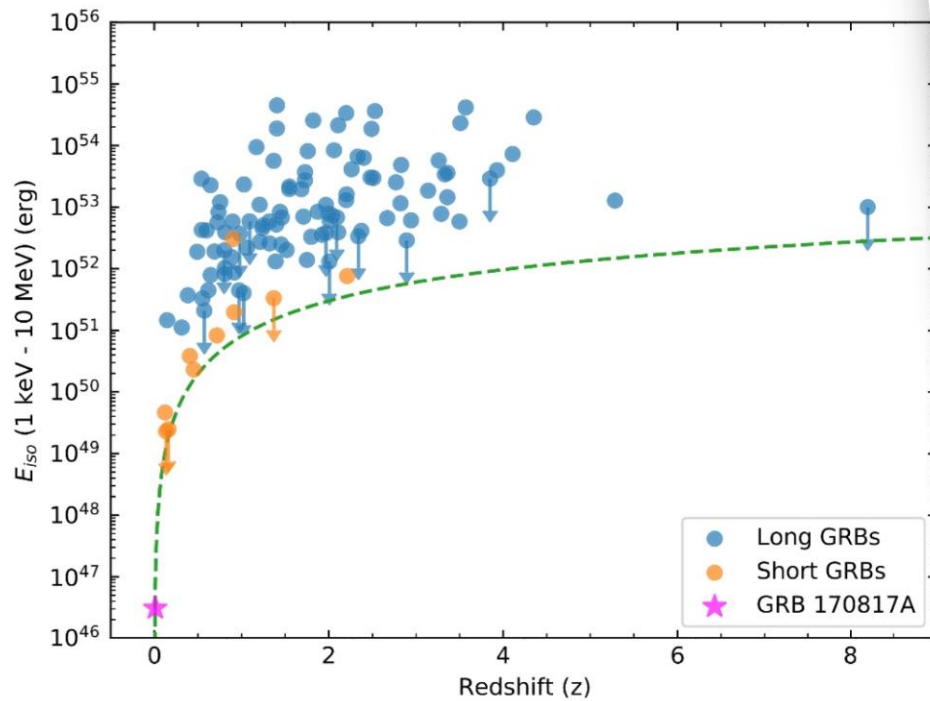
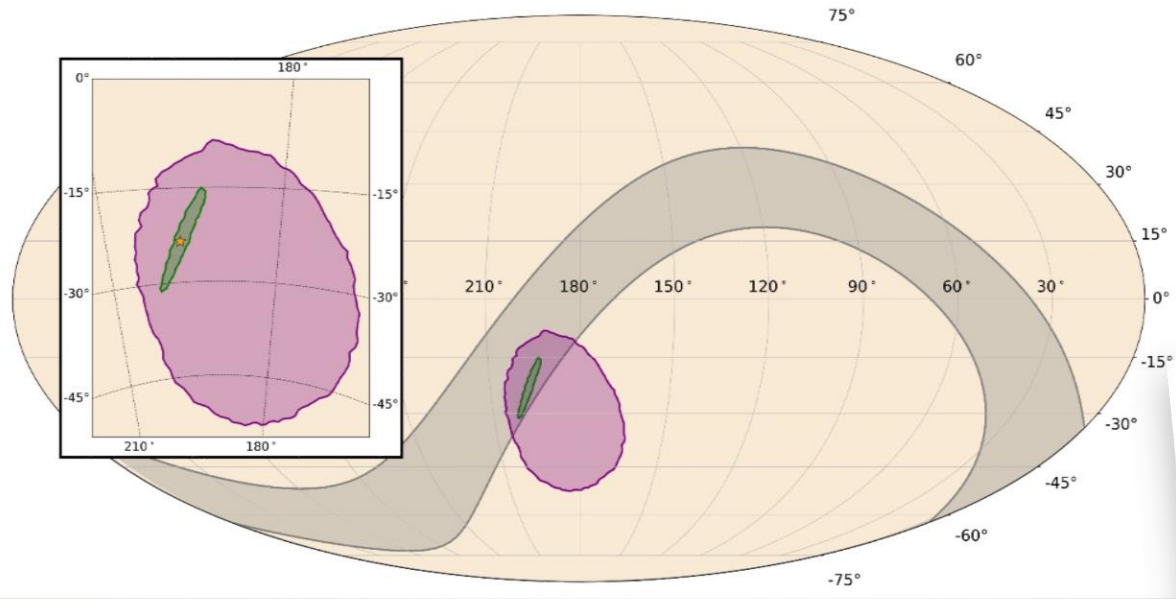
The long-awaited event GW170817

	Low-spin priors ($ \chi \leq 0.05$)	High-spin priors ($ \chi \leq 0.89$)
Primary mass m_1	$1.36-1.60 M_\odot$	$1.36-2.26 M_\odot$
Secondary mass m_2	$1.17-1.36 M_\odot$	$0.86-1.36 M_\odot$
Chirp mass \mathcal{M}	$1.188^{+0.004}_{-0.002} M_\odot$	$1.188^{+0.004}_{-0.002} M_\odot$
Mass ratio m_2/m_1	$0.7-1.0$	$0.4-1.0$
Total mass m_{tot}	$2.74^{+0.04}_{-0.01} M_\odot$	$2.82^{+0.47}_{-0.09} M_\odot$
Radiated energy E_{rad}	$> 0.025 M_\odot c^2$	$> 0.025 M_\odot c^2$
Luminosity distance D_L	40^{+8}_{-14} Mpc	40^{+8}_{-14} Mpc
Viewing angle Θ	$\leq 56^\circ$	$\leq 56^\circ$
Using NGC 4993 location	$\leq 28^\circ$	$\leq 28^\circ$
Combined dimensionless tidal deformability $\tilde{\Lambda}$	≤ 800	≤ 700
Dimensionless tidal deformability $\Lambda(1.4M_\odot)$	≤ 800	≤ 1400

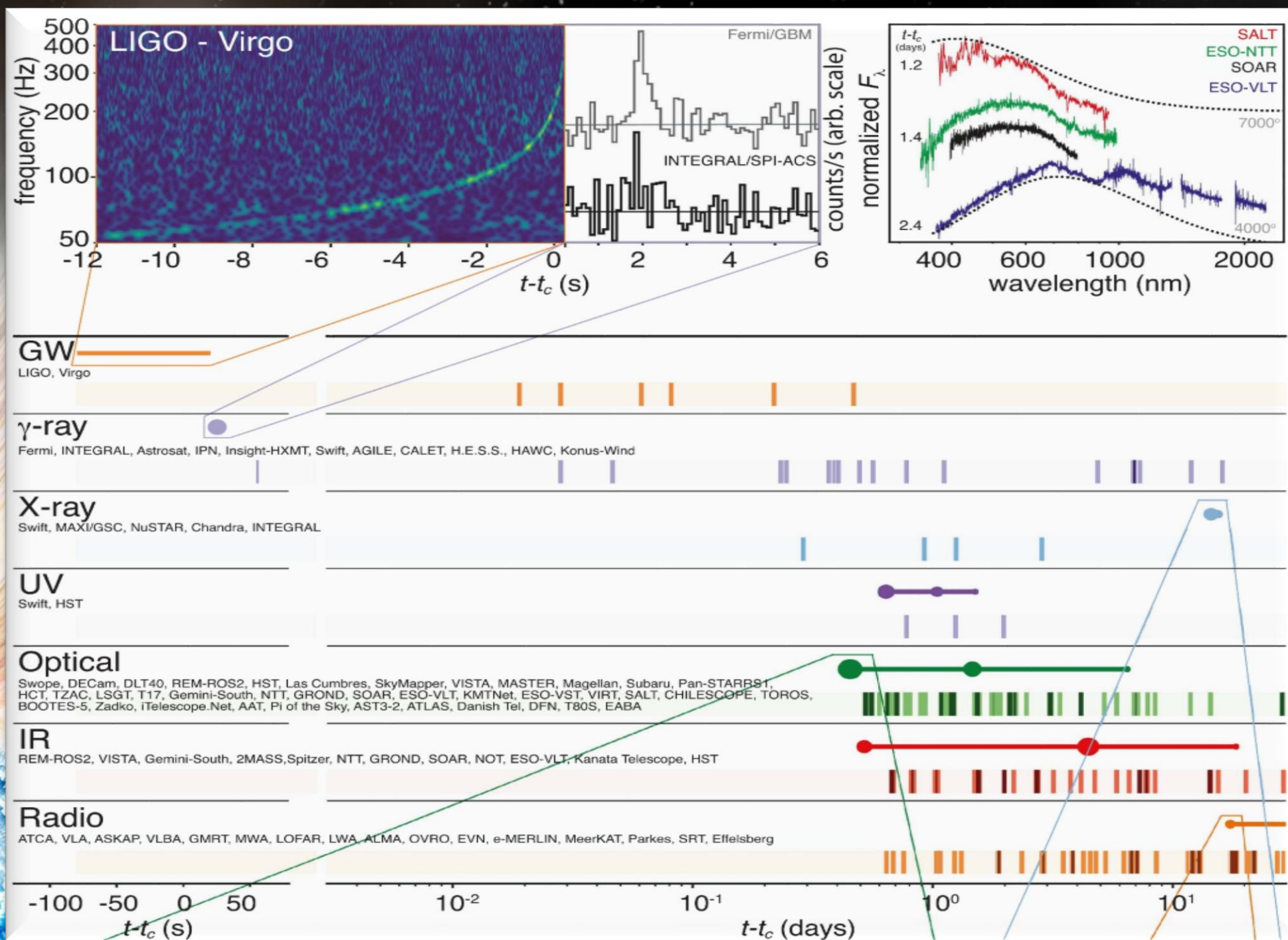
Gravitational Wave GW170817 and Gamma-Ray Emission GRB170817A



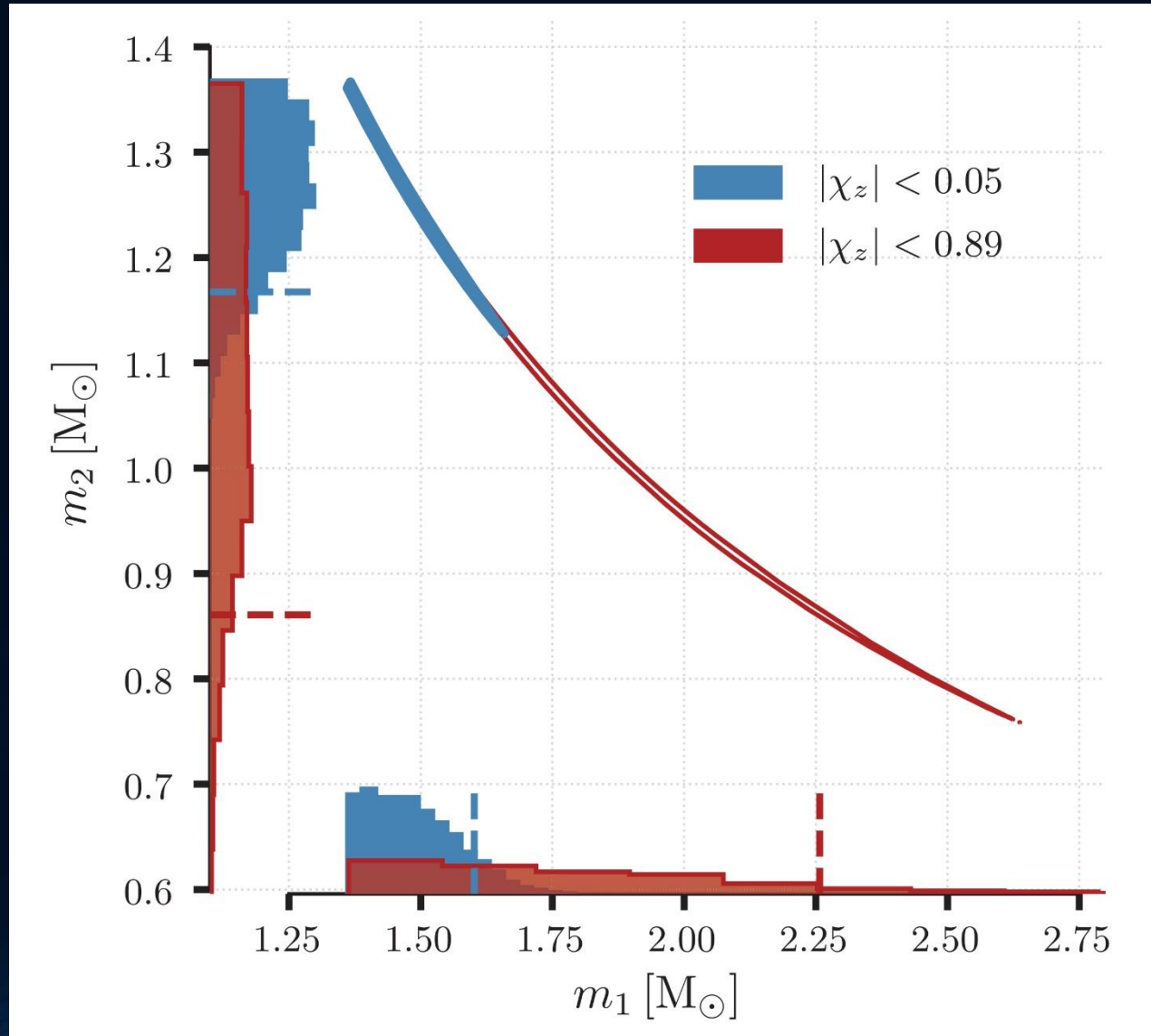
GW170817, GRB170817A Localisation and unusual dimness of GRB



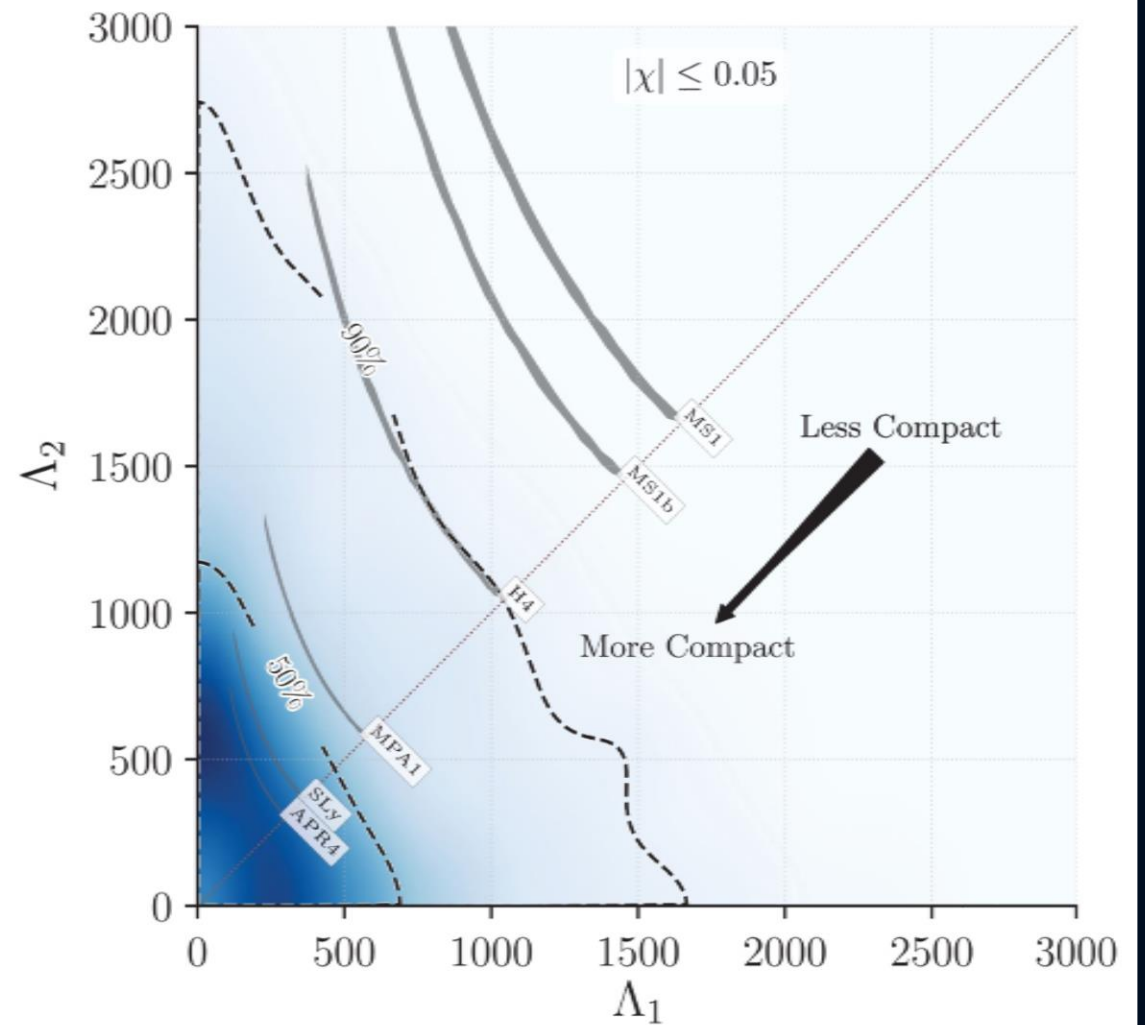
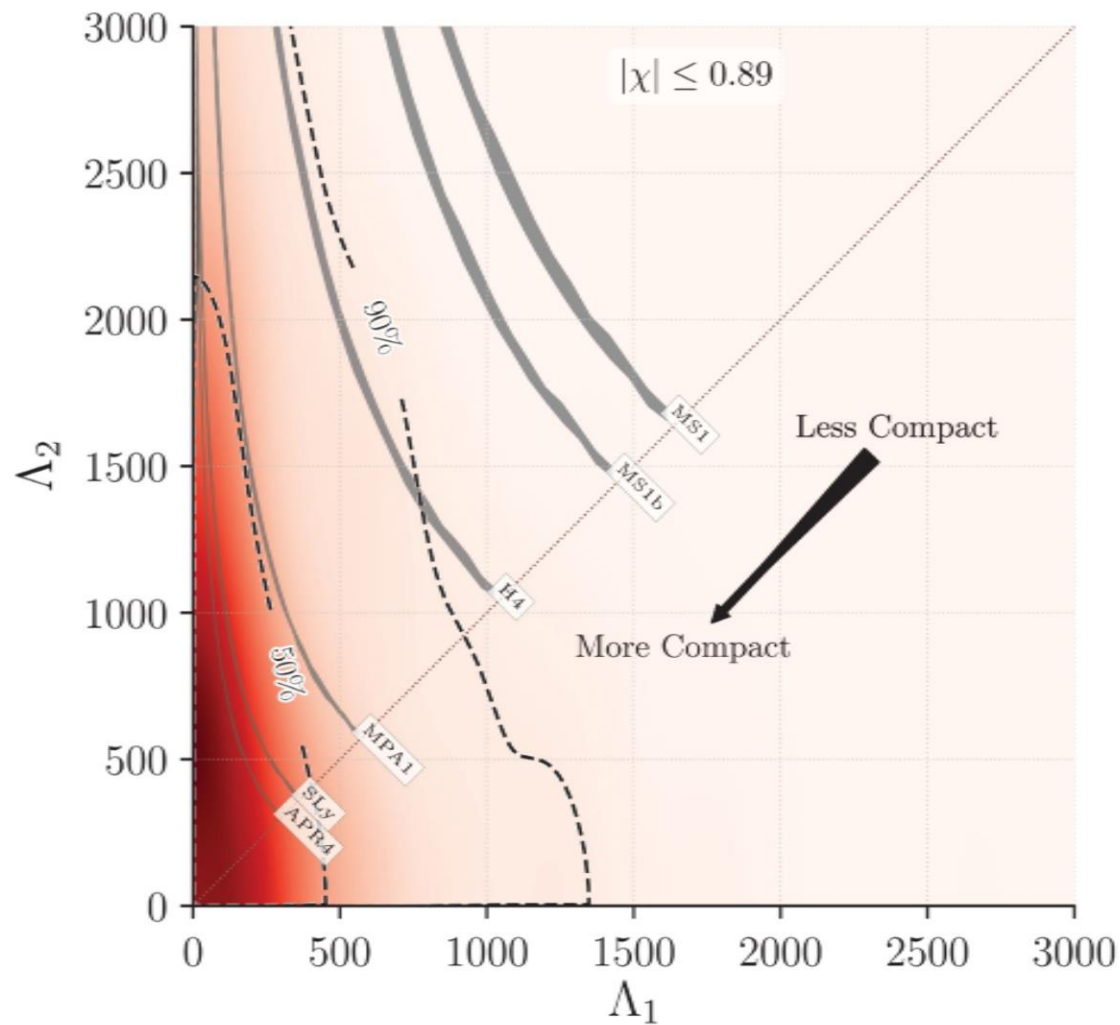
GW170817



Measured Mass Ratio of GW₁₇₀₈₁₇ (for high and low spin assumption)



GW170817: Tidal Deformability Restrictions on the Equation of State (EOS) (for high and low spin assumption)



The Einstein Equation

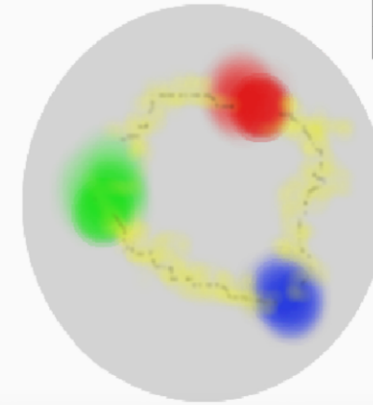
ART	<u>Yang-Mills-Theories</u>
$D_\beta v^\alpha = \partial_\beta v^\alpha + \Gamma_{\sigma\beta}^\alpha v^\sigma$	$D_{\beta a}{}^b = \partial_\beta 1_a{}^b + ig A_{\beta a}{}^b$
$R^\delta{}_{\mu\alpha\beta} v^\mu = [D_\alpha, D_\beta] v^\delta$	$F_{\alpha\beta a}{}^b = \frac{1}{ig} [D_{\alpha a}{}^c, D_{\beta c}{}^b]$
$R^\delta{}_{\mu\alpha\beta} = \Gamma_{\mu\alpha \beta}^\delta - \Gamma_{\mu\beta \alpha}^\delta$ $+ \Gamma_{\nu\beta}^\delta \Gamma_{\mu\alpha}^\nu + \Gamma_{\nu\alpha}^\delta \Gamma_{\mu\beta}^\nu$	$= A_{\beta a}{}^b _\alpha - A_{\alpha a}{}^b _\beta$ $+ \frac{1}{ig} [A_{\alpha a}{}^c, A_{\beta c}{}^b]$
$\mathcal{L}_G = R + \underbrace{(c_1 R_{\mu\nu} R^{\mu\nu} + \dots)}_{\equiv 0 \text{ for ART}}$	$\mathcal{L}_{YM} = \frac{1}{4} F_{\mu\nu a}{}^b F^{\mu\nu}{}_a{}^b$

Quantum ChromoDynamic:

($SU(3)_{(c)}$ - Color Yang-Mills-Gauge Theory)

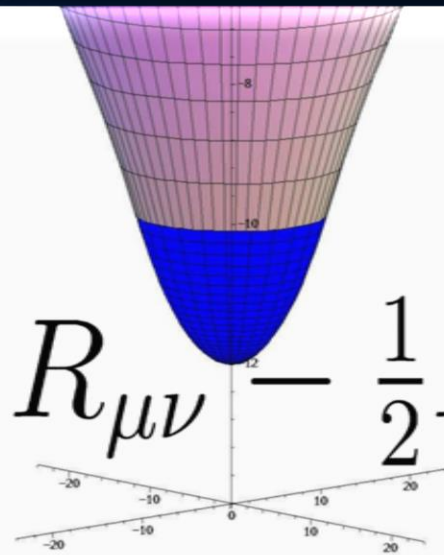
$$D_{\beta A}{}^B = \partial_\beta 1_A{}^B + ig G_{\beta A}{}^B$$

$A, B = \text{red, green, blue}$



$$\psi_A^f = \begin{pmatrix} \psi_r^f \\ \psi_g^f \\ \psi_b^f \end{pmatrix}$$

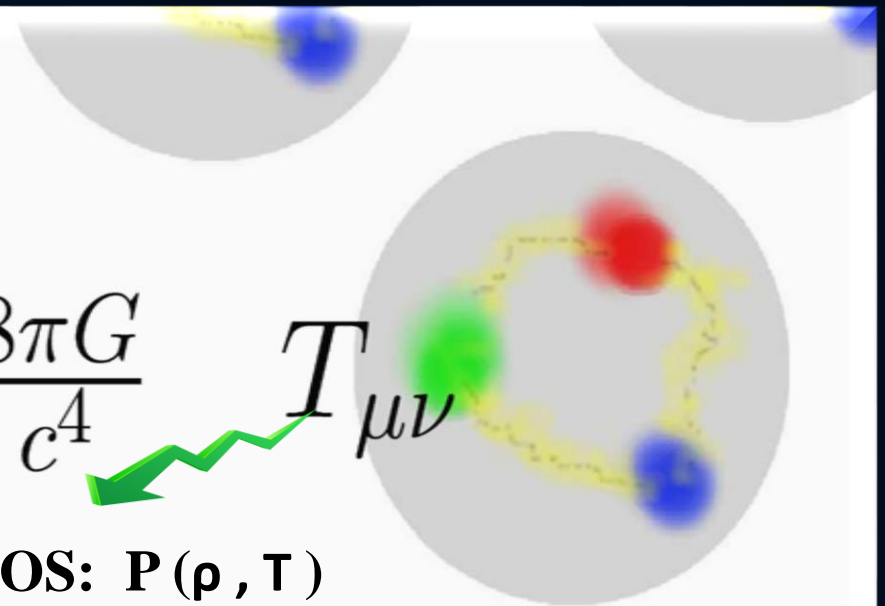
Confinement
chiral symmetry, ...



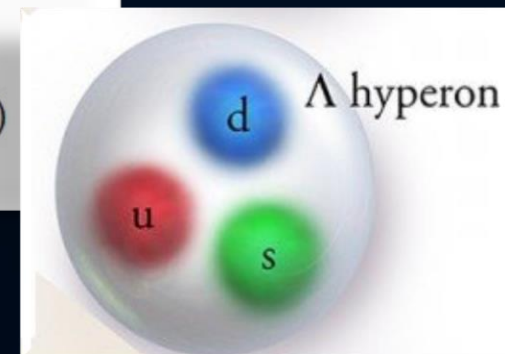
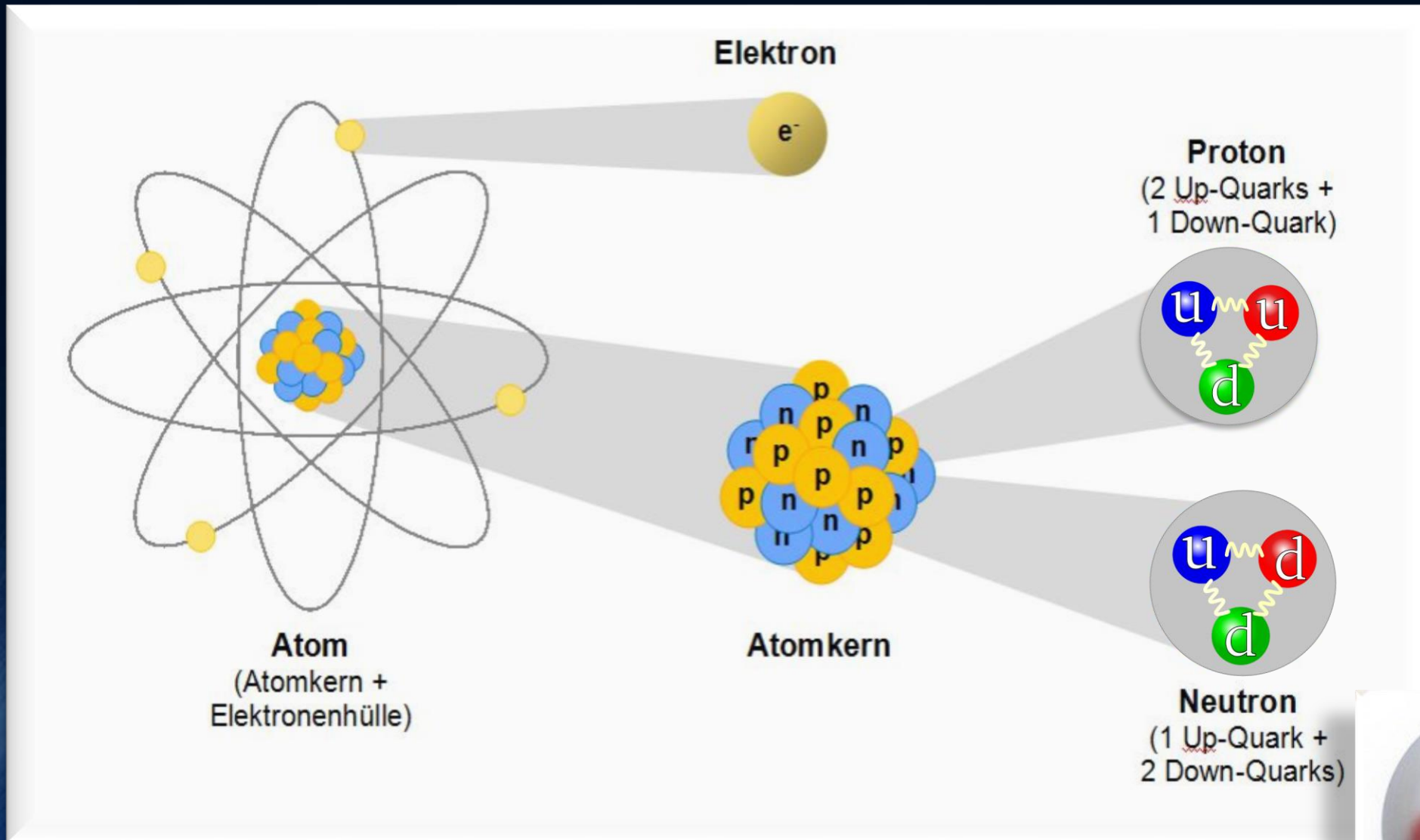
$$R_{\mu\nu} - \frac{1}{2} R g_{\mu\nu} =$$

$$\frac{8\pi G}{c^4} T_{\mu\nu}$$

EOS: $P(\rho, T)$

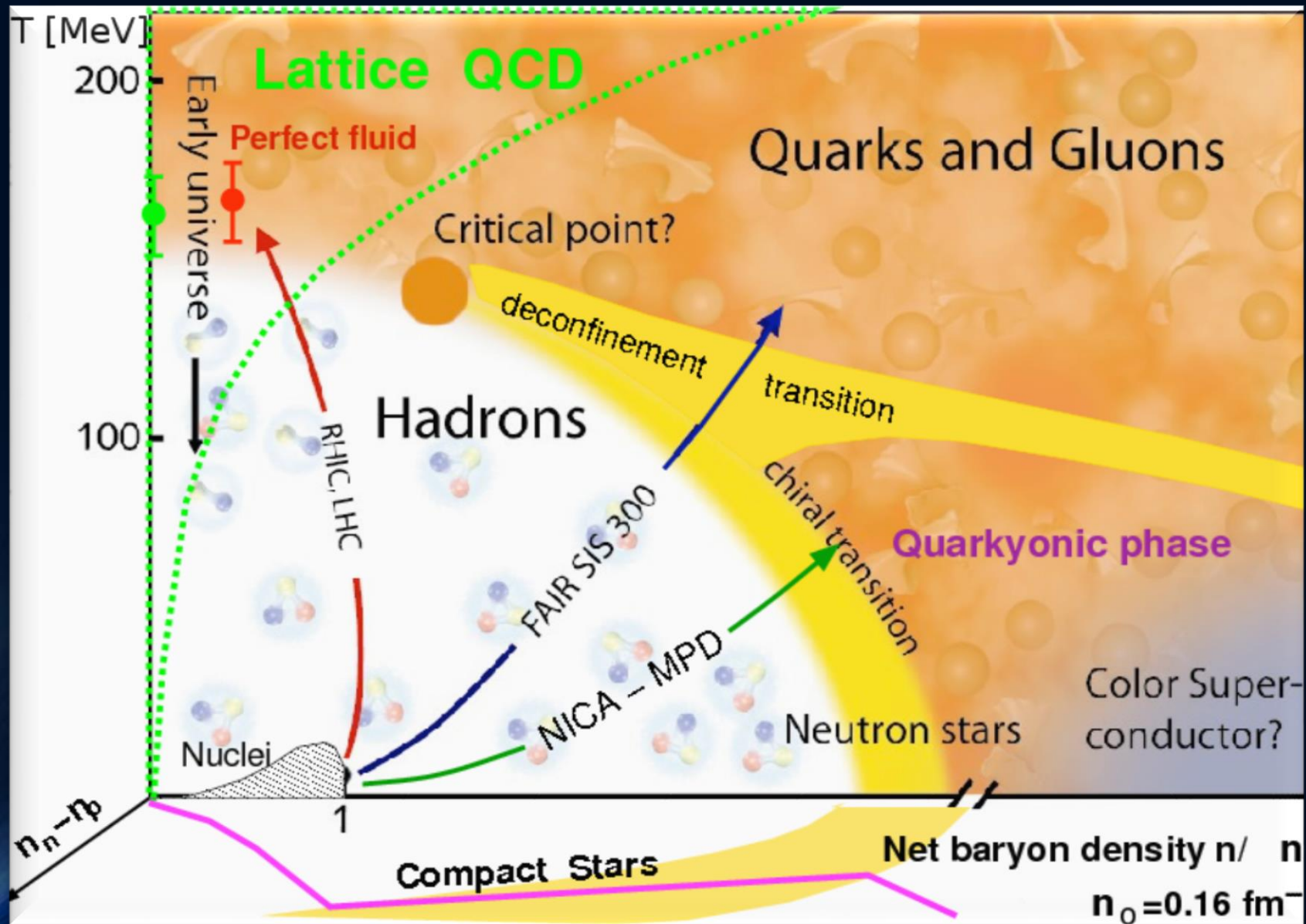


Elementary Matter



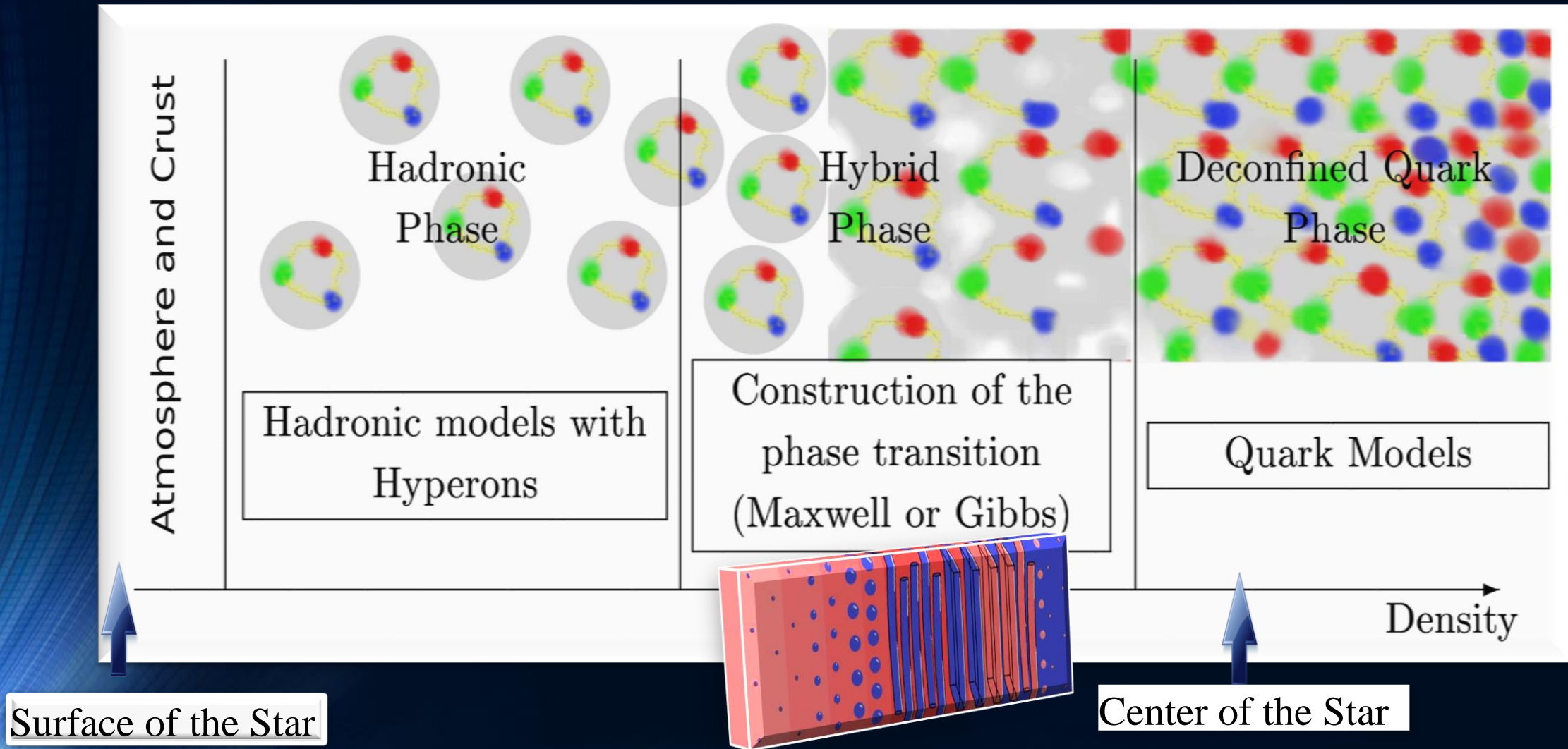
If the densities or temperatures are very high, additional Hyperonic Particles can occur

The Hadron-Quark Phase Transition



Credits to http://inspirehep.net/record/823172/files/phd_qgp3D_quarkyonic2.png

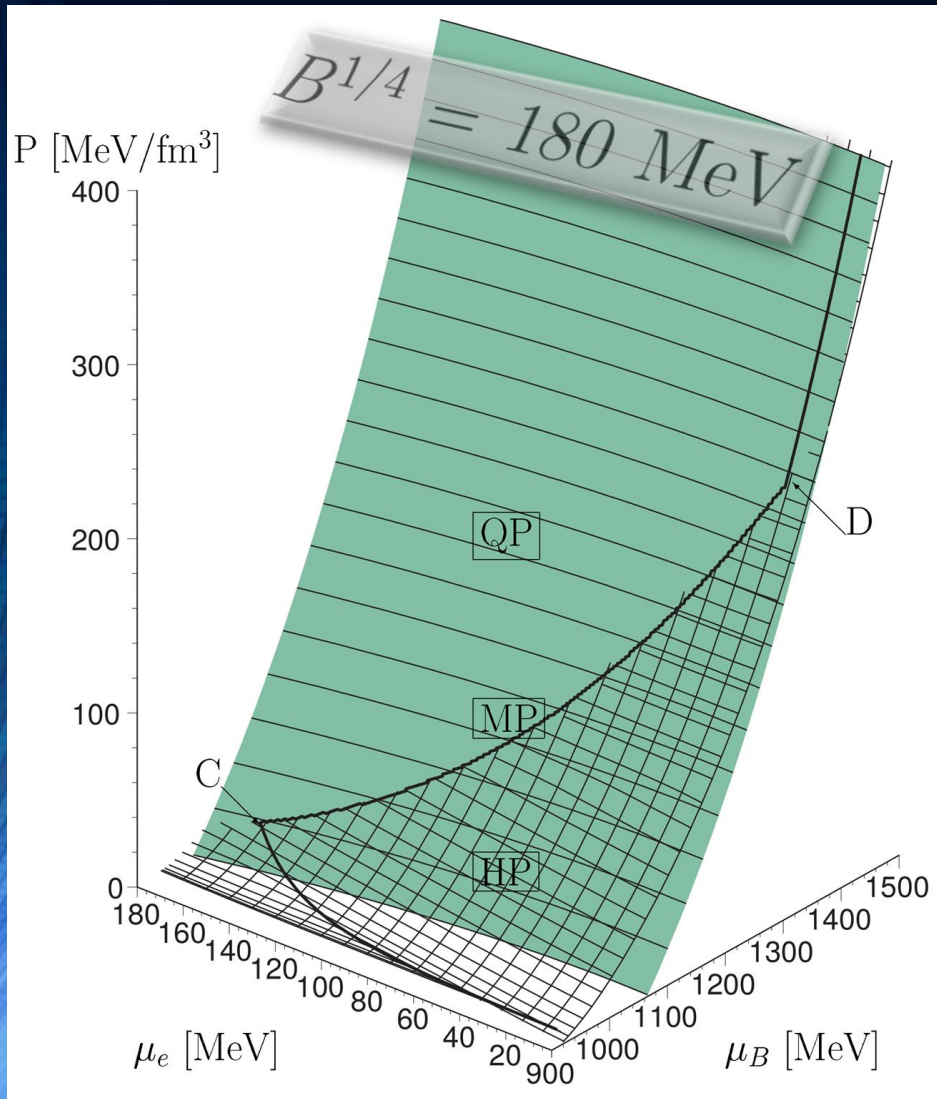
The QCD – Phase Transition and the Interior of a Hybrid Star



See: *Stable hybrid stars within a SU(3) Quark-Meson-Model*,
A.Zacchi, M.Hanuske, J.Schaffner-Bielich, PRD 93, 065011 (2016)

The Gibbs Construction

Hadronic and quark surface:

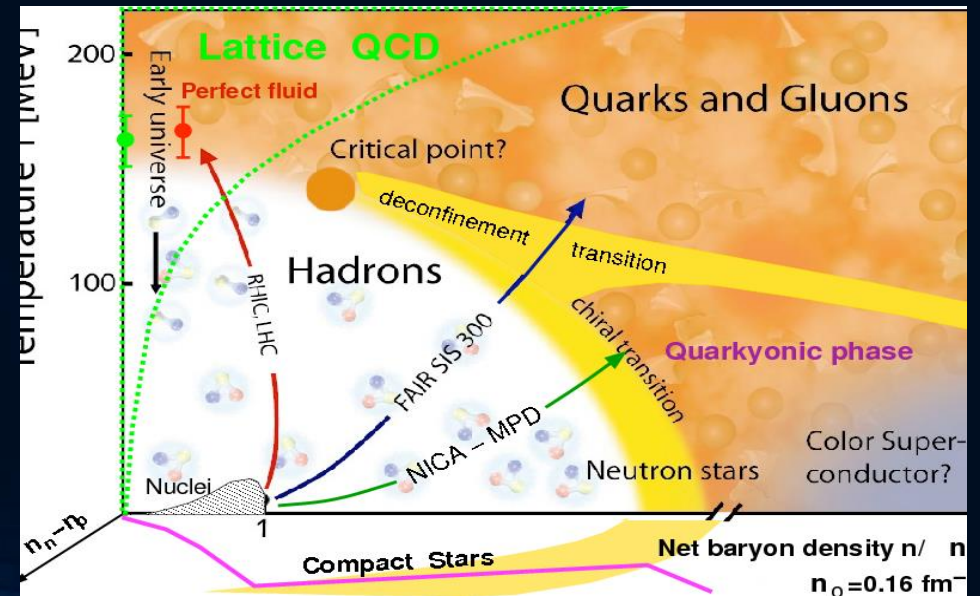


Charge neutrality condition is only globally realized

$$\rho_e := (1 - \chi)\rho_e^H(\mu_B, \mu_e) + \chi\rho_e^Q(\mu_B, \mu_e) = 0.$$

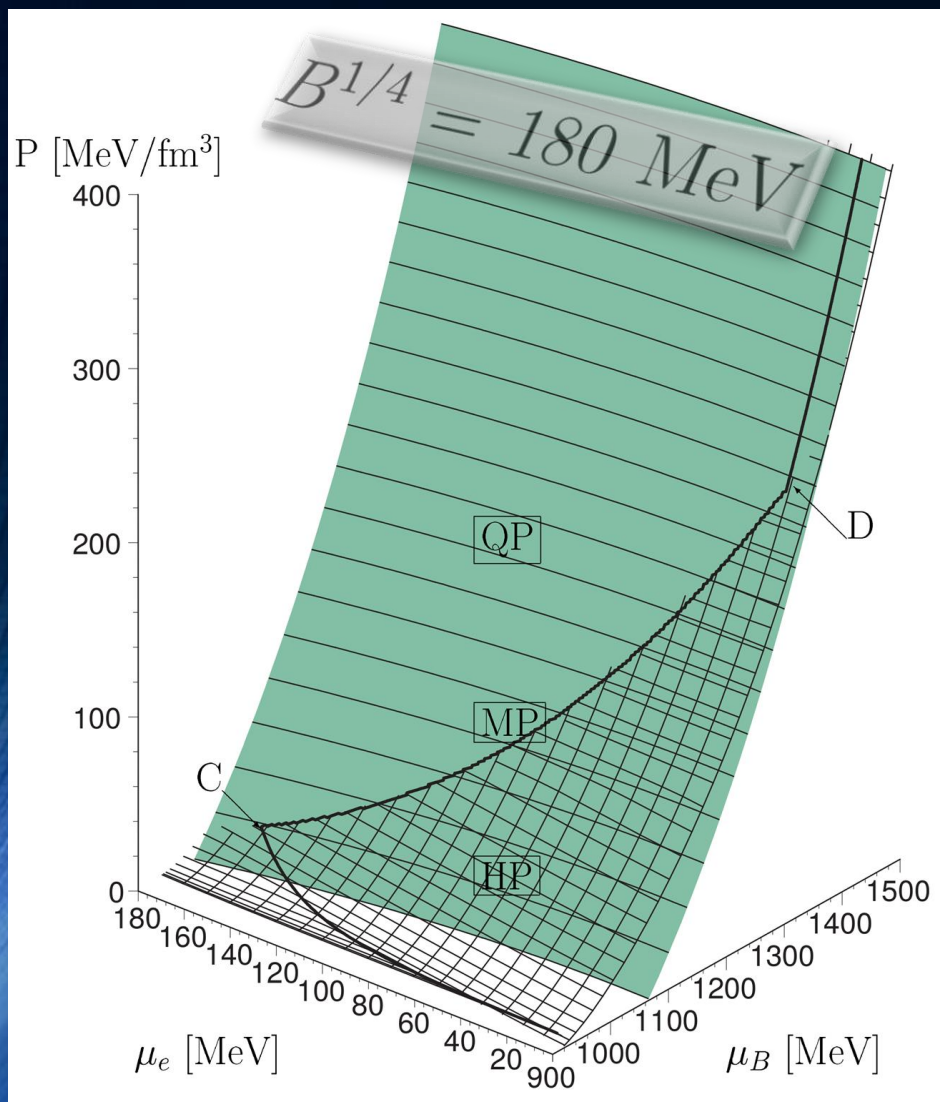
The pressure in the mixed phase depends on two independent chemical potentials

$$\begin{aligned} P^H(\mu_B, \mu_e) &= P^Q(\mu_B, \mu_e), \\ \mu_B &= \mu_B^H = \mu_B^Q, \\ \mu_e &= \mu_e^H = \mu_e^Q \end{aligned}$$

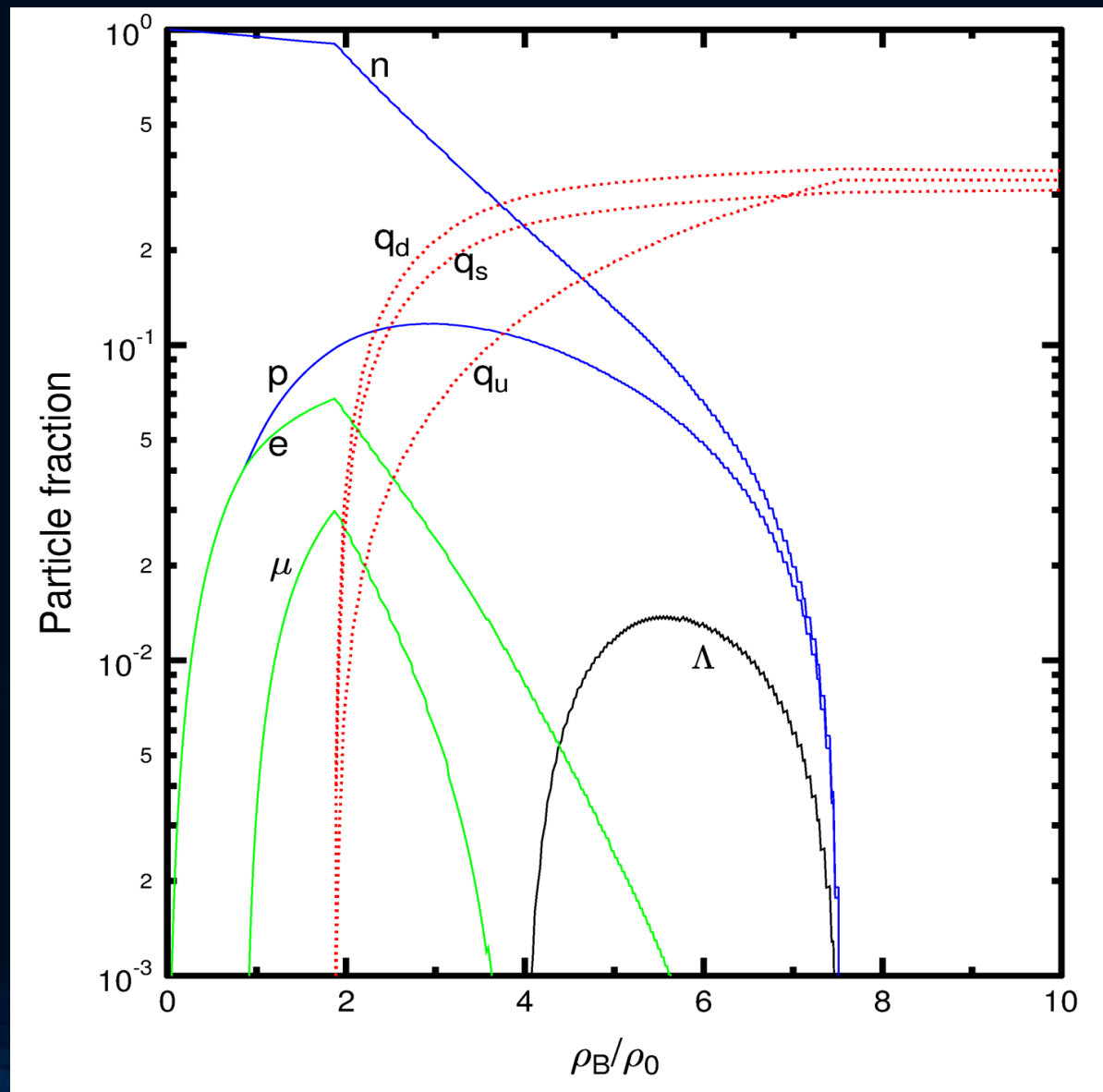


The Gibbs Construction

Hadronic and quark surface:

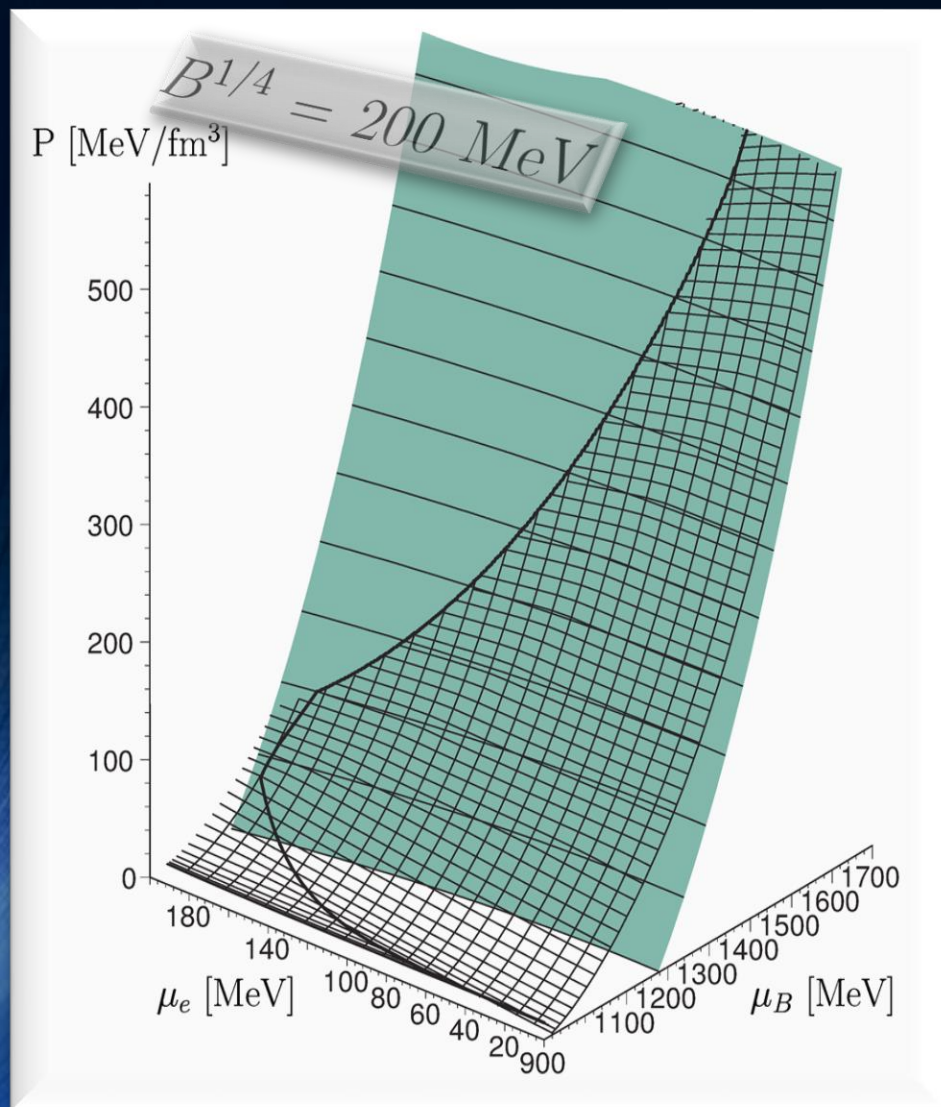


Particle composition:

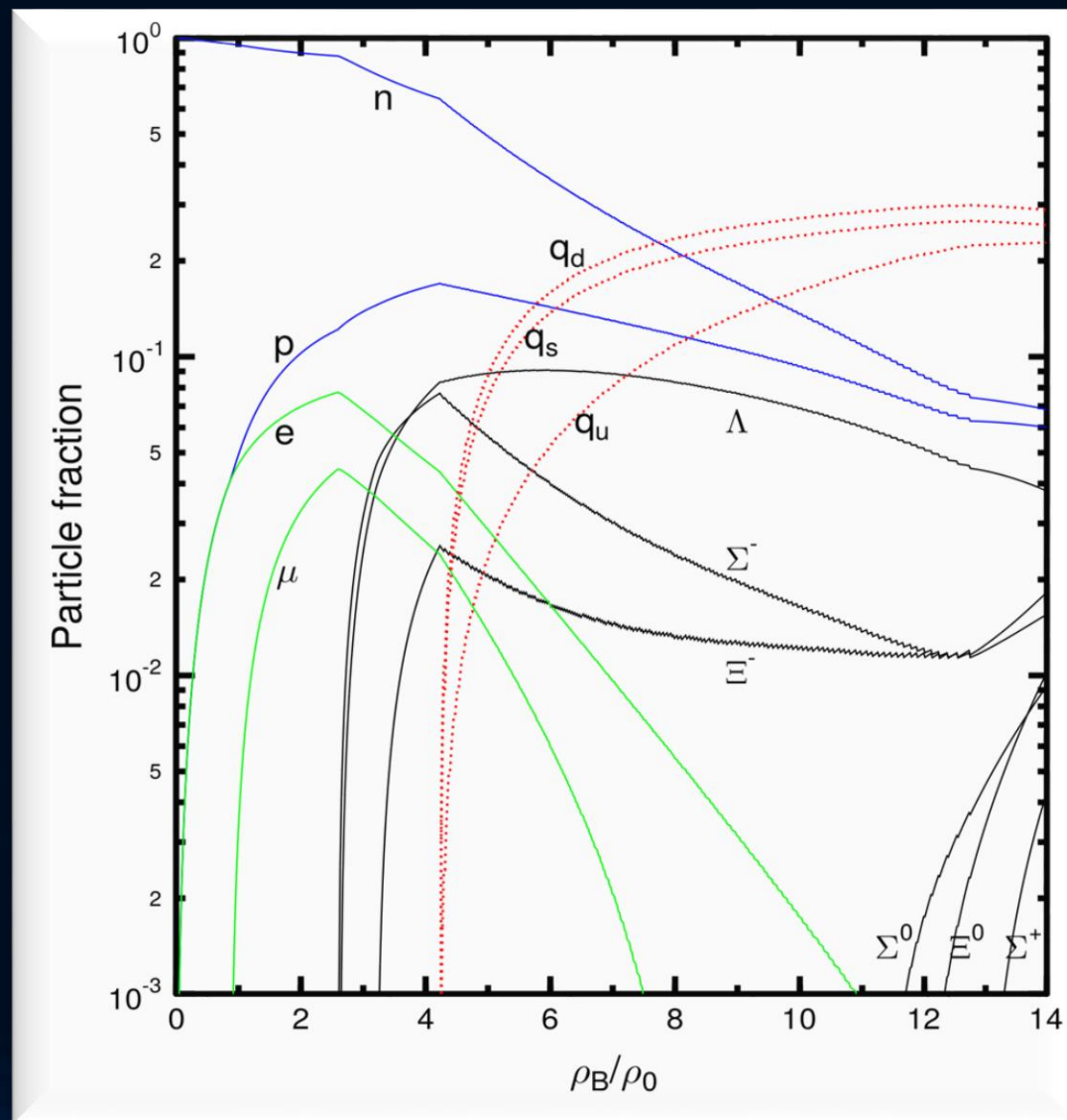


The Gibbs Construction

Hadronic and quark surface:

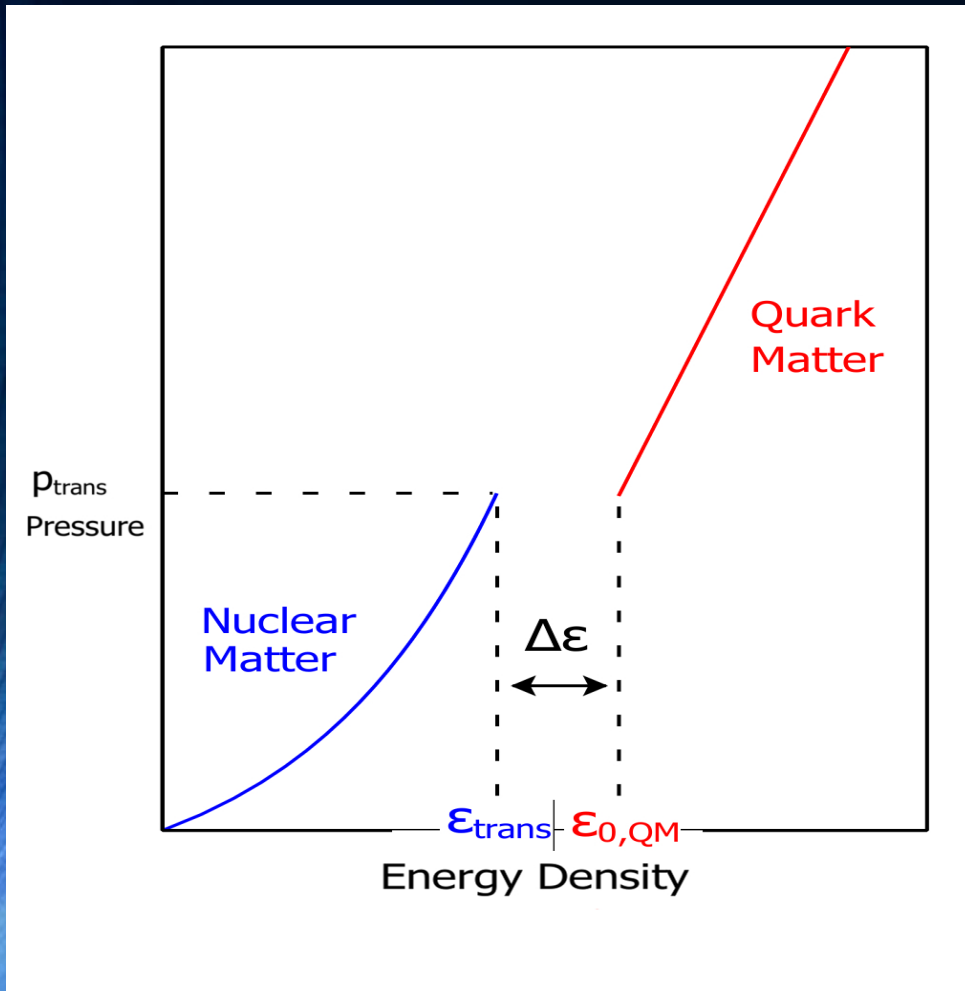


Particle composition:

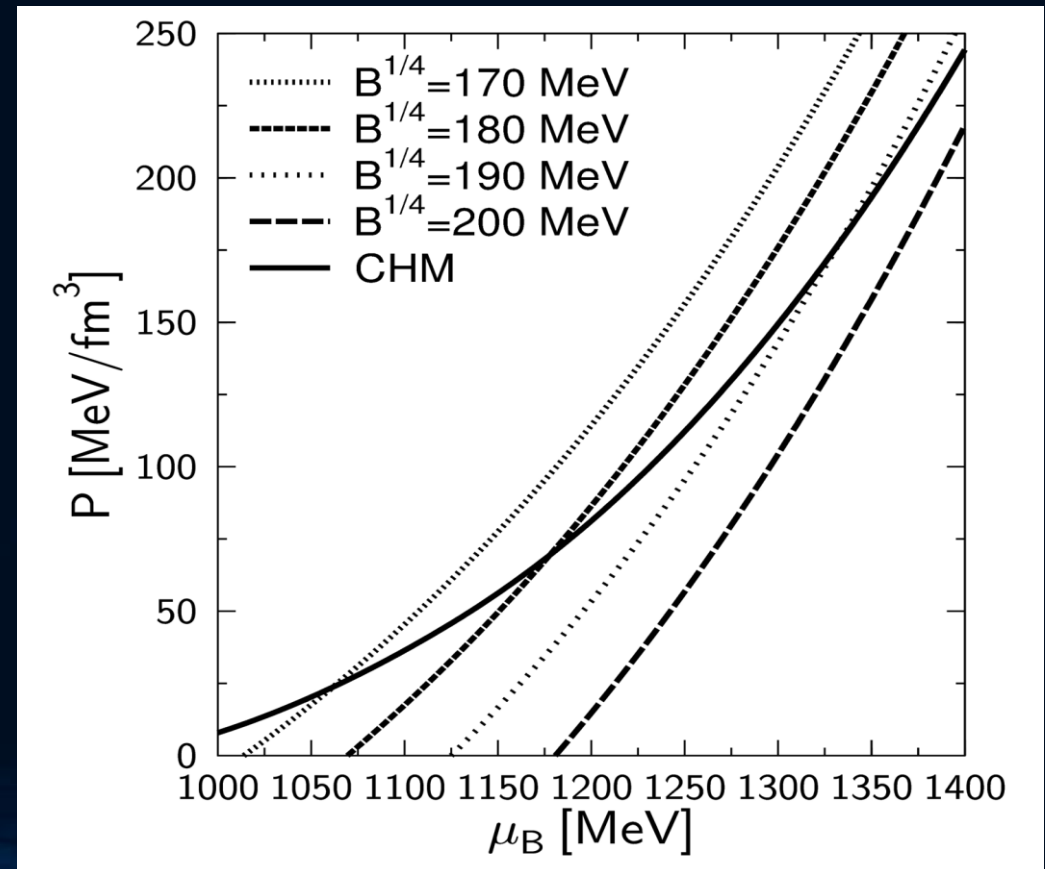


The Maxwell Construction

If the surface tension between the hadron and quark phase is relatively large, the mixed phase could completely disappear, so that a sharp boundary between the two phase exists. The Hadron-quark phase transition is then described using a Maxwell construction.



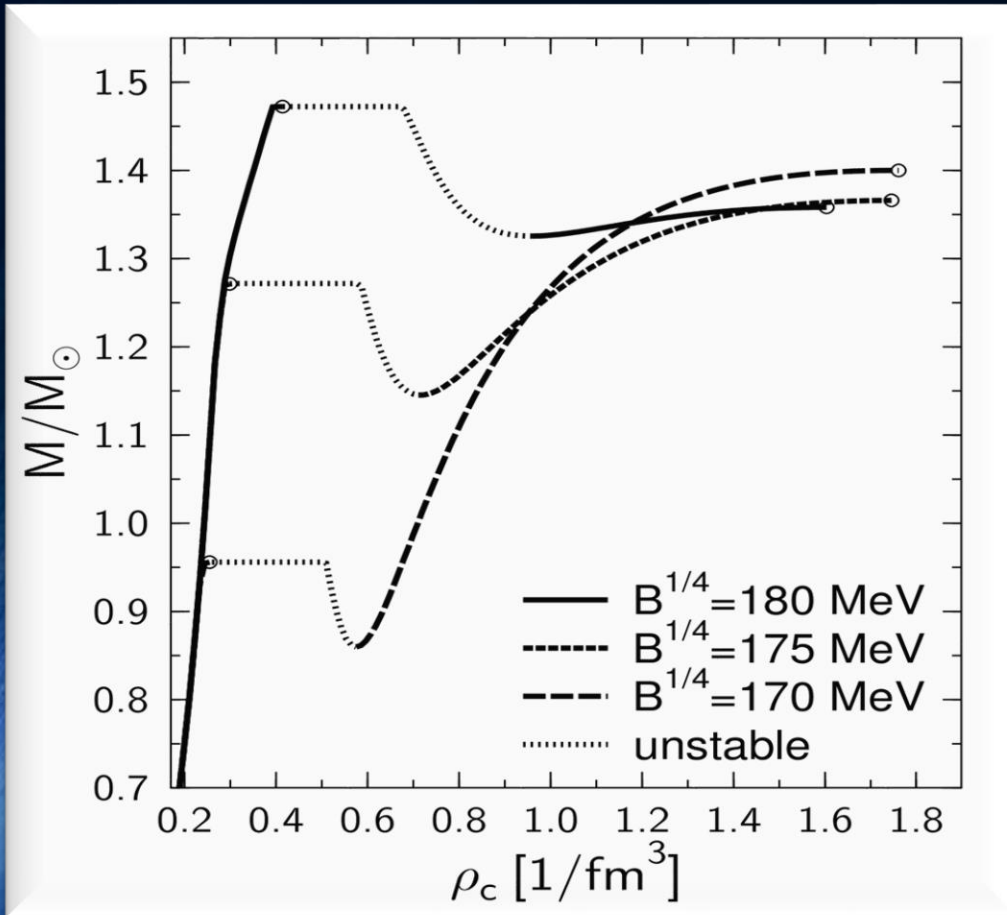
Pressure and baryon chemical potential stays constant, while the density and the charge chemical potential jump discontinuously during the phase transition.



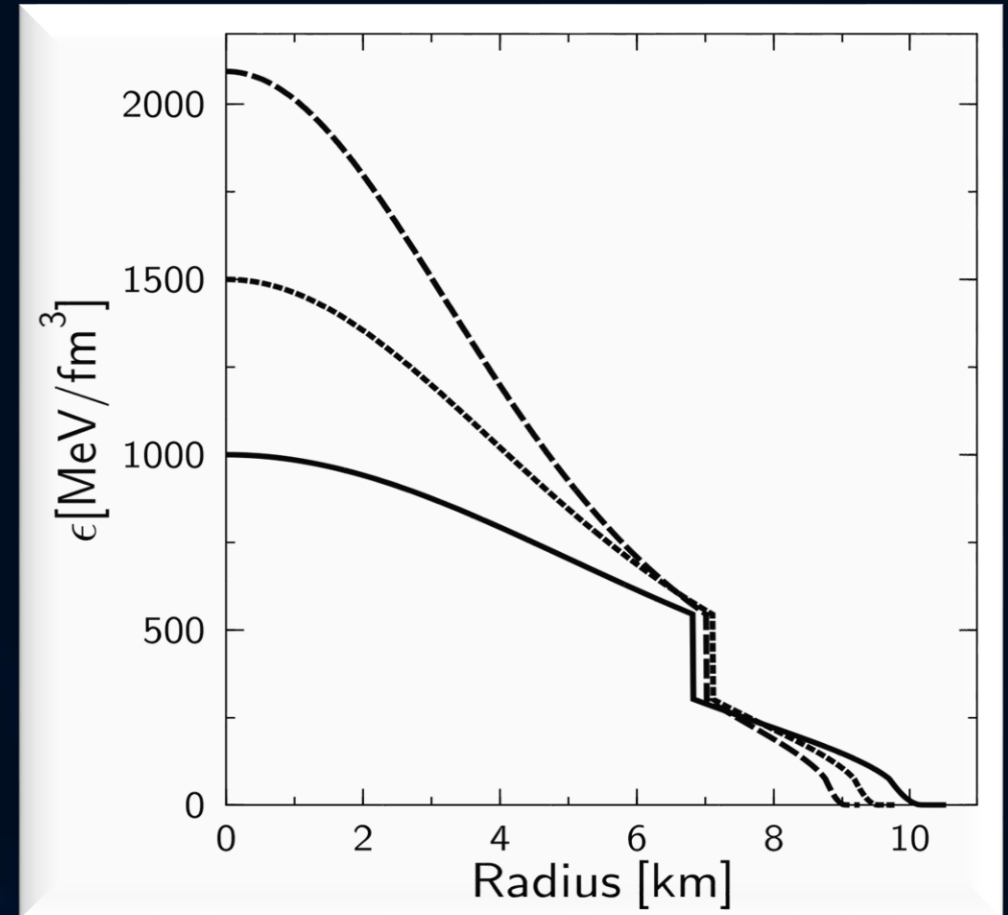
Hybrid Star Properties

In contrast to the Gibbs construction, the star's density profile within the Maxwell construction (see right figure) will have a huge density jump at the phase transition boundary. Twin star properties can be found more easily when using a Maxwell construction.

Mass-Density relation

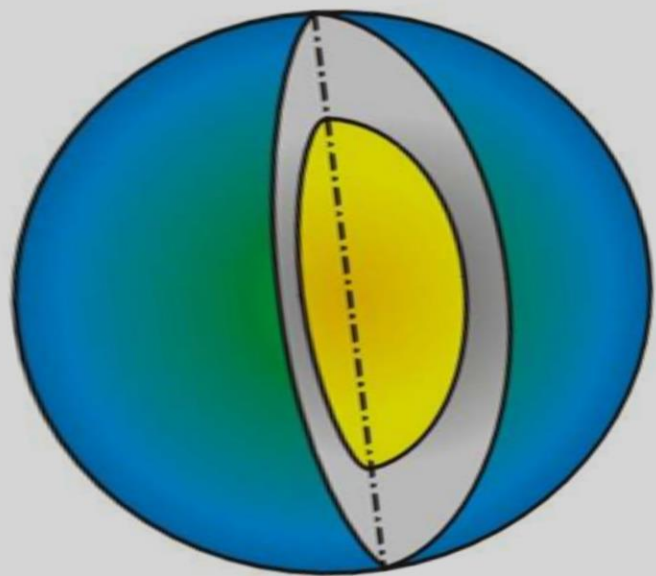


Energy-density profiles

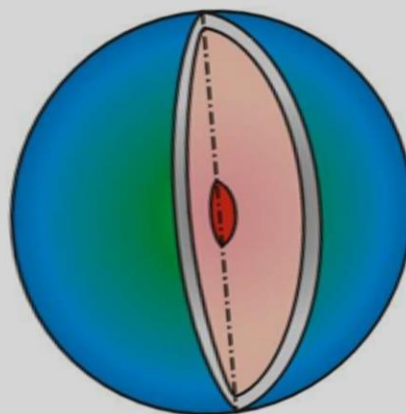


Neutron Stars, Hybrid Stars, Quark Stars and Black Holes

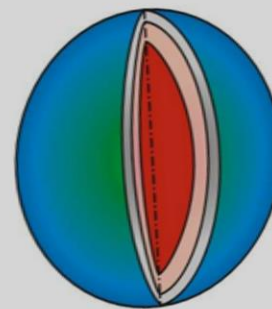
Neutron Stars



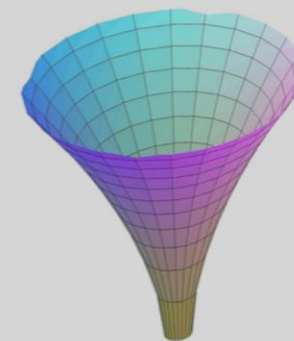
Hybrid Stars



Quark Stars



Black Holes



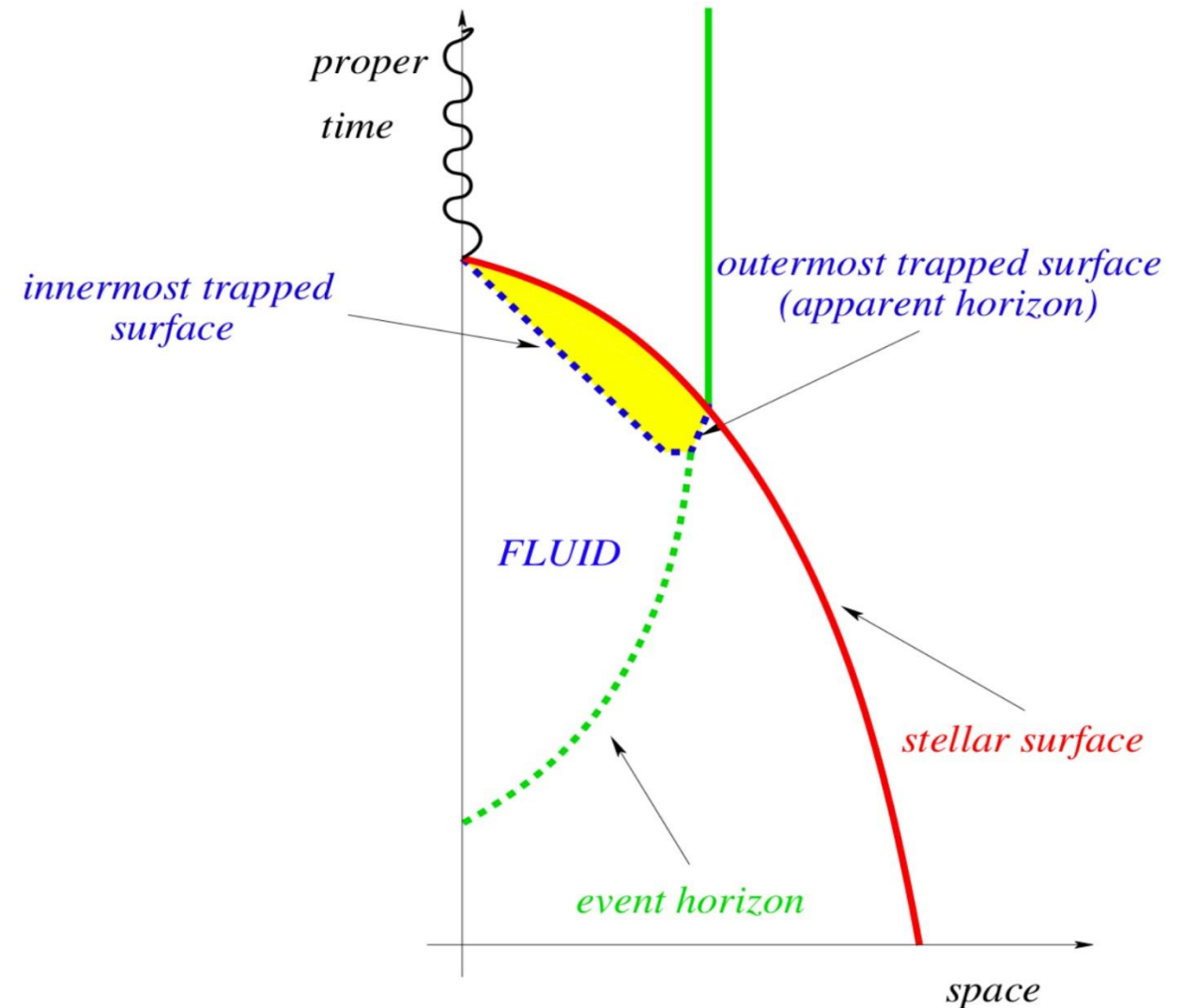
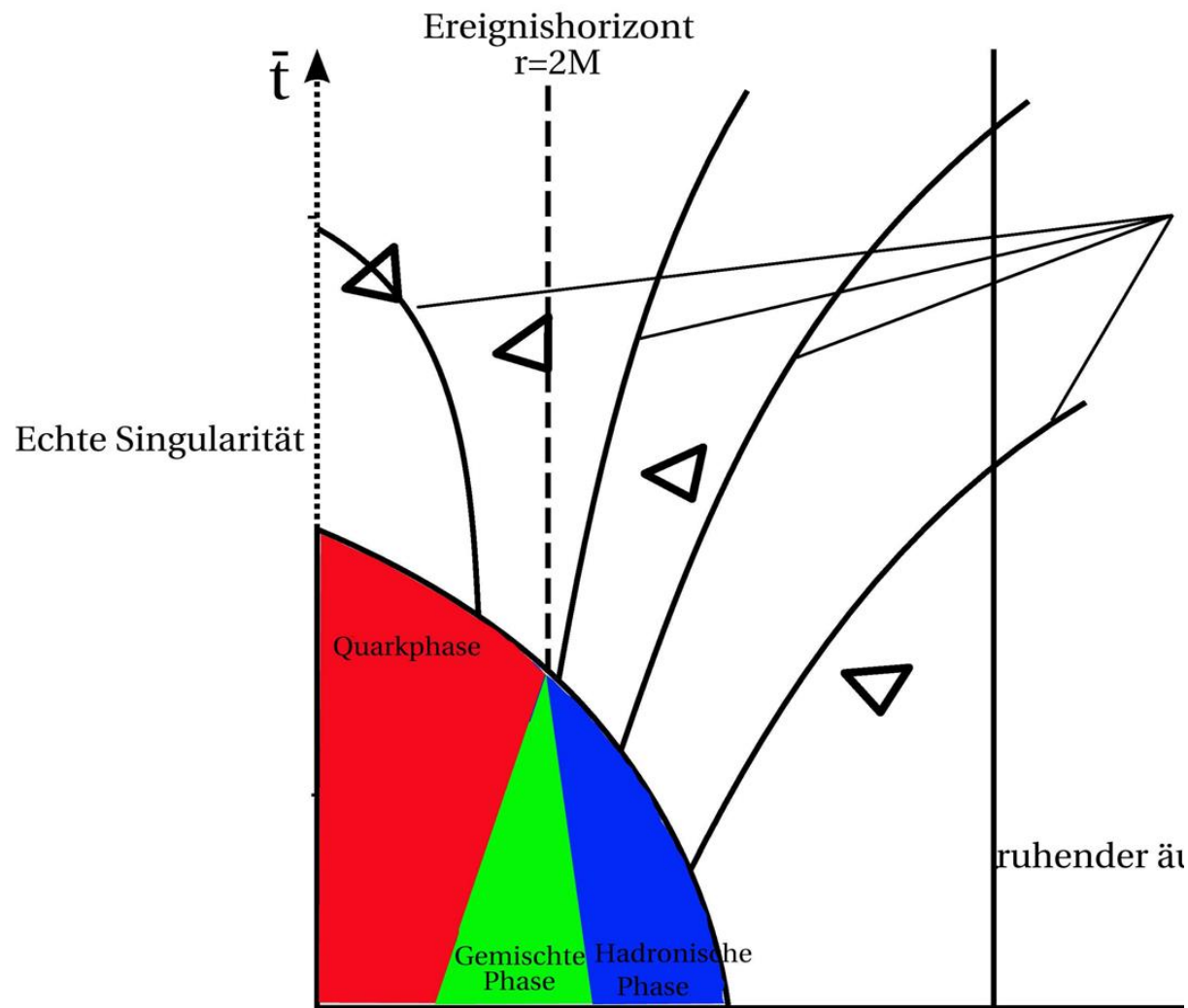
$\rho_c = \rho_0$
Central density ρ_c in the star
($\rho_0 := 0.15/\text{fm}^3$)

$\approx 2 \rho_0$

$\approx 5 \rho_0$

... ∞

The Formation of the Event Horizon of the Black Hole and the Deconfinement of Elementary Matter



Numerical Relativity and Relativistic Hydrodynamics of Binary Neutron Star Mergers

Numerical simulations of a merger of two compact stars are based on a (3+1) decomposition of spacetime of the Einstein and hydrodynamic equations.

$$R_{\mu\nu} - \frac{1}{2}g_{\mu\nu}R = 8\pi T_{\mu\nu}$$

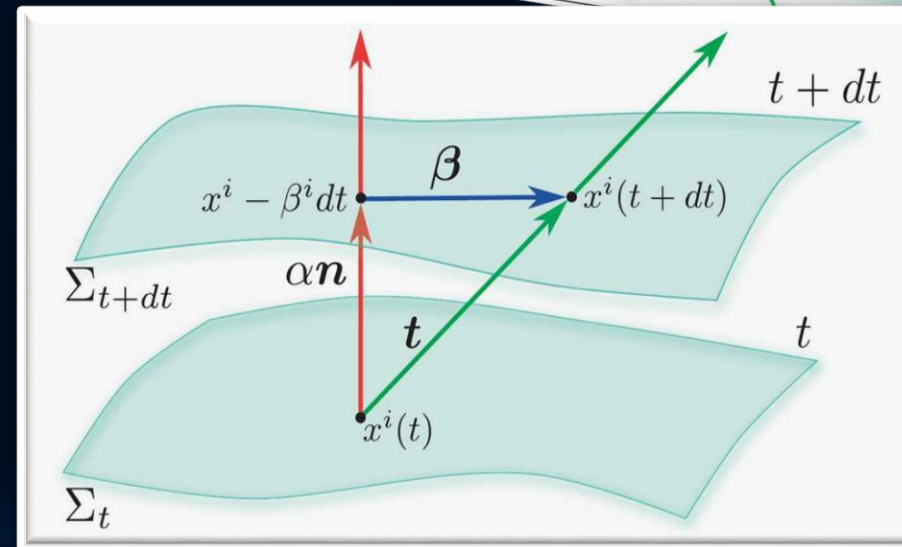
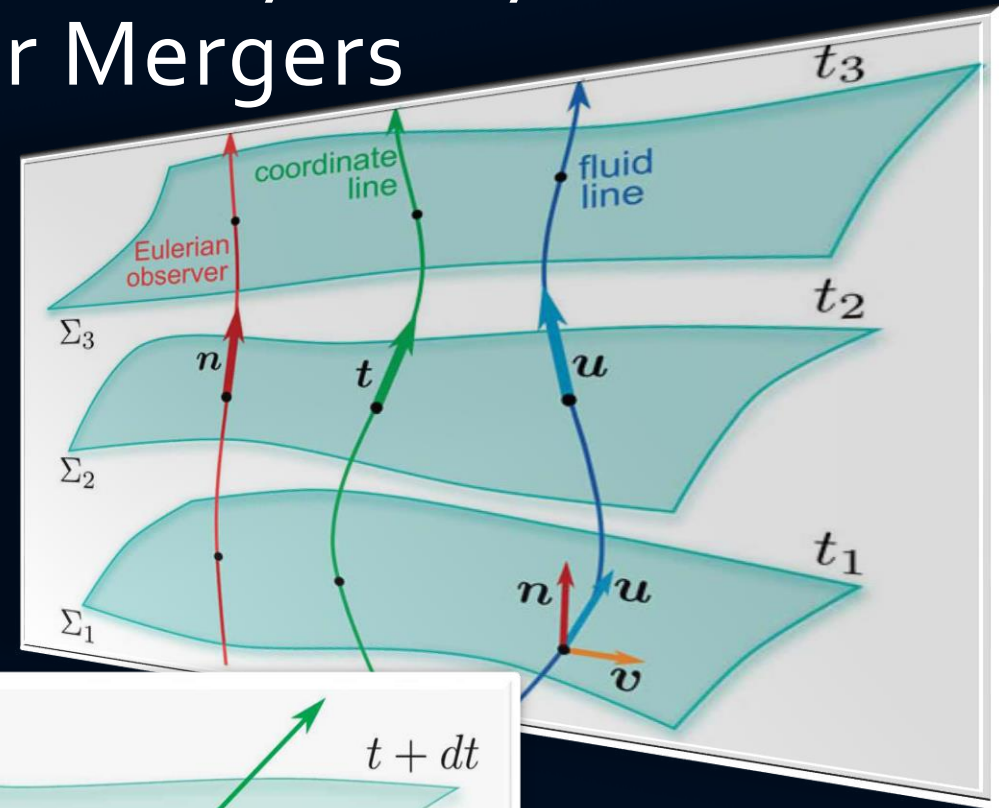
$$\begin{aligned}\nabla_{\mu}(\rho u^{\mu}) &= 0, \\ \nabla_{\nu}T^{\mu\nu} &= 0.\end{aligned}$$

(3+1) decomposition of spacetime

$$g_{\mu\nu} = \begin{pmatrix} -\alpha^2 + \beta_i\beta^i & \beta_i \\ \beta_i & \gamma_{ij} \end{pmatrix}$$

$$d\tau^2 = \alpha^2(t, x^j)dt^2$$

$$x^i_{t+dt} = x^i_t - \beta^i(t, x^j)dt$$



The ADM equations

The ADM (Arnowitt, Deser, Misner) equations come from a reformulation of the Einstein equation using the (3+1) decomposition of spacetime.

$$\begin{aligned}\partial_t \gamma_{ij} &= -2\alpha K_{ij} + \mathcal{L}_\beta \gamma_{ij} \\ &= -2\alpha K_{ij} + D_i \beta_j + D_j \beta_i\end{aligned}$$

$$\begin{aligned}\partial_t K_{ij} &= -D_i D_j \alpha + \beta^k \partial_k K_{ij} + K_{ik} \partial_j \beta^k + K_{kj} \partial_i \beta^k \\ &+ \alpha \left({}^{(3)}R_{ij} + K K_{ij} - 2K_{ik} K^k_j \right) + 4\pi\alpha [\gamma_{ij} (S - E) - 2S_{ij}]\end{aligned}$$

Time evolving part of ADM

$$D_j (K^{ij} - \gamma^{ij} K) = 8\pi S^i$$

$${}^{(3)}R + K^2 - K_{ij} K^{ij} = 16\pi E$$

Constraints on each hypersurface

Three dimensional covariant derivative

$$D_\nu := \gamma^\mu_\nu \nabla_\mu = (\delta^\mu_\nu + n_\nu n^\mu) \nabla_\mu$$

Three dimensional Riemann tensor

$${}^{(3)}R^\mu_{\nu\kappa\sigma} = \partial_\kappa {}^{(3)}\Gamma^\mu_{\nu\sigma} - \partial_\sigma {}^{(3)}\Gamma^\mu_{\nu\kappa} + {}^{(3)}\Gamma^\mu_{\lambda\kappa} {}^{(3)}\Gamma^\lambda_{\nu\sigma} - {}^{(3)}\Gamma^\mu_{\lambda\sigma} {}^{(3)}\Gamma^\lambda_{\nu\kappa}$$

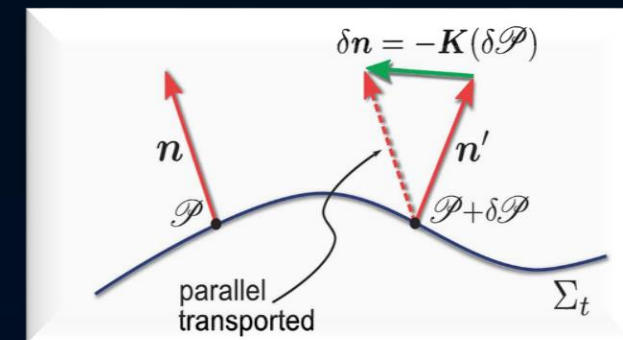
$${}^{(3)}\Gamma^\alpha_{\beta\gamma} = \frac{1}{2} \gamma^{\alpha\delta} (\partial_\beta \gamma_{\gamma\delta} + \partial_\gamma \gamma_{\delta\beta} - \partial_\delta \gamma_{\beta\gamma})$$

Spatial and normal projections of the energy-momentum tensor:

$$\begin{aligned}S_{\mu\nu} &:= \gamma^\alpha_\mu \gamma^\beta_\nu T_{\alpha\beta}, \\ S_\mu &:= -\gamma^\alpha_\mu n^\beta T_{\alpha\beta}, \\ S &:= S^\mu_\mu, \\ E &:= n^\alpha n^\beta T_{\alpha\beta},\end{aligned}$$

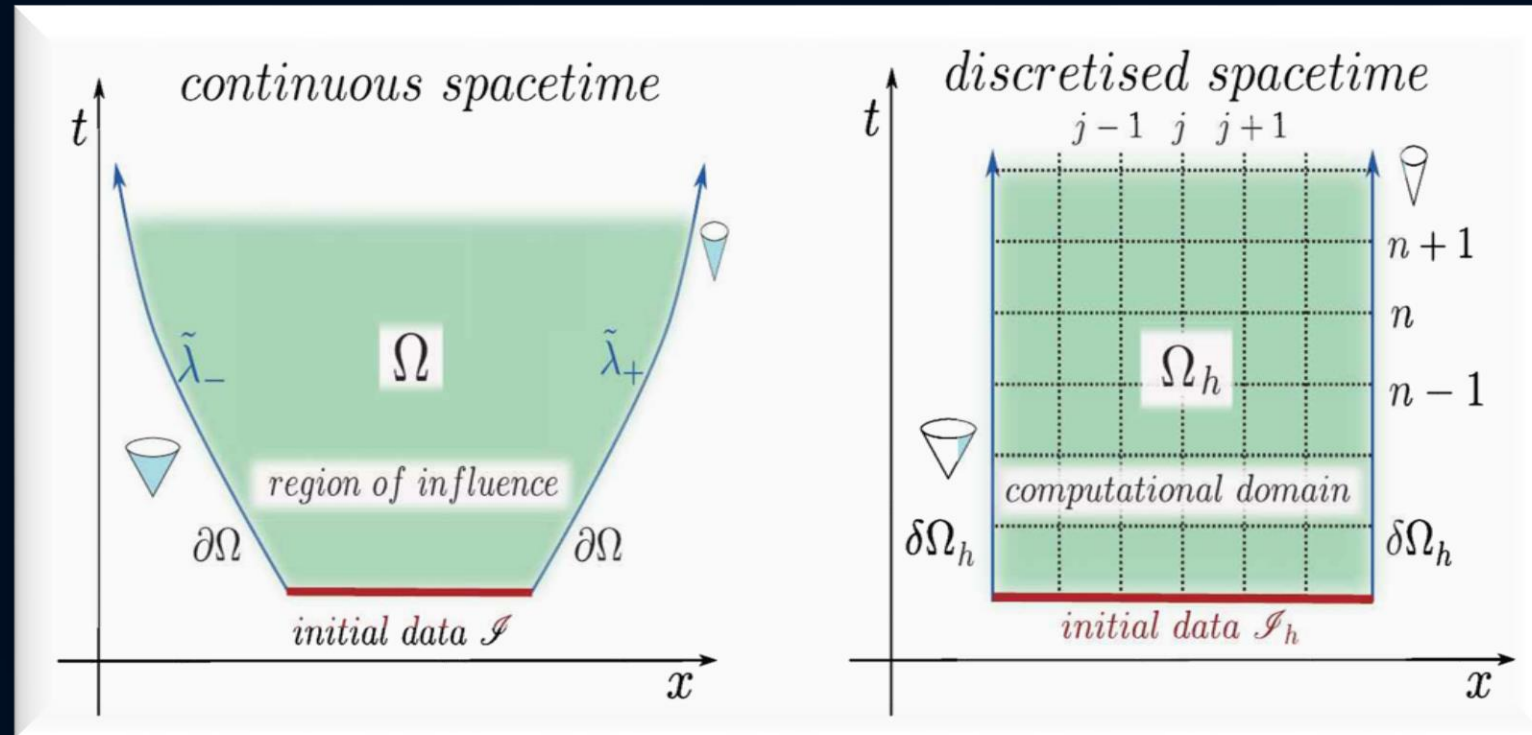
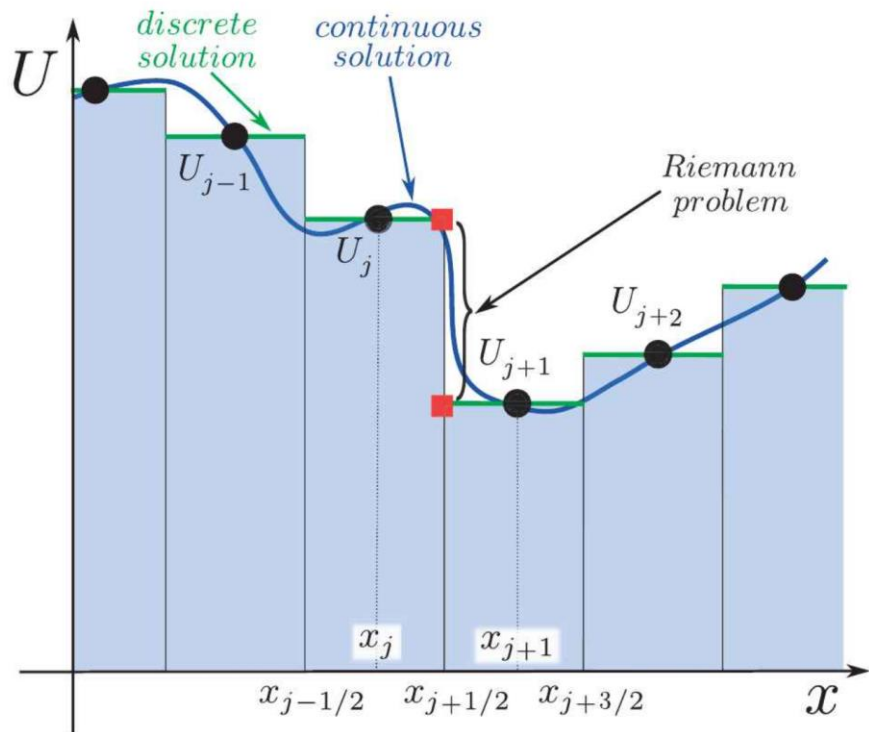
Extrinsic Curvature:

$$K_{\mu\nu} := -\gamma^\lambda_\mu \nabla_\lambda n_\nu$$



Finite difference methods

Discretisation of a hyperbolic initial value boundary problem.



High resolution shock capturing methods (HRSC methods) are needed, when Riemann problems of discontinuous properties and shocks needs to be evolved accurately.

From ADM to BSSNOK

Unfortunately the ADM equations are only weakly hyperbolic (mixed derivatives in the three dimensional Ricci tensor) and therefore not "well posed". It can be shown that by using a conformal traceless transformation, the ADM equations can be written in a hyperbolic form. This reformulation of the ADM equations is known as the BSSNOK (Baumgarte, Shapiro, Shibata, Nakamuro, Oohara, Kojima) formulation of the Einstein equation. Most of the numerical codes use this (or even better the CCZ4) formulation.

The 3+1 Valencia Formulation of the Relativistic Hydrodynamic Equations

$$\begin{aligned}\nabla_{\mu}(\rho u^{\mu}) &= 0, \\ \nabla_{\nu}T^{\mu\nu} &= 0.\end{aligned}$$

To guarantee that the numerical solution of the hydrodynamical equations (the conservation of rest mass and energy-momentum) converge to the right solution, they need to be reformulated into a conservative formulation. Most of the numerical "hydro codes" use here the 3+1 Valencia formulation.

Computersimulation of a Neutron Star Merger in full General Relativity

**Credits: Cosima Breu, David Radice
and Luciano Rezzolla**



Density

8.5 14



$\lg(\rho)$ [g/cm³]

Temperature

0 50



T [MeV]

Numerical Setup

BSSNOK conformal traceless formulation of the ADM equations.
3+1 Valencia formulation and high resolution shock capturing methods for the hydrodynamic evolution. Full general relativity using the **Einstein-Toolkit** and the **WHISKY/WhiskyTHC code** for the general-relativistic hydrodynamic equations.

Grid Structure:

Adaptive mesh refinement (six ref. levels)

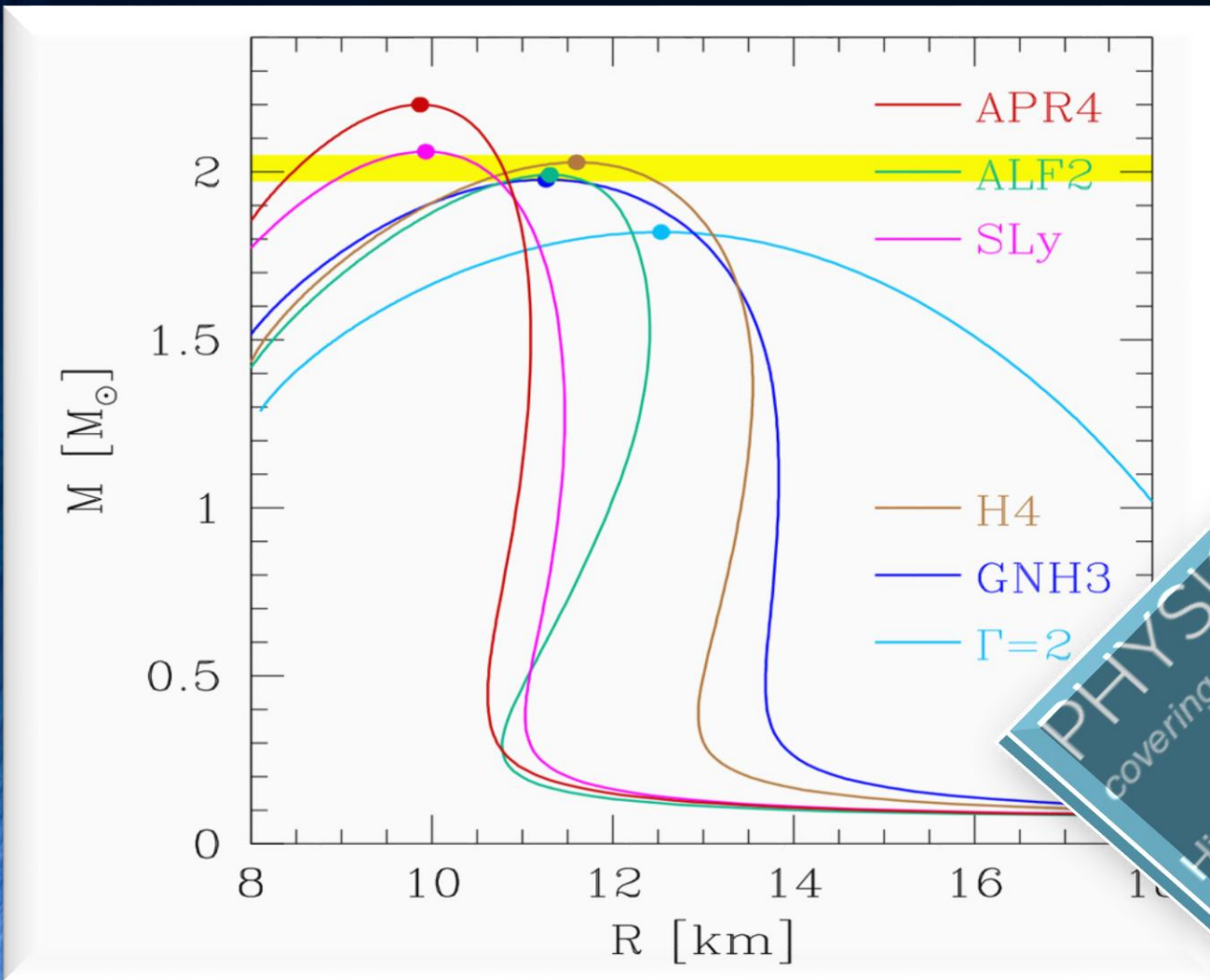
Grid resolution: (from 221 m to 7.1 km)

Outer Boundary: 759 km

Initial separation of stellar cores: 45 km

HMNS Evolution for different EoSs

High mass simulations ($M=1.35 M_{\text{solar}}$)



Mass-Radius relation for different EoSs

PHYSICAL REVIEW D
covering particles, fields, gravitation, and cosmology

Highlights Recent Accepted Authors Referees Search Press About

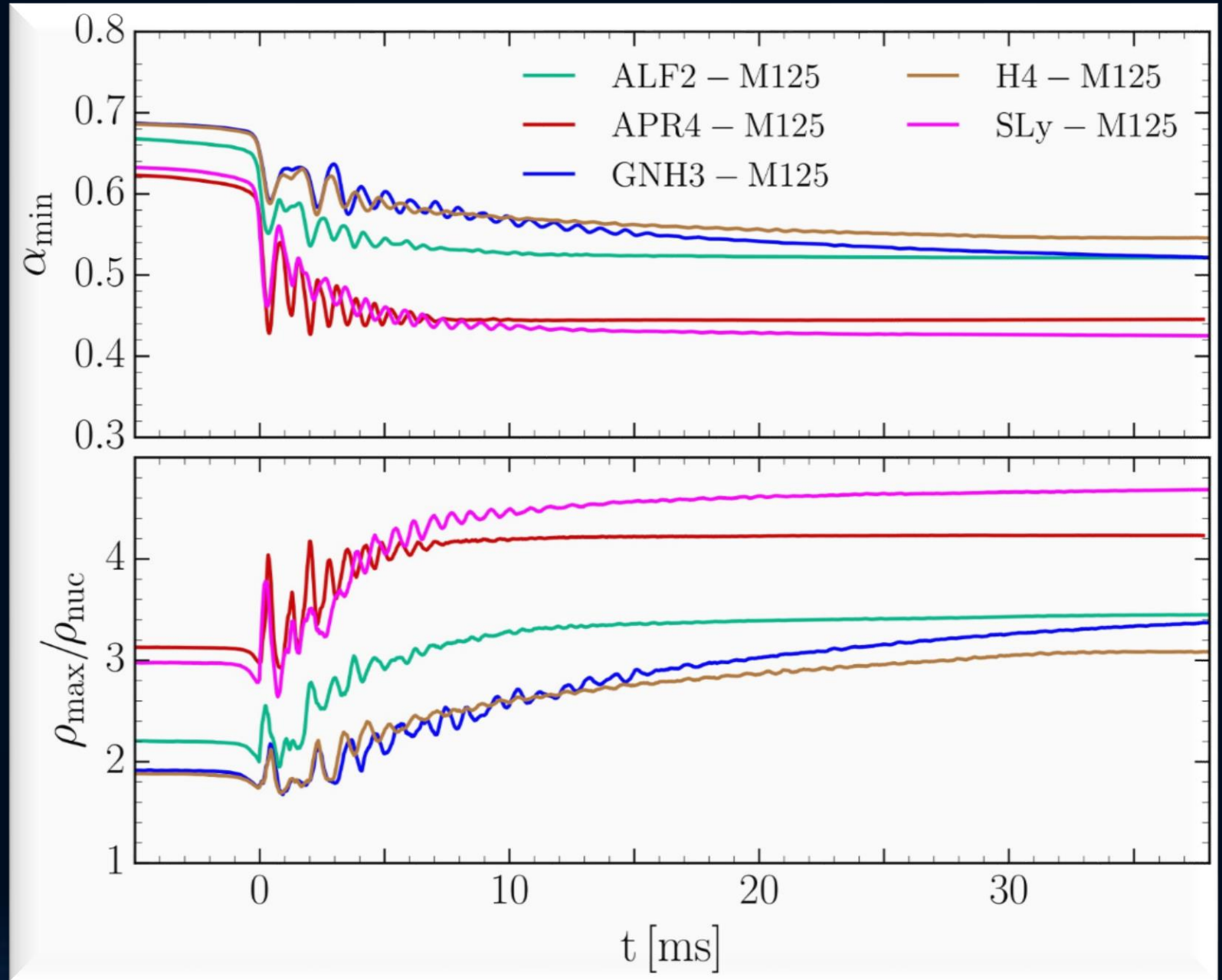
Rotational properties of hypermassive neutron stars from binary mergers

Matthias Hanauske, Kentaro Takami, Luke Bovard, Luciano Rezzolla, José A. Font, Filippo Galeazzi, and Horst Stöcker
Phys. Rev. D **96**, 043004 – Published 7 August 2017

HMNS Evolution for different EoSs

High mass simulations
($M=1.25 M_{\text{solar}}$)

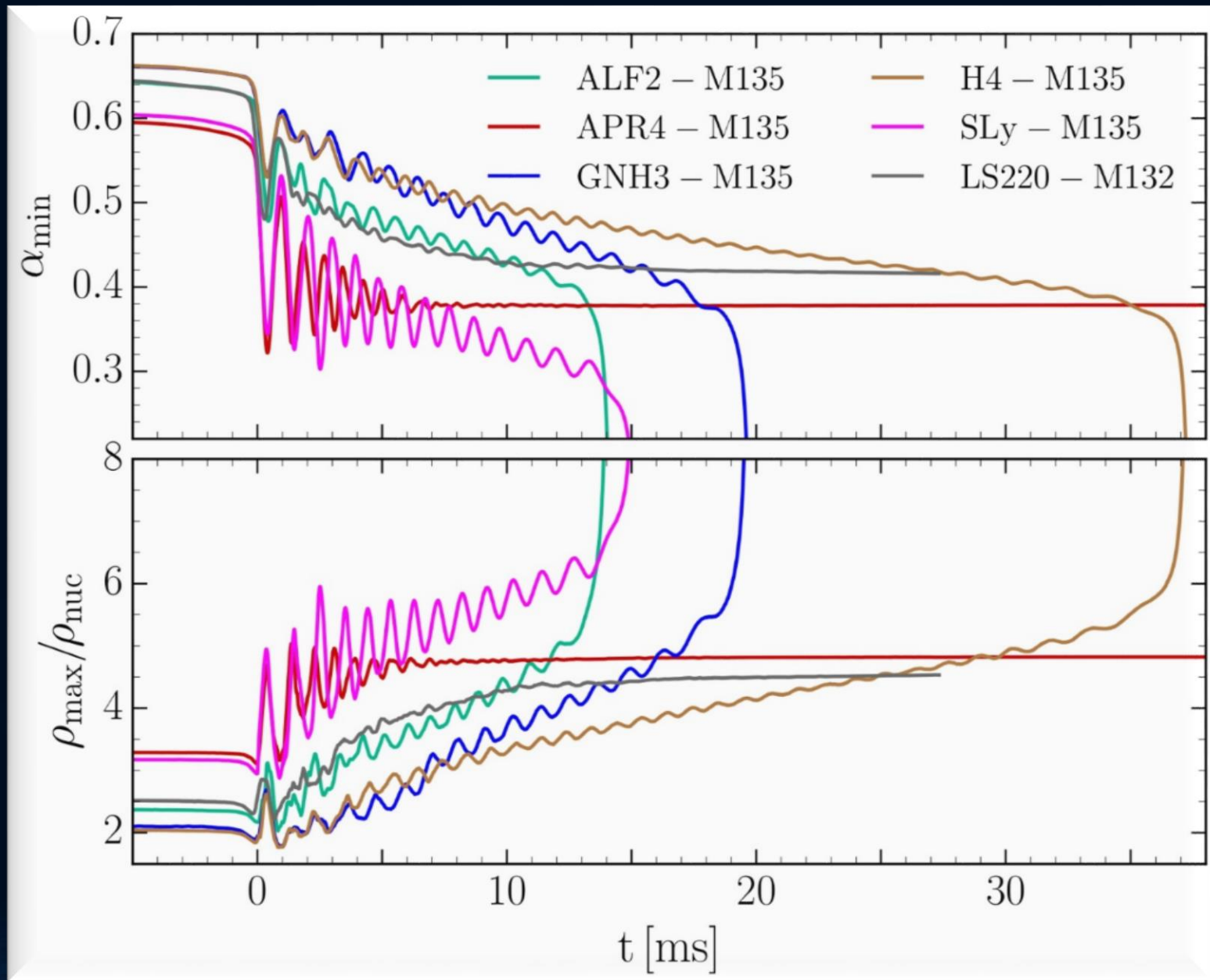
Central value of the lapse function α_c (upper panel) and maximum of the rest mass density ρ_{max} in units of ρ_0 (lower panel) versus time for the high mass simulations.



HMNS Evolution for different EoSs

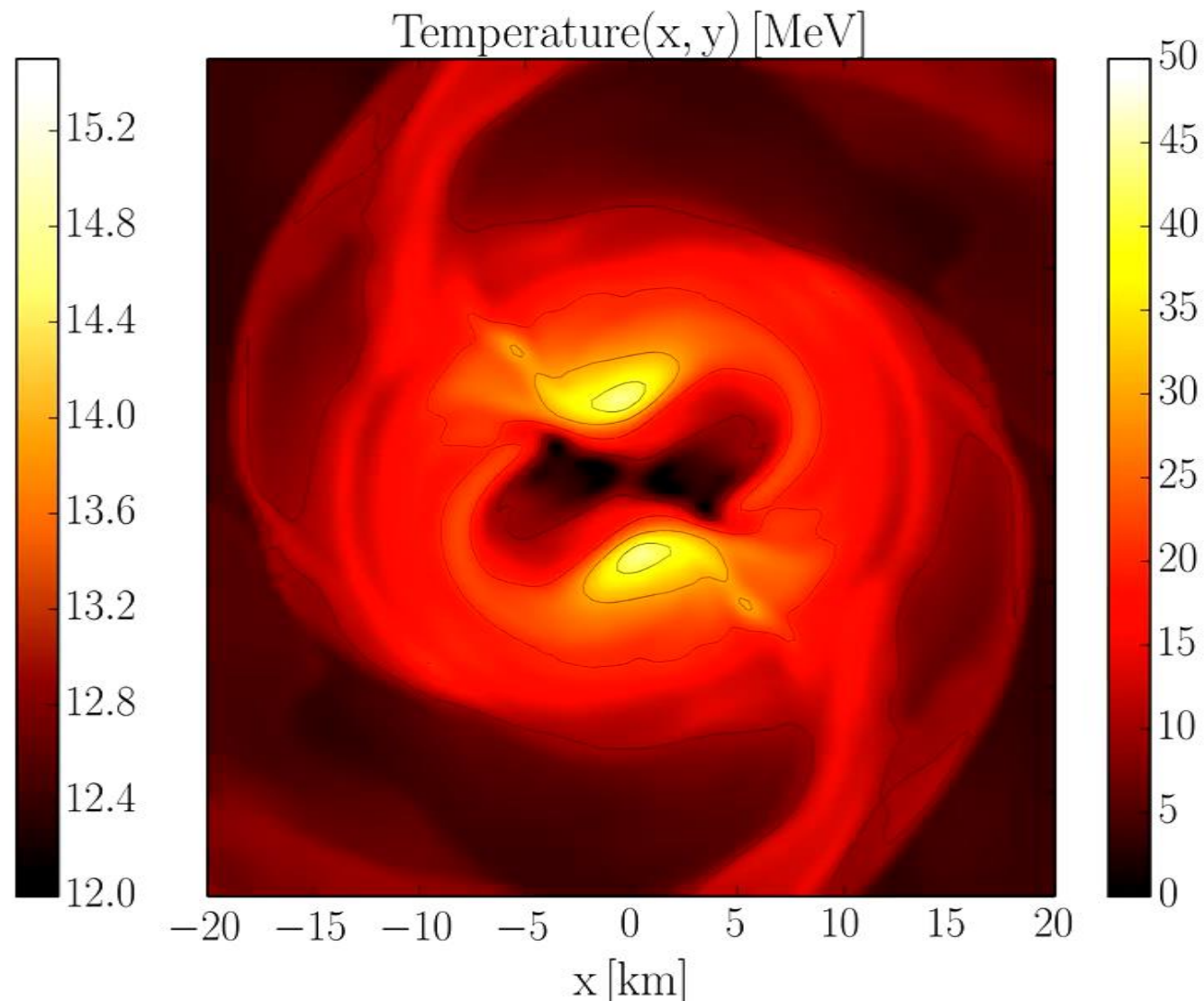
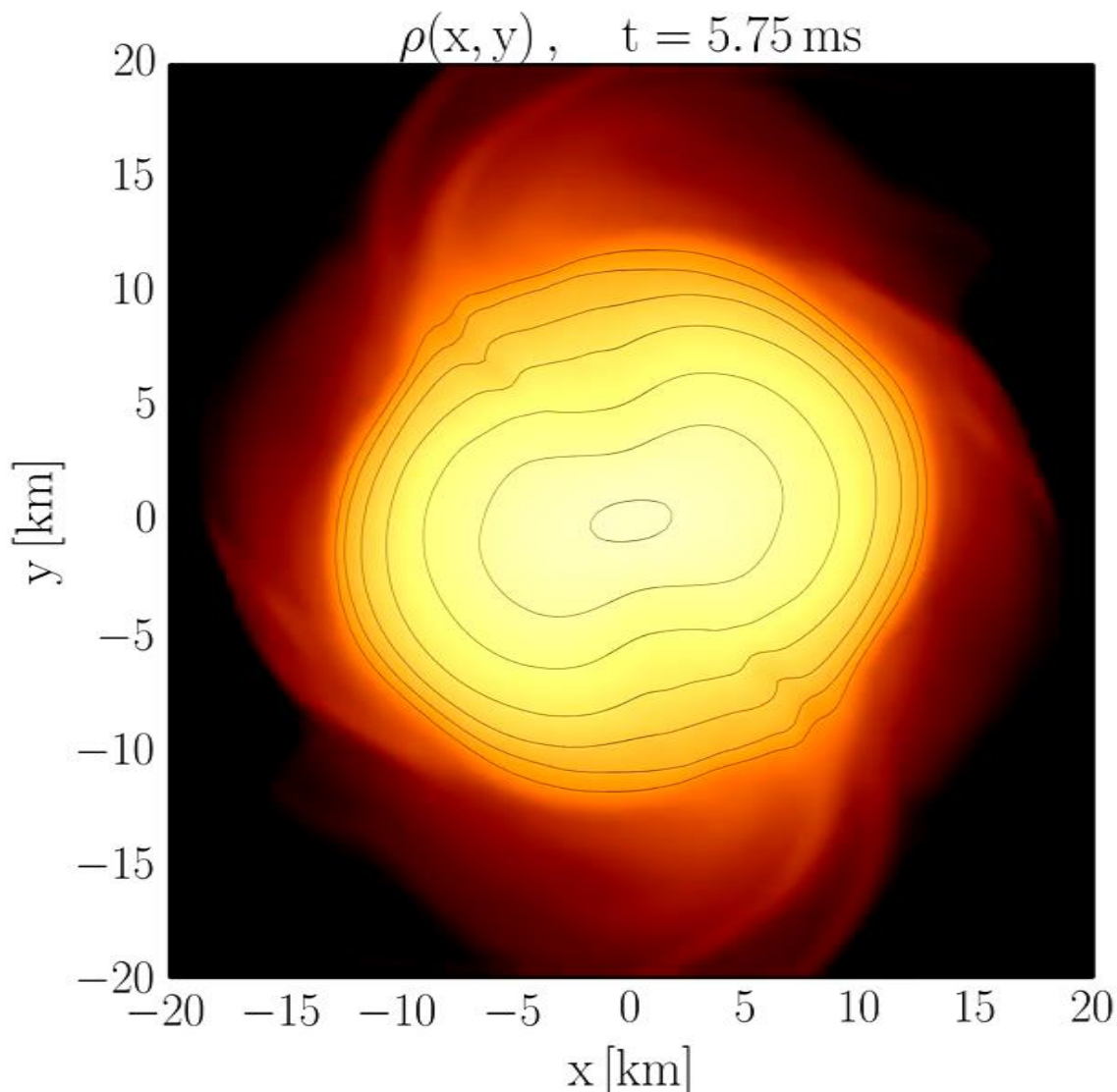
High mass simulations
($M=1.35 M_{\text{solar}}$)

Central value of the lapse function α_c (upper panel) and maximum of the rest mass density ρ_{max} in units of ρ_0 (lower panel) versus time for the high mass simulations.



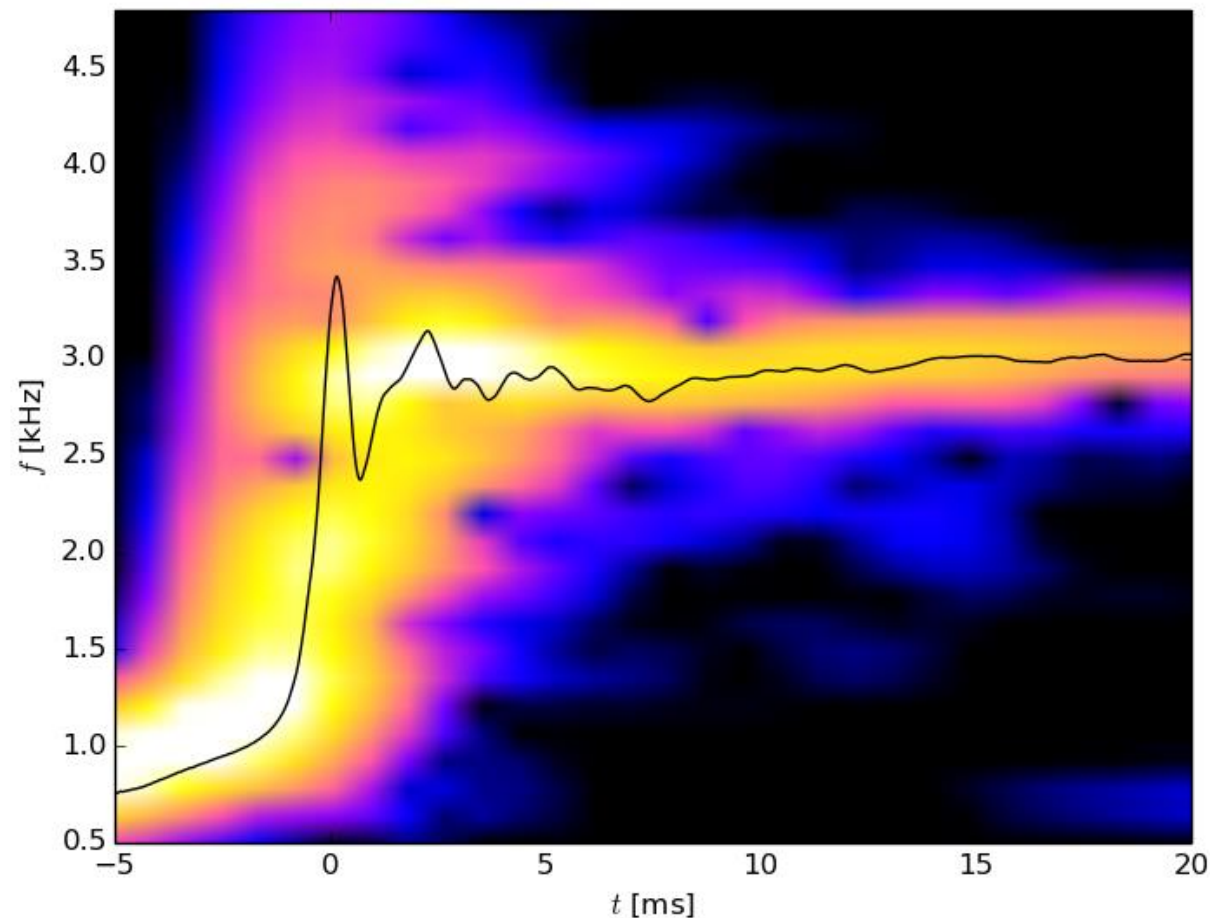
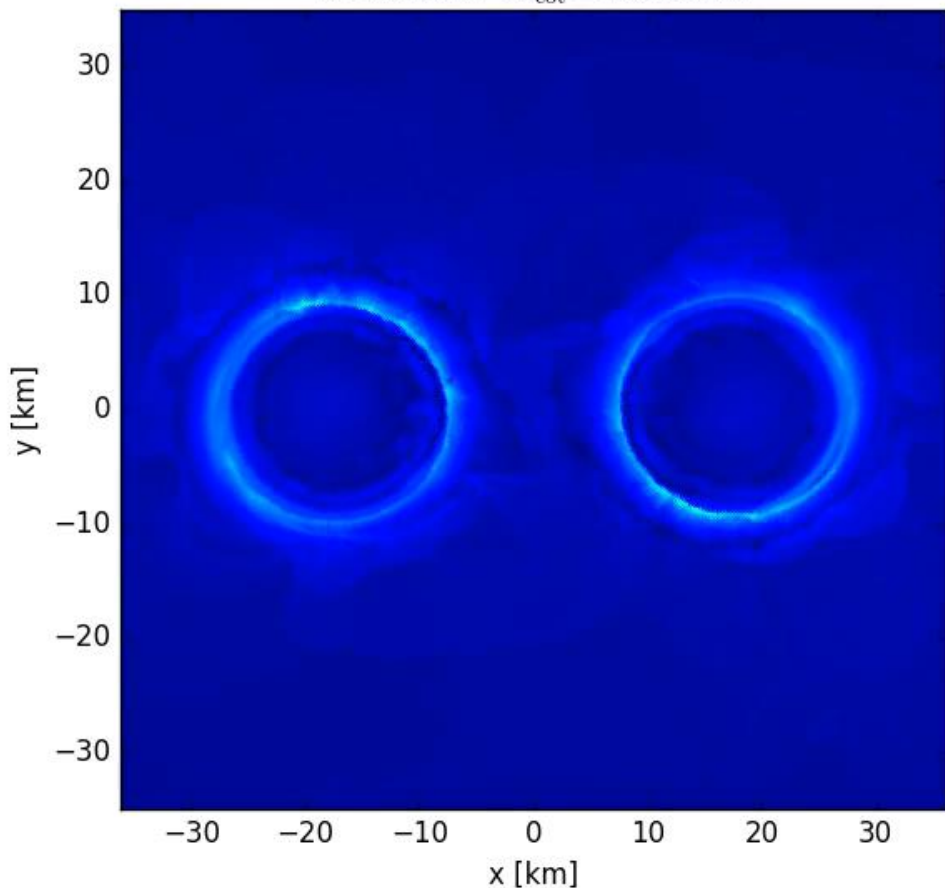
Logarithm of the density

Temperature



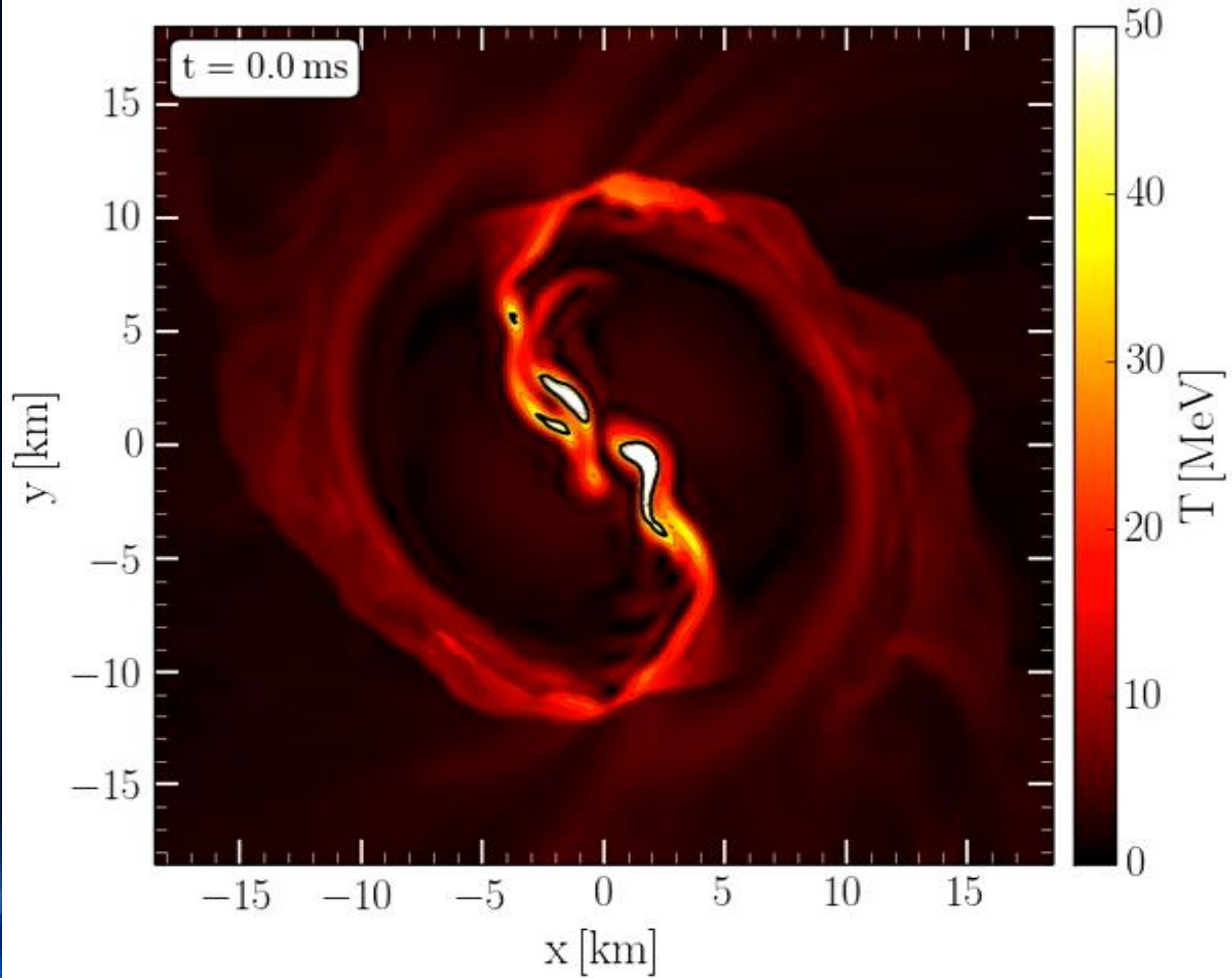
The Co-Rotating Frame

$t = 9.58\text{ms}$ $\Omega_{\text{cot}} = 387.20\text{Hz}$



- ² Note that the angular-velocity distribution in the lower central panel of Fig. 10 refers to the corotating frame and that this frame is rotating at half the angular frequency of the emitted gravitational waves, Ω_{GW} . Because the maximum of the angular velocity Ω_{max} is of the order of $\Omega_{\text{GW}}/2$ (cf. left panel of Fig. 12), the ring structure in this panel is approximately at zero angular velocity.

Simulation and movie has been produced by Luke Bovard

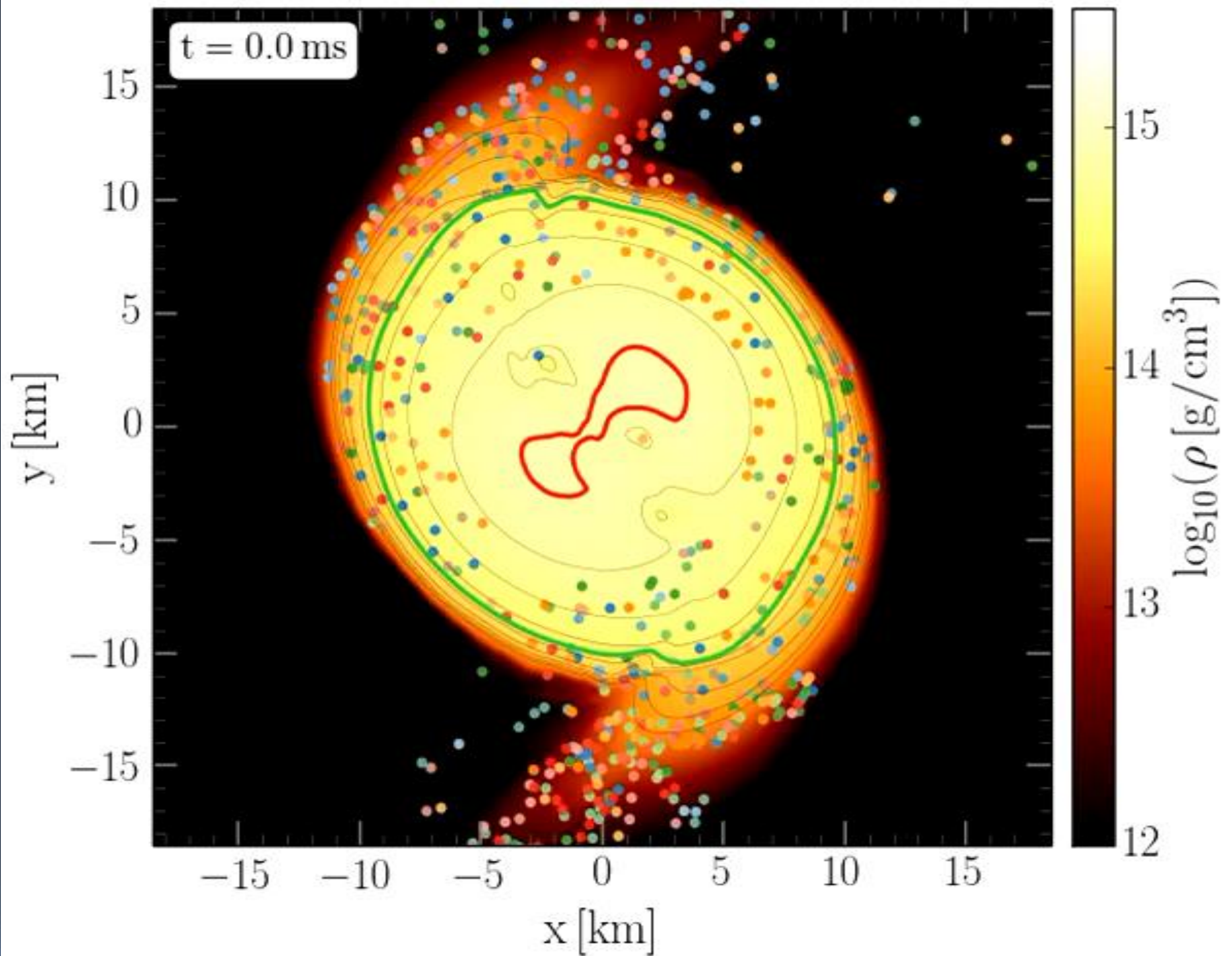


Evolution of Tracer-particles tracking individual fluid elements in the equatorial plane of the HMNS at post-merger times

M.G. Alford, L. Bovard, M. Hanauske, L. Rezzolla and K. Schwenzer

“On the importance of viscous dissipation and heat conduction in binary neutron-star mergers” (submitted to PRL, see arxiv)

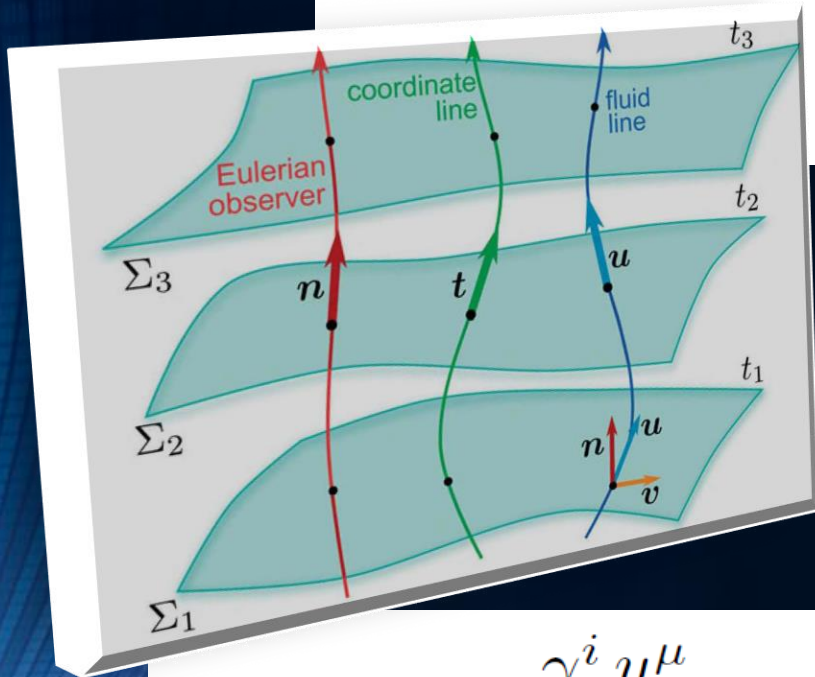
Different rotational behaviour of the quark-gluon-plasma produced in non-central ultra-relativistic heavy ion collisions
L. Adamczyk et.al., “Global Lambda-hyperon polarization in nuclear collisions: evidence for the most vortical fluid”, Nature 548, 2017



The Angular Velocity in the (3+1)-Split

$$\Omega(x, y, z, t) = \Omega = \frac{d\phi}{dt} = \frac{dx^\phi}{dt} = \quad \text{with: } x^\mu = (t, r, \phi, \theta) \quad (1)$$

$$= \frac{dx^\phi}{dt} = \frac{\frac{dx^\phi}{d\tau}}{\frac{dt}{d\tau}} = \frac{u^\phi}{u^t} \quad \text{with: } u^\mu = \frac{dx^\mu}{d\tau}$$



The angular velocity Ω in the (3+1)-Split is a combination of the lapse function α , the ϕ -component of the shift vector β^ϕ and the 3-velocity v^ϕ of the fluid (spatial projection of the 4-velocity \mathbf{u}):

$$v^i = \frac{\gamma^i_\mu u^\mu}{-n_\mu u^\mu} = \frac{1}{\alpha} \left(\frac{u^i}{u^t} - \beta^i \right) \quad \text{with: } i = 1, 2, 3 \text{ and } \mu = 0, 1, 2, 3$$

$$\Leftrightarrow \frac{u^i}{u^t} = \alpha v^i - \beta^i \quad \text{Insert in (1)} \Rightarrow \quad \Omega = \frac{d\phi}{dt} = \frac{u^\phi}{u^t} = \alpha v^\phi - \beta^\phi$$

The Angular Velocity in the (3+1)-Split

The angular velocity Ω in the (3+1)-Split is a combination of the lapse function α , the ϕ -component of the shift vector β^ϕ and the 3-velocity v^ϕ of the fluid (spatial projection of the 4-velocity \mathbf{u}):

**(3+1)-decomposition
of spacetime:**

$$\Omega(x, y, z, t) = \frac{u^\phi}{u^t} = \alpha v^\phi - \beta^\phi$$

$$g_{\mu\nu} = \begin{pmatrix} -\alpha^2 + \beta_i \beta^i & \beta_i \\ \beta_i & \gamma_{ij} \end{pmatrix}$$

Angular velocity
 Ω

Lapse function
 α

Φ -component of
3-velocity v^ϕ

Frame-dragging
 β^ϕ

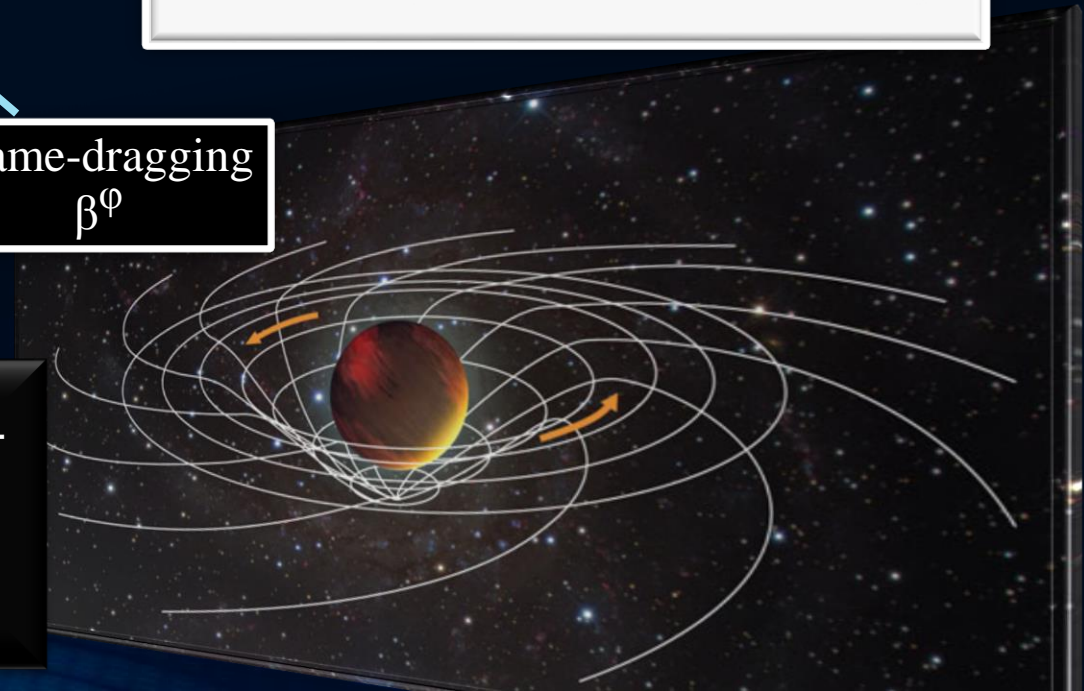
Focus: Inner core of the differentially rotating HMNS

M. Shibata, K. Taniguchi, and K. Uryu, Phys. Rev. D 71, 084021 (2005)

M. Shibata and K. Taniguchi, Phys. Rev. D 73, 064027 (2006)

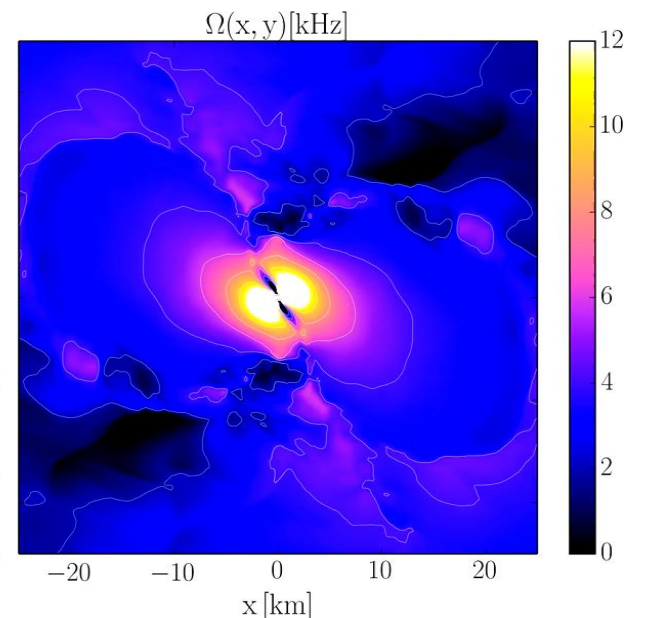
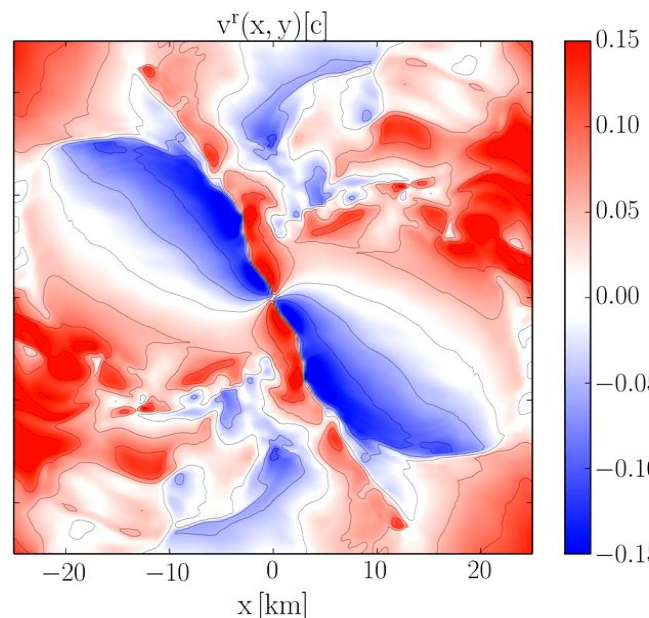
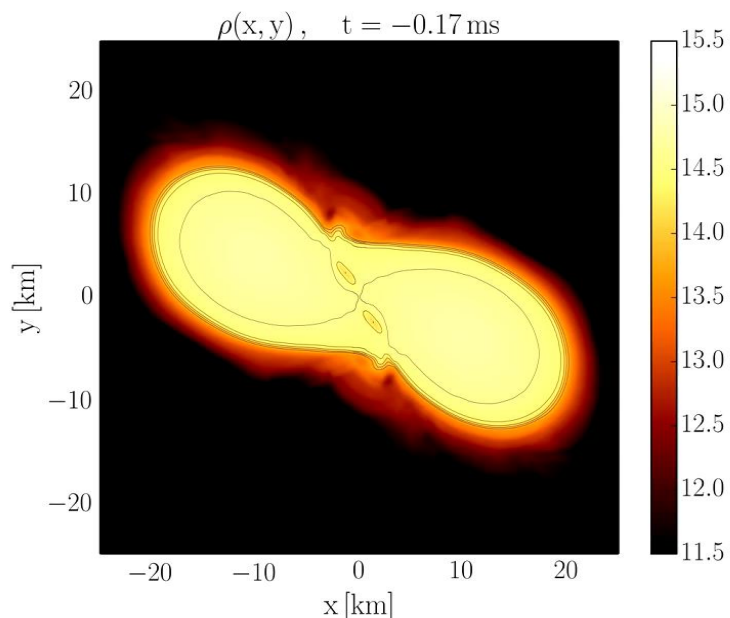
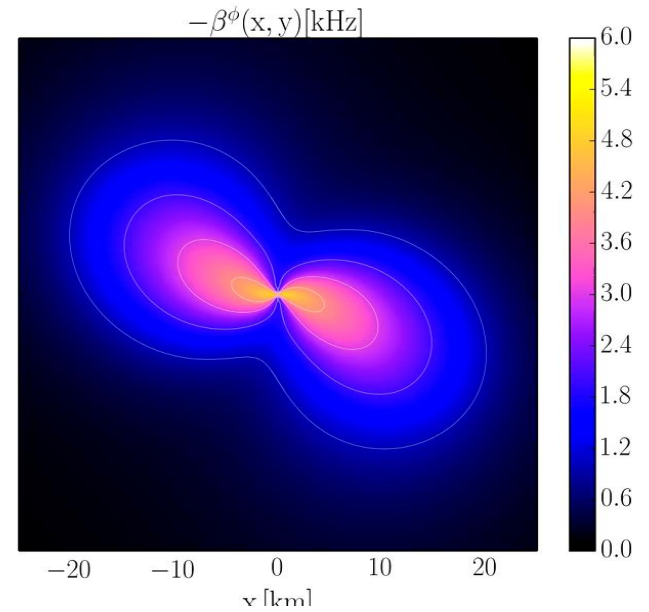
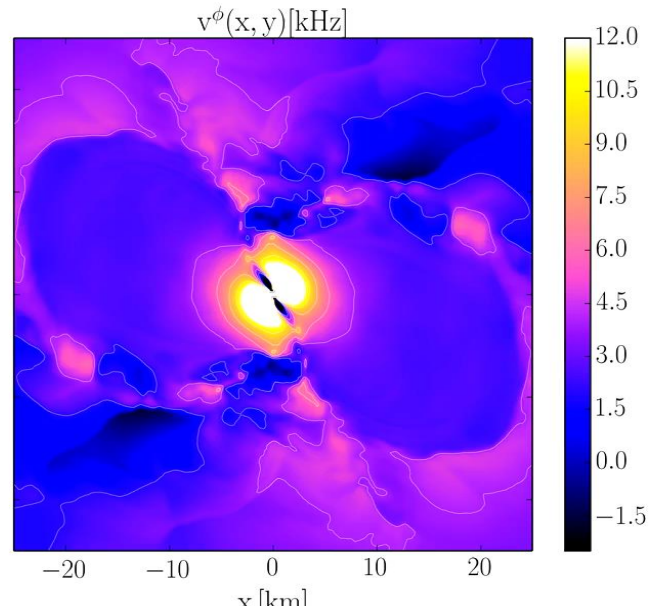
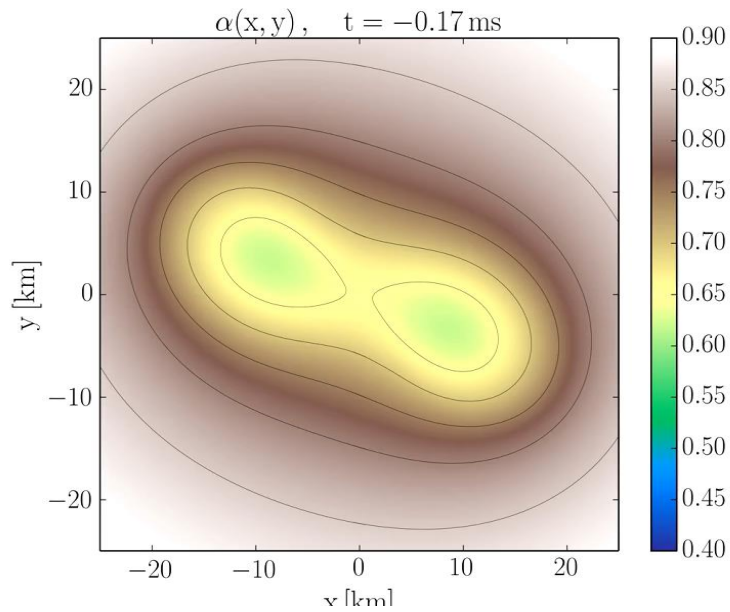
F. Galeazzi, S. Yoshida and Y. Eriguchi, A&A 541, p. A156 (2012)

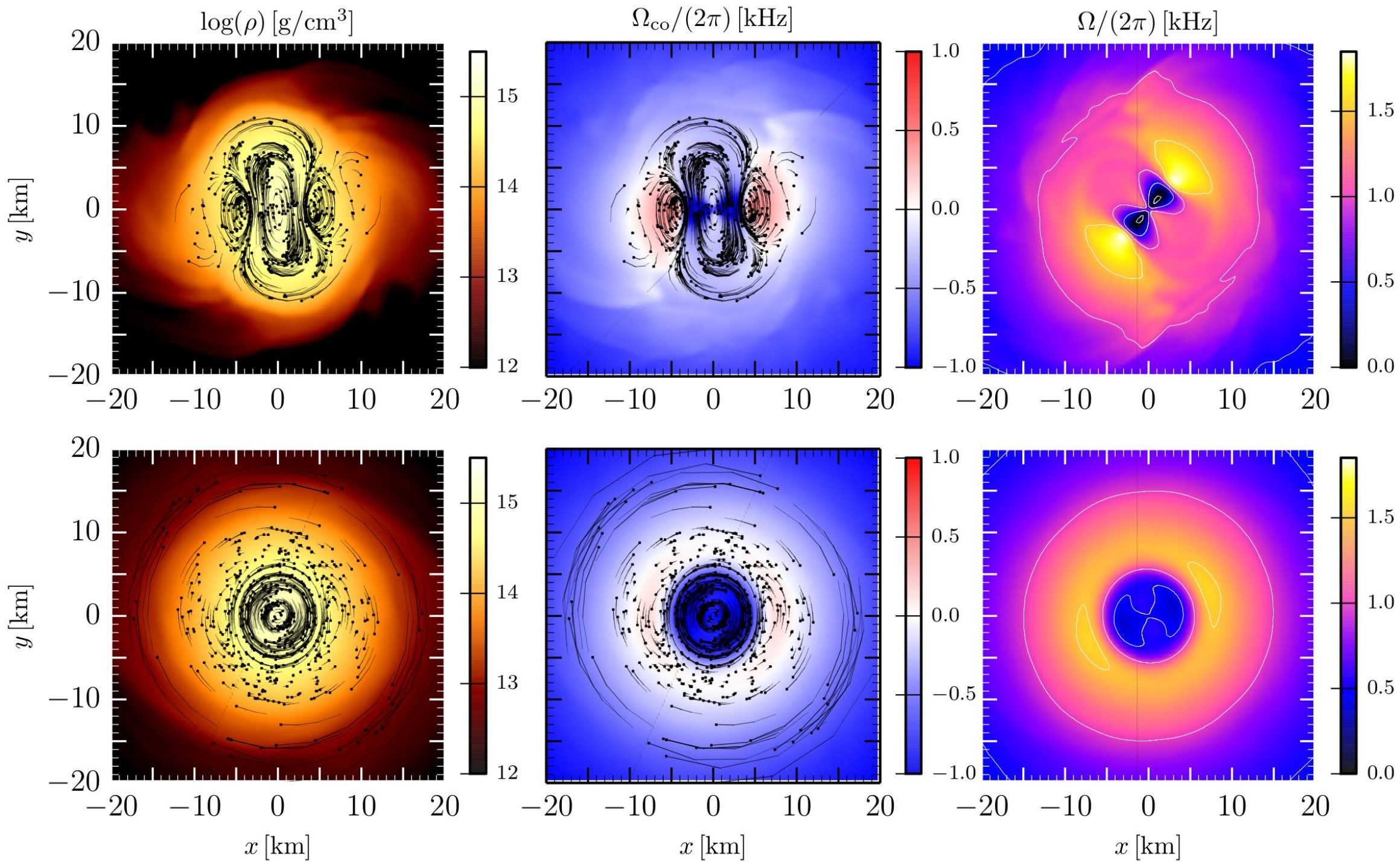
W. Kastaun and F. Galeazzi, Phys. Rev. D 91, p. 064027 (2015)

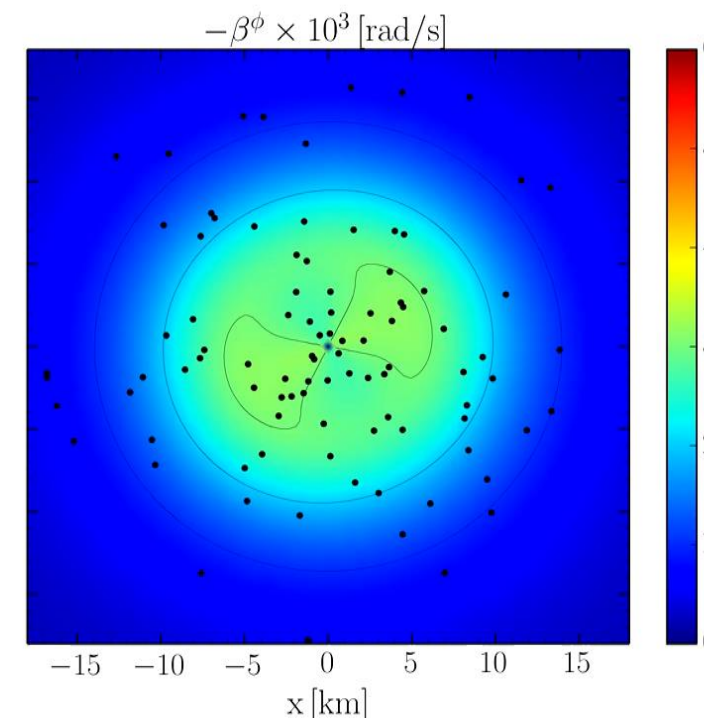
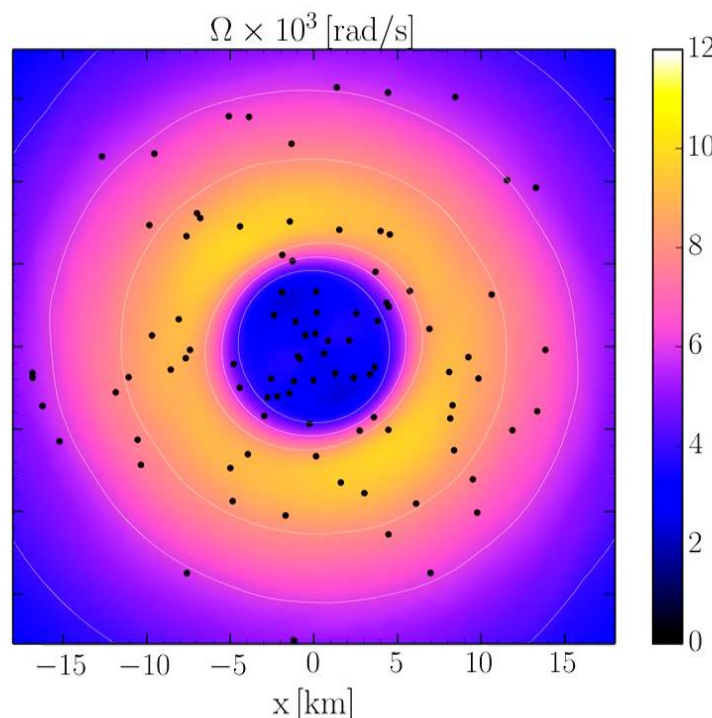
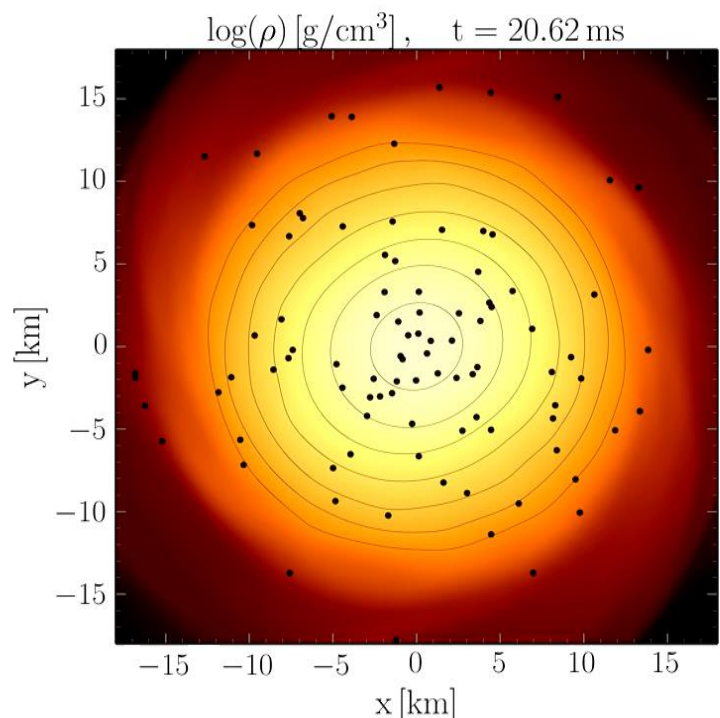
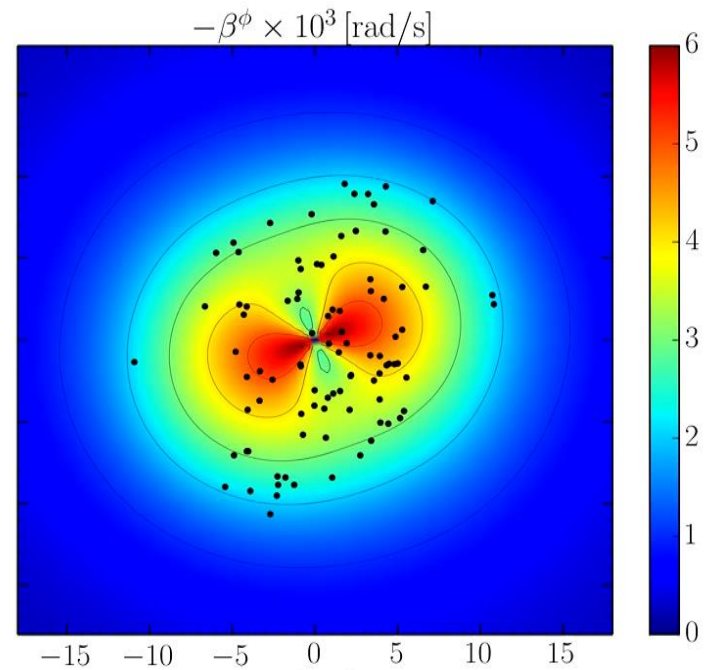
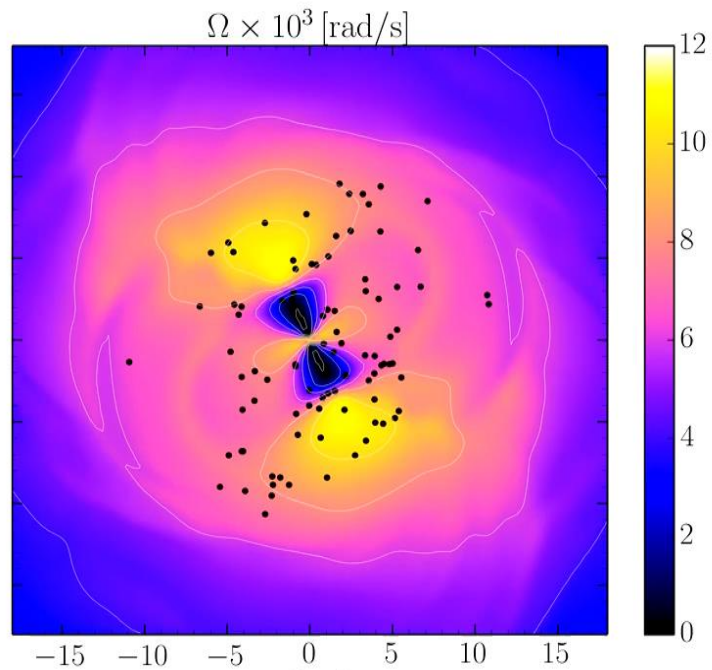
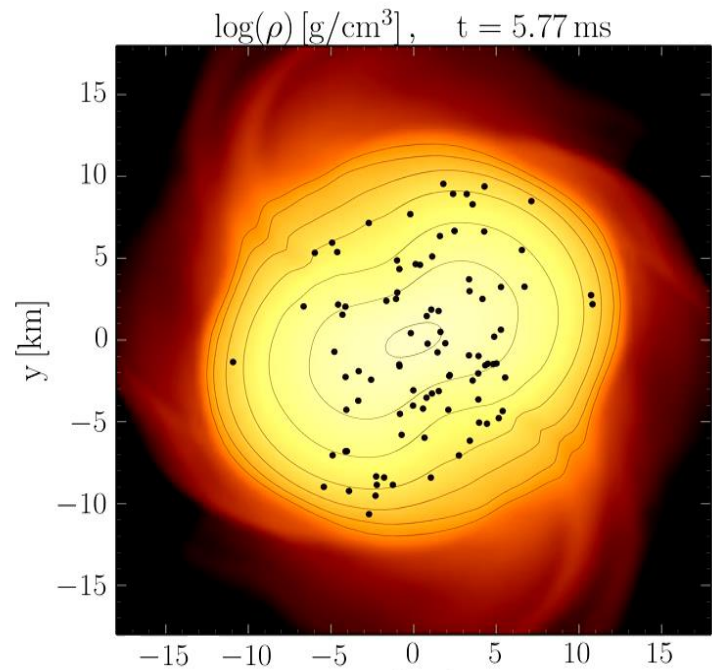


The Structure of Ω

$$\Omega(x, y, z, t) = \frac{u^\phi}{u^t} = \alpha v^\phi - \beta^\phi$$

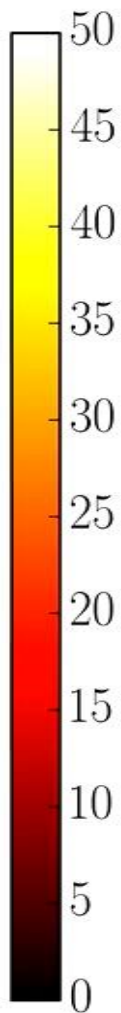
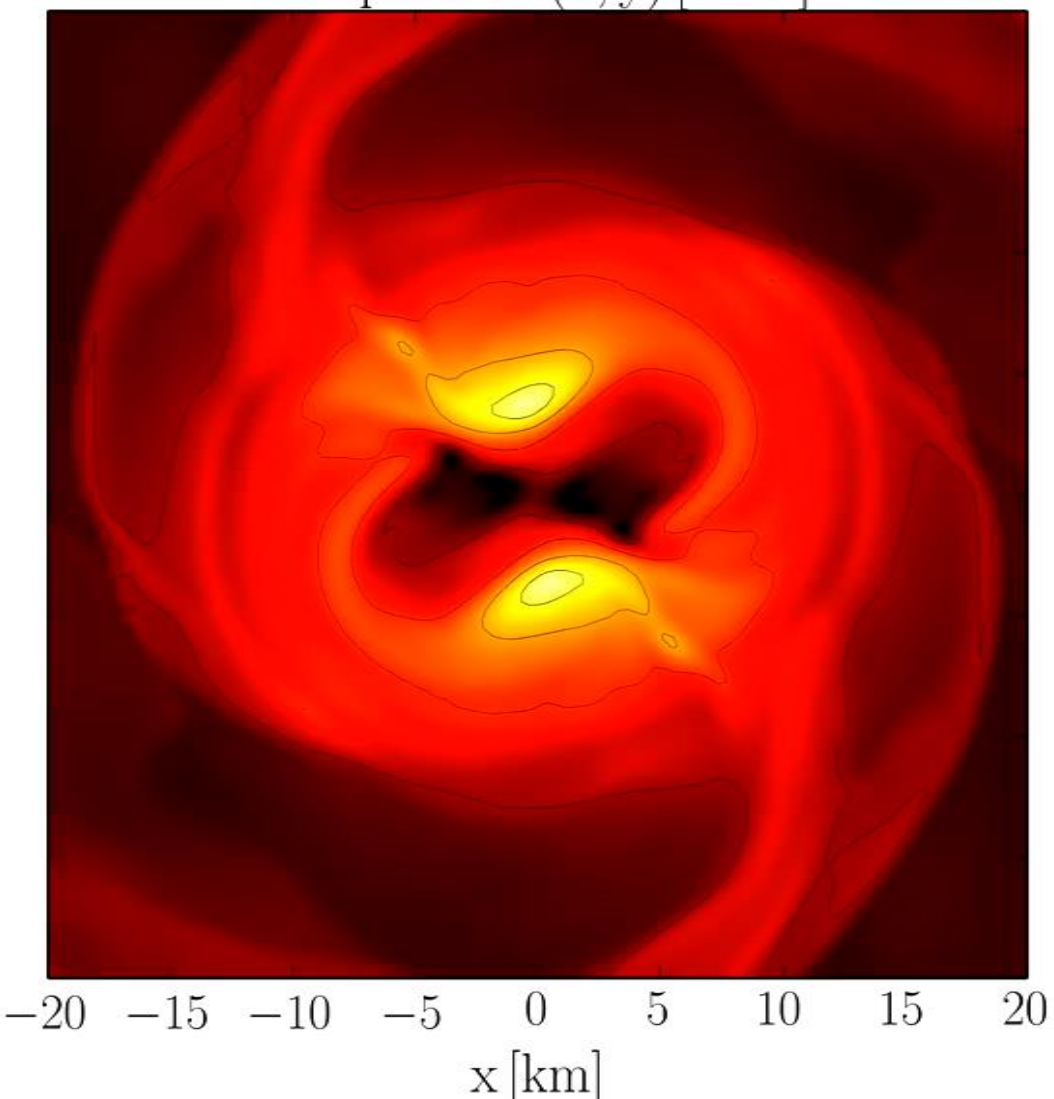






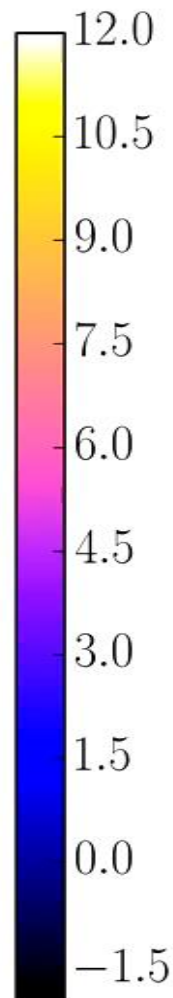
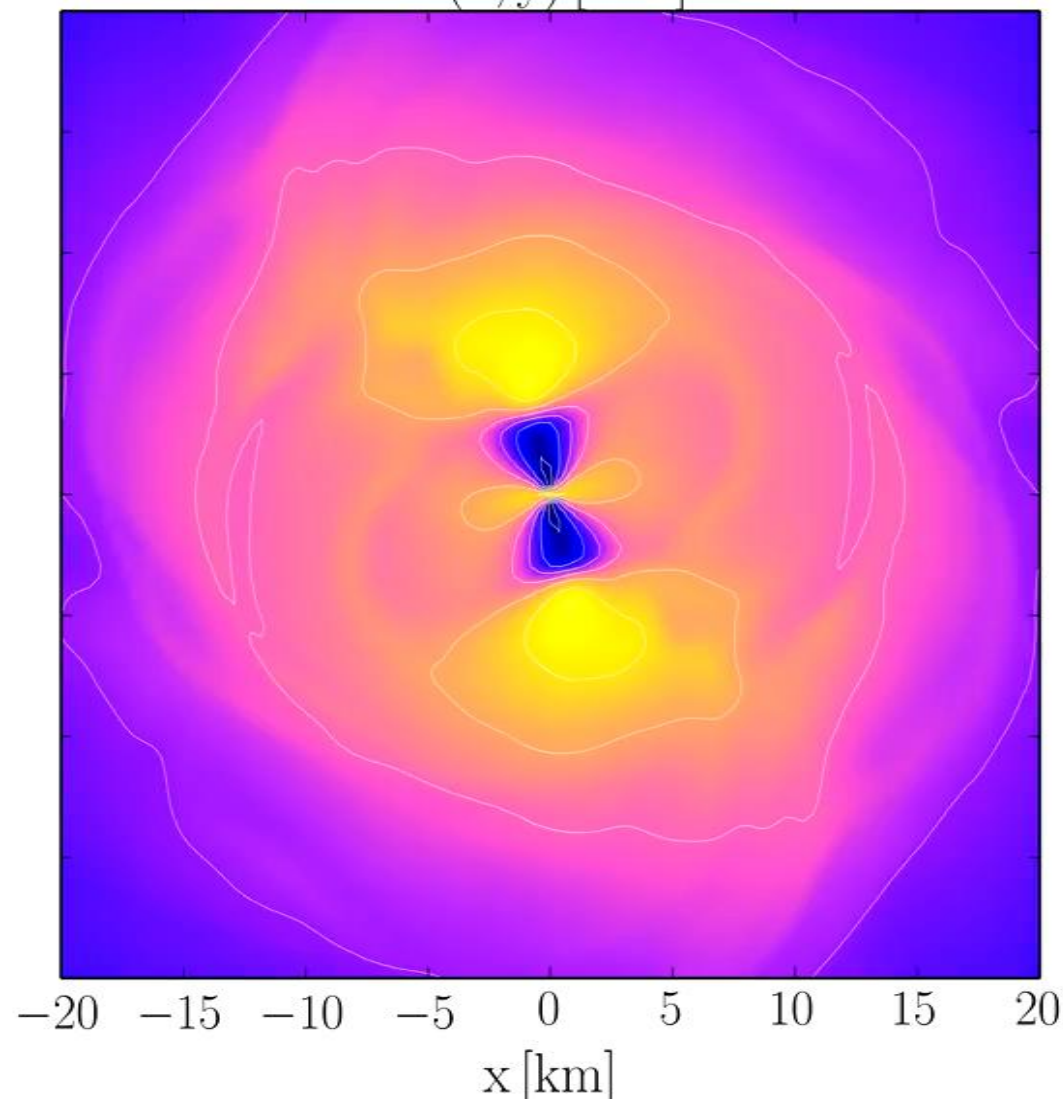
Temperature

Temperature(x, y) [MeV]



Angular Velocity

$\Omega(x, y)$ [kHz]



Averaging Procedure for Ω

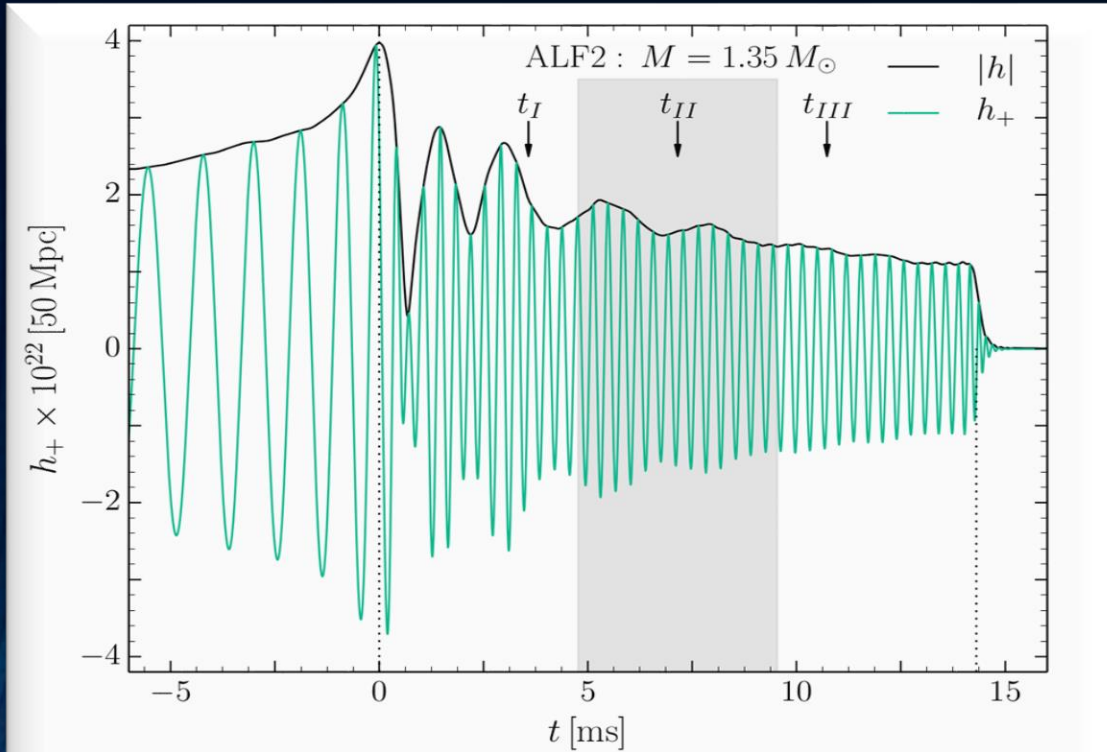


FIG. 2. Gravitational wave amplitude $|h|$ and h_+ at a distance of 50 Mpc for the ALF2-M135 model.

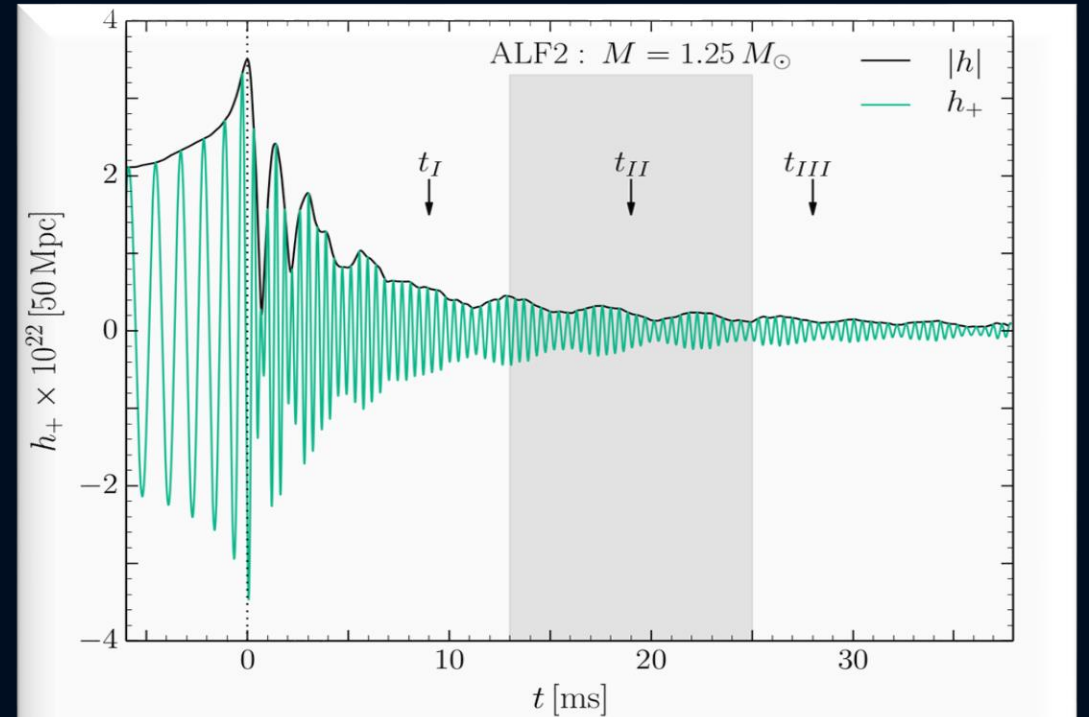
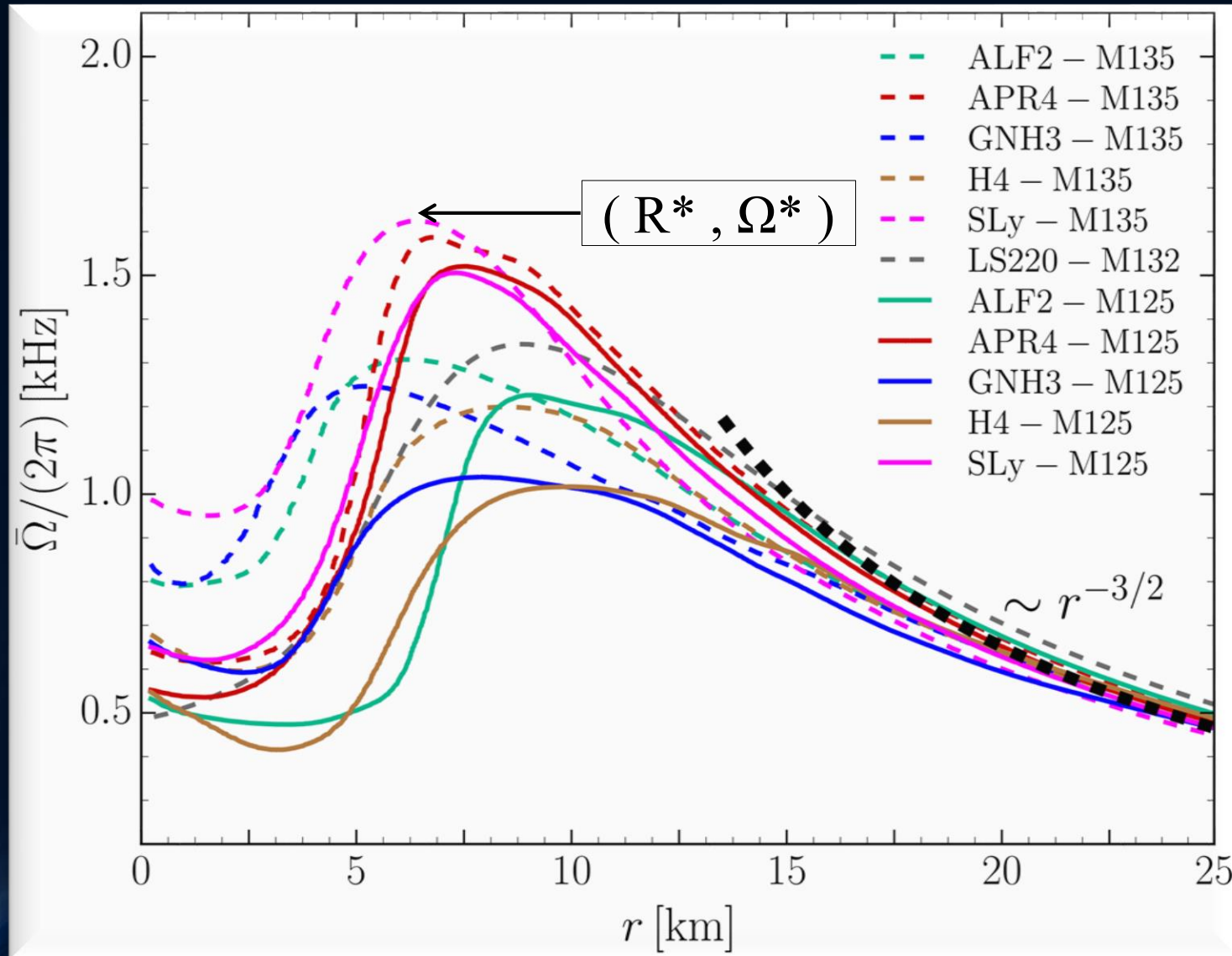


FIG. 10. Gravitational wave amplitude h_+ and $|h|$ at a distance of 50 Mpc for the ALF2-M125 model.

$$\bar{\Omega}(r, t_c) = \int_{t_c - \Delta t/2}^{t_c + \Delta t/2} \int_{-\pi}^{\pi} \Omega(r, \phi, t') d\phi dt'$$

In order to compare the structure of the rotation profiles between the different EOSs, a certain time averaging procedure has been used:

Time-averaged Rotation Profiles of the HMNSs



Soft EoSs:

Sly
APR4

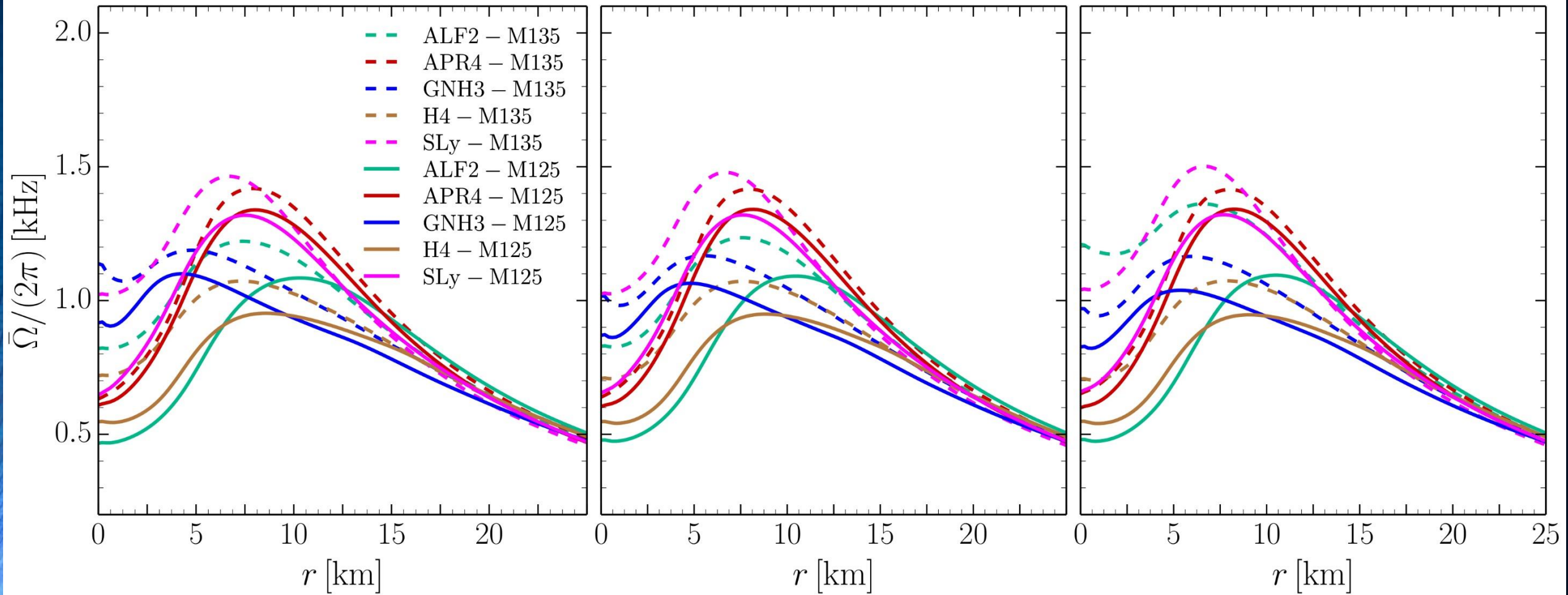
Stiff EoSs:

GNH3
H4

Time-averaged rotation profiles for different EoS
Low mass runs (solid curves), high mass runs (dashed curves).

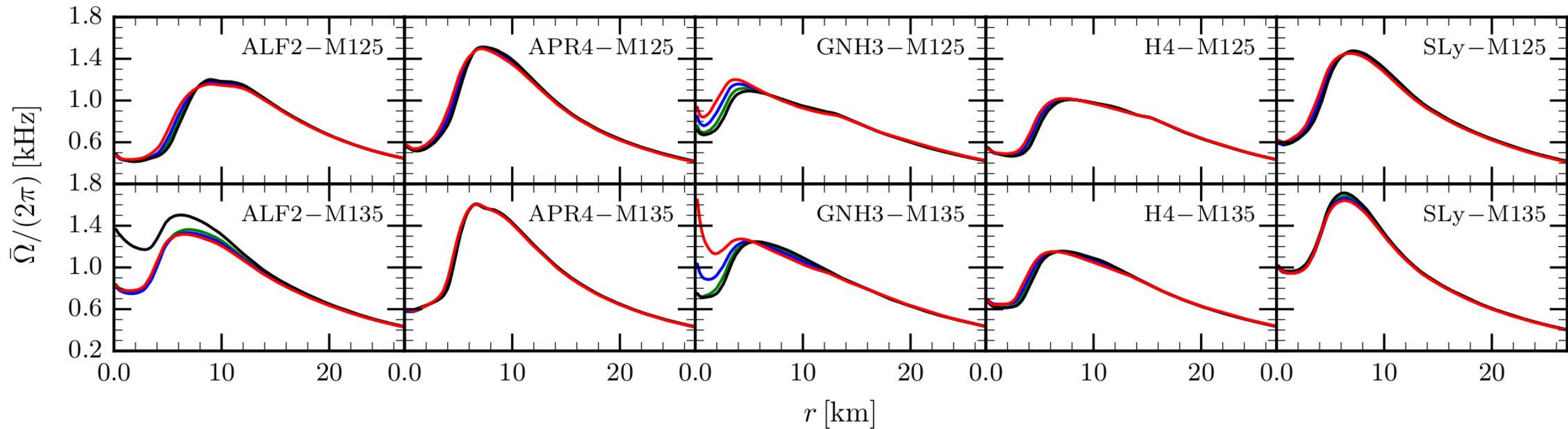
Dependence on the time averaging window

For all EOS the same time averaging window. From the left to right the data refer to time windows [6 ; 11]; [6 ; 13] and [6 ; 15] ms, respectively.

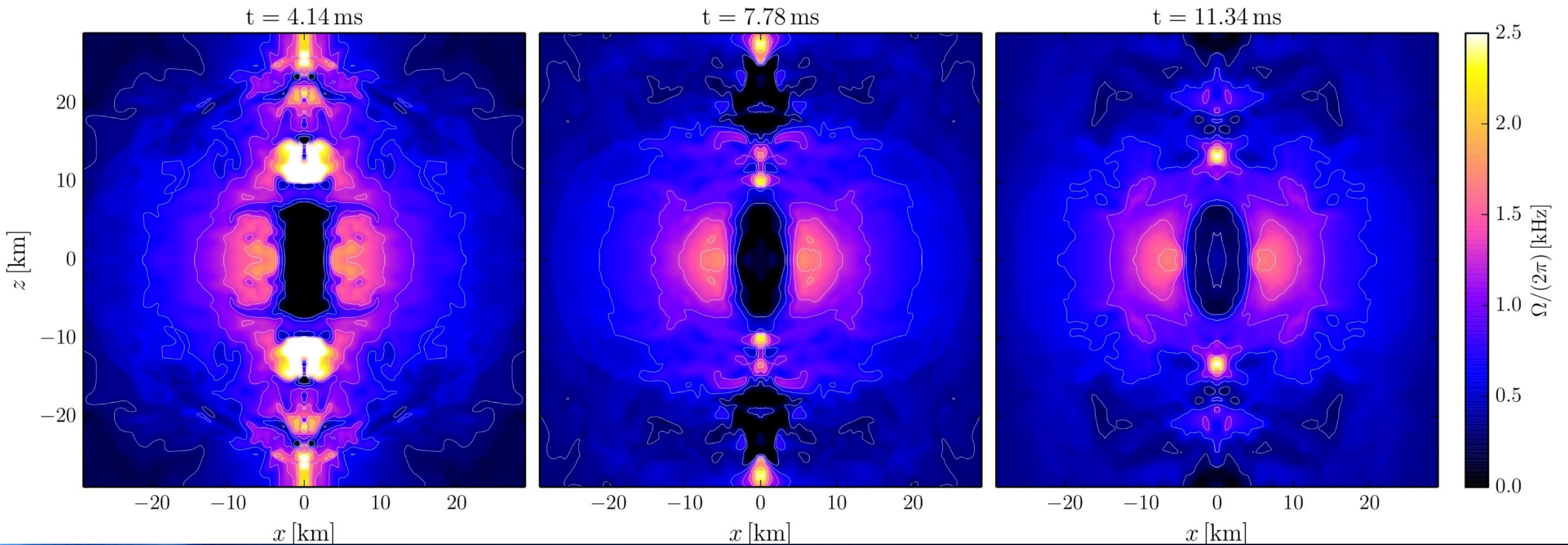


Dependence on the time averaging window

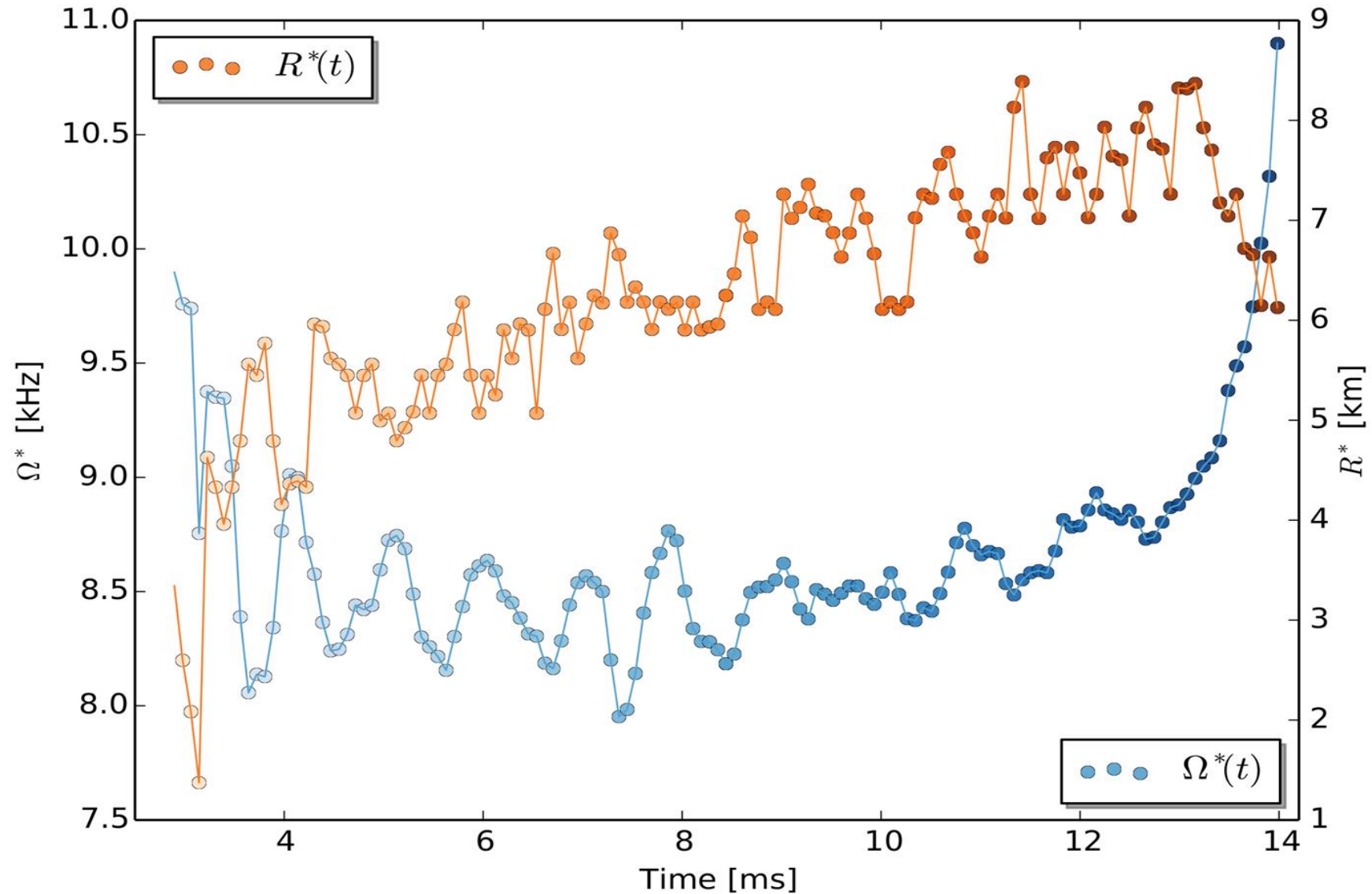
Averaged angular-velocity profiles when the averaging window is set to be 7 ms for all EOSs and masses, but where the initial averaging time is varied and set to be 5 (red line), 6 (blue line), 7 (green line), and 8 ms (black line), respectively. The four lines refer to averaging windows given by [5; 12], [6; 13], [7; 14], and [8; 15] ms, respectively; note that the top part of each panel refers to the low-mass binary, while the bottom one to the high-mass one.



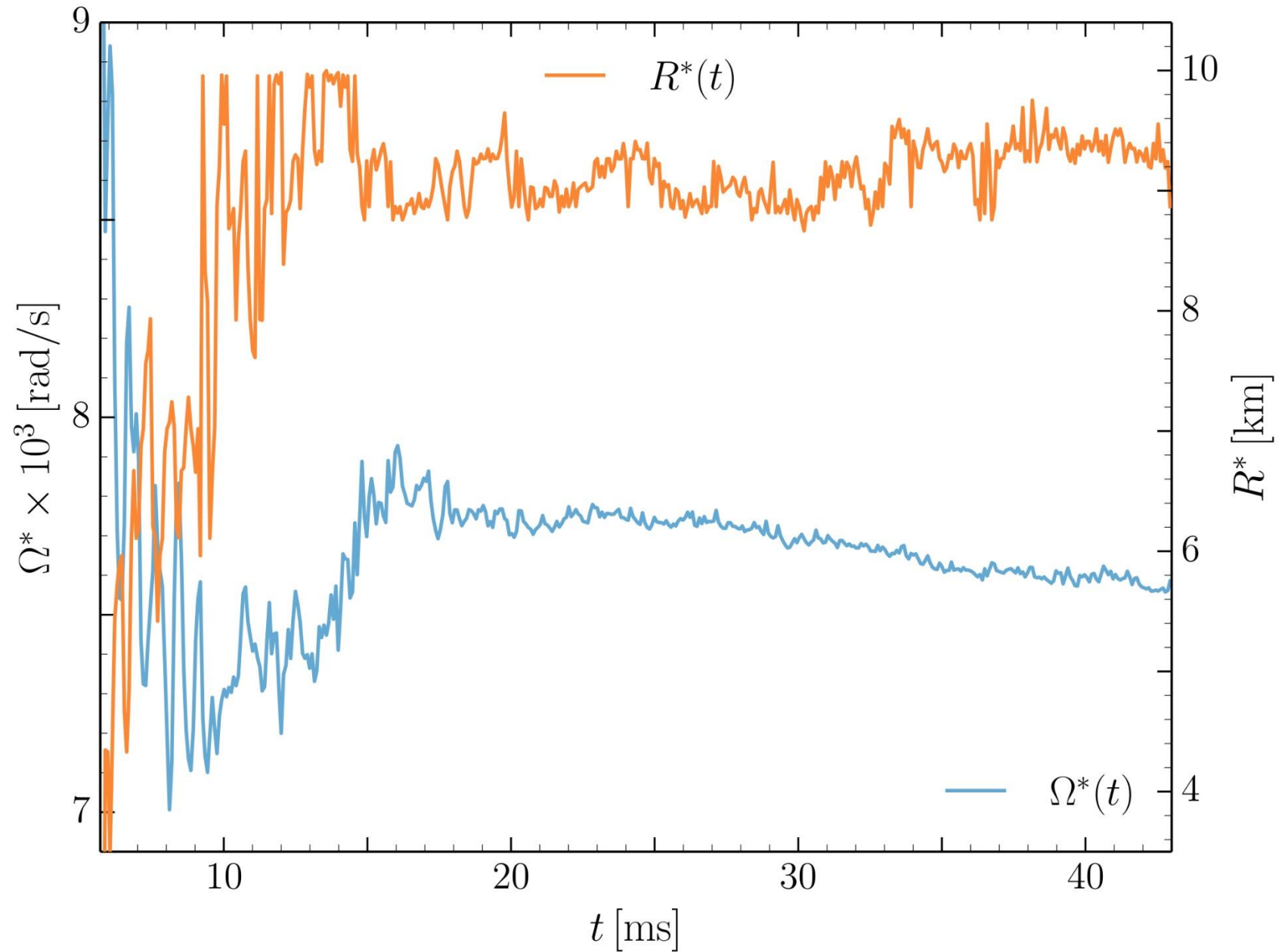
Angular Velocity away from the equatorial plane



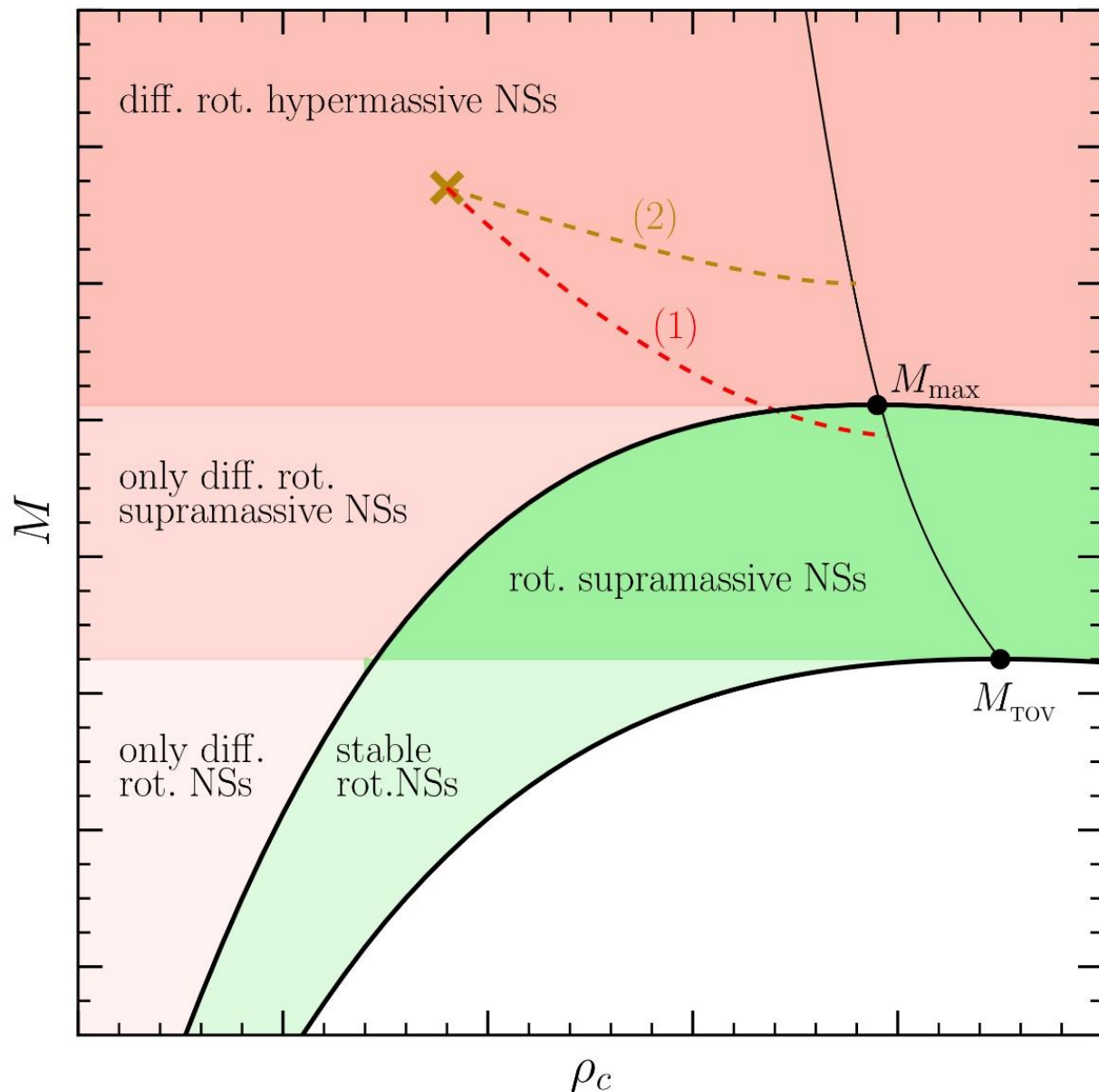
$\Omega^*(t)$ [rad/s] and $R^*(t)$ for ALF2, $M=1.35$



Maximum of the rotation profile $\Omega^*(t)$ (blue) and its radial position $R^*(t)$ (orange) for the non-collapsing simulation (ALF2, $M=1.25$)



GW170817: Evolution of the HMNS until BH formation



The highly differentially rotating hypermassive/supramassive neutron star will spin down and redistribute its angular momentum (e.g. due to magnetic braking). After ~ 1 second it will cross the stability line as a uniformly rotating supramassive neutron star (close to M_{max}) and collapse to a black hole. Parts of the ejected matter will fall back into the black hole producing the gamma-ray burst.

GW170817: Constraining the Maximum Mass and the EOS

USING GRAVITATIONAL-WAVE OBSERVATIONS AND QUASI-UNIVERSAL RELATIONS TO CONSTRAIN THE MAXIMUM MASS OF NEUTRON STARS

LUCIANO REZZOLLA^{1,2}, ELIAS R. MOST¹, AND LUKAS R. WEIH¹

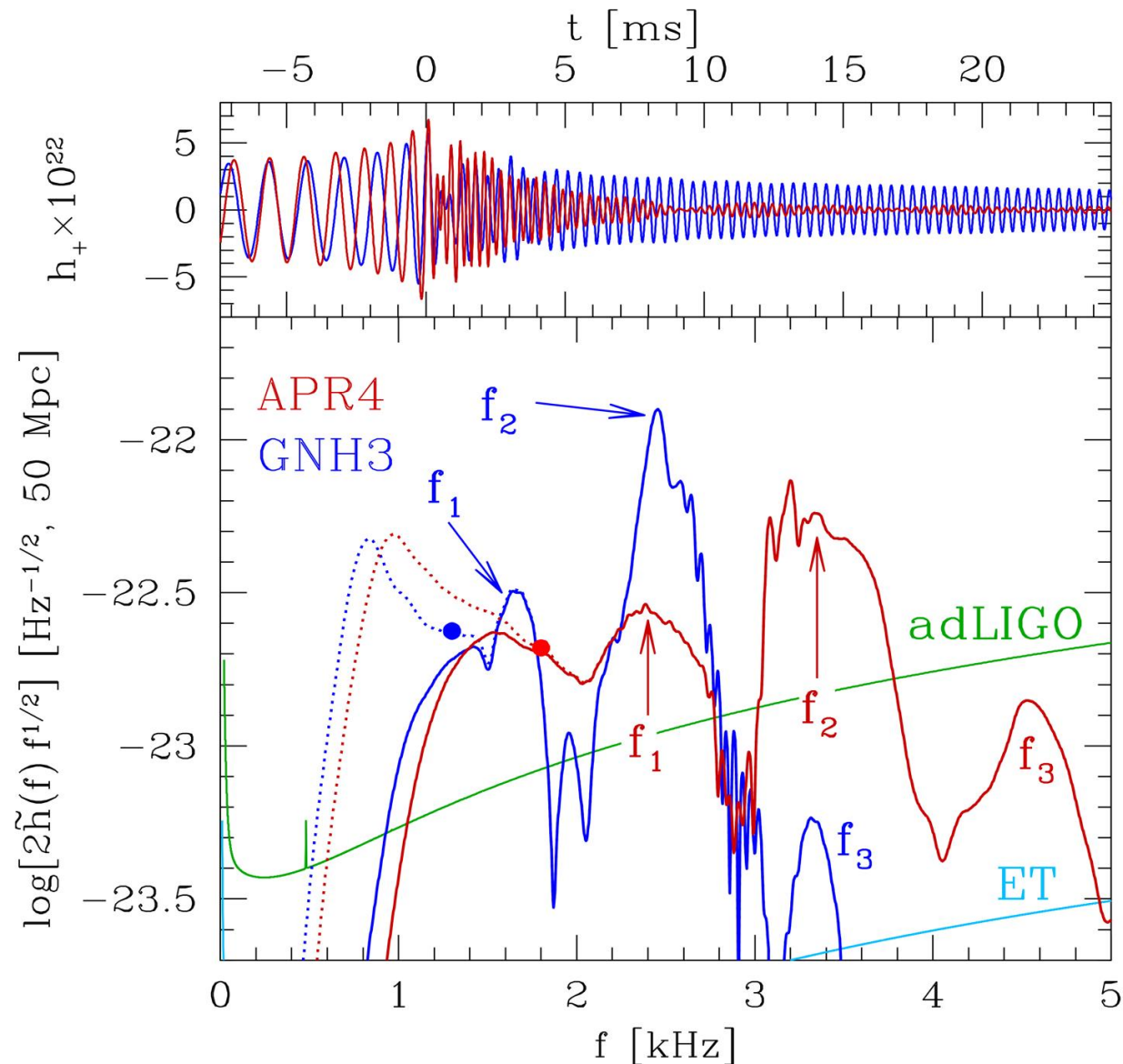
Draft version November 2, 2017

ABSTRACT

Combining the gravitational-wave observations of merging systems of binary neutron stars and quasi-universal relations we set constraints on the maximum mass that can be attained by nonrotating stellar models of neutron stars. More specifically, exploiting the recent observation of the gravitational-wave event GW170817 ([Abbott et al. 2017b](#)) and the quasi-universal relation between the maximum mass of nonrotating stellar models M_{TOV} and the maximum mass that can be supported through uniform rotation $M_{\text{max}} = (1.203 \pm 0.022) M_{\text{TOV}}$ ([Breu & Rezzolla 2016](#)), we set limits for the maximum mass to be $2.01 \pm 0.04 \leq M_{\text{TOV}}/M_{\odot} \lesssim 2.16 \pm 0.03$, where the lower limit in this range comes from pulsar observations ([Antoniadis et al. 2013](#)). Our estimate, which follows a very simple line of arguments and does not rely on the interpretation of the electromagnetic signal, can be further refined as new detections become available. We also briefly discuss the impact that our conclusions have on the equation of state of nuclear matter.

See arXiv:1711.00314v1 [astro-ph.HE] 1 Nov 2017

GW-Spectrum for different EOSs



See:

Kentaro Takami, Luciano Rezzolla, and Luca Baiotti, *Physical Review D* 91, 064001 (2015)

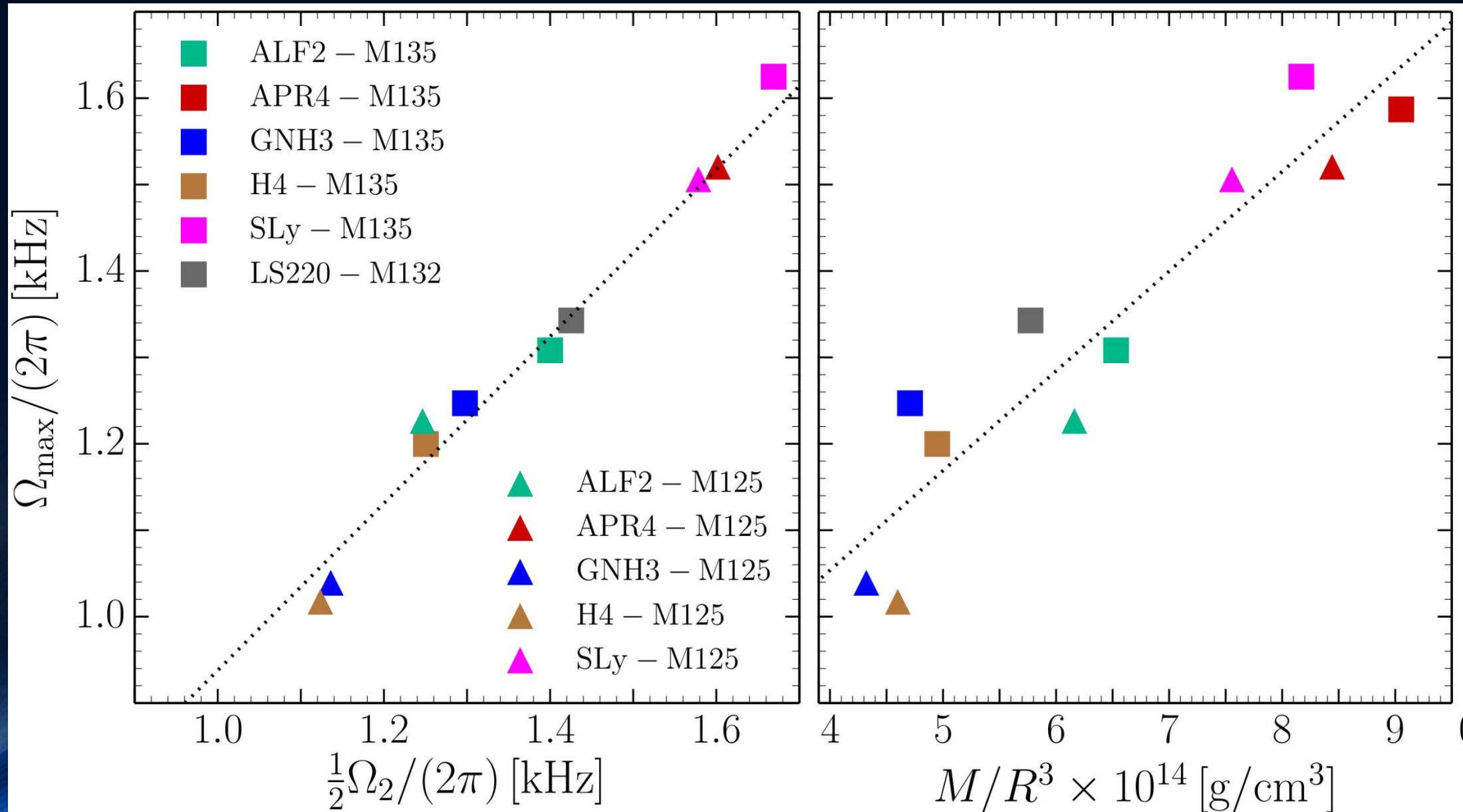
Hotokezaka, K., Kiuchi, K., Kyutoku, K., Muranushi, T., Sekiguchi, Y. I., Shibata, M., & Taniguchi, K. (2013). *Physical Review D*, 88(4), 044026.

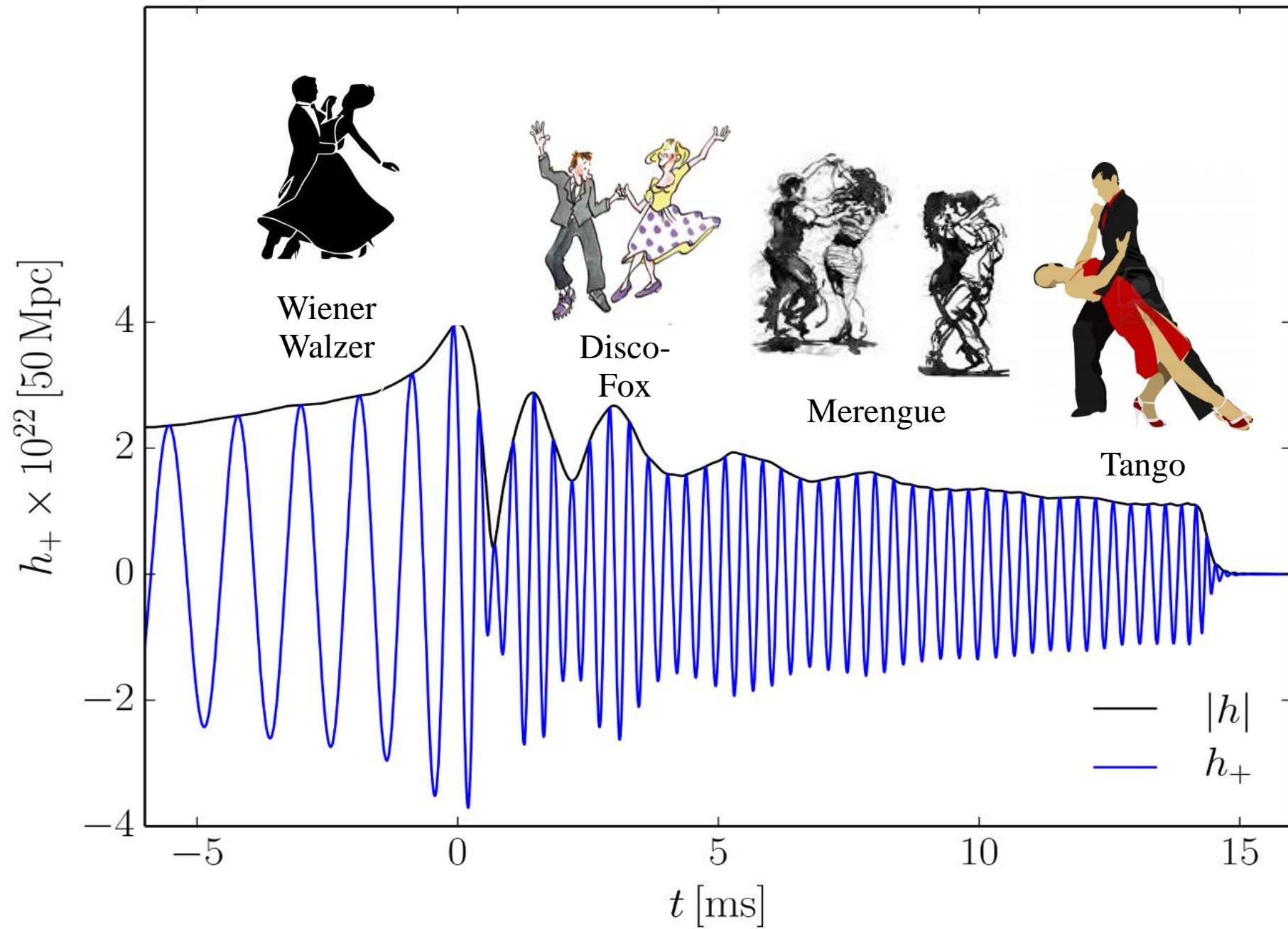
Bauswein, A., & Janka, H. T. (2012). *Physical review letters*, 108(1), 011101.

Clark, J. A., Bauswein, A., Stergioulas, N., & Shoemaker, D. (2015). *arXiv:1509.08522*.

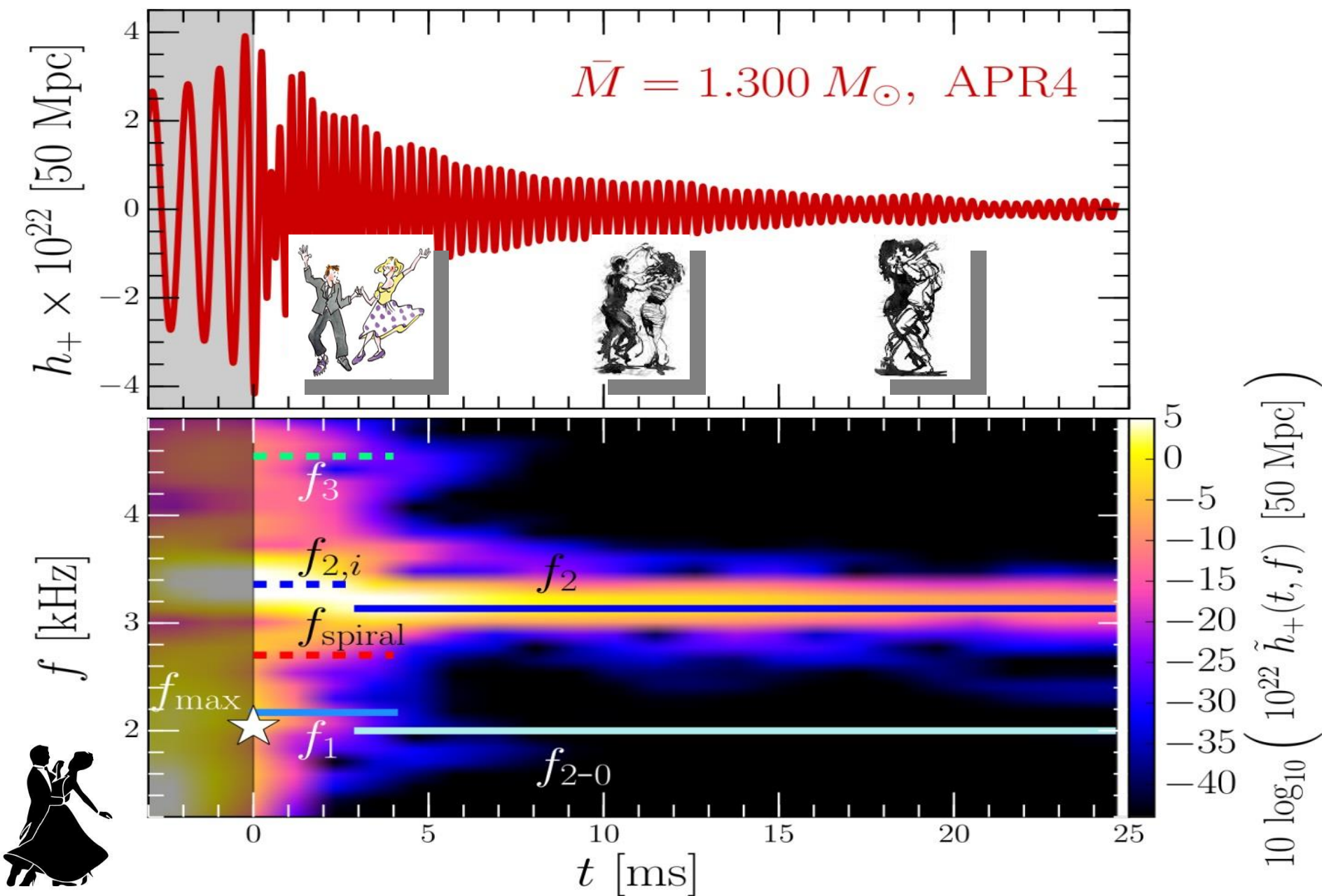
Bernuzzi, S., Dietrich, T., & Nagar, A. (2015). *Physical review letters*, 115(9), 091101.

Gravitational Waves and the Maximum of the Rotation Profile



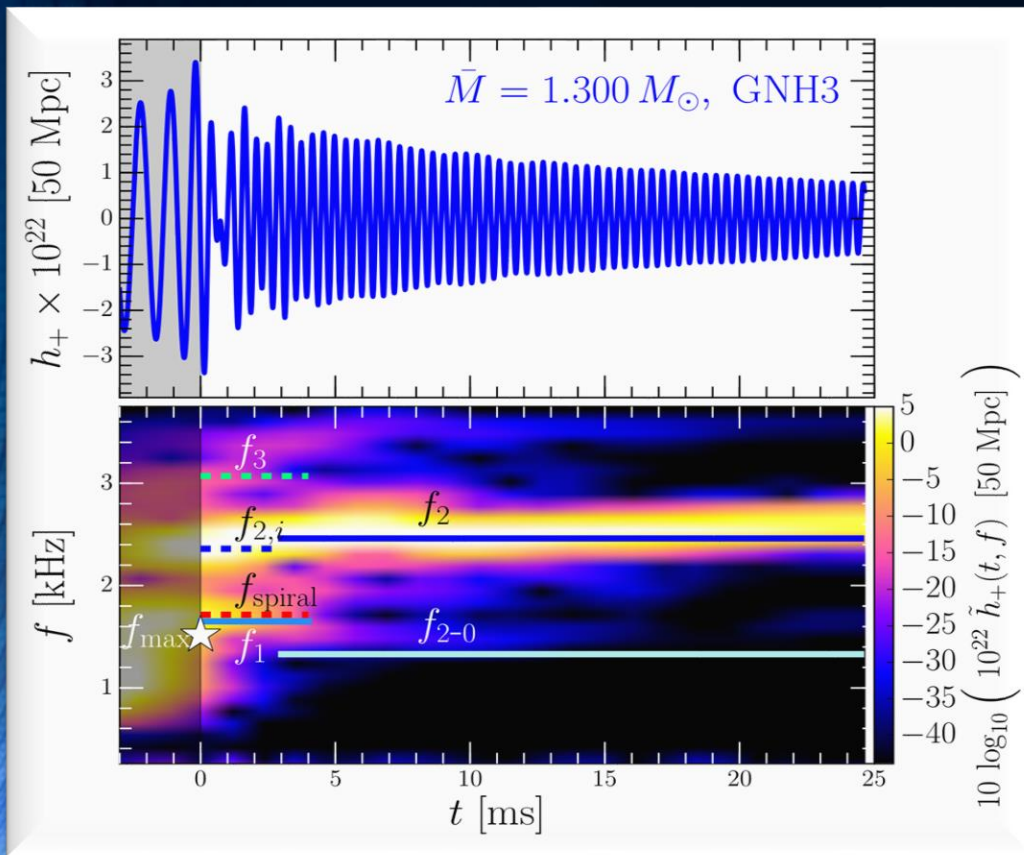


The different Phases during the Postmergerphase of the HMNS

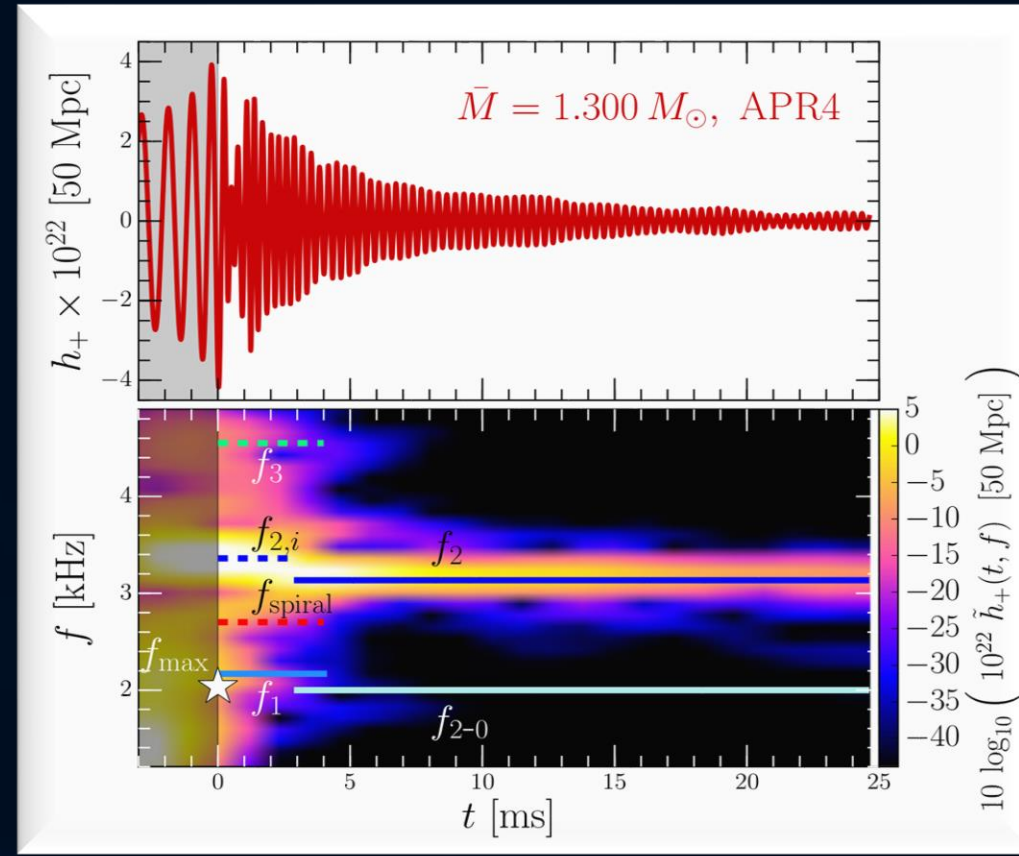


Time Evolution of the GW-Spectrum

The power spectral density profile of the post-merger emission is characterized by several distinct frequencies f_{\max} , f_1 , f_2 , f_3 and f_{2-0} . After approximately 5 ms after merger, the only remaining dominant frequency is the f_2 -frequency (See L.Rezzolla and K.Takami, arXiv:1604.00246)



Stiff EOS



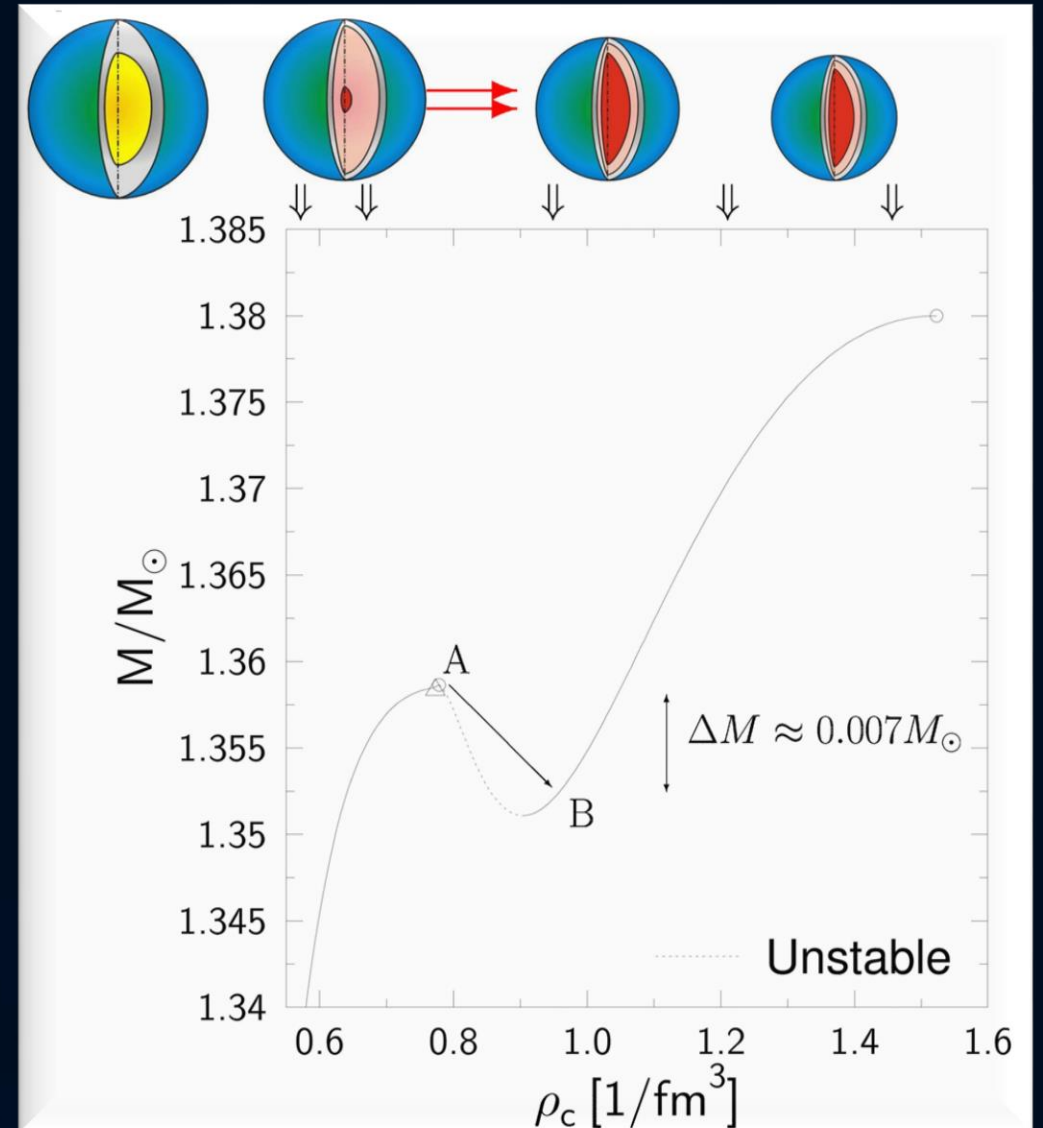
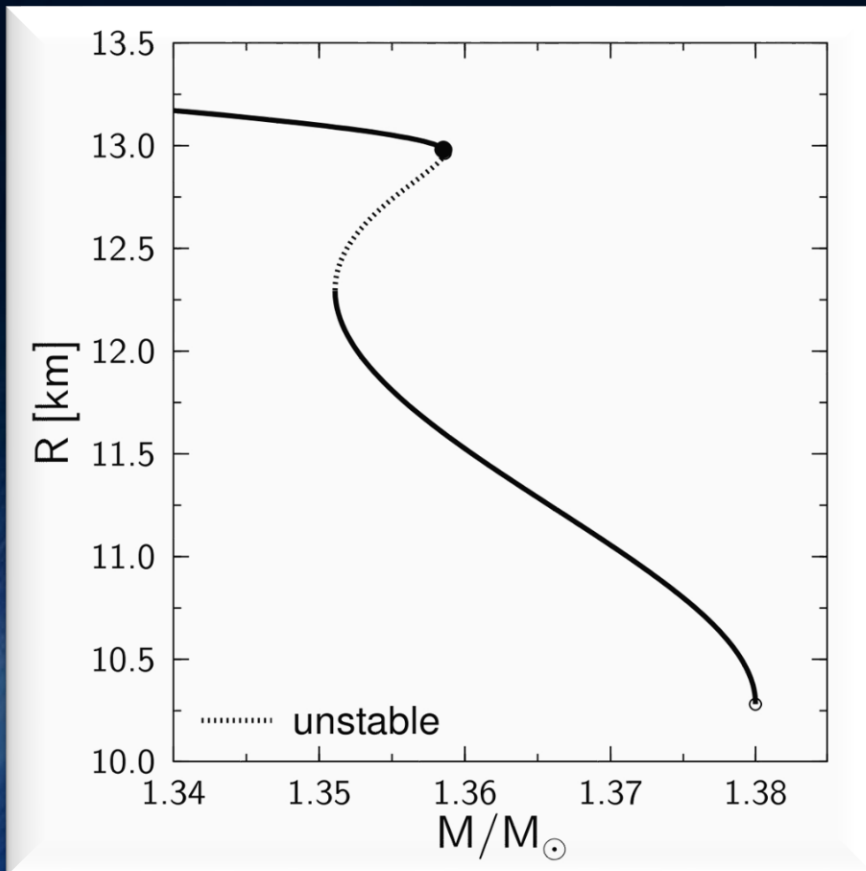
Soft EOS

Unfortunately, due to the low sensitivity at high gravitational wave frequencies, no post-merger signal has been found in GW170817.

But advanced detectors / next-generation detectors will be able to detect!

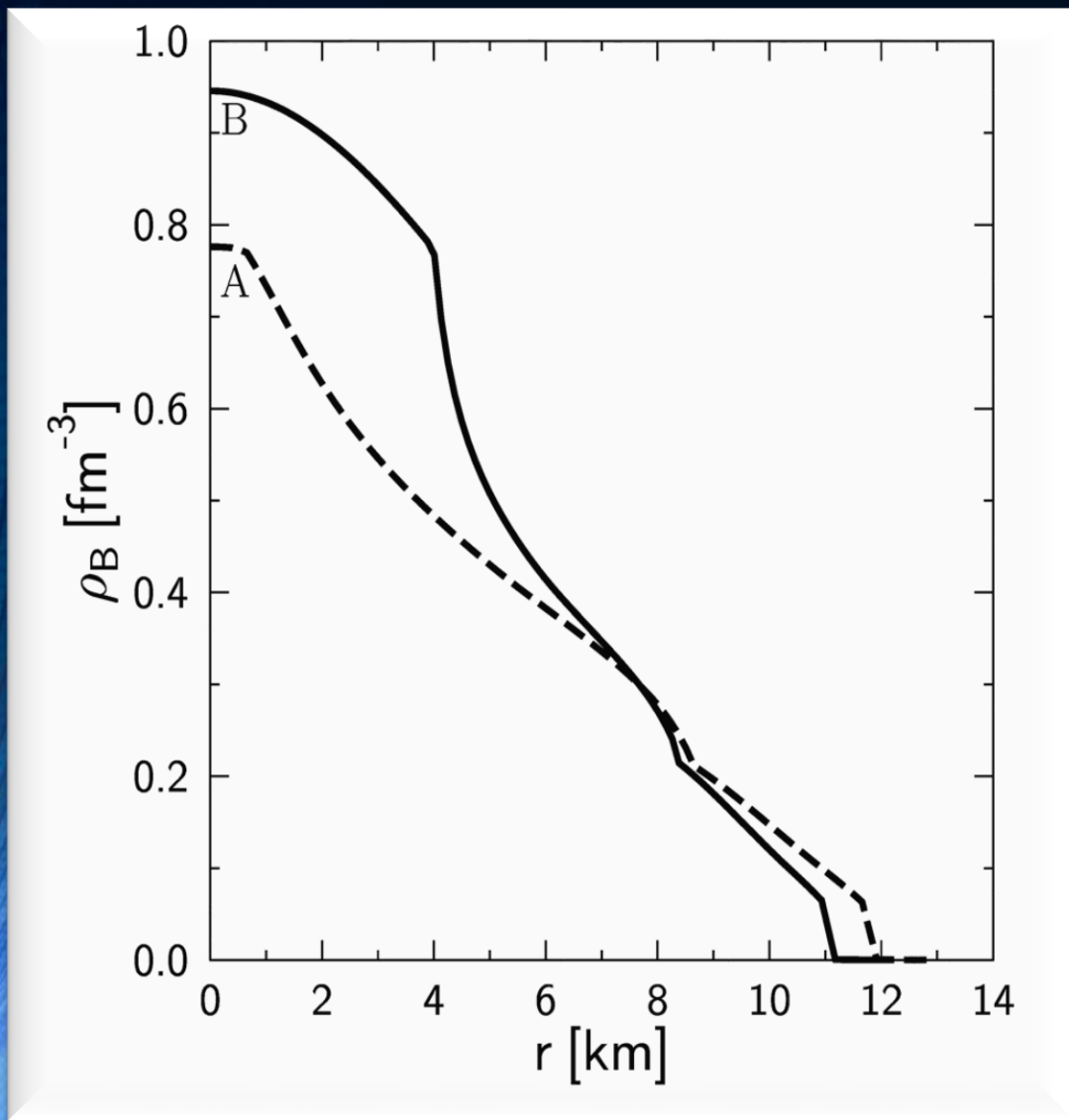
Twin Stars

Usually it is assumed that this loss of stability leads to the collapse into a black hole. However, realistic calculations open another possibility: the collapse into the twin star on the second sequence.

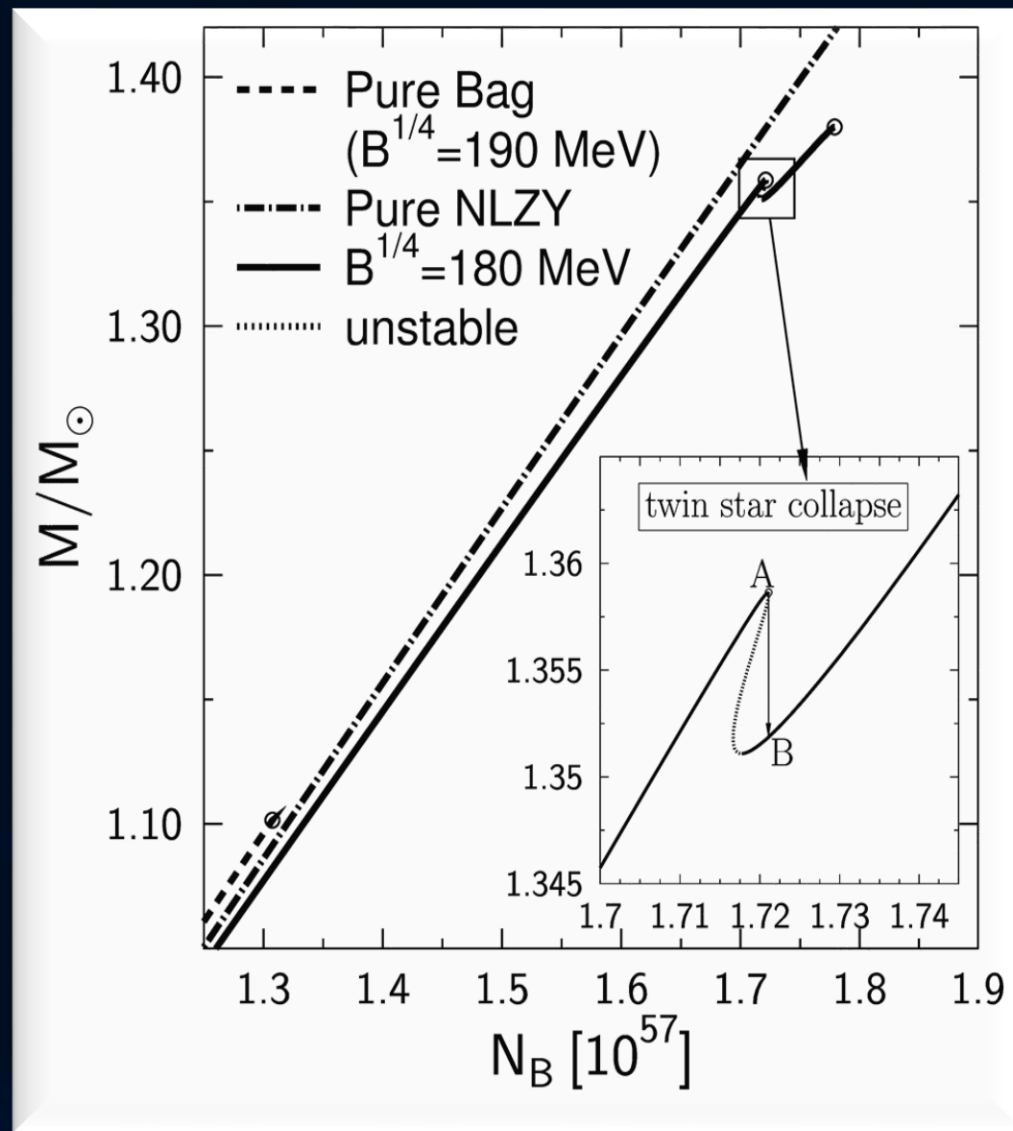


The Twin Star Collapse

Density profiles of the two twins

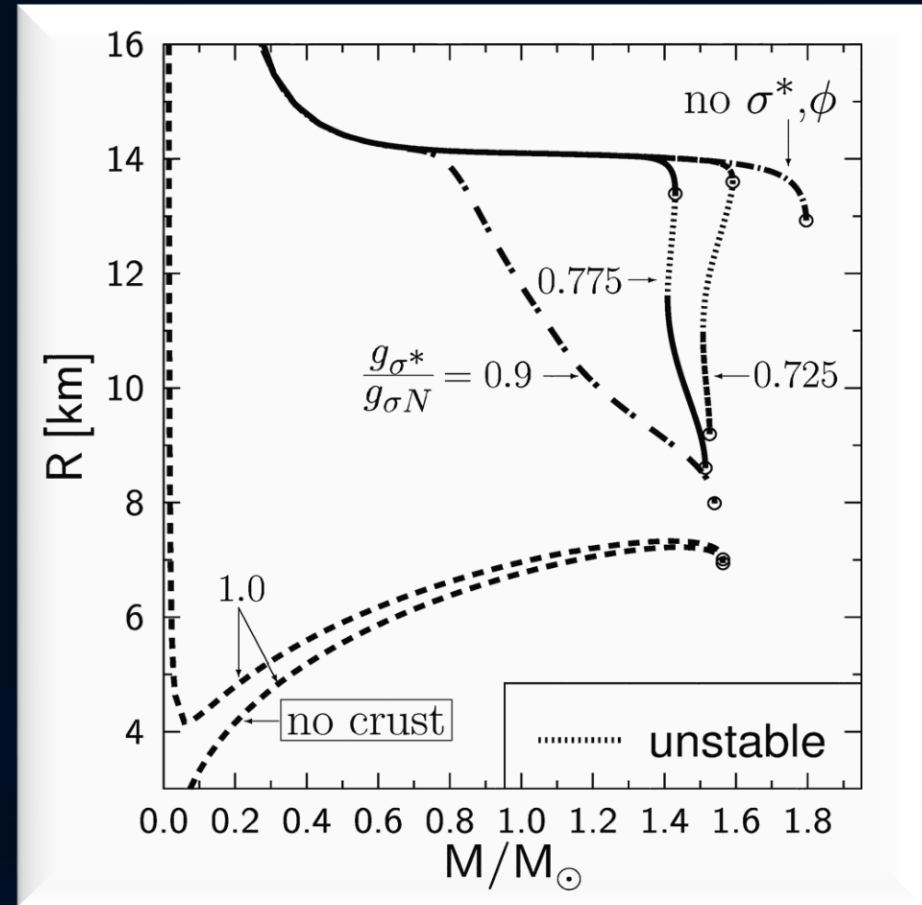
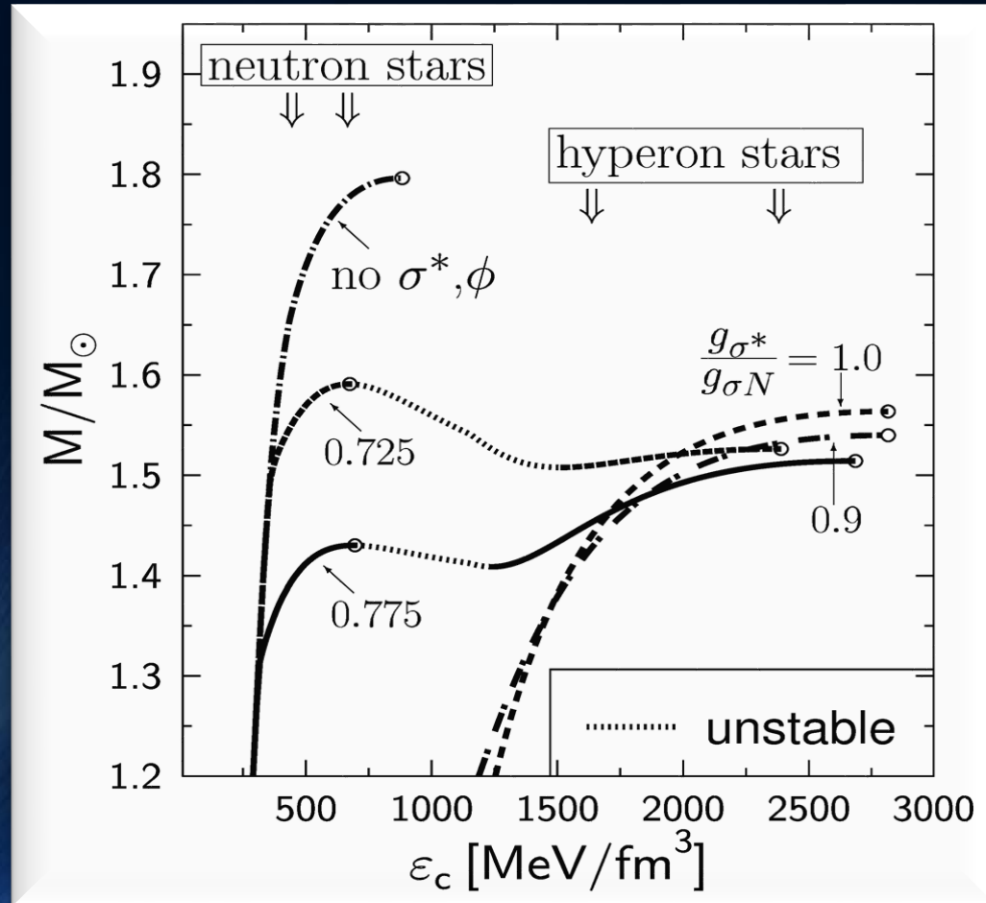


Conservation of total baryonic mass

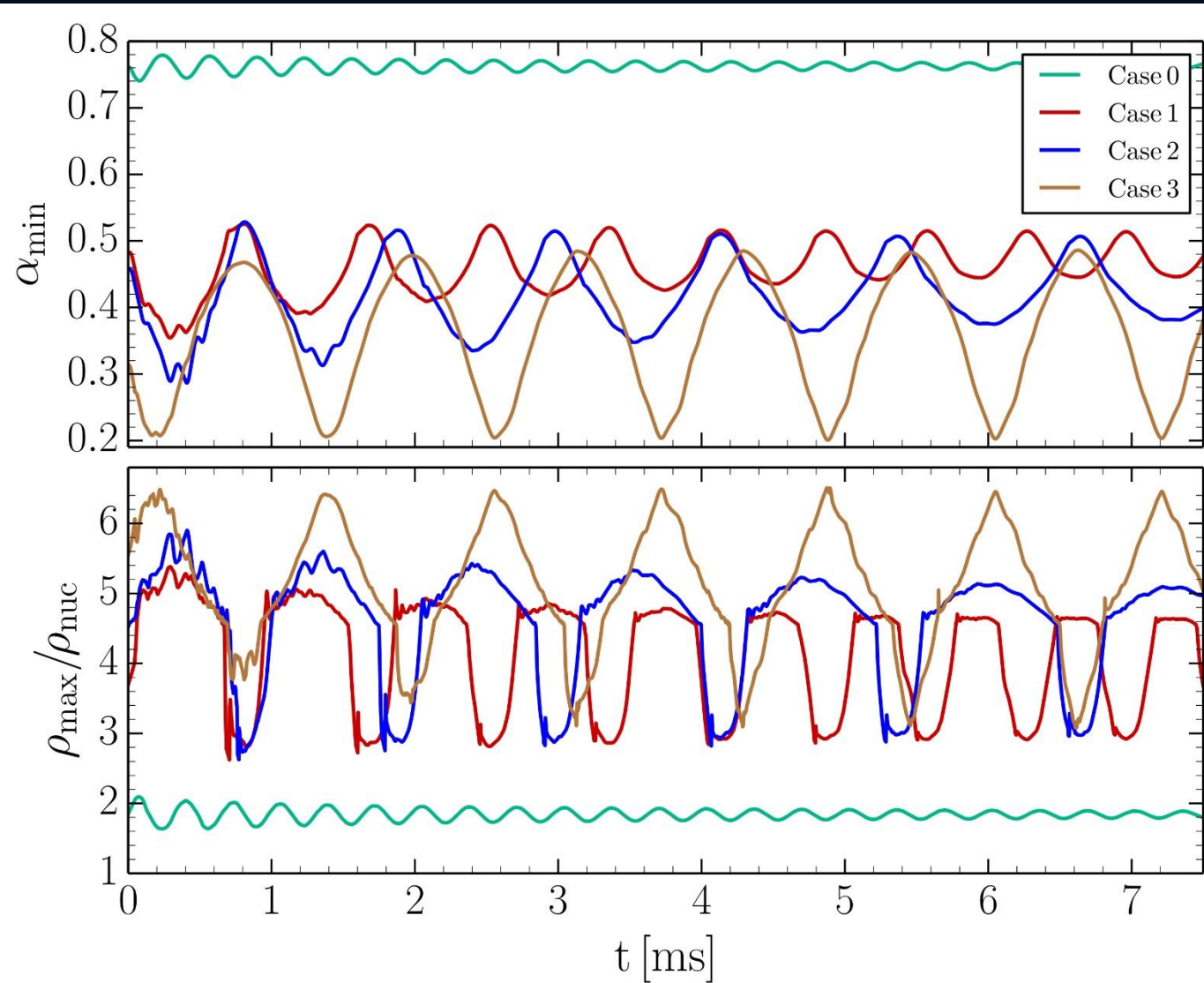
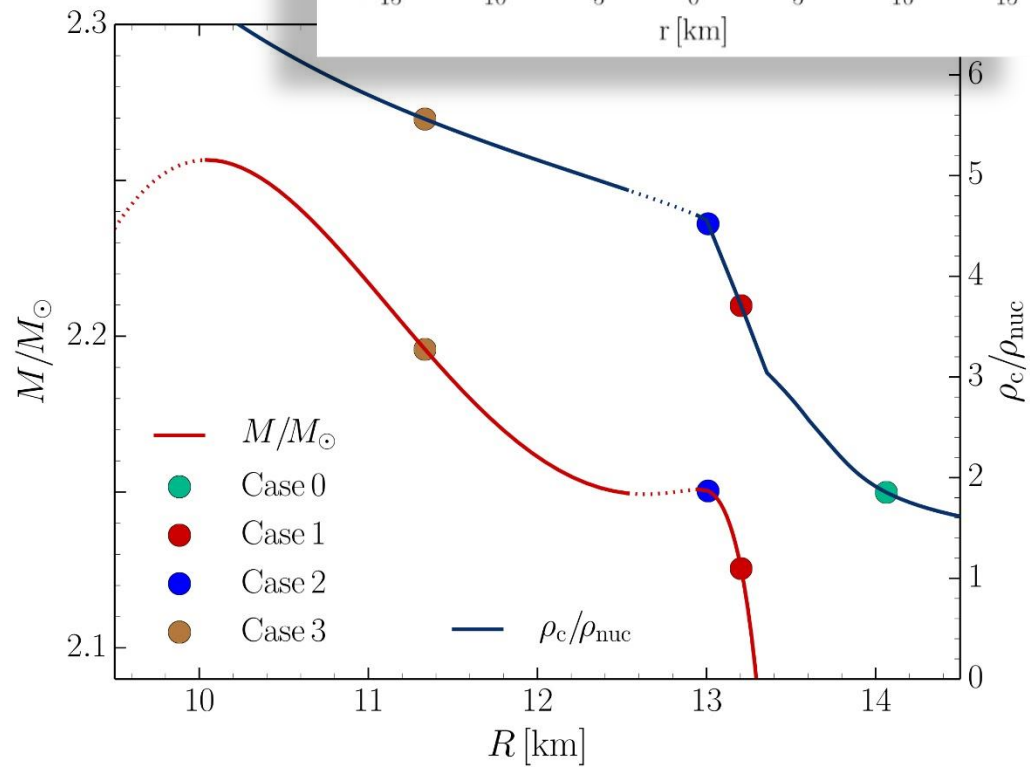
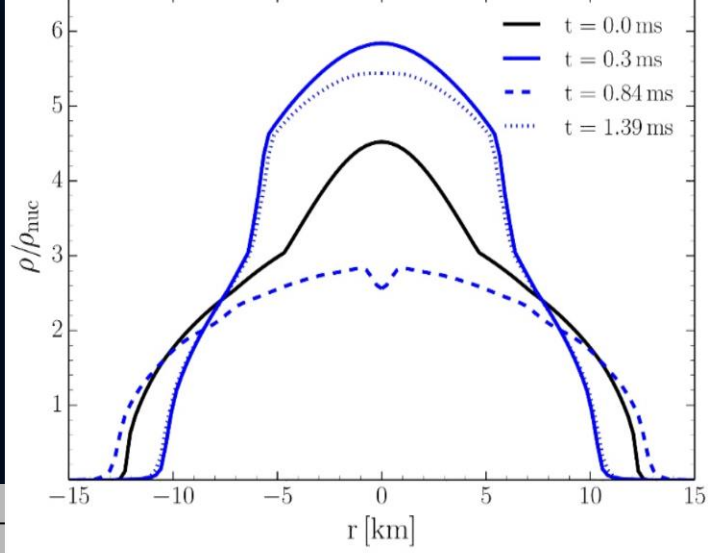


Exotic Stars

But, unfortunately, twin stars can not be created solely by a Hadron-Quark phase transition. Extremely bound hyperon matter, or kaon condensation could also form a twin star behaviour.



The Twin Star collapse



Radial oscillations of twin star configurations

M. Hanauske, Z.S. Yilmaz, C. Mitropoulos, L. Rezzolla and H. Stöcker

"Gravitational waves from binary compact star mergers in the context of strange matter", in Proceedings SQM2017

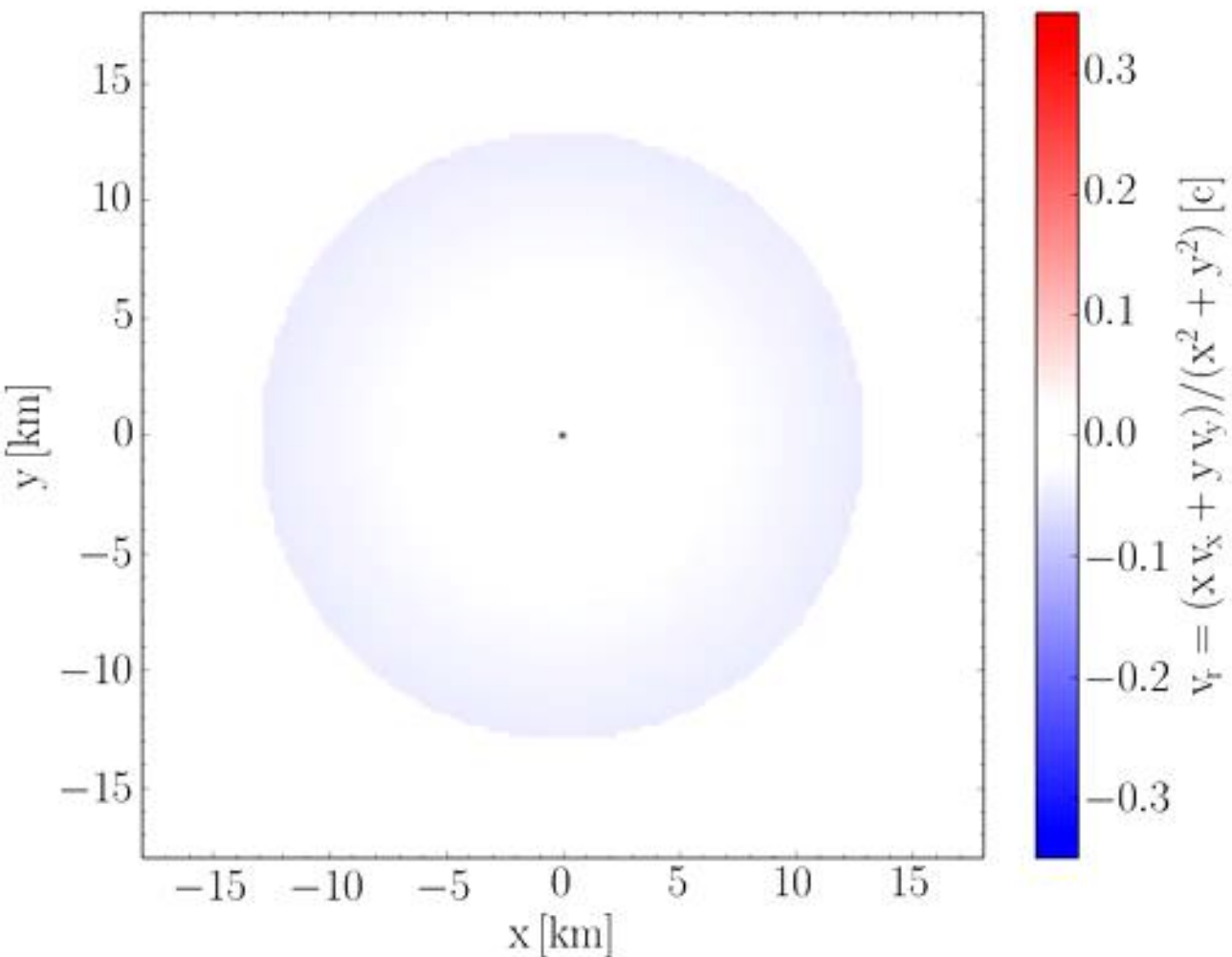
The Twin Star Collapse (red)

Green contour line: Nuclear Matter density

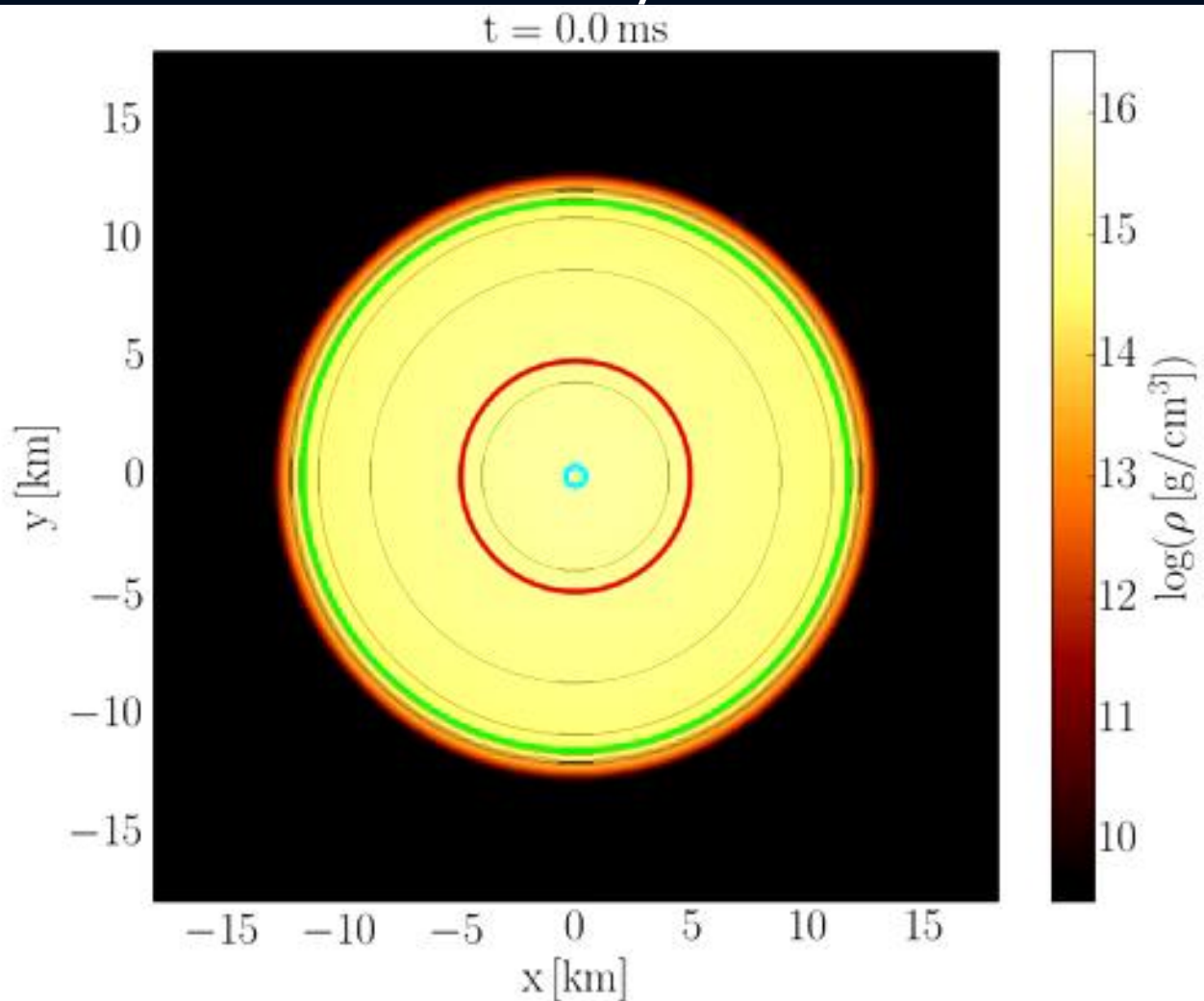
Red contour line: Beginning of PT

Cyan contour line: End of PT

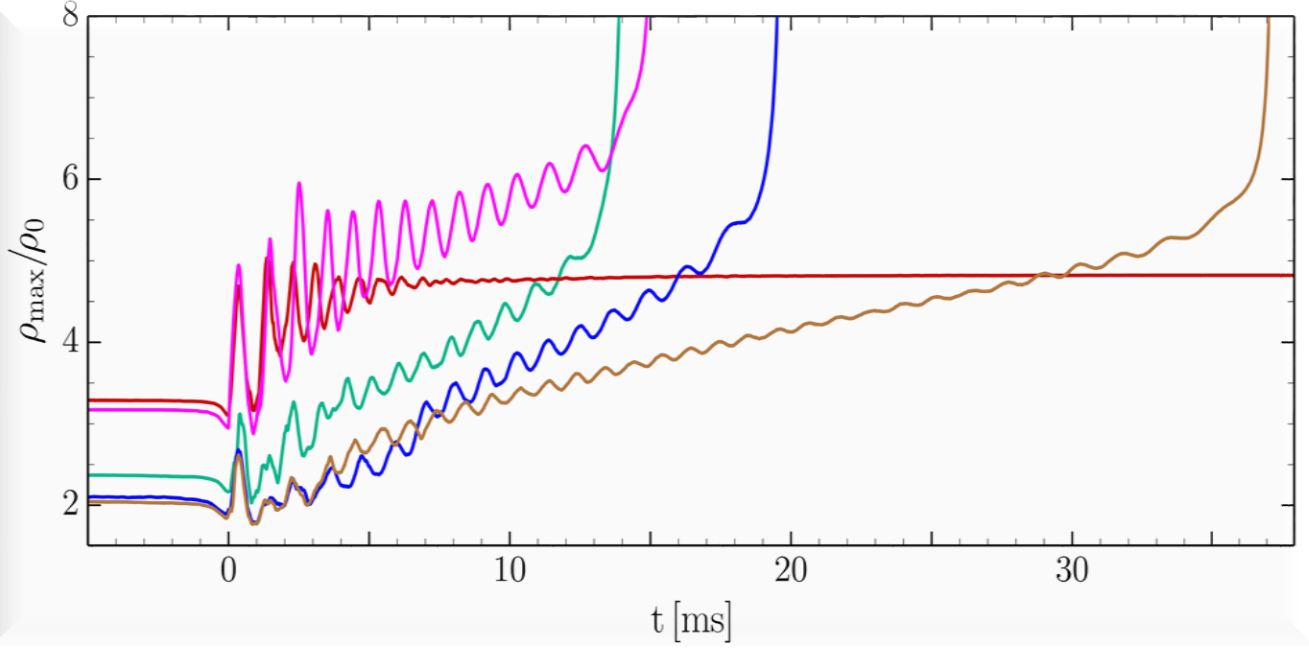
Radial velocity



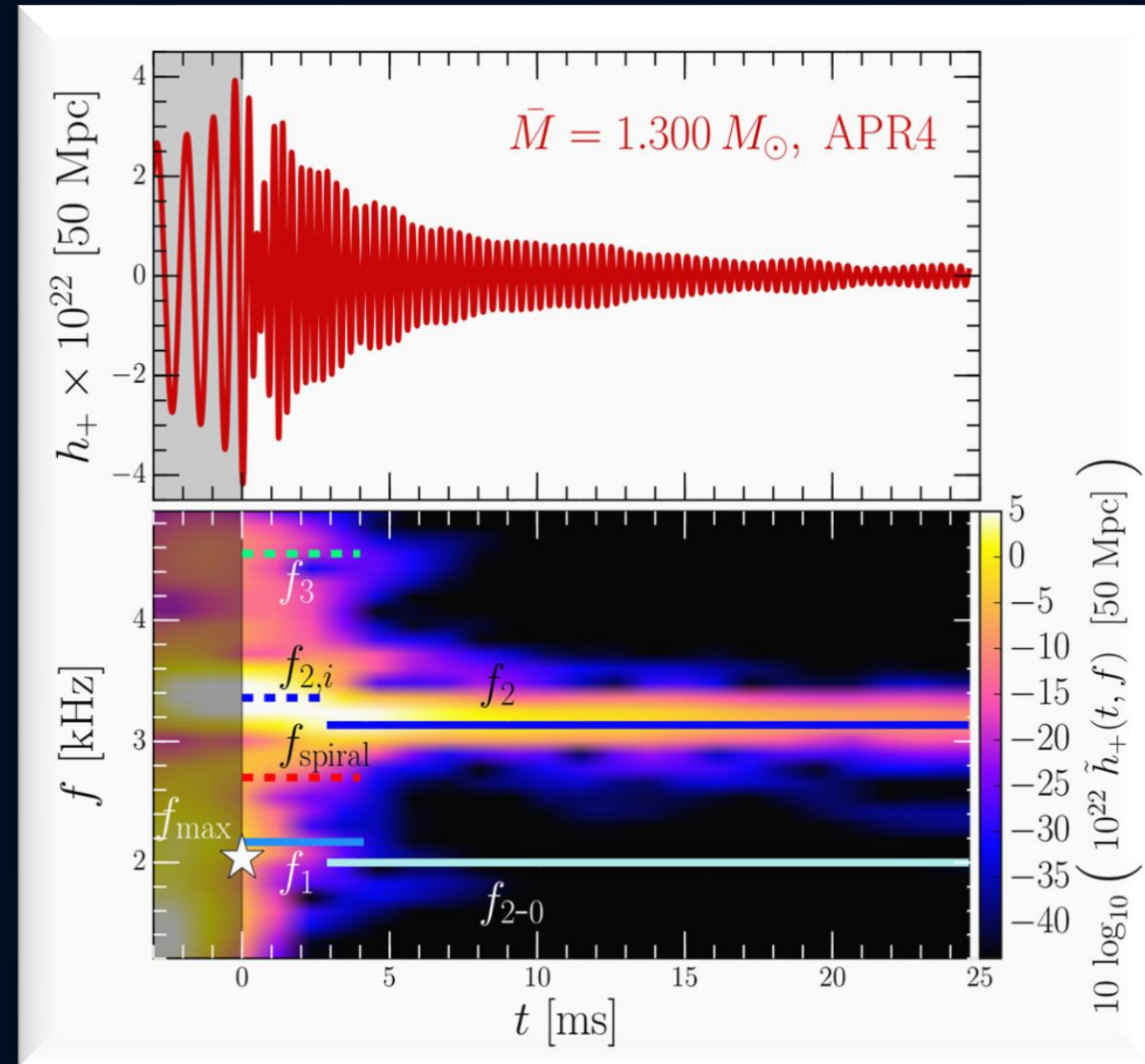
Density



How to observe the QGP with gravitational waves from NS mergers?



The appearance of the hadron-quark phase transition in the interior region of the HMNS will change the spectral properties of the emitted GW if it is strong enough. If the unstable twin star region will be reached during the “post-transient” phase, the f_2 -frequency peak of the GW signal will change rapidly due to the sudden speed up of the differentially rotating HMNS.



Hybrid star mergers represent optimal astrophysical laboratories to investigate the QCD phase structure and in addition with the observations from heavy ion collisions it will be possibly reach a conclusive picture on the QCD phase structure at high density and temperature.

On r-process nucleosynthesis from matter ejected in binary neutron star mergers

Luke Bovard,¹ Dirk Martin,² Federico Guercilena,¹ Almudena Arcones,² Luciano Rezzolla,^{1,3} and Oleg Korobkin⁴

¹*Institut für Theoretische Physik, Johann Wolfgang Goethe-Universität, Max-von-Laue-Straße 1, 60438 Frankfurt, Germany*

²*Institut für Kernphysik, Technische Universität Darmstadt, Schlossgartenstraße 9, 64289 Darmstadt, Germany*

³*Frankfurt Institute for Advanced Studies, Ruth-Moufang-Straße 1, 60438 Frankfurt, Germany*

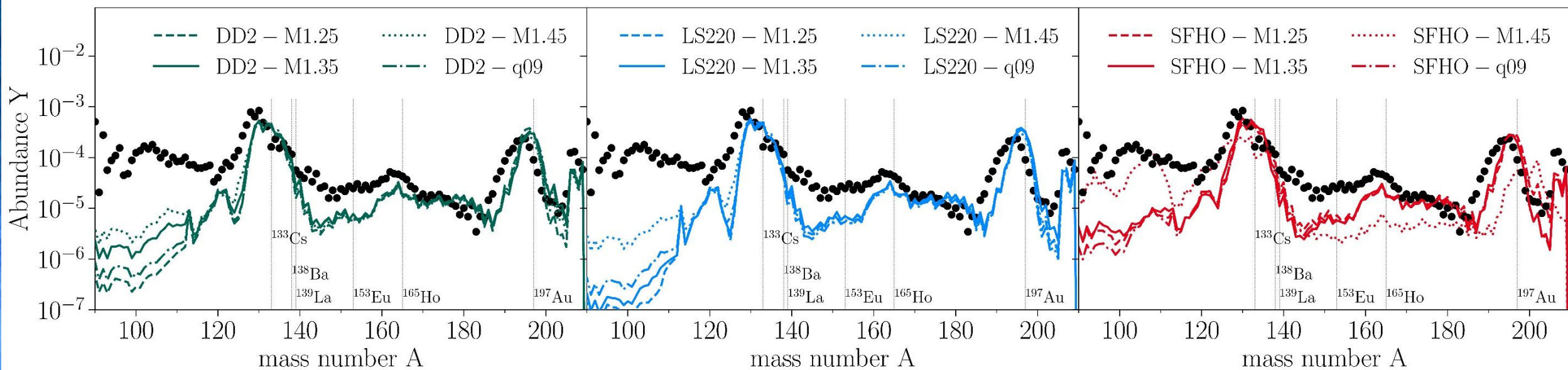
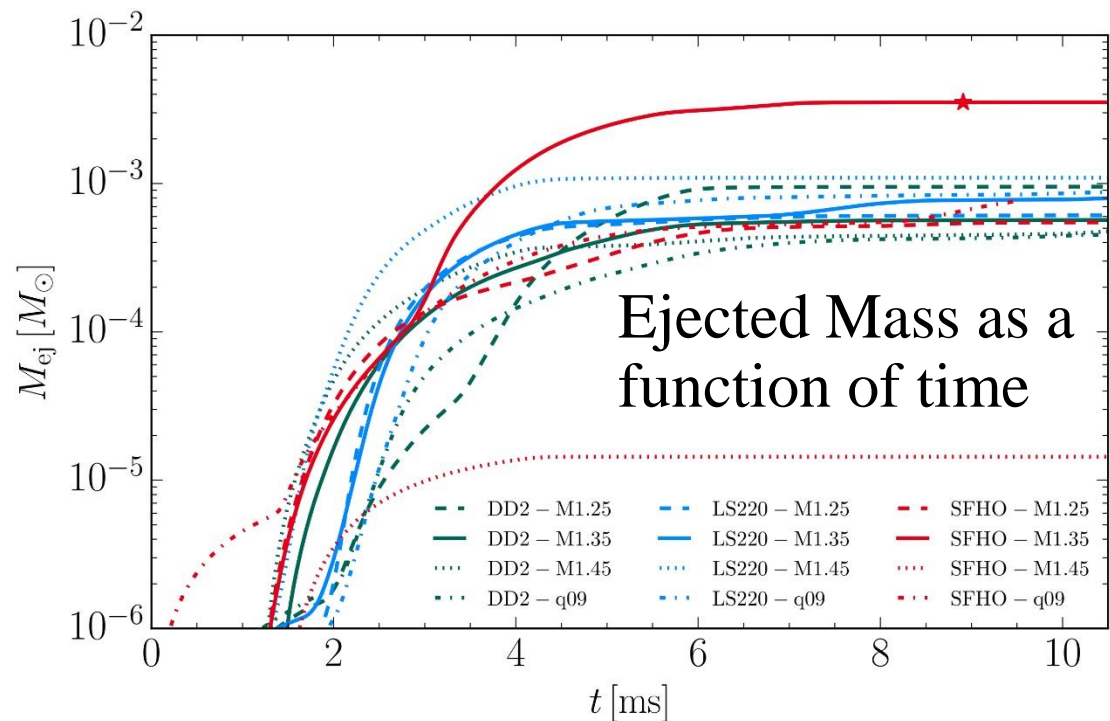
⁴*Center for Theoretical Astrophysics, Los Alamos National Laboratory, Los Alamos, NM 87545, USA*

When binary systems of neutron stars merge, a very small fraction of their rest mass is ejected, either dynamically or secularly. This material is neutron-rich and its nucleosynthesis could provide the astrophysical site for the production of heavy elements in the universe, together with a kilonova signal confirming neutron-star mergers as the origin of short gamma-ray bursts. We perform full general-relativistic simulations of binary neutron-star mergers employing three different nuclear-physics EOSs, considering both equal- and unequal-mass configurations, and adopting a leakage scheme to account for neutrino radiative losses. Using a combination of techniques, we carry out an extensive and systematic study of the hydrodynamical, thermodynamical, and geometrical properties of the matter ejected dynamically, employing the `WinNet` nuclear-reaction network to recover the relative abundances of heavy elements produced by each configurations. Among the results obtained, three are particularly important. First, we find that both the properties of the dynamical ejecta and the nucleosynthesis yields are robust against variations of the EOS and masses, and match very well the observed chemical abundances. Second, using a conservative but robust criterion for unbound matter, we find that the amount of ejected mass is $\lesssim 10^{-3} M_{\odot}$, hence at least one order of magnitude smaller than what normally assumed in modelling kilonova signals. Finally, using a simplified and gray-opacity model we assess the observability of the infrared kilonova emission finding, that for all binaries the luminosity peaks around $\sim 1/2$ day in the H -band, reaching a maximum magnitude of -13 , and decreasing rapidly after one day. These rather low luminosities make the prospects for detecting kilonovae less promising than what assumed so far.







r-process nucleosynthesis in binary neutron star mergers

Luke Bovard, Dirk Martin, Federico Guercilena, Almudena Arcones, Luciano Rezzolla and Oleg Korobkin
arXiv:1709.09630v1 [gr-qc] 27 Sep 2017

Simulation of the relative abundances of heavy elements produced in a binary neutron star merger.



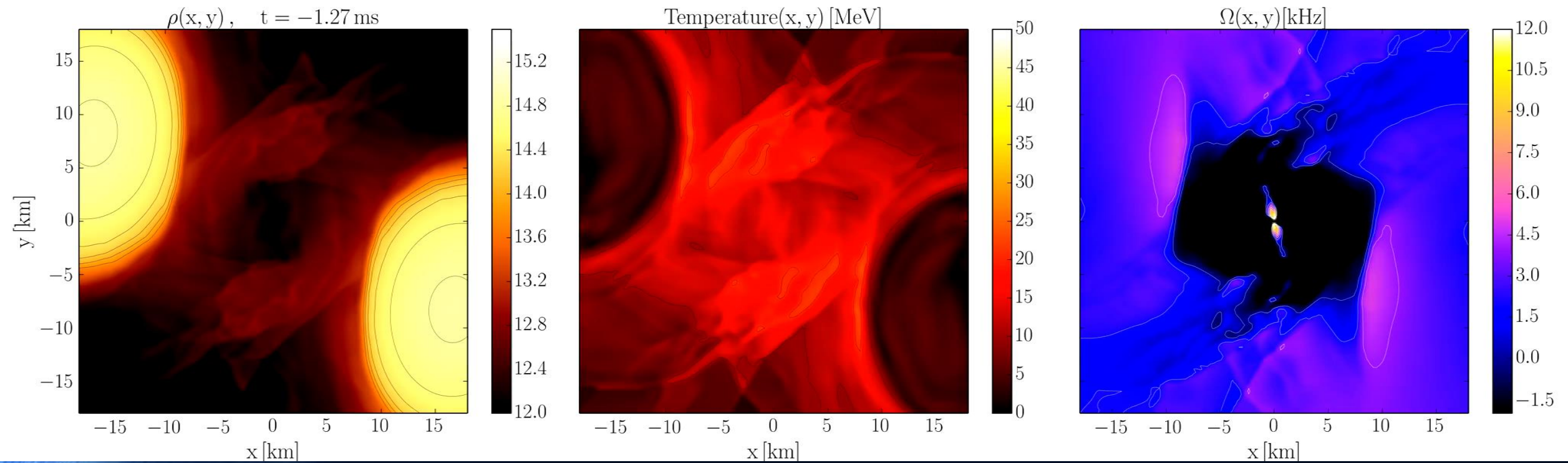
The Origin of the Solar System Elements

1 H	big bang fusion 										cosmic ray fission 					2 He						
3 Li	4 Be	merging neutron stars? 										exploding massive stars 					5 B	6 C	7 N	8 O	9 F	10 Ne
11 Na	12 Mg	dying low mass stars 										exploding white dwarfs 					13 Al	14 Si	15 P	16 S	17 Cl	18 Ar
19 K	20 Ca	21 Sc	22 Ti	23 V	24 Cr	25 Mn	26 Fe	27 Co	28 Ni	29 Cu	30 Zn	31 Ga	32 Ge	33 As	34 Se	35 Br	36 Kr					
37 Rb	38 Sr	39 Y	40 Zr	41 Nb	42 Mo	43 Tc	44 Ru	45 Rh	46 Pd	47 Ag	48 Cd	49 In	50 Sn	51 Sb	52 Te	53 I	54 Xe					
55 Cs	56 Ba		72 Hf	73 Ta	74 W	75 Re	76 Os	77 Ir	78 Pt	79 Au	80 Hg	81 Tl	82 Pb	83 Bi	84 Po	85 At	86 Rn					
87 Fr	88 Ra																					
		57 La	58 Ce	59 Pr	60 Nd	61 Pm	62 Sm	63 Eu	64 Gd	65 Tb	66 Dy	67 Ho	68 Er	69 Tm	70 Yb	71 Lu						
		89 Ac	90 Th	91 Pa	92 U	93 Np	94 Pu	Very radioactive isotopes; nothing left from stars														

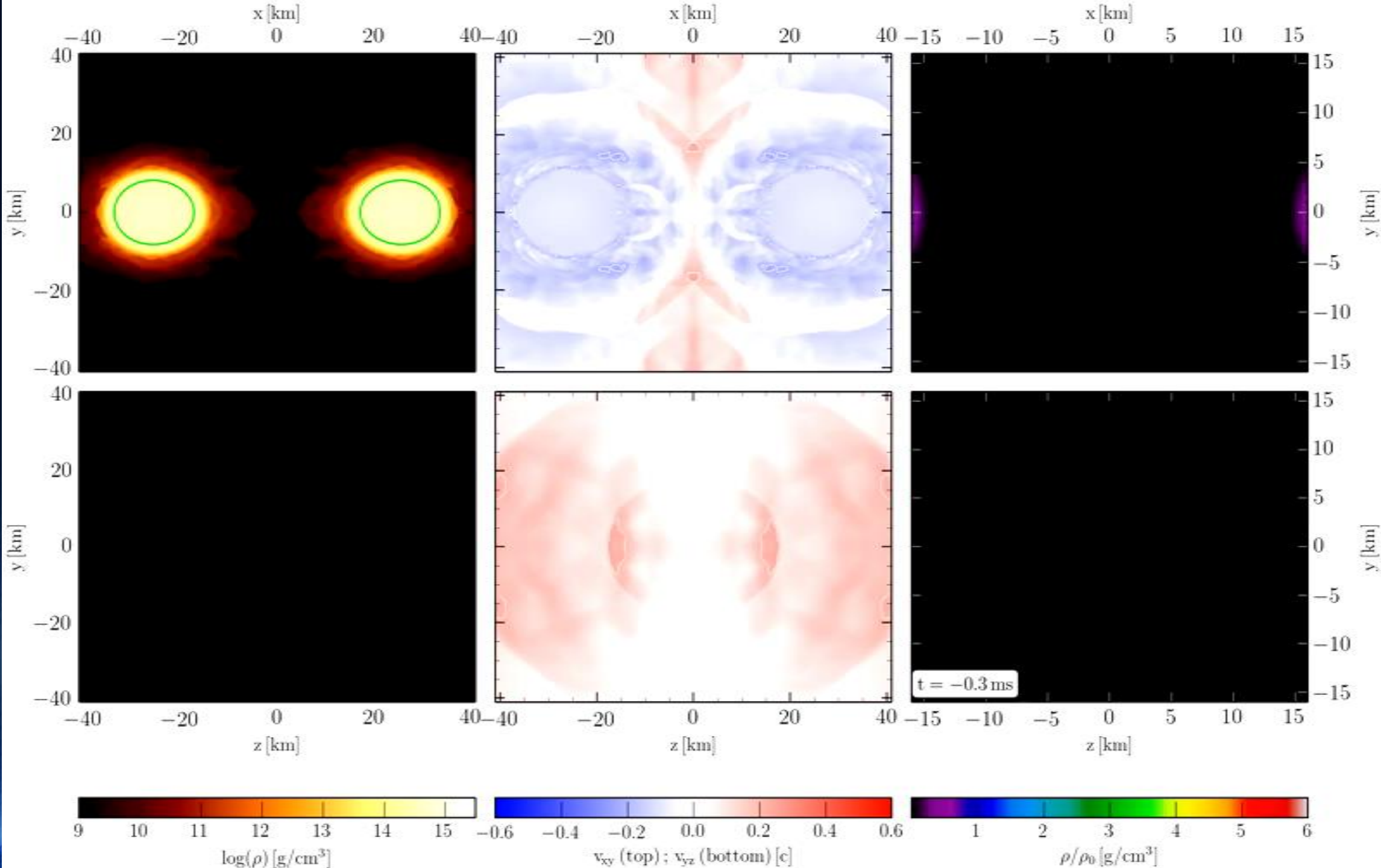
Graphic created by Jennifer Johnson
<http://www.astronomy.ohio-state.edu/~jaj/nucleo/>

Astronomical Image Credits:
 ESA/NASA/AASNova

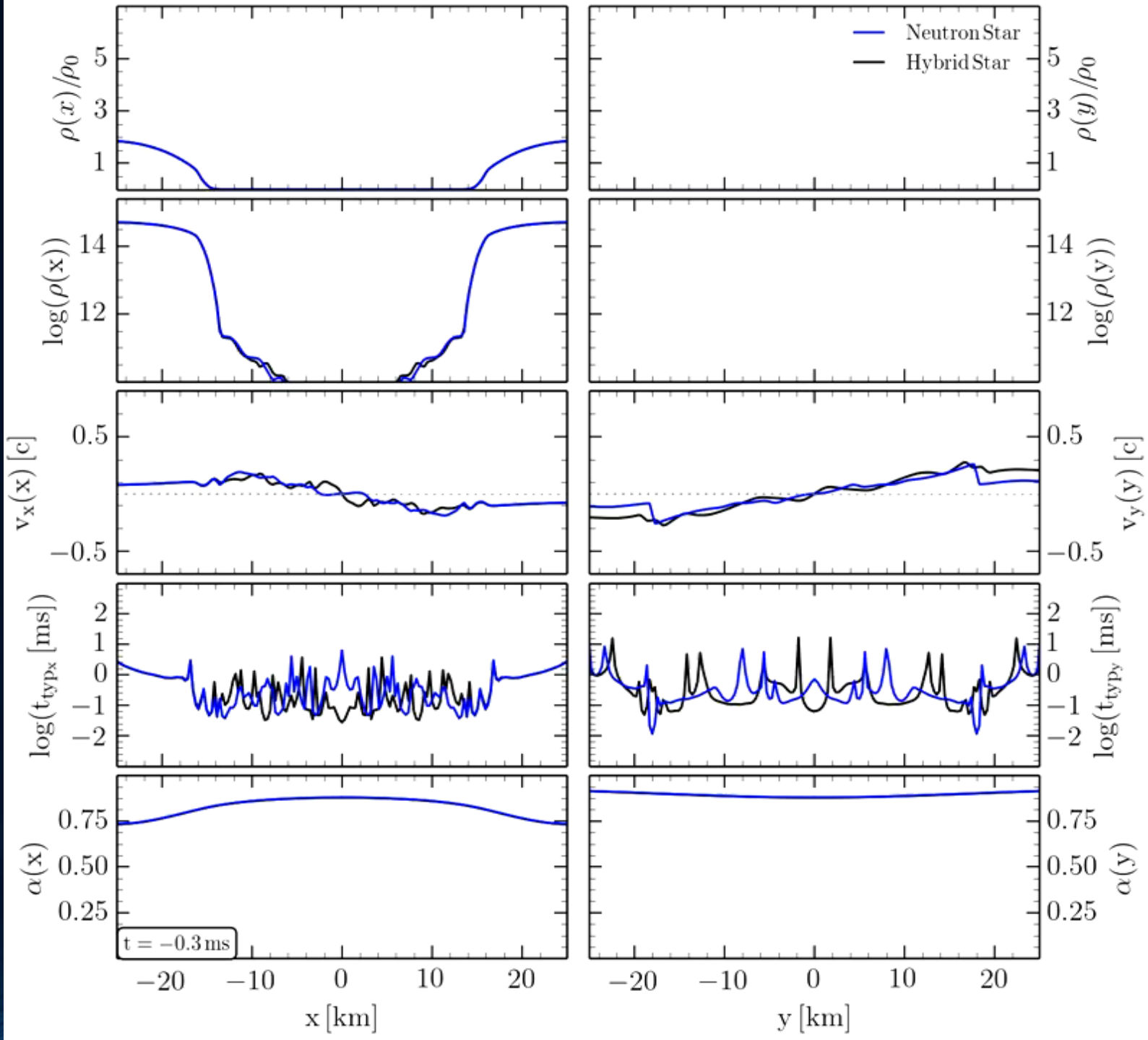
Merger Product from an eccentric colliding Neutron Star Binaries



Head-On Collision of Neutron Stars



Head-On Collision Comparison: Neutron Stars - Hybrid Stars



Vorlesung besteht aus drei Teilen

Allgemeine Relativitätstheorie mit dem Computer von Dr.phil.nat.Dr.rer.pol. Matthias Hanauske

[Home](#) [Research](#) [Contact](#)

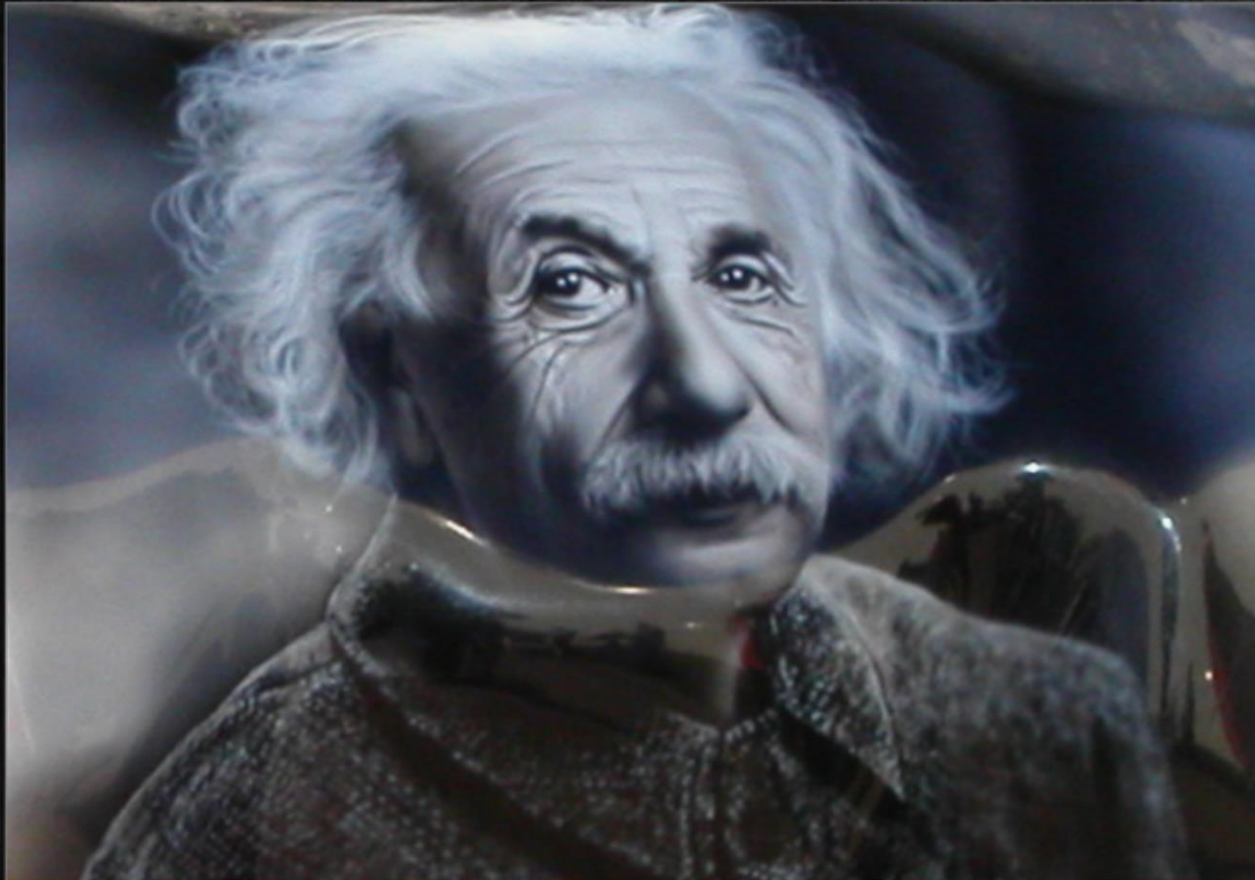
[Einführung](#)

[Teil I](#)

[Teil II](#)

[Teil III](#)

[E-Learning](#)



www.fias.uni-frankfurt/~hanauske/VARTC/

Allgemeine Relativitätstheorie mit dem Computer (General Theory of Relativity on the Computer) Vorlesung SS 2016, Mo. 16-18.00 Uhr, PC-Pool 01.120

In dieser Vorlesung werden die mathematisch anspruchsvollen Gleichungen der Allgemeinen Relativitätstheorie (ART) in diversen Programmierumgebungen analysiert. Im ersten Teil des Kurses erlernen die Studierenden die Verwendung von Computeralgebra-Systemen (Maple und Mathematica). Die oft komplizierten und zeitaufwendigen Berechnungen der tensoriellen Gleichungen der ART können mit Hilfe dieser Programme erleichtert werden. Diverse Anwendungen der Einstein- und Geodätengleichung werden in Maple implementiert, quasi analytische Berechnungen durchgeführt und entsprechende Lösungen berechnet und visualisiert. Der zweite Teil des Kurses befasst sich mit der numerischen Berechnung von Neutronensternen und Weißen Zwergen mittels eines C/C++ Programms. Nach einer kurzen Auffrischung der grundlegenden Programmierkenntnisse, erstellen die Studierenden, gemeinsam mit dem Betreuer, ein Programm, das die Tolman-Oppenheimer-Volkov-Gleichung numerisch löst und visualisieren die Ergebnisse. Zusätzlich wird hierbei in die Grundkonzepte der parallelen Programmierung eingeführt und eine MPI- und OpenMP-Version des C/C++ Programms erstellt. Im dritten Teil des Kurses werden zeitabhängige numerische Simulationen der ART mittels des Einstein Toolkit durchgeführt und deren Ergebnisse mittels Python/Matplotlib visualisiert. Inhaltlich wird hierbei ebenfalls auf den, dem Programm zugrunde liegenden (3+1)-Split der ART eingegangen und, abhängig von den Vorkenntnissen der Studierenden, mehrere fortgeschrittene, astrophysikalisch relevante Probleme simuliert. Mögliche Themen dieses abschließenden Teils könnten die folgenden Systeme

[Intro 介绍](#)

[Chapter I 第一章](#)

[Chapter II 第二章](#)

[Chapter III 第三章](#)

[e-learning 电子学习](#)

Spring School on Numerical Relativity and Gravitational Wave Physics

15th-25th May 2017, Beijing
Room 6620, ITP New Building, Beijing



Invited Lecturers:

Niels Warburton (University College Dublin)
Andrea Taracchini (Max Planck Institute for Gravitational Physics)
David Hilditch (Theoretical Physics Institute, University of Jena)
David Weir (Helsinki Institute of Physics, University of Helsinki)
Koutarou Kyutoku (KEK, IPNS)
Matthias Hanauskę (Goethe University Frankfurt)

(Spring School on Numerical Relativity and Gravitational Wave Physics)

Vorlesungsreihe (6 Vorlesungen) über
Gravitationswellen von kollidierenden kompakten Sternen und die
Eigenschaften seltsamer Materie
(Gravitational waves from colliding compact star binaries in the context of
strange/exotic matter)
致密星碰撞引起的引力波和奇异物质的性质
Beijing, China, 15.-25. May 2017

Die im Jahre 2017 gehaltene Vorlesungsreihe führt einerseits in die Allgemeine Relativitätstheorie ein, andererseits fokussiert sie sich auf den speziellen Teilaspekt der relativistischen Astrophysik kollidierender hybrider Neutronensterne, in deren innerem Bereich es zur Bildung seltsamer und exotischer Materie kommen kann. Kollabiert ein instabiler Neutronenstern zu einem schwarzen Loch oder zu einem Quark Stern? Wie kann man anhand des ausgesandten Gravitationswellen-Signals zweier kollidierender kompakter Sterne die Eigenschaften der Nuklearen- und Quark-Materie entschlüsseln?

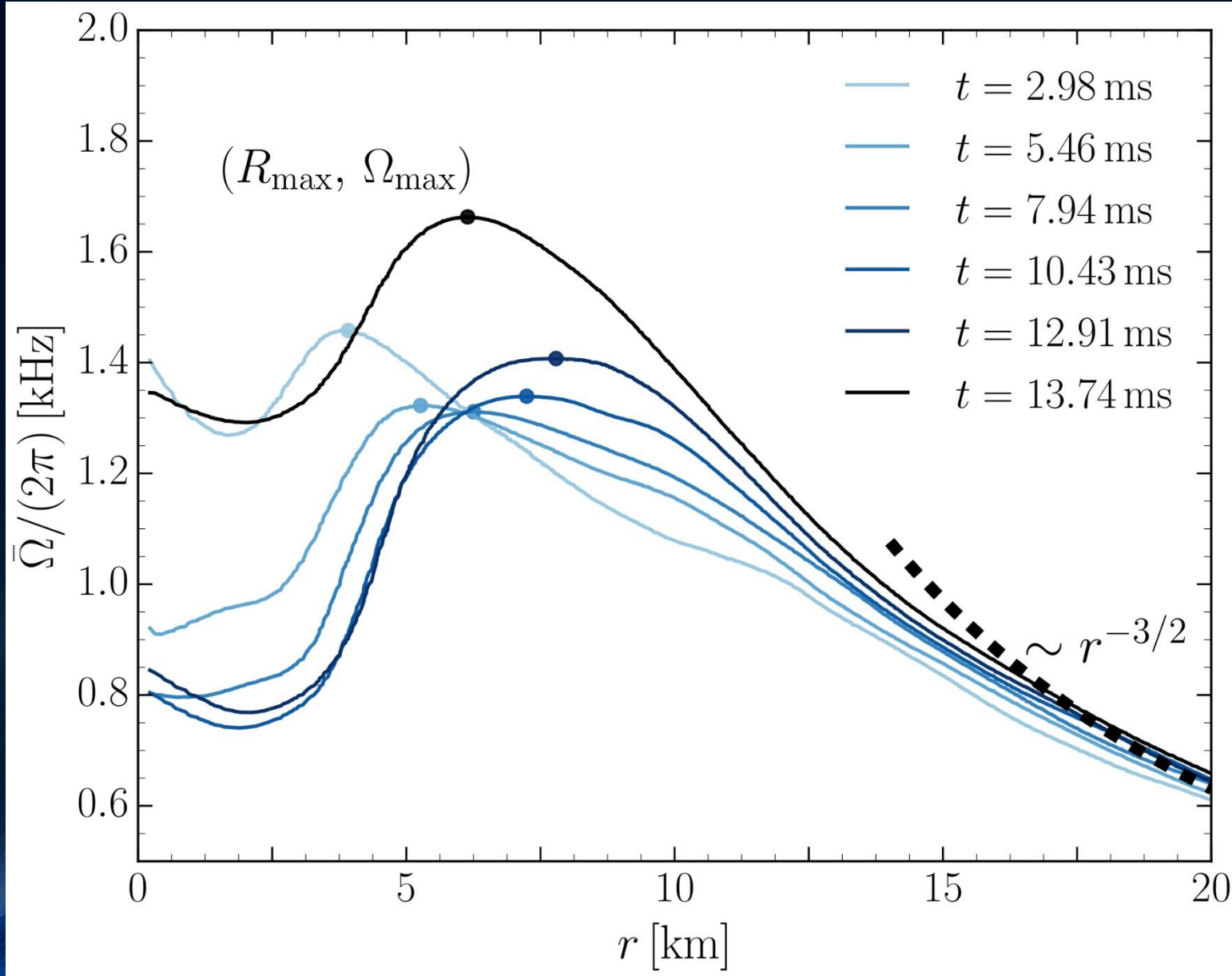
(The series of lectures held in 2017. Topics: theory of general relativity theory, relativistic astrophysics of colliding hybrid neutron stars, strange and exotic matter in the interior of compact stars. Questions: Does an unstable neutron star collapse to a black hole or quark star? How can we extract the strange properties of high density nuclear and quark matter by means of the emitted gravitational wave signal of two colliding compact stars?)

在2017年开设的课程,一方面介绍广义相对论理论,另一方面聚焦于相对论天体物理中的一个特殊部分:混合致密星碰撞,以及在其内部可能生成的奇异和异常物质。一个不稳定的中子星是会坍缩成黑洞还是夸克星?如何根据两个致密星碰撞发射的引力波信号来解码核物质和夸克物质的奇异特性?

Summary

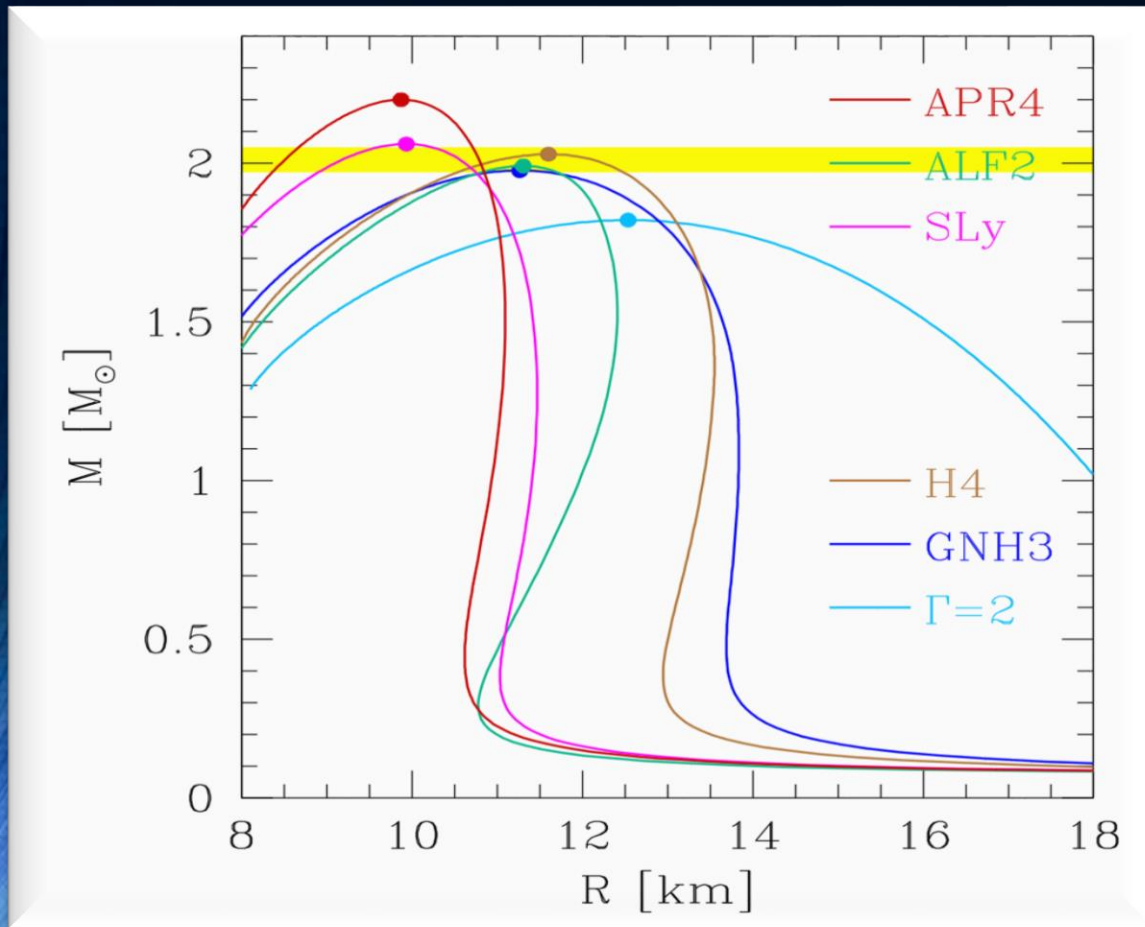
- On August 17, 2017, a long-awaited event has taken place: the Advanced LIGO and Virgo gravitational-wave detectors have recorded the signal from the inspiral and merger of a binary neutron-star system.
- The analysis of the gravitational wave data in combination with the independently detected gamma-ray burst and electromagnetic counterpart results in a neutron star merger scenario which is in good agreement with numerical simulations of binary neutron star mergers performed in full general relativity.
- During the late post-merger simulation, the value of central rest-mass density will reach extreme values and it is expected that a hadron-quark phase transition will be present in the interior region of the HMNS.
- Astrophysical observables of the hadron-quark phase transition may be detectable when advanced gravitational wave detectors reach design sensitivity or with next-generation detectors.

Time dependence of the Rotation Profile



Averaged fluid angular velocity on the equatorial plane for the ALF2-M135 binary as averaged at different times and with intervals of length $t = 1$ ms.

Several different EOSs : ALF₂, APR₄, GNH₃, H₄ and SLy, approximated by piecewise polytopes. Thermal ideal fluid component ($\Gamma=2$) added to the nuclear-physics EOSs.



EOSs

composed of a “cold” nuclear-physics part and of a “thermal” ideal-fluid component¹ [56]

$$p = p_c + p_{\text{th}}, \quad \epsilon = \epsilon_c + \epsilon_{\text{th}}, \quad (6)$$

where p and ϵ are the pressure and specific internal energy,

The “cold” nuclear-physics contribution to each EOS is obtained after expressing the pressure and specific internal energy ϵ_c in the rest-mass density range $\rho_{i-1} \leq \rho < \rho_i$ as (for details see [36, 64–66])

$$p_c = K_i \rho^{\Gamma_i}, \quad \epsilon_c = \epsilon_i + K_i \frac{\rho^{\Gamma_i-1}}{\Gamma_i - 1}. \quad (7)$$

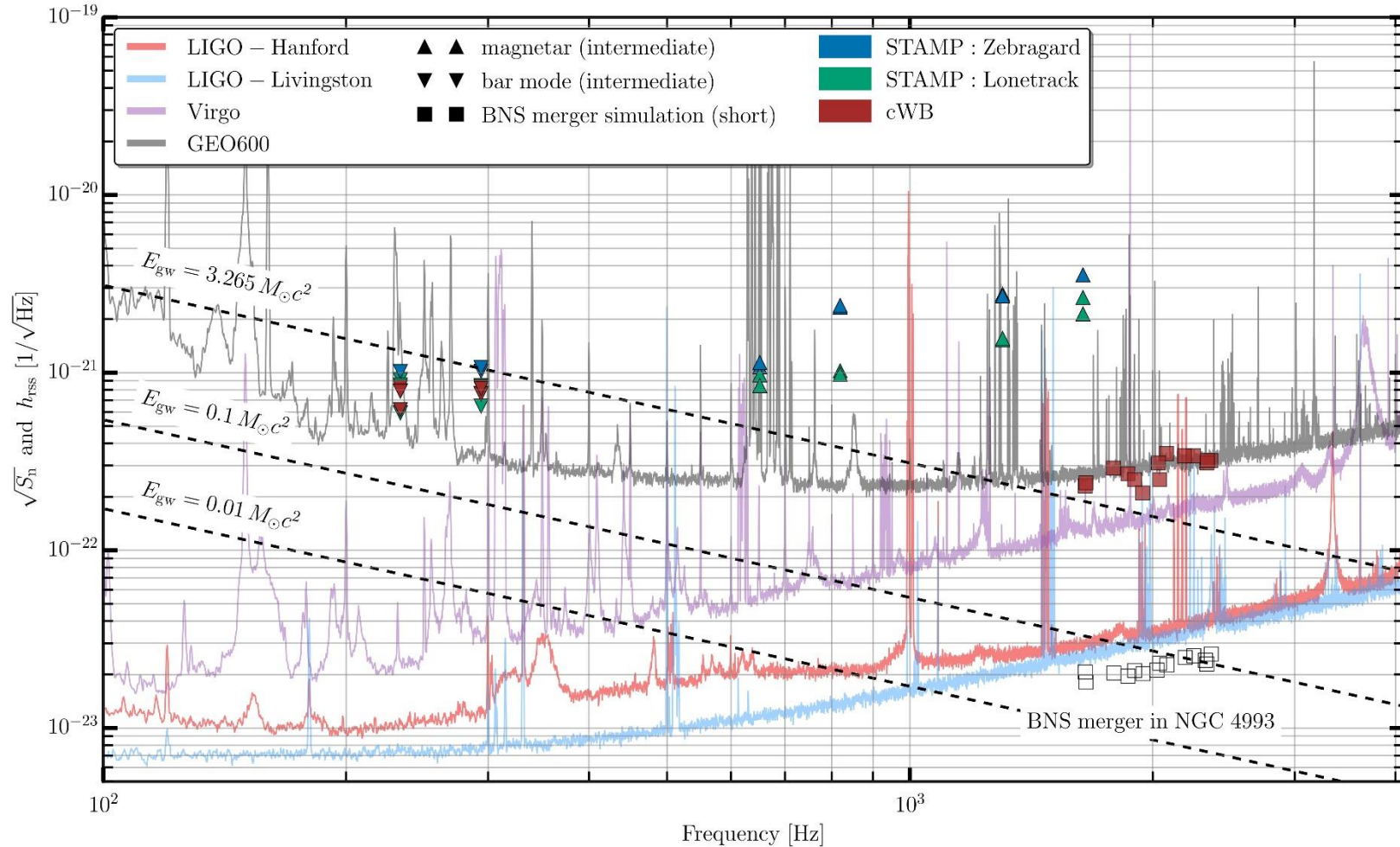
($\Gamma_1 = 4.070$ and $\Gamma_2 = 2.411$). Finally, the “thermal” part of the EOS is given by

$$p_{\text{th}} = \rho \epsilon_{\text{th}} (\Gamma_{\text{th}} - 1), \quad \epsilon_{\text{th}} = \epsilon - \epsilon_c. \quad (8)$$

where the last equality in (8) is really a definition, since ϵ refers to the computed value of the specific internal energy. In all of the simulations reported hereafter we use $\Gamma_{\text{th}} = 2.0$

Additionally LS220-EOS used: Density and Temperature dependent EOS-table (Lattimer-Swesty)

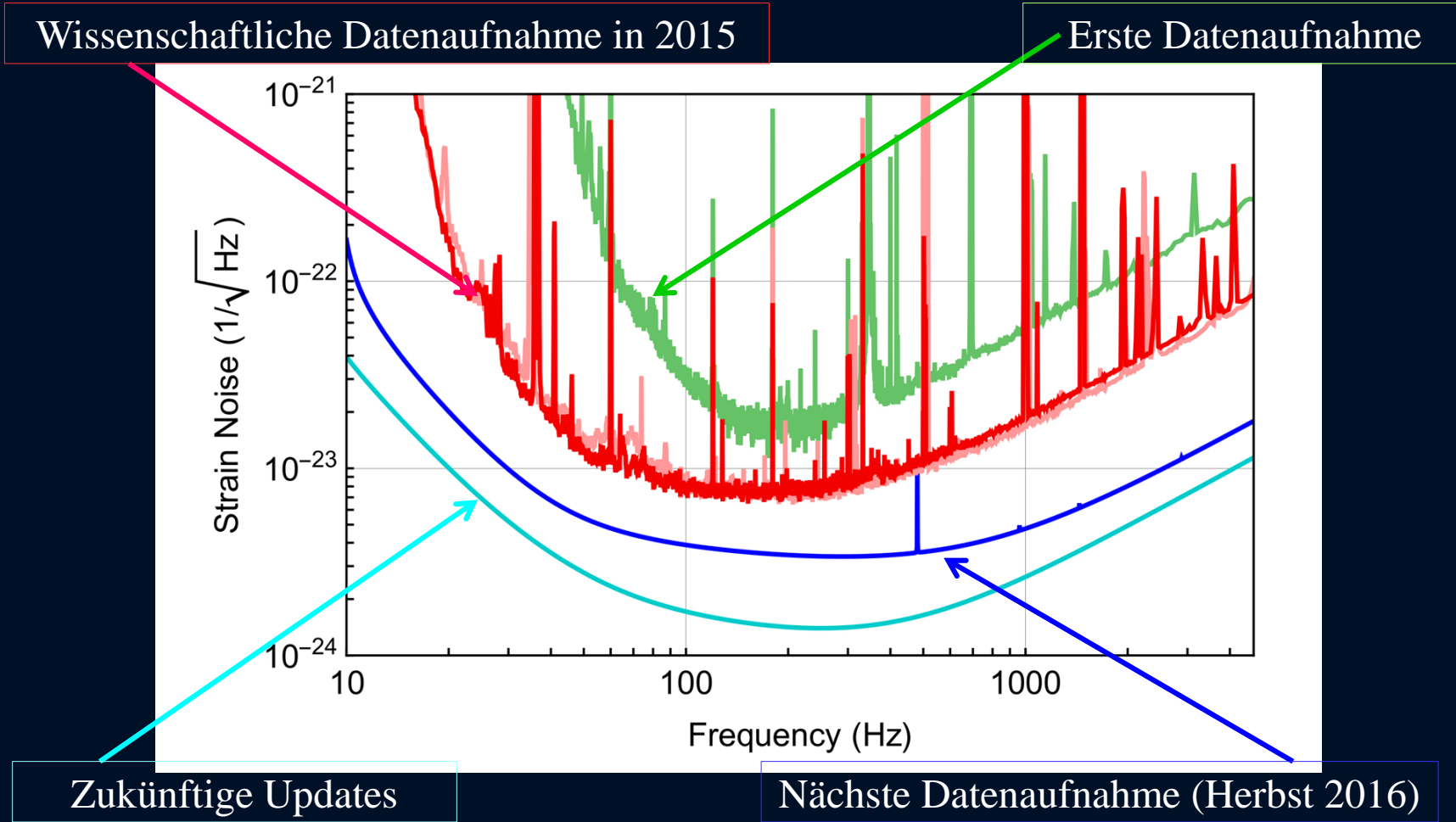
SEARCH FOR POST-MERGER GRAVITATIONAL WAVES FROM THE REMNANT OF THE BINARY NEUTRON STAR MERGER GW170817 (see arXiv:1710.09320v1)



Unfortunately, due to the low sensitivity at high gravitational wave frequencies, no post-merger signal has been found in GW170817.

But, the results indicate that post-merger emission from a similar event may be detectable when advanced detectors reach their design sensitivity or with next-generation detectors.

Warum (noch) keine Gravitationswellen von kollidierenden Neutronensternen?



Gauge Conditions

On each spatial hypersurface, four additional degrees of freedom need to be specified: A slicing condition for the lapse function and a spatial shift condition for the shift vector need to be formulated to close the system. In an optimal gauge condition, singularities should be avoided and numerical calculations should be less time consuming.

Bona-Massó family of slicing conditions:

$$\partial_t \alpha - \beta^k \partial_k \alpha = -f(\alpha) \alpha^2 (K - K_0)$$

“1+log” slicing condition:

$$f = 2/\alpha$$

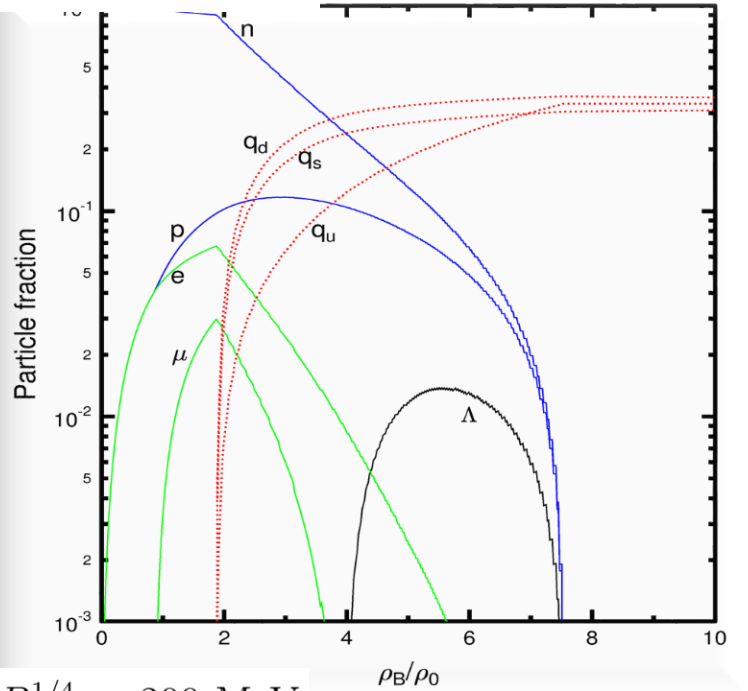
$$\text{where } f(\alpha) > 0 \text{ and } K_0 := K(t = 0)$$

“Gamma-Driver” shift condition:

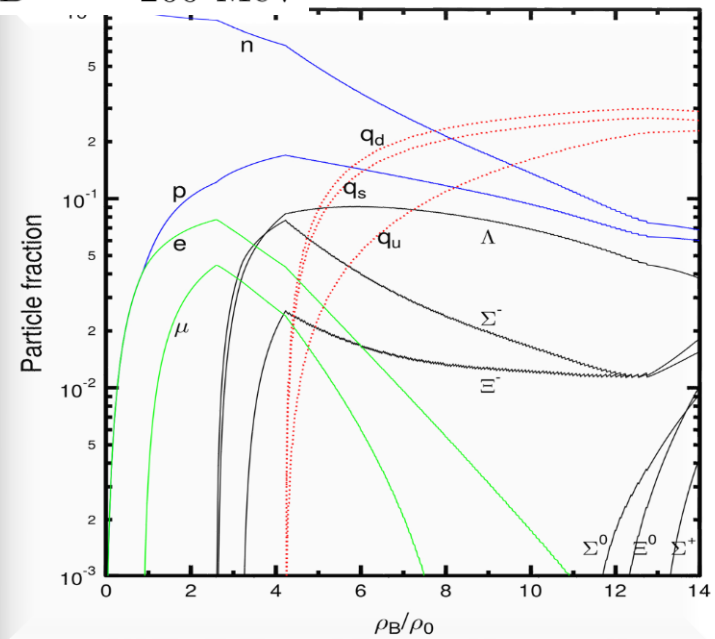
$$\partial_t \beta^i - \beta^j \partial_j \beta^i = \frac{3}{4} B^i,$$

$$\partial_t B^i - \beta^j \partial_j B^i = \partial_t \tilde{\Gamma}^i - \beta^j \partial_j \tilde{\Gamma}^i - \eta B^i$$

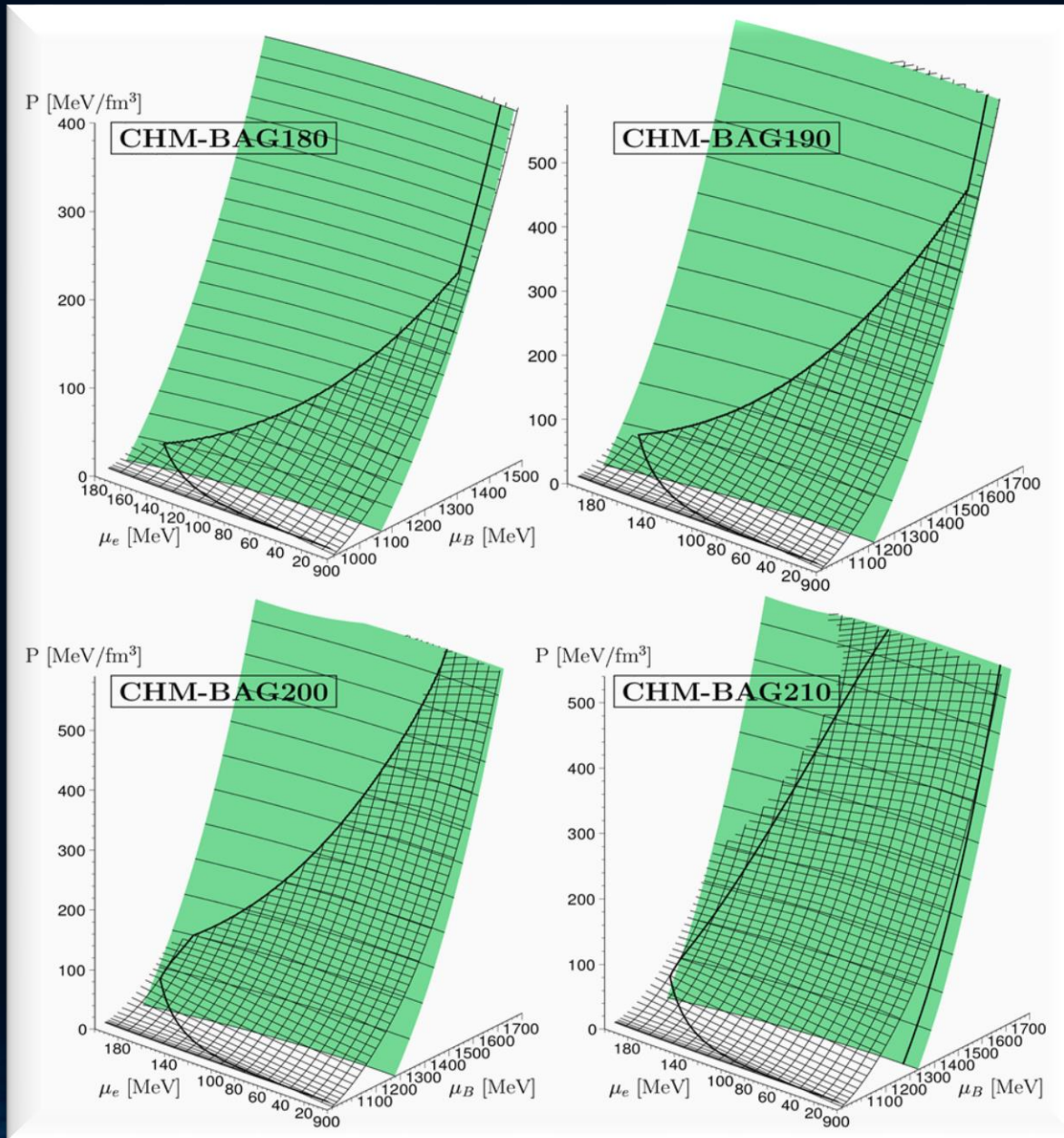
$B^{1/4} = 180 \text{ MeV}$



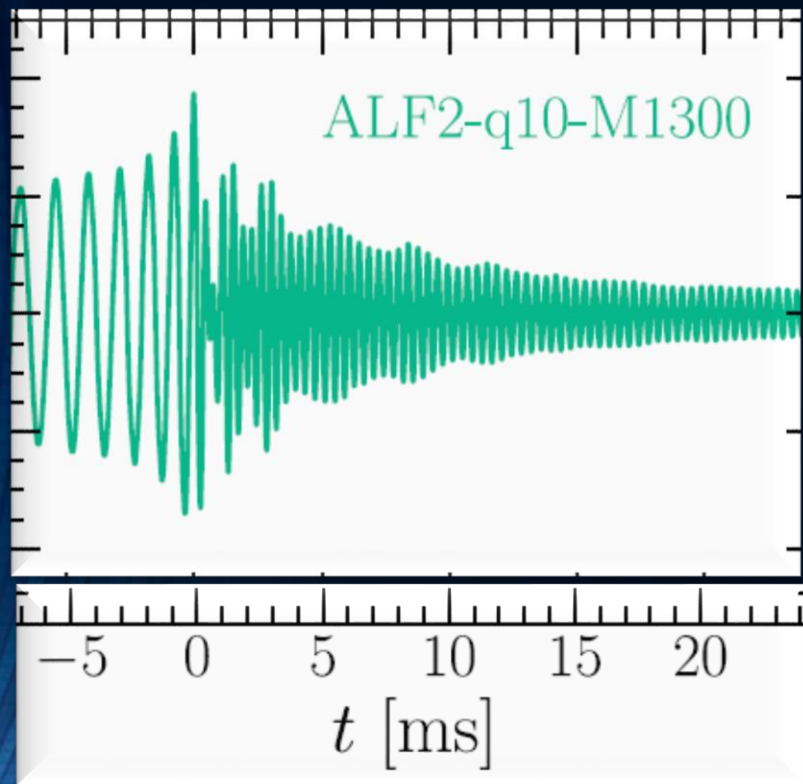
$B^{1/4} = 200 \text{ MeV}$



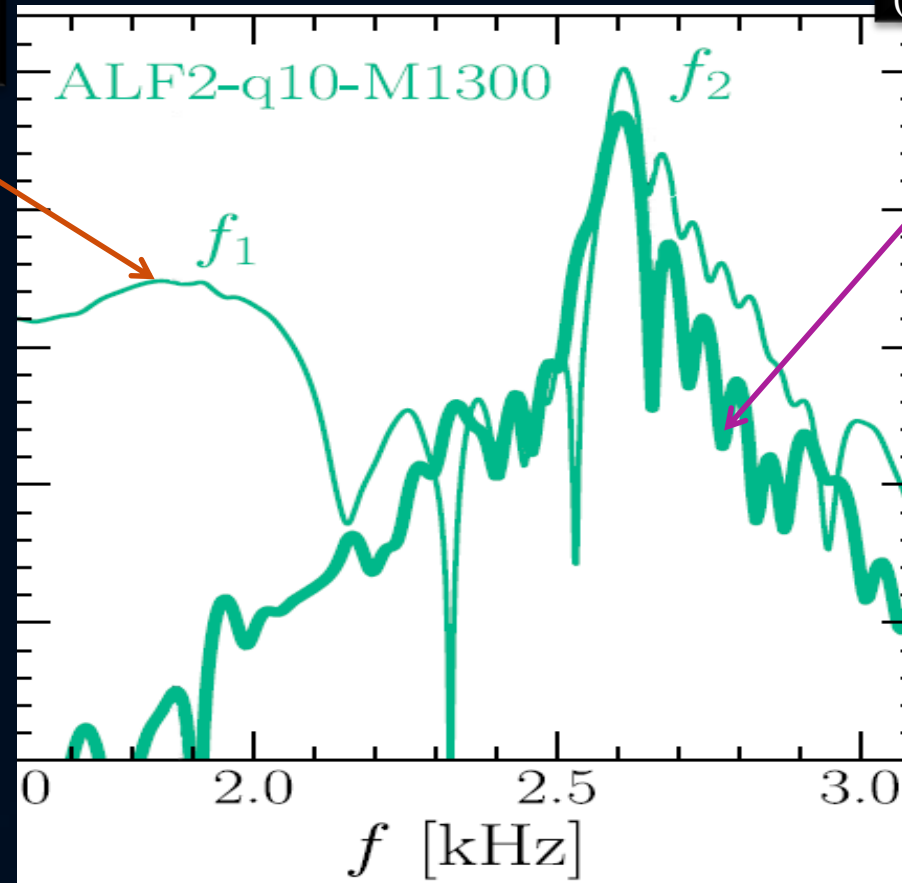
The Gibbs Construction



Spectral Properties of GWs



Full spectral profile
(thin curve)

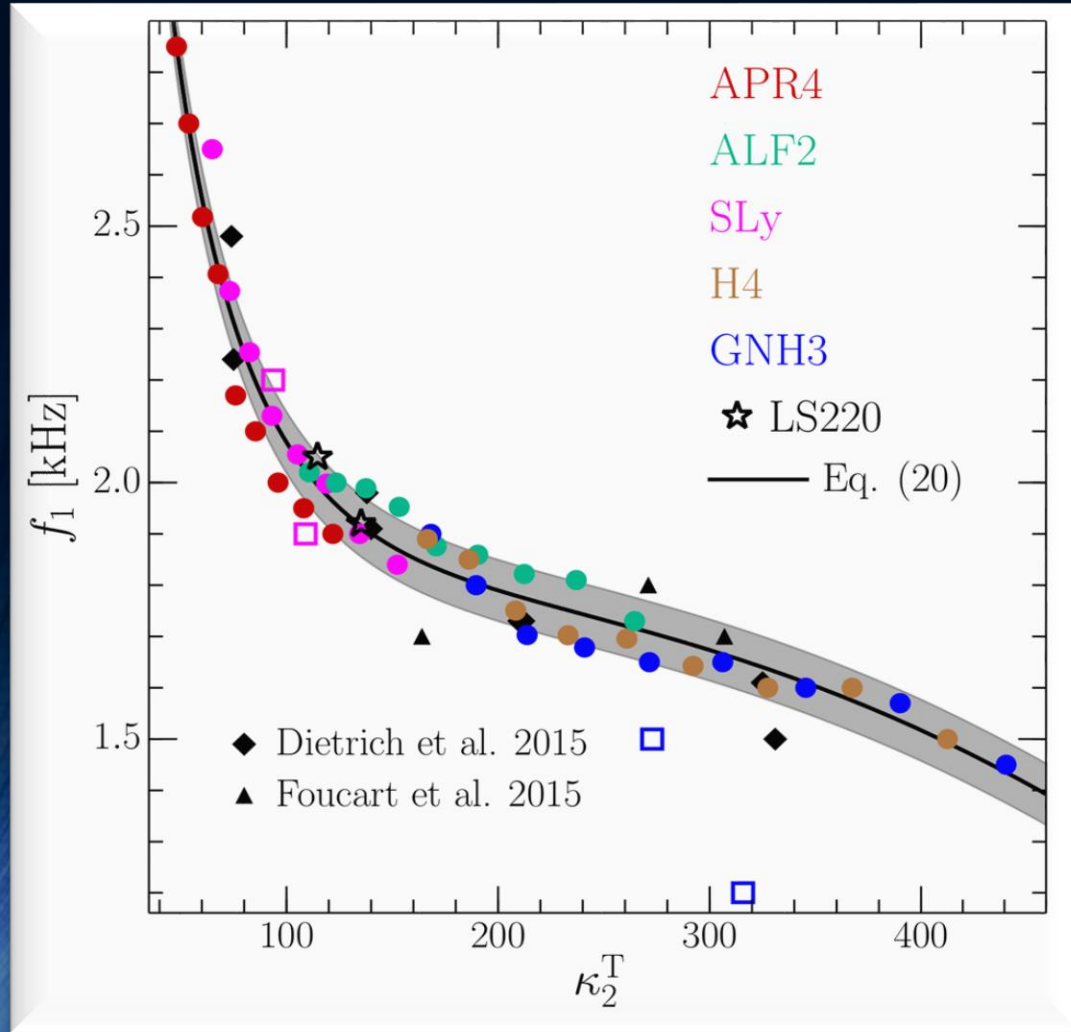


Spectral profile
($t > 3$ ms)
(thick curve)

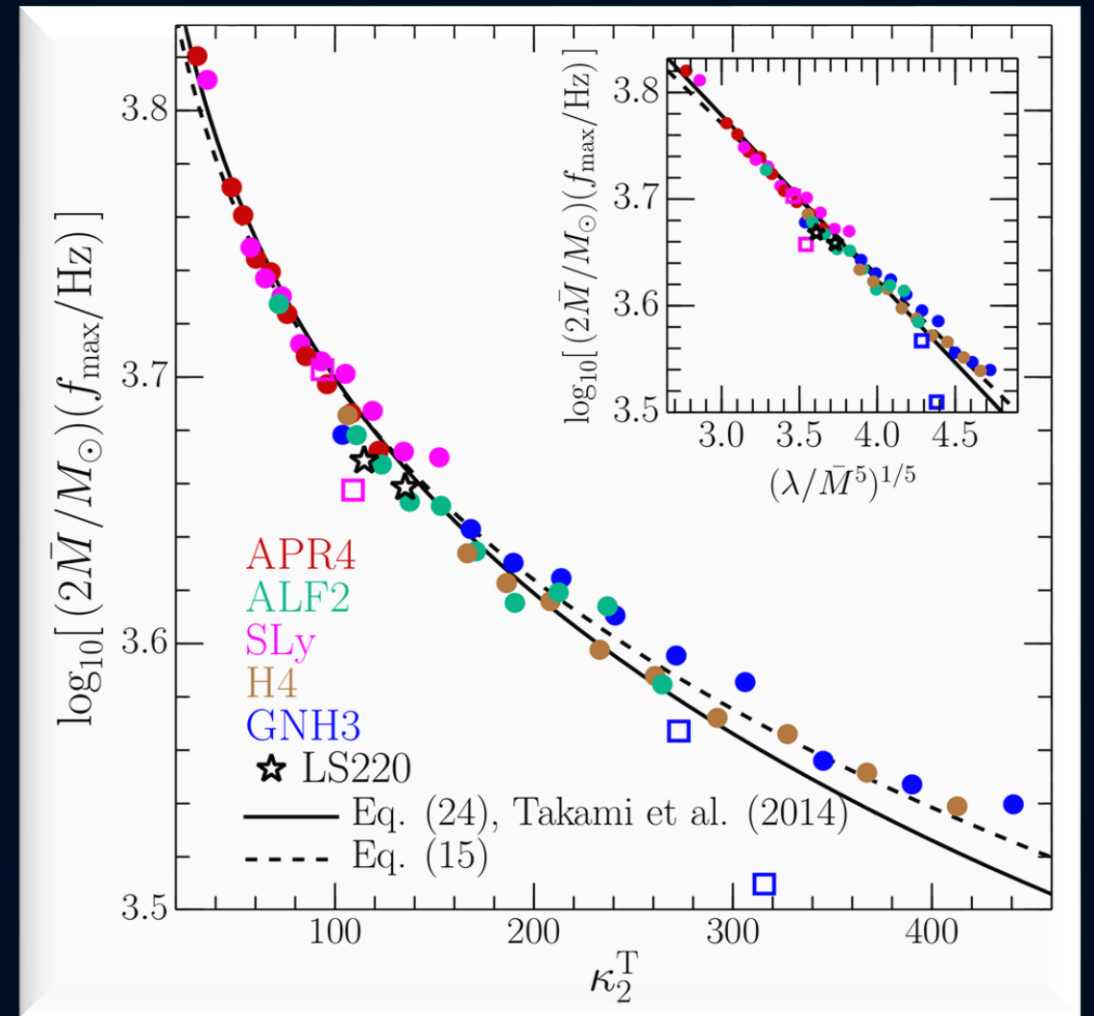
Two characteristic GW frequency peaks (f_1 and f_2);

the origin of f_1 comes from $t < 3$ ms. By measuring M , f_1 and f_2 one can set high constraints on the EoS.

Universal Behavior of f_1 and f_{\max}



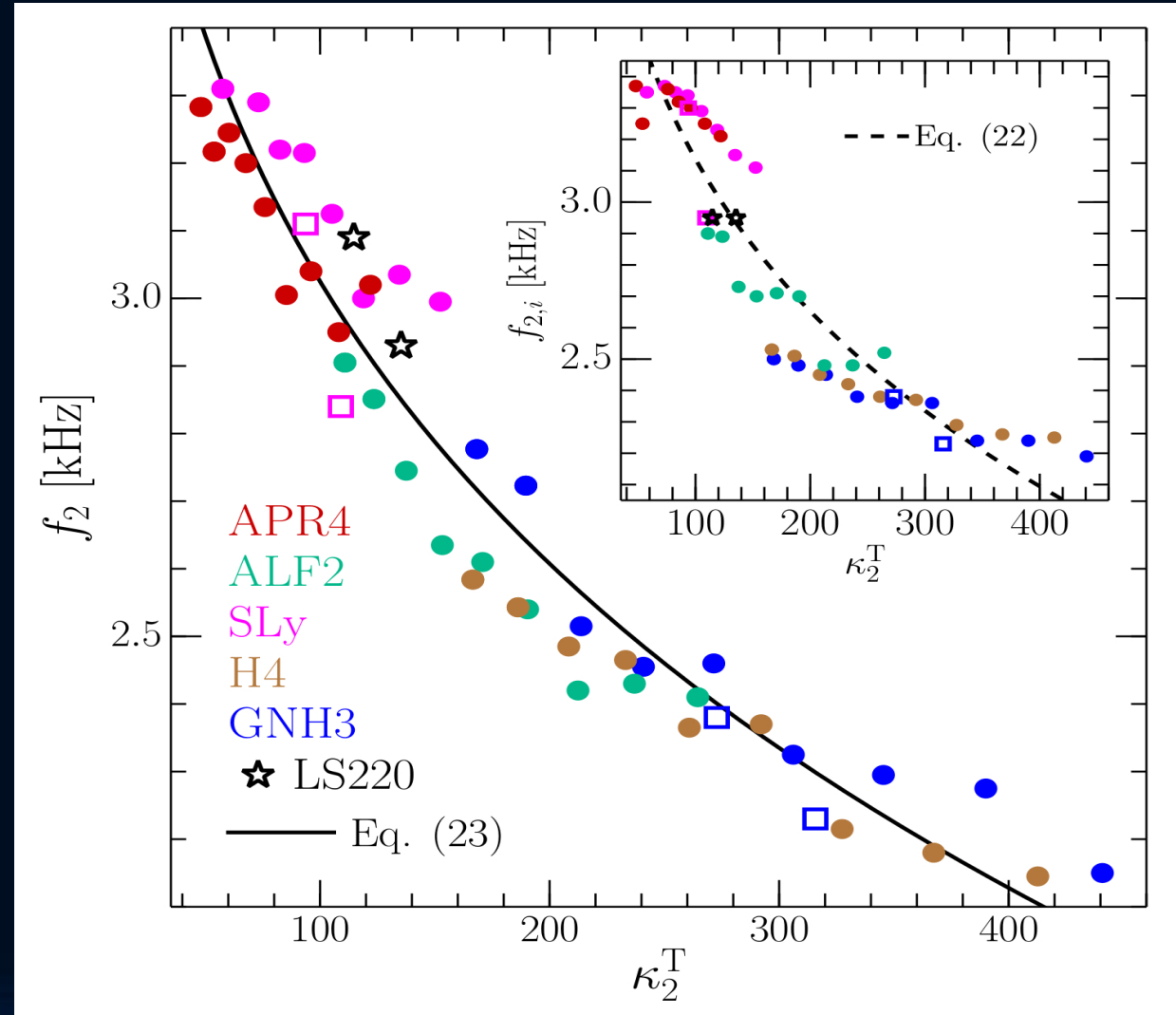
Values of the low-frequency peaks f_1 shown as a function of the tidal deformability parameter κ_2^T .



Mass-weighted frequencies at amplitude maximum f_{\max} shown as a function of the tidal deformability parameter κ_2^T .

Universal behavior of the f_2 -peak

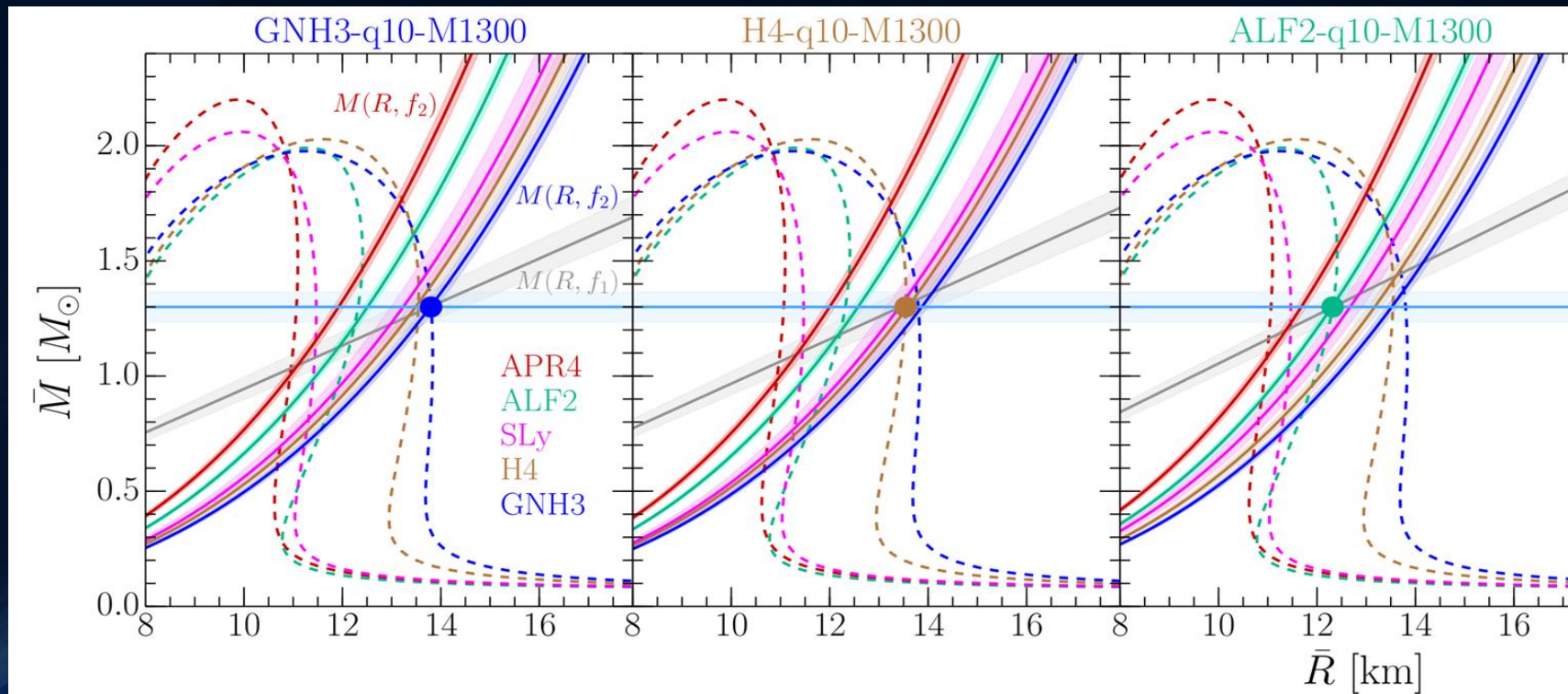
Values of the high-frequency peaks f_2
Shown as a function of the
tidal deformability
parameter κ_2^T .



Gravitational Waves → Equation of State

The detection of GWs from merging neutron star binaries can be used to determine the high density regime of the EOS.

With the knowledge of f_1 , f_2 and the total mass the system, the GW signal can set tight constraints on the EOS.



The deconfined Quark Matter will be Macroscopically Confined by the Event Horizon

